

Bone Aging in DNA Repair Deficient Trichothiodystrophy Mice

Botveroudering in trichothiodystrophy muizen
met een defect in DNA schadeherstel

ISBN: 978-90-8559-915-9

Omslag: Ruud Koppenol en Karin Diderich

Lay-out en drukwerk: Optima Grafische Communicatie

Dit proefschrift kwam tot stand binnen de vakgroep Celbiologie en Genetica van de faculteit der Geneeskunde en Gezondheidswetenschappen van de Erasmus Universiteit Rotterdam.

De vakgroep maakt deel uit van het Medisch Genetisch centrum Zuid-West Nederland.

Het onderzoek is financieel ondersteund door de Nederlandse Organisatie voor Wetenschappelijk Onderzoek via het Research Institute for Diseases of the Elderly, the National Institutes of Health, the National Institute of Environmental Health Sciences, de Stichting Koningin Wilhelmina Fonds voor de Nederlandse Kankerbestrijding en de Europese Commissie.

Bijdragen in de drukkosten zijn verkregen van de Erasmus Universiteit Rotterdam, de Nederlandse Paget patiënten vereniging en DNage BV, Leiden.

Bone Aging in DNA Repair Deficient Trichothiodystrophy Mice

Botveroudering in trichothiodystrophy muizen
met een defect in DNA schadeherstel

Proefschrift ter verkrijging van de graad van doctor
aan de Erasmus Universiteit Rotterdam

op gezag van de rector magnificus Prof.dr. H.G. Schmidt
en volgens besluit van het College voor Promoties.

De openbare verdediging zal plaatsvinden op
woensdag 6 januari 2010 om 13.30 uur

door Karin Elin Maria Diderich
geboren te Rotterdam



Promotiecommissie

Promotoren: Prof.dr. J.H.J. Hoeijmakers
Prof.dr. G.T.J. van der Horst
Prof.dr. J.P.T.M. van Leeuwen

Overige leden: Prof.dr. H. van Steeg
Prof.dr.ir. A.P.N. Themmen
Prof.dr.ir. H. Weinans

“Als mijn proefschrift klaar is, zal er met geen woord gewag worden gemaakt van
ontvelde schouders, geschaafde knieën, de beukende hoofdpijn, de muggen en de
vleesetende vliegen.”

Uit “Nooit meer slapen” van Willem Frederik Hermans

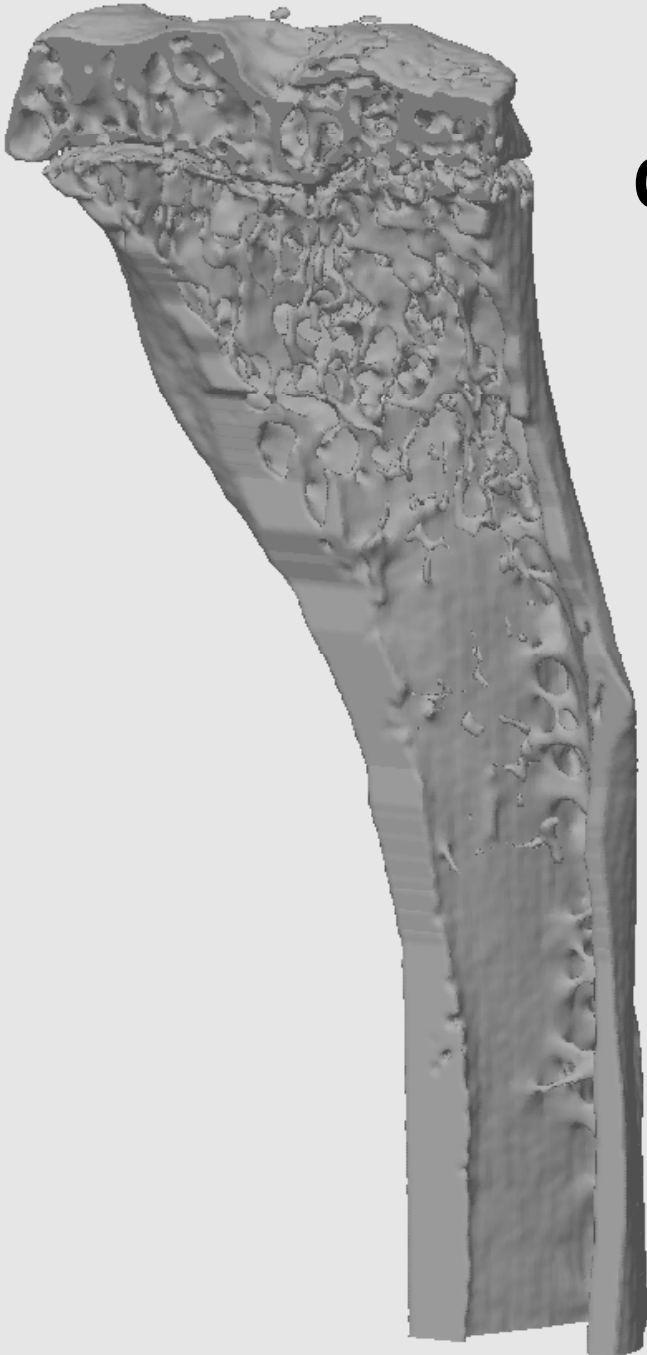
Voor mijn moeder

In memoriam

Ragnhild Hellestam
Prof.dr. J. Sanders-Woudstra

Contents

Chapter 1 Introduction	9
1 Premature aging in DNA repair deficient disorders	11
2 Trichothiodystrophy and bone aging	24
3 Bone metabolism	25
4 Scope of this thesis	37
Chapter 2 Osteoporosis and decline in stem cells in prematurely aging DNA repair deficient trichothiodystrophy mice	51
Chapter 3 Age-related skeletal dynamics in DNA repair deficient male trichothiodystrophy mice	75
Chapter 4 Increased bone mass in vertebrae of DNA repair deficient trichothiodystrophy mice strongly resembling patients	93
Chapter 5 Endocrine parameters in relation to accelerated bone loss in prematurely aging DNA repair deficient trichothiodystrophy mice	107
Chapter 6 Concluding remarks and future perspectives	133
Summary/ Samenvatting	141
Appendix I Accelerated aging pathology in <i>ad libitum</i> fed <i>Xpd^{TTD}</i> mice is accompanied by features suggestive of caloric restriction	147
Appendix II Dysregulation of the peroxisome proliferator-activated receptor target genes by XPD mutations	169
Appendix III Impaired Genome Maintenance Suppresses the GH/IGF1 Axis in Cockayne Syndrome Mice	195
Curriculum vitae	231
Dankwoord	237
Colour figures	241



CHAPTER 1

Introduction

1 Premature aging in DNA repair deficient disorders

1.1.1 DNA damage

Our genome is continuously damaged by environmental, endogenous agents as well as by the intrinsic instability of DNA. For example, UV light gives rise to helix-distorting cyclobutane pyrimidine dimers (CPDs) and pyrimidine-(6,4)-pyrimidone adducts (6-4PPs). Ionizing radiation can cause both single and double strand breaks in DNA and numerous types of oxidative lesions. Chemotherapeutics, that are used in cancer therapy, and other environmental chemical agents, which are present in e.g. polluted air and tobacco smoke, induce a plethora of DNA lesions, including intra- and inter-strand cross-links and mono-adducts. In addition, endogenous agents cause a wide variety of DNA lesions. Metabolic processes within our cells lead to reactive oxygen species (ROS), which react with proteins, lipids and DNA. Although ROS participate in beneficial physiological processes as growth factor signal transduction (1), these by-products of metabolism also underlie a broad spectrum of oxidative DNA lesions, including 8-oxo-2'-deoxyguanosine (8-oxodG), thymine glycols, cylopurines, as well as single and double strand breaks (2). Finally, lesions in the DNA can also form without a direct damaging agent. E.g. spontaneous hydrolysis or modifications of nucleotides occurs in cells, which leaves non-informative a-basic sites or altered, miscoding nucleotides (3).

1.1.2 Consequences of DNA damage

Lesions in DNA have immediate effects on cell function as well as long-term consequences. For instance, DNA lesions will interfere with transcription and replication (4,5). This causes dysfunctioning of cells and -depending on the damage load- will lead to cell cycle arrest or programmed cell death (apoptosis) (6). Apoptosis is a way of eliminating cells that are at risk of malignant transformation. In addition to apoptosis, cellular senescence, i.e. limited growth potential followed by growth arrest, can neutralize potentially malignant cells (7). De Waard and co-workers found that different cell types exhibit different responses to DNA damage (8). For instance, pluripotent embryonic stem cells show increased apoptosis after treatment with several types of DNA damaging agents compared to differentiated keratinocytes (8).

Persistent DNA lesions that are misinterpreted by the replication machinery, result in the induction of mutations. These mutations, as well as other changes in the DNA that result from genome instability or miss-segregation (rearrangements, deletions, insertions, loss of heterozygosity and numerical aberrations), can on the long-term give rise to cancer or inborn diseases. Furthermore, cellular dysfunction or depletion of proliferative capacity of cells by senescence or apoptosis can contribute to aging (9,10). These processes lead to compromised tissue homeostasis, most likely through diminished self-renewal or altered tissue structure

(11). For example, cells that are lost via apoptosis might be replaced by progenitors and in time this may exhaust the regenerative capacity of a tissue.

1.2.1 Repair mechanisms

To counteract the deleterious effects of DNA damage, the cell is equipped with a wide variety of genome caretaking mechanisms (12,13) (Figure 1). On the one hand, a transient block in the cell cycle can provide an extended time window for repair to take place (14). Various DNA repair machineries exist to repair the different DNA lesions (reviewed by (12,13)). On the other hand, cells with persisting DNA damage may bypass DNA damage during replication at the risk of mutation induction. This process is called trans-lesion synthesis and involves several polymerases that are more or less error-prone (15-17).

Nucleotide excision repair (NER), which is discussed in more detail below, functions by a 'cut and patch'-like mechanism, in which damage recognition, opening of the DNA helix around the lesion, damage excision, and gap-filling are the successive steps (reviewed by (12,18,19)). This repair mechanism can remove numerous types of helix-distorting and bulky lesions.

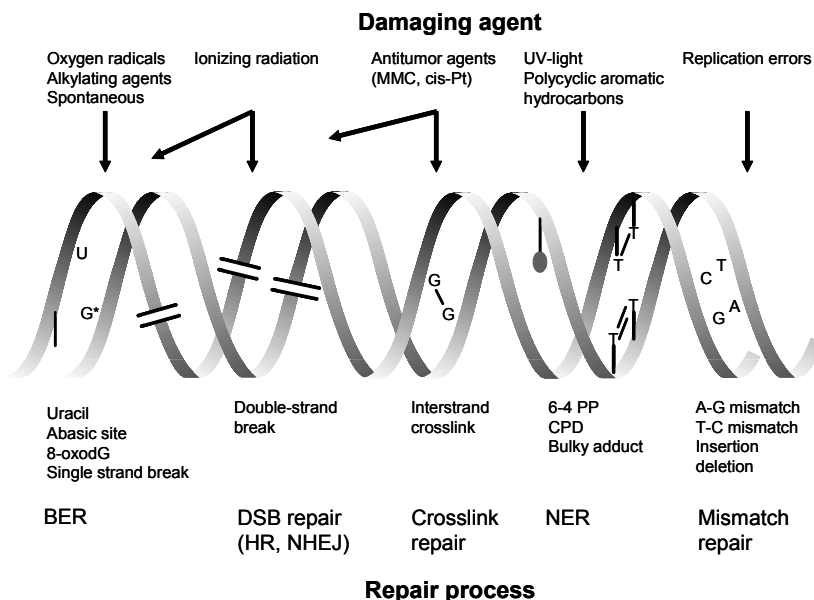


Figure 1: DNA lesions and repair mechanisms.

At the top of the figure, examples of common DNA damaging agents are depicted. As indicated by the arrows, many DNA damage inducing agents produce a spectrum of different (classes of) lesions. Oppositely, different DNA damaging agents can cause similar DNA lesions. The middle part of the figure shows the DNA helix, with several DNA lesions, as depicted under the figure. The lower part of the figure shows the various repair pathways that cells use to remove these lesions (adapted from de Boer et al., Carcinogenesis 2000).

Base excision repair (BER) is another 'cut and patch'-like mechanism that involves the concerted interplay of different specialized proteins. A battery of glycosylases with overlapping lesion specificity recognize and remove the lesions from the DNA. These different glycosylases allow BER to remove a wide variety of (non helix-distorting) nucleotide modifications (reviewed by (20,21)). As BER removes base adducts from ROS, methylation, deamination, and hydroxylation, it is considered as the main guardian against DNA lesions caused by cellular metabolism.

Mismatch repair is a 'cut and patch'-like mechanism that removes single base-base mismatches and small insertion/deletion loops caused by erroneous base incorporation, and slippage of DNA polymerases during replication or recombination (reviewed by (22)). As such it prevents the accumulation of these mutagenic lesions and is important in the prevention of cancer. This is illustrated by the fact that mutations in mismatch repair genes cause Lynch syndrome (previously called hereditary non-polyposis colorectal cancer or HNPCC) (23).

Double strand breaks (DSBs) are deleterious lesions that arise from ionizing radiation, free radicals or chemicals, or are formed during replication of single strand breaks. Cells are equipped with at least two double strand break repair mechanisms: homologous recombination and non-homologous end joining (NHEJ) (reviewed by (24,25)). The first uses the homologous sequence of the sister chromatid, present after DNA replication (or in meiosis the homologous chromosome) to accurately repair the DSB in an error-free manner. In contrast, NHEJ simply links two DNA ends together with little or no use of homologous sequences present in the ends and is thus an error-prone pathway.

Cross-link repair is capable of removing the highly toxic inter-strand cross-links. While the components of the Fanconi Anemia/ BRCA pathway are being unraveled, its mechanism is still not fully understood. This is probably due to the fact that it depends on many factors involved in other repair processes (NER, homologous recombination, mismatch repair and trans-lesion synthesis) and as such seems to be the result of a combination of interwoven repair pathways (reviewed by (26-32)).

1.2.2 Nucleotide excision repair

One of the most versatile DNA repair mechanisms is nucleotide excision repair (NER). This repair system can remove a wide variety of DNA helix-distorting lesions of both exogenous and endogenous origin. For example, NER is responsible for the removal of CPDs and 6-4PPs induced by UV light. NER can also remove bulky chemical adducts, intra-strand cross-links and several forms of oxidative damage such as cyclopurines induced by reactive chemicals as ROS or tobacco smoke (12,33).

NER is composed of two sub-pathways that differ in the way lesions are recognized: global genome NER and transcription-coupled NER (Figure 2). In global genome NER, the hHR23B/XPC complex recognizes the lesion. This recognition is dependent on the degree of helix distortion and as a consequence CPDs, that only mildly disturb the helix, are inefficiently

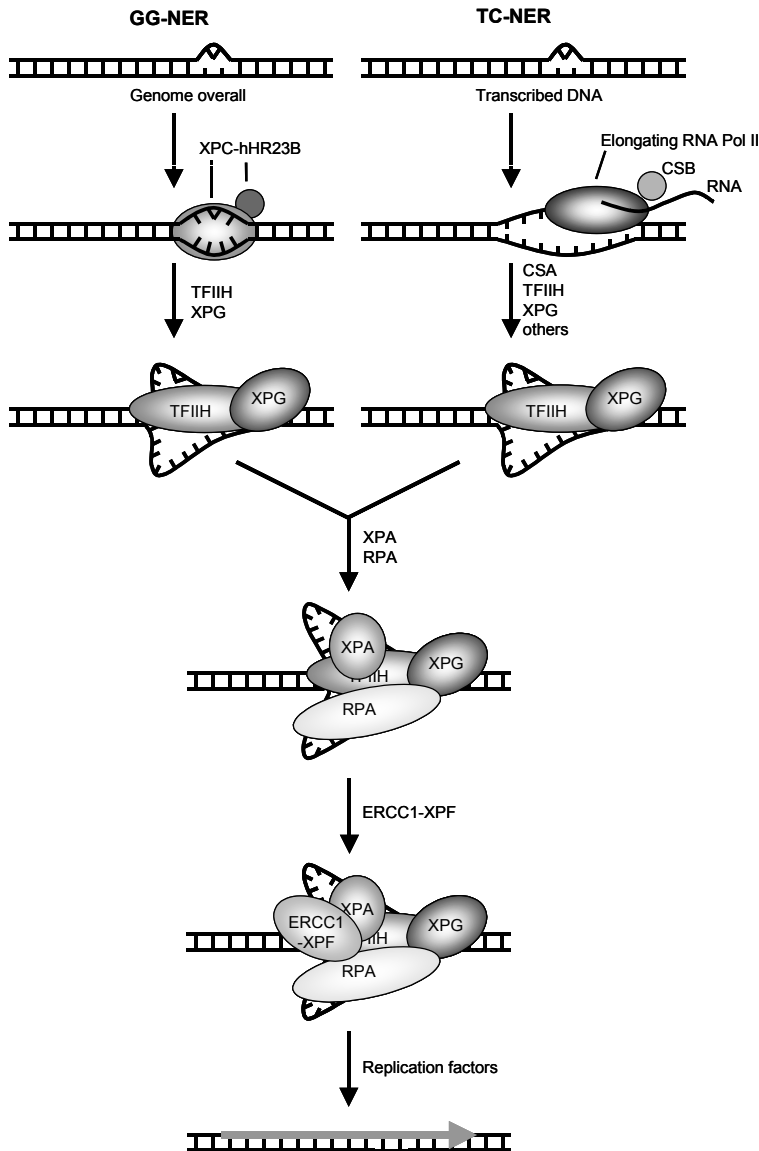


Figure 2: Mechanism of nucleotide excision repair.

This figure shows the principle of nucleotide excision repair (NER) and its two subpathways, global genome NER (GG-NER) and transcription-coupled NER (TC-NER). In GG-NER, the XPC/hHR23B protein complex recognizes the helix distorting lesion. When RNA polymerase II is stalled upon a lesion, TC-NER is initiated by the CSA and CSB protein. In both GG-NER and TC-NER the lesion recognition step is followed by recruitment of TFIIH. The XPB and XPD helicases from the TFIIH complex unwind the DNA around the lesion. The initial open complex is stabilized by XPG. Next, XPA verifies the lesion and RPA stabilizes the open intermediate by binding single stranded DNA. The structure specific endonucleases XPG and ERCC1/XPF cleave 3' and 5' of the lesion, respectively. The resulting 24-32 nucleotide fragment, containing the lesion, is subsequently removed and the remaining single strand gap is filled by the regular replication machinery and the resulting nick is sealed by ligase I or ligase III (adapted from Hoeijmakers, Nature 2001).

repaired. In contrast, blockage of the elongating RNA polymerase II is believed to initiate repair in transcription-coupled NER. Lesions that block transcription as for example CPDs are efficiently repaired by transcription-coupled NER (34). This process requires the CSB and CSA proteins (19). In both global genome NER and transcription-coupled NER, the lesion recognition step is followed by recruitment of the ten subunit transcription factor TFIIH. TFIIH contains the XPB and XPD helicases that unwind ~30bp of DNA around the lesion with respectively its ATPase activity and its helicase activity (35). XPA then demarcates the damage and together with the single strand binding protein complex RPA stabilizes the NER complex. Next, endonucleases XPG and ERCC1/XPF cleave 3' and 5' of the lesion, respectively. Finally, the ssDNA gap is filled by the regular replication machinery and the resulting nick is sealed by ligase I or ligase III (36). In vivo, the NER complex assembles at the site of damage in a few seconds and remains stable for about 4 minutes during which the repair reaction is believed to take place (37). Global genome NER repairs lesions in the entire genome and is as such important in preventing cancer whereas transcription-coupled NER repairs lesions in transcribed strands enabling unhindered transcription. Transcription-coupled repair may be more extensive including transcription-coupled BER as well.

1.3.1 Repair-related disorders

A variety of rare (autosomal recessive) disorders illustrate the importance of DNA repair mechanisms and other vital genome caretaking processes (reviewed by (38)). Most of these DNA repair associated disorders show an elevated cancer risk and thus demonstrate the important function of DNA repair in preventing cancer. As mentioned previously, Lynch syndrome (hereditary non-polyposis colorectal cancer) is caused by mutations in mismatch repair genes (23), whereas autosomal recessive adenomatous polyposis is caused by biallelic mutations in MYH, a glycosylase involved in BER (39,40). Ataxia telangiectasia, ataxia telangiectasia-like disorder and Nijmegen breakage syndrome are DSB-repair related disorders and all display cancer predisposition and several aspects of accelerated aging as well as hypersensitivity to ionizing radiation and chromosomal instability (41). Mutations in genes involved in NER underlie three rare autosomal recessive disorders: xeroderma pigmentosum (XP), Cockayne syndrome (CS) and trichothiodystrophy (TTD) (reviewed by (42,43)).

1.3.2 Xeroderma pigmentosum

The diagnostic features of XP are a dry scaly skin (xeroderma), abnormal pigmentation in sun-exposed skin-areas (pigmentosum), photosensitivity, and a 1000-fold increased risk of developing UV-induced skin cancer (mainly squamous cell carcinomas and basal cell carcinomas). However, these symptoms are heterogeneous in occurrence as well as in severity among the different XP patients. In addition to skin cancer predisposition, patients have a 10-20 fold increased risk of developing several types of internal cancers before the age of 20 (43).

Complementation studies have shown the involvement of 7 genes: *XPA* through *XPG*. XP-C and XP-E are specifically deficient in the global genome repair pathway (44-47) leaving the transcription-coupled NER intact. This is probably why, except for the cancer risk, XP-C and XP-E patients generally show mild XP features. The other five complementation groups display defects in both global genome repair and transcription-coupled NER. However, many mutations in *XP* genes do not cause a complete inactivation of proteins and thus provide the cell with residual repair capacity, which probably explains the milder forms of XP (reviewed in (43)). Most XP patients develop almost normally but die of cancer, which reduces their average life span by approximately 30 years (48).

However, about 20-30% of XP patients show progressive neurological degeneration with a variable course. Features observed in these patients include diminished or absent deep tendon reflexes, high frequency hearing loss, abnormal gait, swallowing difficulties and mental retardation (49). A minority of patients show microcephaly and growth retardation, (43,50-52). The neurological symptoms in XP are caused primarily by neuronal degeneration (53) (54).

The diagnosis of XP is based on the level of unscheduled DNA synthesis (UDS) measured by the incorporation of 3H- thymidine in non-S phase nuclei after UV-irradiation of skin fibroblasts from patients. When UDS levels are lower compared to control fibroblasts, the patient fibroblasts are subjected to complementation assays.

1.3.3 Cockayne syndrome and XP/CS

As is the case for XP, patients with Cockayne syndrome can display photosensitivity of the skin. However, CS is not associated with an increased skin cancer risk. This low cancer predisposition in CS patients is probably associated with functional global genome NER in addition to increased apoptosis of premutagenic cells due to improper TCR. In addition, CS patients display additional features that are not observed in XP.

These features include a characteristic facies with deep set eyes, prominent ears and a wizened facial appearance (bird-like face), short stature, kyphosis, impaired sexual development, caries, thin hair, cachexia, and osteoporosis. Neurological features include progressive microcephaly, increased deep tendon reflexes, progressive sensorineural deafness, progressive visual loss with pigmentary retinal degeneration and involvement of the lens and cornea, progressive ataxia, delayed psychomotor development, and mental retardation (49). Brain imaging shows absence of myelin, cerebral atrophy and prominent calcification of among others the basal ganglia (49). The cerebral atrophy is due to degeneration of neurons, but the most striking neuropathological feature is abnormal myelination (53,54).

Many of these features resemble aging and classify CS as a progeroid disease (reviewed by (43,55)). The mean age of death, mainly caused by respiratory infections, resulting from a poor overall condition, is 12.5 years.

Similar to XP, CS is a heterogeneous disease. In order to diagnose CS, cellular studies must show impaired UV survival and lack of RNA synthesis recovery, which is the start of transcription after a temporary UV-induced block in transcription. Cerebro-oculo-facio-skeletal syndrome (COFS) can be regarded as a severe form of CS (56). Symptoms of COFS include reduced birth weight, early microcephaly with subsequent brain atrophy, reduced white matter, patchy grey matter, hypotonia, deep-set eyes and cataracts. In addition, movement is markedly decreased and joint contractures are common.

Defects in two genes, *CSA* and *CSB*, can cause CS (55). However, a correlation between complementation group and severity of CS has not been observed. Only few patients are known to suffer from COFS, but the genes that are known to be involved are *CSB*, *XPG*, *XPB* and *ERCC1* (57). In addition, a subset of mutations in *XPB*, *XPB* and *XPG* can lead to the combined phenotype of XP and CS including predisposition to cancer (43). Patients with the XP/CS complex have the skin and eye phenotype as observed in XP patients in addition to the somatic and neurological abnormalities of CS patients including short stature, immature sexual development and retinal degeneration(49,58). The reported patients show progressive neurological degeneration.

1.3.4 Trichothiodystrophy and XP/TTD

A third photosensitive disorder is trichothiodystrophy (TTD). TTD involves a broad spectrum of symptoms and as a result the nomenclature can be confusing. Over the years, many syndromes, such as the syndrome of Pollit, Tay's syndrome, Sabinas syndrome, ONMR syndrome (onychotrichodysplasia with neutropenia and mental retardation), and Amish brittle hair disease, have been described that retrospectively belong to the spectrum of TTD (59-61). PIBIDS is an acronym that is often used for the combination of symptoms that is displayed by TTD patients: photosensitivity, ichthyosis (scaly skin), brittle hair and nails, impaired intelligence, decreased fertility, and short stature (43,60). TTD encompasses PIBIDS, IBI(D)S and BI(D)S as well as SIBIDS

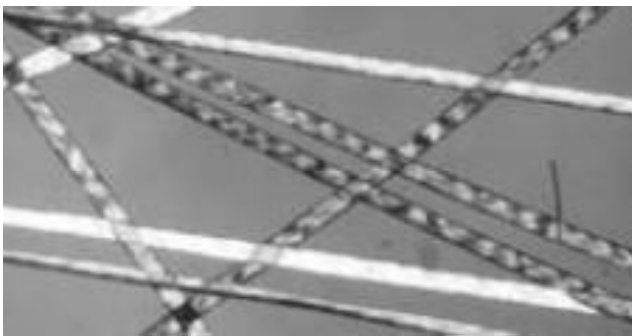


Figure 3: 'Tiger tail banding' in hair from a TTD patient.

Adapted from Liang et al., *J Invest Dermatol.* 2006.

(osteosclerosis or skeletal abnormality and IBIDS) (43,62). The hallmark of TTD is the hair with its characteristic 'tiger tail' pattern (when viewed with polarised microscopy; Figure 3) that is dry, sparse and easily broken, as a result of the absence of cysteine-rich matrix proteins in the hair shaft (63).

A recent literature review describes features of 112 patients that were included based on having at least two of four abnormalities ((1) presence of brittle hair and/or hair shaft abnormalities; (2) tiger tail banding; (3) decreased sulphur or cysteine content of hair; and (4) a DNA repair abnormality) (61). In this review, the spectrum of clinical features varied from mild disease with only hair involvement to severe disease with profound developmental defects, recurrent infections and a high mortality at a young age. The median age of these patients was 6 years (ranging from 12 weeks to 47 years of age). DNA repair abnormalities or gene defects were reported in 41 of these patients; 32 patients were reported as having mutations in XPD, two in XPB and two in TTDA. Five showed cellular UV hypersensitivity, but no specific gene defect determined. In addition, 6 patients had a mutation in the newly discovered *TTDN1* gene. The majority of patients exhibited hair, skin and nail abnormalities: in addition to brittle hair or hair shaft abnormalities (96%), tiger tail banding (73%), and decreased sulfur or cysteine (71%), sparse hair (48%) and alopecia (39%) were described. 79% of patients had skin abnormalities; most frequently ichthyosis (65%) and photosensitivity (42%). Noteworthy, 37% of the patients with ichthyosis presented with a collodion membrane at birth. The nail abnormalities (63%) included onychodystrophy (37%), brittle nails (14%), hypoplasia (13%), and koilonychias, ie. spoonshaped nails (12%). 86% of patients presented with developmental delay or intellectual impairment. A notably sociable or outgoing behaviour, which is also a feature in Cockayne syndrome, was observed in 17% of patients. Further neurological abnormalities included microcephaly (50%), abnormal gait/ataxia (26%), sensorineural hearing loss (5 out of 25 patients who underwent audiologic examination), increased deep tendon reflexes (13%), spasticity (10%), and tremor (7%). In 23% of patients neuroimaging abnormalities were described: dysmyelination (14%), cerebellar atrophy (4%), and dilated ventricles (4%), which are similar to features found in CS. Growth abnormalities (81%) including short stature (73%) as well as facial dysmorphism (66%) were reported. In addition to microcephaly, large or protruding ears (30%), micrognathia (29%), and an aged (9%) or "bird-like" appearance (8%) were recorded. Ocular abnormalities were reported in 51% of patients; most frequently cataracts (29%) of which 8/32 congenital cataracts, nystagmus (14%), and strabismus (10%). Infections were commonly (46%) reported and 65% of the 20 reported deaths were related to infections. The high mortality rate, which might show some selection bias, highlights the potential severity of TTD in the neonatal and early childhood period. In less than half of the patients a radiological examination was performed. In total 38% patients showed radiographic bone abnormalities including (axial) osteosclerosis (14%), delayed bone age (13%), (distal) osteopenia (9%), and kyphosis 6%. In addition, 19% showed dental abnormalities, most frequently caries (19%).

Haematologic abnormalities as anaemia and neutropenia, sexual/reproductive abnormalities like hypogonadism, cryptorchidism or delayed pubertal development, and cardiac defects including cardiomyopathy, pulmonic stenosis and ventricular septal defect were reported in respectively 21%, 14% and 7% of patients. Several of these features are shared with CS and categorize TTD as a premature aging syndrome.

TTD results from phenotype-specific mutations in *XPB*, *XPD*, *TTDA*, which codes for TFIIH subunit p8, or the recently discovered *TTDN1* gene (64-67). Notably, most patients have a defect in *XPD*. Several years ago, some patients with a combined form of XP/TTD have been described (68). So far, only mutations in *XPD* have been shown to cause XP/TTD. Interestingly, *XPD* mutations can thus cause several different diseases: XP, XP with additional neurological features, COFS, TTD and the combinations XP/TTD and XP/CS. The photosensitivity is due to a NER defect, but several other symptoms cannot be explained by a repair defect alone. The first clue in understanding the paradox of one gene causing these very different clinical phenotypes came from the discovery that *XPB* and *XPD* are part of a transcription factor, TFIIH that is required for transcription initiation (69,70). The role of TFIIH in repair and transcription is discussed further in the next paragraph. Impaired transcription (depressed RNA synthesis due to DNA damage) may account for some clinical features, such as growth retardation, neurological abnormalities, skin abnormalities, and brittle hair and nails.

1.3.5 TFIIH

Already in 1993 it was known that *XP-B*, *XP-D* and *XP-G* can cause XP, XP/CS as well as PIBIDS (71). How features as neurodysmyelination, retarded development and brittle hair could originate from a repair defect was however not yet understood (71). This was especially difficult to understand since some of these features are not observed in completely NER deficient XPA patients (71). The first clue came by the discovery from the group of Egly in collaboration with the genetics department of the Erasmus MC that *XPB* was part of the transcription factor TFIIH (70). Thus, the CS features neurodysmyelination and retarded development and the brittle hair in TTD could be due to a subtle transcription defect (71). One year later, it was discovered that *XPD* was part of the TFIIH complex as well (69). Both *XPB* and *XPD* are DNA helicases unwinding DNA in the 3'-5' and 5'-3' direction respectively (69,72).

The TFIIH complex opens DNA around the lesion as well as around the promoter site in DNA repair and initiation of basal transcription respectively (19,73-77). The role of *XPD* in these two processes is however quite different. Whereas DNA repair is dependent on the helicase activity of *XPD*, transcription initiation just requires the structural presence of *XPD* for stability of the complex (53,78-80). The helicase activity of *XPD* unwinds DNA in the 5'-3' direction (69,72), but the fairly low activity is stimulated by the interaction with p44 (81). In contrast, the *XPB* helicase activity is required for transcription initiation (35,53). As a consequence many mutations in *XPD* result in severe repair defects while they have little effects on transcription and thus viability (53). Indeed many different viable mutations have been detected in the

XPD gene whereas only few mutations in *XPB* are tolerated (82-87). Still, genotype-phenotype relationships have turned out to be exceedingly complicated, partly because most patients are compound heterozygotes. Dubaele and co-workers studied *XPD* mutations causing XP or TTD and found that additional effects on the stability of TFIIH can explain the different degree of severity of the clinical features in TTD patients (88). This difference in stability of TFIIH may also account for the difference in cancer risk between XP and TTD patients (89).

It is now known that TFIIH consist of 10 subunits of which the *XPB* helicase, p62, p52, p44, p34 and p8 form a tight 'core' complex (67). The *XPD* helicase interacts with p44 and thus serves as a bridge between the core and the ternary cyclin-activating-kinase (CAK) complex, consisting of CDK7, MAT1 and cyclinH (67,90-92). In addition, it was found that TFIIH also has a mechanical role in transcription regulation, ie. it functions as a kinase that phosphorylates nuclear hormone receptors (92,93).

In summary, TFIIH is involved in RNA-pol I transcription, RNA-pol II driven (basal) transcription initiation, transcription regulation, global genome NER, transcription-coupled NER and perhaps general transcription-coupled repair as well. In addition some forms may have implications in cell-cycle regulation (70,94-99).

1.3.5.1 *TFIIH* in TTD

In the case of TTD, disease-causing mutations are all found in components of the dual functioning TFIIH complex. Consequently, a link between defective basal transcription and the clinical onset of these TTD features has been made (62,71,88,100-103). For example, in the hair shafts that show transverse fractures, a 'tiger-tail' pattern, and severely damaged or absent cuticle, a strong reduction in the class of ultra-high sulphur-rich matrix proteins is observed. These proteins are composed of up to 30% of cysteine residues that are involved in disulfide cross-links (43). In addition, the cutaneous symptoms, such as acanthosis and hyperkeratosis, have been proposed to be associated with reduced transcription of the skin-specific, differentiation-related gene *SPRR2*, a member of the small proline-rich protein (*SPRR*) family expressed in the dermis (60). *SPRR2* encodes a structural component of the cornified envelope and is expressed in the final stage of terminal differentiation (60). Lehmann and co-workers also found that almost all TTD patients with an *XPD* mutation have elevated levels of haemoglobin A2 and reduced levels of β -globin in erythrocytes without a defect in a haemoglobin gene (53,104). It has been proposed that low TFIIH levels and/or the defect in TFIIH become apparent in terminally differentiated, enucleated cells, like keratinocytes and erythrocytes, which need to produce abundant protein.

Recently, it was shown that TFIIH can function as a co-activator for thyroid hormone-dependent gene regulation, and it was speculated that the loss of this co-activator function of TFIIH is responsible for some of the major neurological abnormalities observed in TTD patients (105).

1.3.5.2 The 3D-structure of the XPD protein

Studies of the crystal structure of the XPD protein have recently given some insight in the genotype-phenotype correlation of XPD mutations which could not be understood solely by their position along the gene as adjacent mutations can cause different diseases (106). The XPD protein is folded into four differently active domains, two helicase domains (HD1 and HD2), the 4FeS domain involved in DNA- and ATP-binding and the Arch domain, named by its arch-shaped conformation (106). XP mutations are located along the ATP-binding edge of HD1 and the DNA-binding channel of HD1 and impair helicase activity essential for NER (106). XP/CS mutations not only impair helicase activity, but also have an effect on the functional flexibility of the HD1 and HD2 domains which likely affects protein-protein interactions within the TFIIH complex as well as with other critical protein partners including XPG (106). TTD mutations may effect helicase activity, but map to sites in all four domains expected to cause framework defects impacting TFIIH integrity (106). These mutations are thought to result in destabilization of the interaction with p44 or the XPD structure itself and therefore TFIIH (107).

1.4.1 TTD mouse model

Mice carrying an XPD point mutation (Arg⁷²²→Trp (R⁷²²W)), which is found in patients, were generated in our laboratory (102). These TTD mice reflect the human disorder to a remarkable extent and display partial defects in transcription and repair (102,108). In addition, it was observed that TTD mice develop premature aging features (Table 1) (100). This initial observation of premature aging features was made in TTD mice in a mixed (C57Bl/6/FVB) background.

Firstly, it was noticed that TTD mice acquire an 'aged' appearance. Whereas TTD mice develop normally, they show cachexia and kyphosis at 16 months of age. In addition, the average life span ranged from less than 12 months to 1,5 year compared to more than 2 years for wild type littermates. Closer examination revealed patchy depigmentation of the skin which was observed earlier and more frequently than in wild type littermates. The skin also showed hyperplasia of sebaceous glands as is observed in human aging. TTD females appeared to lose fertility early and indeed 16 months old TTD mice displayed ovarian dysfunction ranging

Table 1: Premature aging features in TTD patients and mice.

mice	patients
reduced life span	reduced life span
cachexia	cachexia
reduced fertility (in females)	early arrest of sexual development
aged-like appearance, cutaneous symptoms	aged-like appearance
neurological problems	neurological problems
skeletal abnormalities	skeletal abnormalities

from complete anovulation to sporadic, seemingly normal, ovulation. At 6 months of age, TTD mice showed mild normochrome anemia and an enlarged spleen. In addition, significantly reduced levels of the branched-chain amino acids (valine, leucine, and isoleucine) indicative of starvation were found. However, the starvation was not caused by aberrant food uptake or malabsorption.

After this first report, Wijnhoven and co-workers documented the overall phenotype of TTD mice in a pure C57Bl/6 background (109) and divided the observed pathology in three groups: (1) pathology consistent with accelerated aging, (2) trichothiodystrophy-specific pathology and (3) pathology consistent with dietary restriction. The first group includes osteoporosis of the femur, kyphosis, abnormalities in liver, kidney and lymphoid tissue, aortic sarcopenia and reduced hypodermal fat. For example, the increased levels of lipofuscin pigmentation in TTD livers can be related to oxidative damage. The second group harbours anorectal prolapse, which in addition to a general conditional decline is a common cause of death in TTD mice. Furthermore, typical skin lesions as acanthosis, hyperkeratosis and sebaceous hyperplasia are present in this group. Notably, the pathology in the last group that among others includes reduced hypodermal fat, is not caused by a difference in food uptake between TTD and C57Bl/6 control mice. This dietary restriction pathology is in concordance with the observed reduced body weight in TTD mice. It was hypothesized that transcription problems in TTD mice could lead to a metabolic state with inefficient energy uptake. The decrease in metabolic side products as ROS could be favourable for DNA-repair deficient TTD mice.

1.4.2 Mouse models showing premature aging

In many progeroid disorders the underlying defect is a disturbance in DNA metabolism or genome maintenance. Mouse models are powerful tools in the analysis of the effect of defective genome maintenance on aging. Today, several mouse models with defective genome maintenance that also display symptoms of accelerated aging are available (reviewed by (10)). TTD mice with a defect in both global genome repair and transcription-coupled repair as well as transcription-coupled repair-deficient CSB mice show several features of accelerated aging. In both TTD and CSB mice, the features of premature aging are severely enhanced by crossing them to XPA mutant mice that have a total NER defect but no overt features of premature aging. For example, TTD/XPA mice develop dramatically runted growth and extreme cachexia resulting in a severely shortened life span on average of only 22 days (100). In addition, they show disturbed gait and spinal kyphosis. This suggests that a complete NER defect, in combination with a defect in transcription-coupled repair that renders the transcription machinery very sensitive to lesions in transcribed genes, is responsible for the markedly accelerated aging of the double mutant mice (10).

In addition, Ku80 mice with a defect in NHEJ exhibit an early onset of aging characteristics as among others a shortened life span, cancer, reduced weight, osteopenia, and alopecia. In ERCC1 mice, with a defect in NER and inter-strand cross-link repair, liver and kidney abnor-

malities reminiscent of accelerated aging are present in addition to reduced life span, body weight and neuronal function (98).

In many progeroid disorders the underlying defect is a problem in DNA metabolism which strengthens the hypothesis that DNA damage is an important factor in the aging process.

1.5 Aging

Aging is commonly defined as progressive loss of function accompanied by decreasing fertility and increasing mortality with advancing age (110). Time-dependent accumulation of damage is generally accepted to be the cause of aging (1,10,110). Already in 1957, Harman postulated the 'free radical theory' of aging speculating that endogenous radicals were generated in cells and resulted in a pattern of cumulative damage (1). However, endogenously produced ROS do not only cause damage to lipids, proteins and most importantly DNA, but also function as intracellular signalling molecules (1). So ideally there should be a balance: reducing detrimental effects of ROS while keeping oxidative metabolism and the role of ROS as intracellular signalling molecules intact.

1.5.1 Genome maintenance

Humans have high metabolic rate, but keep ROS limited using defence mechanisms as ROS scavenging, damage removal, and repair (111). Indeed, DNA repair capacity of some repair systems has been reported to correlate with mammalian life span in several comparative studies (98). In addition, it has been claimed that MMR, BER, NER and DSB repair become less efficient with age leading to accumulation of mutations (112). As discussed above, inborn defects in proteins involved in DNA repair also give rise to symptoms that resemble segmental accelerated aging (10). As ROS are believed to result in at least 70 different types of DNA lesions (12) and the various DNA repair systems are highly specific, it is not surprising that defects in various DNA repair proteins occasionally result in segmental and not full reconstitution of aging.

Further evidence supporting that premature aging is caused by defects in genome maintenance comes from additional progeroid disorders as Werner syndrome, Bloom syndrome and Rothmund-Thomson syndrome. These syndromes are all triggered by mutations in Rec-Q like DNA helicases. Rec-Q like helicases are involved in DNA repair and replication and thereby safeguard genome stability. Mutations in the genes coding for these helicases lead to accelerated aging features including early alopecia (loss of hair), osteoporosis, malignancies, atherosclerosis, diabetes, cataracts, telangiectasia, skin atrophy and greying of hair (113). Ataxia telangiectasia (AT) is caused by Ataxia Telangiectasia mutated (ATM) protein, which is a DNA damage sensing signalling protein kinase. Symptoms of AT include skin atrophy/sclerosis, telangiectasia, immuno-deficiencies, malignancies (mainly lymphomas), greying of hair and neurodegeneration ((10) and references therein).

Mutations in the LMNA gene, which encodes for type A nuclear lamins are responsible for Hutchinson-Gilford progeria syndrome (HGPS) and atypical Werner syndrome. LMNA is a structural component of the nuclear envelope and is involved in regulating mitotic signaling pathways. Mutations in LMNA cause nuclear fragility, rendering the nucleus sensitive to mechanical stress, reduced mitotic stability, shortened telomere length and diminished DNA repair (114,115). HGPS is known as a progeria of childhood with features including atrophy of subcutaneous fat, alopecia, short stature, premature atherosclerosis and a panel of musculoskeletal abnormalities.

In conclusion, DNA maintenance is not only important in preventing cancer, but has a role in preventing premature aging as well.

2 Trichothiodystrophy and bone aging

The TTD mouse model resembles the phenotype of TTD patients remarkably well. In order to gain insight in the premature aging phenotype, we focus on one tissue, the bone. In both TTD patients and mice skeletal abnormalities as osteoporosis have been described.

2.1 Skeletal abnormalities in trichothiodystrophy patients

TTD patients exhibit photosensitivity, ichthyosis (scaly skin), brittle hair and nails, impaired intelligence, decreased fertility, and short stature (60,116). In addition to these features, skeletal abnormalities, like a bird-like face, thoracic kyphosis, axial osteosclerosis, and peripheral osteoporosis, have been described. In 1979 Leupold described a 13-year-old girl with axial osteosclerosis and peripheral osteopenia who was later thought to have suffered from TTD (117). In 1980 Price et al. introduced the term trichothiodystrophy in an article where they report a male patient who at the age of 7 years showed axial and cranial osteosclerosis and demineralisation in the distal bones on roentgenographic examination (63). Chapman reported another patient, a 5-year old boy who showed osteosclerosis in the axial skeleton and proximal limbs while the bone density was decreased further down in the limbs and the distal parts were osteopenic (118). In 1989, Civitelli et al. describe a 9-year-old boy with marked axial osteosclerosis and peripheral osteopenia (119). Besides low serum osteocalcin, no abnormalities in mineral homeostasis were noted. Histological analysis of the iliac crest specimen showed marked increase in trabecular bone whereas the femoral neck specimen showed decrease in cortical thickness and increased porosity (119). McCuaig et al. report three patients with striking osteosclerosis of the vertebral column and skull and additionally mentions two previously reported patients with osteopenia and osteosclerosis (59,120,121). Toelle et al. reported on two sisters with TTD and severe cardiac and neurological involvement who also have kyphosis, sclerosis and osteopenia (122). A few years ago, Wakeling et al. reported a boy with normal bone density at 3 months of age, increased bone density at 5

years of age, and marked increase in density of the spine, ribs, scapulae, clavicles, skull, facial bones and proximal humeri at 7 years of age (123). At that time, he also had a mild kyphosis. In her review, Wakeling suggests that central osteosclerosis and peripheral osteoporosis are distinctive features of TTD that may easily remain undetected (123).

2.2 Premature bone changes in TTD mice

TTD mice reflect the human disorder to a remarkable extent displaying partial defects in transcription and repair as well as premature aging features. The TTD mouse model showed no skeletal abnormalities around 3 months of age, whereas at 14 months radiographs revealed prominent kyphosis and generalized reduction in radio-density of the skeleton (100). The TTD skull, however, showed higher radio-density. The kyphosis was thought to be a result of the osteoporosis (100). However, as commented by Gerhard and Kasales, osteoporosis is not the only factor that can underlie kyphosis (124). Next to deformity of the vertebral bodies caused by osteoporosis, growth plate abnormalities, osteosclerosis, annulus degeneration, and muscular dystrophy or degeneration can lead to kyphosis (124). Indeed, the initial roentgenographic analysis of the TTD skeleton as described by de Boer et al. (100) should be followed up by a more detailed analysis of the bone phenotype as described in this thesis.

3 Bone metabolism

3.1 The constituents of bone

For better comprehension of bone loss with aging, the structure of bone, bone forming and bone resorbing cells, the extracellular matrix (paragraph 3.1) as well as the remodelling process and factors that influence bone metabolism will be discussed separately (paragraph 3.2).

3.1.1 Cortical and trabecular bone

The skeleton contains two types of bone: cortical bone and trabecular bone. Long bones, as femurs and tibiae have more cortical bone, which is calcified to a much larger extent than trabecular bone, rendering optimal structure and strength for their mechanical and protective function. In contrast, vertebrae and flat bones as the skull and pelvis mainly consist of trabecular bone. Trabecular bone has a metabolic function: storage of essential minerals, including calcium thus aiding optimal calcium homeostasis (see paragraph 3.2.3 on calcium homeostasis).

In addition, the loss of bone occurs in different ways in trabecular and cortical bone. The cortical bone volume is regulated by periosteal bone formation, remodelling within the cortex (leading to increased porosity) and endosteal bone resorption whereas loss of trabecular bone is caused by complete perforation and fragmentation of trabeculae when bone resorption outpaces bone formation.

3.1.2 Osteoblasts

The bone forming osteoblasts are derived from mesenchymal stem cells that can also differentiate into chondrocytes, adipocytes, myoblasts, and fibroblasts (125,126). In the case of the bone forming cells, mesenchymal stem cells differentiate into osteoprogenitor cells and later further into osteoblasts (see Figure 4). The osteoprogenitor cells contribute to maintenance of the osteoblast population. Osteoblasts produce the components of the extracellular matrix, such as collagen (125-128). The newly produced, non-calcified bone matrix is called osteoid. Osteoblasts are also able to induce mineralization of the bone matrix. This calcification occurs at a later stage, which is about 10 days after deposition of osteoid in humans. Two types of osteoblasts reside on the bone surface: active cuboidal osteoblasts and inactive, i.e. not active bone matrix producing osteoblasts, flat lining cells. Active osteoblasts are found in clusters of 100-400 cells per bone-forming site. When the process of bone formation has taken place, osteoblasts can either go into apoptosis, become osteocytes or lining cells. Within the calcified bone matrix thousands of osteocytes are embedded. Osteocytes are terminally differentiated osteoblasts that got trapped in the bone matrix they produced (129). They have long processes that are in contact with other osteocytes, osteoblasts, lining cells at the bone surface and the blood supply. These processes are created before and during matrix synthesis and form a network that permeates the entire bone matrix through thin channels called canaliculi. The primary function of this network is considered to be mechanosensory, by transducing and translating mechanical signals into biological signals and activity and to regulate osteoblast and osteoclast activity (130). Osteocytes can produce various bioactive peptides of which the recently identified, sclerostin, is a very important one. The *SOST* gene, encoding sclerostin, was found by linkage analysis of families with sclerosteosis and

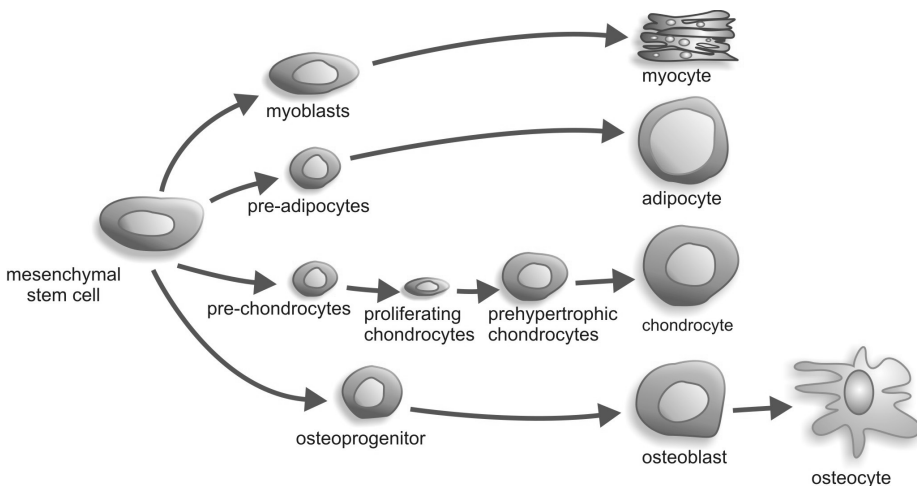


Figure 4: Different lineages derived from the mesenchymal stem cell.

van Buchem disease, two closely related bone disorders characterized by progressive bone thickening due to increased bone formation (131,132). Sclerosteosis is associated with mutations in the *SOST* gene whereas in van Buchem disease a 52 kb deletion downstream of the *SOST* gene, which probably affects transcription of the gene, is found (131). Sclerostin inhibits osteoblast proliferation, differentiation and mineralization (133). Sclerostin expression is reduced by mechanical loading thereby providing a mechanism by which bone formation is increased after mechanical loading (133). Osteocytes can reside in healthy bone for long periods of time. They have an average half-life of 25 years (129). In aging bone, however, empty or mineralized lacunae have been observed as well as an increase in the percentage of dead osteocytes (134-136). To date it is known that osteocytes can go into apoptosis upon aging and that this eventually is followed by resorption of the matrix (129,137). It was shown that osteocyte death is induced by fatigue loading and microcracks and that this coincides with osteoclastic bone resorption (138). In addition, a correlation between osteocyte apoptosis and the withdrawal of oestrogen was found (139). In contrast, no correlation between the percentage of empty lacunae and age was found in trabecular bone of the iliac crest (140). It has been suggested that this difference can be explained by different sites. Indeed, one group found a decrease in viable osteocytes in femur heads of older patients whereas they found no difference in viability in the second lumbar vertebra (136).

3.1.3 Osteoclasts

Osteoclasts are the cells responsible for bone resorption. The process of resorption consists of osteoclast formation and activation, polarization, formation of a ruffled border, resorption by secretion of proteolytic enzymes and hydrogen ions, and ultimately apoptosis, which terminates the activity of osteoclasts and thus resorption (125) (see Figure 5). This process of apoptosis is favoured by estrogens. When estrogen levels decline after menopause or gonad-

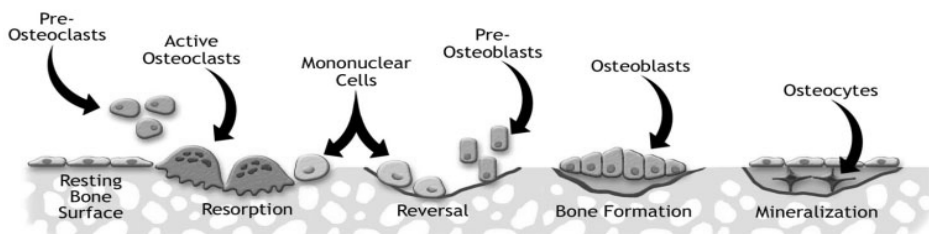


Figure 5: Bone remodelling phases.

During bone remodeling resting bone lining cells secrete RANKL which activates mononuclear cells of the haematopoietic lineage to fuse on the activated bone surface and form differentiated active osteoclasts. Subsequently, osteoclasts resorb bone after which formation is coupled to resorption by the appearance of pre-osteoblasts in the resorption cavity. A cement line is formed which marks the limit of resorption and acts as attachment or glue between the old and new bone. Finally, in the formation phase osteoblasts fill the resorption cavity with new bone. Initially this is osteoid, unmineralized bone matrix, which then becomes mineralized.

ectomy, osteoclast apoptosis decreases and consequently bone resorption increases (125). Osteoclasts are large multinucleated cells originating from the mononuclear/phagocytic differentiation lineage of haematopoietic stem cells (141,142). Two molecules, that are secreted by osteoblasts, are essential to promote osteoclastogenesis: macrophage-stimulating factor (M-CSF) and receptor activator of nuclear factor (NF)- κ B (RANK) ligand (RANKL), while osteoblasts also secrete an inhibitor, osteoprotegerin (OPG) which acts as a decoy receptor for RANKL (128,141,142). These proteins together with RANK, the receptor of RANKL on the osteoclast, are the major regulators of osteoclastogenesis, as well as bone resorption and skeletal remodelling (141,142). The importance of RANKL and OPG emphasizes the central role of osteoblasts in this process as these cells express RANKL and OPG and are the actual targets of osteoclastogenic agents (127,141,143). The osteoclastogenic agents enhance RANKL expression and increase the quantity of this molecule relative to that of OPG (141,143). It is the balance between the expression of the stimulator RANKL and of the inhibitor OPG that dictates the quantity of bone resorbed (141,143).

3.1.4 *The extracellular matrix*

About 90% of the total protein in the extracellular matrix consists of collagen type I fibres. Collagen type I fibres are triple-helix molecules that contain two identical chains (α 1) and one different chain (α 2). These α -chains are characterized by repeating Gly-X-Y triplets, where X is usually proline and Y is often hydroxyproline. Several post-translational modifications which are important for both the structural and mechanical properties of the matrix, occur: (1) hydroxylation of certain (hydroxyl-)lysyl residues with glucose and/or galactose residues and (2) formation of distinct intra- and intermolecular covalent cross-links (144). The importance of these post-translational modifications is illustrated by for example Ehlers-Danlos syndrome type V. In this syndrome the level of hydroxylation is reduced to 17% of normal in bone due to a deficiency in the enzyme lysyl hydroxylase and this results in connective tissue dysfunctions such as kyphoscoliosis, osteoporosis and ruptures of eyes and arteries (144). The level of collagen cross-links measured in serum or urine is a reliable marker of bone resorption (145). With aging, the collagen can become denatured and/or accumulate cross-links. Denaturation of collagen can result in reduced toughness while alteration of the cross-link profile affects the stiffness (146,147).

The remaining 10% of the total protein consists of non-collagenous proteins as albumin, osteocalcin and numerous growth factors like bone morphogenetic proteins (BMPs), transforming growth factor- β (TGF β), and insulin-like growth factor-I (IGF-I) (125,148). They seem to play a role in initiation as well as the control of mineralization. For example, the majority of the newly produced osteocalcin is incorporated into the bone matrix, where it binds to hydroxy-apatite during matrix mineralization (149). The remainder of the osteocalcin is released into the circulation where it can be measured as a sensitive marker of bone formation (150). The growth factors stored in the bone matrix can be released during bone resorption and

may play a role in the control of bone formation following the resorption (148,151). A large amount of bone consists of mineral although this percentage can vary with age, anatomic location, diet, and health status. For example, bone mineral content is positively correlated to age whereas it is negatively correlated to the rate of remodelling (152). The mineral provides mechanical rigidity and load bearing strength to the bone. In contrast, the extracellular matrix provides elasticity and flexibility to the bone and determines the structure of the bone. Together they provide the bone with optimal strength and flexibility.

3.2 Bone remodelling

Bone remodelling is a turnover mechanism by which old bone is replaced by new bone in order to maintain optimal bone quality. Bone remodelling occurs in local groups of osteoclasts and osteoblasts called bone multicellular units (BMU) (153). The bone-remodelling process includes five stages: (1) activation of bone multicellular units, (2) bone resorption, (3) 'coupling' or reversal, (4) bone formation and mineralization of the newly formed bone matrix, and (5) the resting stage (154). Frost was the first to describe this activation-resorption-formation sequence of bone remodelling. During activation, resting bone lining cells change from their normal flat shape to a cuboidal shape and then secrete RANKL. Activated by RANKL, mononuclear cells of the haematopoietic lineage fuse on the activated bone surface and form differentiated active osteoclasts. Subsequently, osteoclasts resorb bone after which formation is coupled to resorption by the appearance of pre-osteoblasts in the resorption cavity. A cement line is formed which marks the limit of resorption and acts as attachment or glue between the old and new bone. Finally, in the formation phase osteoblasts fill the resorption cavity with new bone. Initially this is osteoid, unmineralized bone matrix, which then becomes mineralized. Bone formation and bone resorption are coupled: when one goes up or down, the other one follows. However, bone resorption is much faster than bone formation: it takes at least 3 months to rebuild bone that is resorbed in 2-3 weeks (126,128). Thus, increased resorption can cause bone loss even when it is accompanied by increased bone formation, e.g. in estrogen deficiency or hyperparathyroidism (126).

Many factors have effects on bone formation, resorption or the coupling between the two. Among these factors are the previously mentioned growth factors stored in the bone matrix. Growth factors play an important role in the bone microenvironment, acting on the bone cells directly or influencing other factors. As discussed, the RANK signalling pathway controls osteoclastogenesis and bone resorption. The influence of sex steroids, serum calcium homeostasis, leptin, the GH-IGF-I axis and mechanical action on bone remodelling are discussed below.

3.2.1 Sex steroids

Sex steroids play an important role in skeletal homeostasis. However, the mechanism of action of sex steroids on bone is still not entirely clear (155). The actions of estrogen, together

with biomechanical strain, are major physiological mechanisms of bone mass conservation (156). Most importantly, estrogen inhibits bone resorption by inhibiting osteoclastogenesis and osteoclast function and favouring osteoclast apoptosis (125,126). Recently, it was found that estrogen also decreases osteoblast apoptosis (156). In addition, estrogen promotes the development of osteoblasts from the osteoblast-adipocyte-precursor, and increases the production of a number of osteoblast proteins as e.g. IGF-1 in mice (157-159). A decrease in estrogen due to menopause or ovariectomy (OVX) results in increased bone loss and adipocyte formation (160). Estrogens are synthesized in the ovaries as well as in many other tissues including adipose tissue, bone and brain, where androgens are converted to estrogens by aromatase (161,162). This extra-ovarian estrogen synthesis is of great importance in slowing down the rate of postmenopausal bone loss (161). During growth, estrogen is responsible for initiation of the pubertal growth spurt and closure of the growth plate (163).

Testosterone affects bone in several ways. It can be converted into estradiol by aromatase to inhibit bone resorption, but it also seems to inhibit bone resorption directly in males, and to stimulate bone formation in males and females (126). Like estrogen, testosterone increases the lifespan of osteoblasts and decreases that of osteoclasts by affecting apoptosis (164). On the other hand, there is an important difference between testosterone and estrogen that accounts for the larger skeleton that males obtain in puberty; control of bone formation on the outside of the bone, i.e. periosteal apposition.

3.2.2 Periosteal apposition

The size of a bone is of particular importance to bone strength as the resistance of bone to bending or torsional forces is exponentially related to its diameter (165). In other words, a small addition to the circumference of a bone adds considerably to its fracture resistance. Gradual periosteal apposition occurs during childhood and accelerates at puberty in parallel with accelerated growth in bone length (166). The precise mechanism regulating periosteal apposition is unclear. Growth factors, like insulin-like growth factor-I (IGF-I; see below), affect periosteal apposition (167). Sex steroids are likely to be important regulators with androgens having a positive effect while estrogens are believed to have a negative effect on periosteal apposition (156,168,169). Indeed periosteal apposition increases in women after menopause and following subsequent bone loss. However, recent studies have shown that estrogens may stimulate periosteal apposition as well (169,170). It was suggested that a low dose of estrogen (as in males and young girls) promotes periosteal apposition whereas higher concentrations of estrogen (as in females in late puberty and adulthood) inhibit periosteal growth. In addition, the degree of periosteal apposition is likely to be site specific as increases in bone area at central sites were equal in men and women whereas men showed a larger increase in periosteal apposition at peripheral sites (171).

Furthermore, mechanical loading is supposed to be an important modulator of periosteal apposition (172). With aging, increased bending stress on the outer surface of bone due

to endosteal bone loss and subsequent cortical thinning, is thought to lead to stimulation of periosteal bone apposition (173). Noteworthy, there has been an observation on bone resorption on the periosteal surface so that bone size could decrease with aging (165). However, this observation requires further investigation. An interesting link between estradiol and mechanical loading is the observation that the estrogen receptor α is required for the osteogenic response to mechanical loading whereas the role of estrogen receptor β has not been clarified as experiments show apparently contradictory results (174).

3.2.3 Calcium homeostasis

Parathyroid hormone (PTH), 1,25-dihydroxyvitamin D₃ (1,25(OH)₂D) and calcitonin, an inhibitor of osteoclastic bone resorption, regulate serum calcium homeostasis via effects on the intestine, kidney and bone (126,141,175,176). PTH up-regulates RANKL expression and decreases OPG expression (128,142) resulting in an increase in osteoclast differentiation and bone resorption increasing serum calcium. Surprisingly, intermittent PTH treatment favours bone formation instead of increasing bone resorption and has proven to be an effective therapy in osteoporosis, although the mechanism remains poorly understood. However, inhibition of resorption, by e.g. bisphosphonates, has been noted to attenuate or abolish the anabolic effect of PTH. This points to a role for the osteoclast in osteoblast activation (177). Vitamin D is synthesized in the skin or taken up from the diet. After C-25 hydroxylation in the liver, the biologically most active metabolite 1,25(OH)₂D is synthesized in the kidney by 25-hydroxy-vitaminD-1 α -hydroxylase (1 α (OH)ase) (178). PTH and hypocalcemia are potent activators of this enzyme whereas 1,25(OH)₂D itself and hypercalcemia are potent inhibitors of enzyme activity (178). 1,25(OH)₂D is the most potent stimulator of intestinal calcium absorption and renal reabsorption of calcium to increase serum calcium levels (176). In addition, it has been suggested that PTH has a direct effect on the intestine with regard to calcium absorption (179). The resulting increase in serum calcium levels stimulates bone mineralization (176). In addition to calcium, extracellular phosphate is necessary for matrix mineralization. The PTH/ 1,25(OH)₂D axis regulates phosphate homeostasis as well. PTH inhibits phosphate reabsorption in the kidney whereas 1,25(OH)₂D increases phosphate absorption in the small intestines (180).

3.2.4 Central control of bone formation

Recently, much interest has gone out to leptin and its effect on bone formation. Leptin is an endocrine factor synthesized mainly by adipocytes, and acts primarily in the hypothalamus, where the long form of the leptin receptor is expressed, to regulate body weight and fat mass through appetite suppression and increased energy expenditure (126,127,181,182). In ad libitum fed animals, leptin levels are positively correlated to body fat and adipocyte size (181). In addition to the effects on body weight and fat mass, leptin has an inhibitory effect on bone formation (127). For example, leptin deficient ob/ob mice are very obese, and have

high bone mass in spite of low levels of sex steroids and high corticosteroid concentrations (126,127,183). High bone mass with increased bone formation is also observed in leptin receptor-deficient mice as well as in leptin-deficient lean lipodystrophic mice which argues for a role of leptin signalling *per se*, rather than obesity, in the bone phenotype (126). Ob/ob mice and leptin receptor deficient mice are the only known animal models with both hypogonadism and high bone mass (127). Unlike in mice, leptin deficiency cannot override bone loss due to estrogen deficiency in humans as illustrated by bone loss observed in anorexia nervosa patients or amenorrhoeic female athletes with both low levels of leptin and estrogens (126).

When injected in the cerebral ventricles, leptin suppresses bone formation and reduces bone mass (126). In contrast, systemic administration of leptin reduces bone fragility (184). The latter effect could contribute to the high bone mass and low fracture rates observed in obese people (184).

3.2.5 The GH/IGF axis

The GH/IGF-I axis has an important role in the development and growth of the skeleton as well as in the maintenance of bone mass and bone density (185). For example, adults with GH deficiency display osteopenia, increased fat mass and decreased lean body mass (186). Growth hormone (GH) secretion by the pituitary is stimulated by growth hormone releasing hormone (GHRH) and inhibited by somatotropin release-inhibiting factor (SRIF or somatostatin) from the hypothalamus. The effect of GHRH on GH secretion is potentiated by estrogen as well as glucocorticoids. GH can act directly on target tissues, but most prominently indirectly on several tissues via stimulation of IGF-I synthesis and secretion. In the liver, which is the main source of IGF-I, IGF-I synthesis is also regulated by insulin (187). Both GH and IGF-I act on target organs as bone and muscle. They stimulate development, growth, tissue regeneration and the metabolism of carbohydrates and lipids.

In bone IGF-I secretion is stimulated by GH, estrogens, PTH, 1,25(OH)₂D and calcitonin (187). In addition, stored IGF-I is released from the bone matrix during bone resorption. Together with several other growth factors IGF-I stimulates the remodelling process in bone (187). IGF-I stimulates collagen synthesis, bone formation (especially periosteal apposition) as well as mineralization and inhibits collagen degradation (185,187). Reduced levels of autocrine or paracrine IGF-I are thought to play a role in the decline in remodelling and the pathogenesis of osteoporosis at old age (187).

3.2.6 Micro-damage in bone

Low habitual strains maintain bone mass whereas increased strain stimulates bone formation and decreased strain is associated with bone loss (188). Over-loading of bone causes micro-damage in the bone matrix that is observed as micro-cracks, diffuse damage or micro-fractures (152,189). For example, significant levels of microdamage can be found in

the ribs of rowers (190) and the long bones of race horses (191). The effect of strain caused by physical activity on the bone could be due to repair of micro-damage (192). Furthermore, it is known that exercise can reduce bone resorption (192). The amount of micro-damage in both cortical and trabecular bone increases dramatically with increasing age (152,189). This accumulation of micro-damage is due to reduced remodelling and repair and thereby contributes to a decrease in strength of bones with increased fracture risk (189,193). It has been shown that induction of damage in bone is associated with an increase in osteocyte death by apoptosis (137). Furthermore, a decrease in estrogen levels is accompanied by an increase in osteocyte apoptosis (139). Osteocyte apoptosis at the site of microdamage is likely to play a role in the targeting of repair although the specific signals have not yet been identified (137). One model suggests that actually all cortical bone remodelling is initiated by and in close proximity to micro-cracks (194). However, especially early in life, remodelling takes place while no microdamage is present. In contrast, others did not find micro-cracks in physiologically loaded bones and suggested that most of the previously observed cracks were due to preparation artefacts (134). Not surprisingly, micro-cracks are still a topic of much debate. In general, it is believed that evolvment of damage is prevented by repair of micro-cracks by resorption and by bone deposition in areas under high strain (195) and it can be envisaged that impaired repair of microcracks (with aging) can lead to reduced bone strength.

3.3 Age-related bone loss

Age-related bone loss in the human population is an area of broad interest due to the personal consequences of fractures for quality of life, the high morbidity as well as the budgetary implications for our health care system. The more so considering the aging of the population that will cause an increase in age-related diseases of which osteoporosis is a prominent example. Humans reach a peak bone mass at 23-35 years, after which bone is lost at a rate of about 0.4% per year due to incomplete filling of resorption holes. Women undergo two major phases of bone loss: a first phase of accelerated bone loss that begins at menopause and a second phase of slow, continuous bone loss. The first phase accounts for 20-30% of trabecular bone loss, but for only 5-10% of cortical bone loss (see Figure 6) (156). Trabecular bone loss is associated with increased bone resorption; both the number of remodelling units as the duration of the resorption phase are increased (156). The increase in resorption depth leads to trabecular plate perforation and loss of trabecular connectivity (156). This occurs at different rates at different skeletal sites. In cortical bone an increase in cortical porosity is observed. In the second phase, a slow decline in bone mass leads to overall losses of about 20-25% in both cortical and trabecular bone (156). Men lack the early, accelerated phase of bone loss, but have a similar slow phase of bone loss (156).

During aging, periosteal apposition i.e. bone formation on the outside of the bone (periost, see Figure 6), continues in both men and women, and this process partially preserves bone strength as the resistance of bone to bending or torsional forces is exponentially related to its

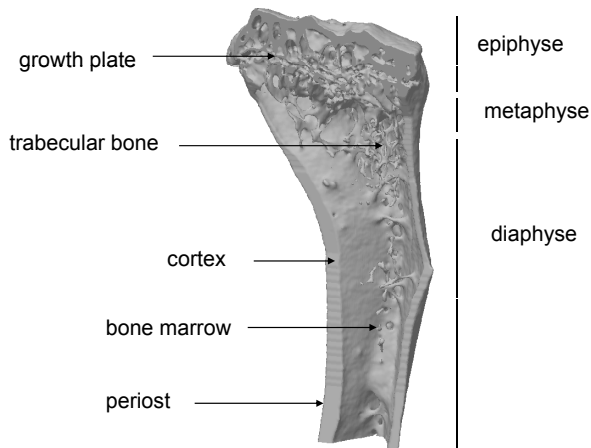


Figure 6: Tibia showing different areas of the long bone.

diameter (156,165,196). Men have more prominent periosteal apposition (197). Nevertheless both men and women are subject to age-related bone loss, increase in bone fragility, and susceptibility to fracture.

The introduction of high resolution quantitative computed tomography (QCT) made it possible to assess age-related changes in more detail (198-201). Riggs et al. used this technique to study age-related changes in volumetric bone mineral density (vBMD), geometry, and bone microstructure in the spine, femur neck, distal radius, and distal tibia in a large population of men (n=323) and women (n=373) aged 20 to 97 yr (171). They observed large decreases in vBMD at all these sites with aging. The decreases in trabecular vBMD were somewhat smaller in men (approximately 46%) compared to women (approximately 55%) at central sites, but were similar (24% and 26%) at peripheral sites. A small midlife acceleration in the slope of the decrease in women accounted for much of the significantly greater decrease in trabecular vBMD at the spine. In contrast, the cortical vBMD at the radius, the distal tibia and femur neck showed little change until midlife in either men or women. Thereafter, cortical vBMD decreased in both sexes, but the decreases were greater in women (25%) than in men (18%) consistent with menopausal-induced increases in bone turnover and porosity. In addition, aging was associated with increases in bone cross-sectional area at various sites due to continued periosteal apposition throughout life. However, the cortical area and thickness decreased as endocortical resorption increased even more than periosteal apposition. The decrease in bone strength resulting from decreased cortical area was partially offset by the outward displacement of the cortex, which increases the strength of bone to bending stresses. The same group studied the microstructure of the forearm and found that men had 28% thicker trabeculae in young adulthood resulting in a 26% greater trabecular bone volume/total volume (BV/TV) (202). BV/TV decreased similarly in women (-27%) and in men (-26%) with aging (202). However, whereas women showed significant decrease in trabecular num-

ber and increase in trabecular spacing, men showed little net change in these parameters, but a greater decrease in trabecular thickness than women. These findings are very similar to earlier studies by Aaron et al. using cadaveric transiliac bone biopsies (203). This suggests that the pattern of changes in trabecular bone may be similar at multiple skeletal sites. In addition, these data suggest that whereas decreases with age in trabecular BV/TV are similar in men and women, the structural basis for the decrease in trabecular volume might be different between the sexes. It has been shown that decrease in trabecular number, leading to loss in connectivity, has a much greater impact on bone strength compared to decreases in trabecular thickness (204), which may help explain the higher risk of fractures in women. In a recent study part of these cross-sectional findings were confirmed by longitudinal data, which showed significant trabecular bone loss at the spine, distal radius, and distal tibia before midlife in men, whereas cortical vBMD remained relatively stable until age 65–70 yr, with loss of cortical bone thereafter (205). Thus, trabecular bone loss begins in young adult life in both sexes whereas cortical bone loss begins after midlife, with overall decreases in vBMD being smaller in men compared to women.

The cellular basis of age-related bone loss as well as osteoporosis is an imbalance in bone remodelling where bone resorption exceeds bone formation (141). With aging, the process of coupled bone formation is affected by the reduction of osteoblast differentiation, activity, and life span, which is due to a higher frequency of apoptosis (125). As the trabecular volume decreases, the adiposity in bone marrow increases and osteoblast development decreases (see paragraph on osteoblasts and sex steroids) (125). In perimenopausal women, the imbalance is further potentiated by hormone deprivation and increased osteoclast activity (see also paragraph on sex steroids) (125). Next to the decline in osteoblast function and hormone secretion, age-related abnormalities in calcium homeostasis and vitamin D metabolism as well as inadequate intake of vitamin D and calcium cause bone loss in subsets of the aging population (156).

3.4 Bone aging in mice

In recent years age-related bone loss has been studied in mice as well. Already in 1987 a study on bone aging in wild type mice was published. Silbermann and co-workers measured a decrease in cortical thickness and a larger width of the total midshaft as well as the medullary diameter in femurs of 28-months-old female C57BL/6 mice compared to 7-months-old mice (206). In addition, they observed cortical porosity and a decrease in number of osteocytes as well as preosteoblasts along the periosteum. Moreover, these preosteoblasts seemed to have lower proliferative capacity. A few years later, Weiss and co-workers studied the femurs of CW-1 female mice over a broad age-range while Bar-Shira-Maymon and co-workers studied the lumbar vertebrae of these mice. It was observed that as in humans, the pattern of age-related bone loss differs at different skeletal sites (207-210). A study in healthy women showed that bone mineral content in the lumbar vertebrae decreased mainly during menopause whereas bone

mineral content in the femoral neck decreased from young adulthood to old age and the femoral shaft remained nearly unaltered until the seventh decade after which bone mineral content declined significantly (210). Another study showed progressive age-related loss of trabecular bone and the development of marrow-filled cavities within cortical bone in proximal femurs whereas the lumbar vertebrae only showed a reduction in number and size of trabeculae.

Recently, several studies on bone development and aging in mostly male C57BL/6 mice were published (143,211-213). Using microcomputed tomography (μ CT) age-related changes in tibiae of male C57BL/6 mice between 1,5 and 24 months of age were studied (211). A decrease in trabecular bone characterized by decreased trabecular number, decreased connectivity and increased trabecular spacing was observed. Cortical bone thickness decreased after 6 months of age whereas cortical bone area remained constant. Using histomorphometry and mechanical testing, the long bones of these aging male C57BL/6 mice were also found to exhibit excessive endocortical resorption and an increase in periosteal apposition but also reduced mechanical strength (212). In addition, 6- and 24- month-old C57BL/6 mice showed increased expression of RANKL and decreased expression of OPG in total bone extracts compared to 6 week old C57BL/6 mice (143). This would be expected to stimulate bone turnover and promote bone loss, which was indeed observed (143). In addition, these changes were shown to be accompanied by an increase in osteoclast progenitor pool (143). This age-associated increase in osteoclast progenitor pool and osteoclast formation was previously studied in 4-6 and 24 month old mice (214). A 20-30% increase in hematopoietic cells obtained from long bones and a 2-3.5-fold increase in macrophage/mononuclear colonies in bone marrow cultures from the aged animals was observed. However, others showed that the functionality of the formed osteoclasts was lower as established by a decrease in bone degradation capacity (214).

3.4.1 Differences in bone metabolism between different mouse strains

It has been established that there are large differences in bone mass between different mouse strains as well as between different skeletal sites. For example, C57BL/6 mice that are widely used have low bone density in long bones and intermediate bone mass in vertebrae. C3H/HeJ mice with a similar body size and adult weight have 53% higher peak bone density in the femora, but have about half the number of trabeculae in the vertebral bodies (215,216). In addition, the pattern of response to mechanical loading differs. It was shown that C57BL/6 mice are more sensitive to endosteal bone loss from hind-limb immobilization than C3H/HeJ mice (215). Furthermore, C57BL/6 mice display significantly more endosteal and periosteal bone formation after loading (217). These strains also differ in calcium metabolism, i.e. at low dietary calcium levels, C57BL/6 mice rely more on mobilization of calcium from bone to maintain extracellular calcium homeostasis than C3H/HeJ mice (218). The effect of ovariectomy on calcium metabolism is also stronger in C57BL/6 mice compared to C3H/HeJ mice. After ovariectomy, C57BL/6 mice show significantly decreased calcium absorption and thus

more calcium in the faeces than non-treated C57BL/6 mice (219). In this regard, C57BL/6 mice are comparable to hypoestrogenic women (219). In addition, the effect of ovariectomy on trabecular bone varies with mouse strain as well as with skeletal site. Trabecular bone volume (BV/TV) in vertebrae and femora declined after ovariectomy in BALB/cByJ, C57BL/6J, CAST/EiJ and DBA/2J mice, but not in C3H/HeJ mice (220). In contrast, at the proximal tibia, C3H/HeJ mice had a greater decline in trabecular BV/TV (-39%) than C57BL/6J (-18%), DBA2/J (-23%), and CAST/EiJ mice (-21%) (220). Ovariectomy induced declines in cortical bone properties, but in contrast to trabecular bone, the effect of ovariectomy did not vary by mouse strain (220). The extent of trabecular bone loss after ovariectomy was greatest in BALB/c mice, which had the highest vertebral trabecular bone volume at baseline (220). In contrast to cortical bone loss, trabecular bone loss thus seems to be partly genetically regulated.

In humans, bodyweight has an important effect on bone mineral density whereas this relation seems to be lacking in mice. No correlation between body weight and femoral or vertebral parameters was found in 11 inbred strains although body weight varied by 86% among the strains (221). C57BL/6J and A/J mice showed differences in bone mass although they were similar in body weight; overall C57BL/6J animals had higher bone mass in both femur and tibia (222). Moreover, Jepsen et al. found that A/J femurs were more brittle than C57BL/6J femurs (223). This was explained by the fact that A/J mice had more slender femurs which was compensated by increased tissue stiffness which ultimately led to increased fragility. Additional differences between A/J, C57BL/6J and C3H/HeJ mice were observed in vertebrae (224). A/J mice had slender axial and appendicular bones with a high mineral content whereas C57BL/6J mice had wider bones with a lower mineral content. The vertebrae of these mice had a similar stiffness, but different failure modes with C57BL/6J again being more ductile. C3H/HeJ femora and vertebrae showed a greater cortical area and mineral content and thus an increased stiffness and fragility. In addition, the architecture of the trabeculae seemed to be coupled to the amount of mineral within the tissue suggesting that these multiple physical traits that explain the genetic variation in whole bone mechanical properties might be co-ordinately regulated. When compared to five other mouse strains, the widely used C57BL/6J mice seem to have an intermediate bone phenotype.

4 Scope of this thesis

Nucleotide excision repair deficient TTD mice display many features of the human syndrome and exhibit signs of segmental premature aging, including skeletal abnormalities. In order to gain insight in the aetiology of premature aging and associated pathology in DNA repair disorders, we set out to extensively analyse the bone phenotype of TTD mice in relation to age. In chapter 2 we describe the age-related changes in the structure of long bones of wild type and TTD female mice by microCT and histomorphometric analysis, mechanical test-

ing, as well as by characterizing osteoprogenitor cells in bone marrow cultures. In chapter 3 we extend this study to male wild type and TTD mice to address the question whether the TTD bone phenotype is subject to gender differences. In chapter 4 we describe the aging-associated changes in the vertebrae of female TTD mice. Finally, chapter 5 addresses whether aging-associated changes in endocrine parameters that relate to bone metabolism are altered in TTD mice.

References

1. Finkel T, Holbrook NJ 2000 Oxidants, oxidative stress and the biology of ageing. *Nature* **408**(6809):239-47.
2. Cadet J, Douki T, Gasparutto D, Ravanat JL 2003 Oxidative damage to DNA: formation, measurement and biochemical features. *Mutat Res* **531**(1-2):5-23.
3. Lindahl T 1993 Instability and decay of the primary structure of DNA. *Nature* **362**(6422):709-15.
4. Lehmann AR, Kirk-Bell S, Mayne L 1979 Abnormal kinetics of DNA synthesis in ultraviolet light-irradiated cells from patients with Cockayne's syndrome. *Cancer Res* **39**(10):4237-41.
5. Mayne LV, Lehmann AR 1982 Failure of RNA synthesis to recover after UV irradiation: an early defect in cells from individuals with Cockayne's syndrome and xeroderma pigmentosum. *Cancer Res* **42**(4):1473-8.
6. Bernstein C, Bernstein H, Payne CM, Garewal H 2002 DNA repair/pro-apoptotic dual-role proteins in five major DNA repair pathways: fail-safe protection against carcinogenesis. *Mutat Res* **511**(2):145-78.
7. Campisi J 2001 Cellular senescence as a tumor-suppressor mechanism. *Trends Cell Biol* **11**(11):S27-31.
8. de Waard H 2004 Genome caretaking and differentiation *Cell Biology and Genetics*. Erasmus University Rotterdam, Rotterdam, pp 141.
9. Mitchell JR, Hoeijmakers JH, Niedernhofer LJ 2003 Divide and conquer: nucleotide excision repair battles cancer and ageing. *Curr Opin Cell Biol* **15**(2):232-40.
10. Hasty P, Campisi J, Hoeijmakers J, van Steeg H, Vijg J 2003 Aging and genome maintenance: lessons from the mouse? *Science* **299**(5611):1355-9.
11. Chen JH, Hales CN, Ozanne SE 2007 DNA damage, cellular senescence and organismal ageing: causal or correlative? *Nucleic Acids Res* **35**(22):7417-28.
12. Hoeijmakers JH 2001 Genome maintenance mechanisms for preventing cancer. *Nature* **411**(6835):366-74.
13. Friedberg EC 2003 DNA damage and repair. *Nature* **421**(6921):436-40.
14. Bartek J, Lukas J 2001 Mammalian G1- and S-phase checkpoints in response to DNA damage. *Curr Opin Cell Biol* **13**(6):738-47.
15. Baynton K, Fuchs RP 2000 Lesions in DNA: hurdles for polymerases. *Trends Biochem Sci* **25**(2):74-9.
16. Friedberg EC, Wagner R, Radman M 2002 Specialized DNA polymerases, cellular survival, and the genesis of mutations. *Science* **296**(5573):1627-30.
17. McGowan CH 2003 Running into problems: how cells cope with replicating damaged DNA. *Mutat Res* **532**(1-2):75-84.
18. Aboussekhra A, Biggerstaff M, Shivji MK, Vilpo JA, Moncollin V, Podust VN, Protic M, Hubscher U, Egly JM, Wood RD 1995 Mammalian DNA nucleotide excision repair reconstituted with purified protein components. *Cell* **80**(6):859-68.
19. de Laat WL, Jaspers NG, Hoeijmakers JH 1999 Molecular mechanism of nucleotide excision repair. *Genes Dev* **13**(7):768-85.
20. Fortini P, Pascucci B, Parlanti E, D'Errico M, Simonelli V, Dogliotti E 2003 The base excision repair: mechanisms and its relevance for cancer susceptibility. *Biochimie* **85**(11):1053-71.
21. Krokan HE, Nilsen H, Skorpen F, Otterlei M, Slupphaug G 2000 Base excision repair of DNA in mammalian cells. *FEBS Lett* **476**(1-2):73-7.
22. Marti TM, Kunz C, Fleck O 2002 DNA mismatch repair and mutation avoidance pathways. *J Cell Physiol* **191**(1):28-41.

23. Peltomaki P 2003 Role of DNA mismatch repair defects in the pathogenesis of human cancer. *J Clin Oncol* **21**(6):1174-9.
24. Valerie K, Povirk LF 2003 Regulation and mechanisms of mammalian double-strand break repair. *Oncogene* **22**(37):5792-812.
25. van Gent DC, Hoeijmakers JH, Kanaar R 2001 Chromosomal stability and the DNA double-stranded break connection. *Nat Rev Genet* **2**(3):196-206.
26. Dronkert ML, Kanaar R 2001 Repair of DNA interstrand cross-links. *Mutat Res* **486**(4):217-47.
27. Kennedy RD, D'Andrea AD 2005 The Fanconi Anemia/BRCA pathway: new faces in the crowd. *Genes Dev* **19**(24):2925-40.
28. Mirchandani KD, D'Andrea AD 2006 The Fanconi anemia/BRCA pathway: a coordinator of cross-link repair. *Exp Cell Res* **312**(14):2647-53.
29. Bergstralh DT, Sekelsky J 2008 Interstrand crosslink repair: can XPF-ERCC1 be let off the hook? *Trends Genet* **24**(2):70-6.
30. Thompson LH, Hinz JM, Yamada NA, Jones NJ 2005 How Fanconi anemia proteins promote the four Rs: replication, recombination, repair, and recovery. *Environ Mol Mutagen* **45**(2-3):128-42.
31. Niedernhofer LJ, Lalai AS, Hoeijmakers JH 2005 Fanconi anemia (cross)linked to DNA repair. *Cell* **123**(7):1191-8.
32. Levitus M, Joenje H, de Winter JP 2006 The Fanconi anemia pathway of genomic maintenance. *Cell Oncol* **28**(1-2):3-29.
33. Smith JR, Pereira-Smith OM 1996 Replicative senescence: implications for in vivo aging and tumor suppression. *Science* **273**(5271):63-7.
34. Bohr VA, Smith CA, Okumoto DS, Hanawalt PC 1985 DNA repair in an active gene: removal of pyrimidine dimers from the DHFR gene of CHO cells is much more efficient than in the genome overall. *Cell* **40**(2):359-69.
35. Coin F, Oksenyk V, Egly JM 2007 Distinct roles for the XPB/p52 and XPD/p44 subcomplexes of TFIIH in damaged DNA opening during nucleotide excision repair. *Mol Cell* **26**(2):245-56.
36. Moser J, Kool H, Giakzidis I, Caldecott K, Mullenders LH, Foustier MI 2007 Sealing of chromosomal DNA nicks during nucleotide excision repair requires XRCC1 and DNA ligase III alpha in a cell-cycle-specific manner. *Mol Cell* **27**(2):311-23.
37. Hoogstraten D, Nigg AL, Heath H, Mullenders LH, van Driel R, Hoeijmakers JH, Vermeulen W, Houtsmuller AB 2002 Rapid switching of TFIIH between RNA polymerase I and II transcription and DNA repair in vivo. *Mol Cell* **10**(5):1163-74.
38. Hakem R 2008 DNA-damage repair; the good, the bad, and the ugly. *Embo J* **27**(4):589-605.
39. Al-Tassan N, Chmiel NH, Maynard J, Fleming N, Livingston AL, Williams GT, Hodges AK, Davies DR, David SS, Sampson JR, Cheadle JP 2002 Inherited variants of MYH associated with somatic G:C->T:A mutations in colorectal tumors. *Nat Genet* **30**(2):227-32.
40. Cheadle JP, Sampson JR 2003 Exposing the MYTH about base excision repair and human inherited disease. *Hum Mol Genet* **12 Spec No 2**:R159-65.
41. Thompson LH, Schild D 2002 Recombinational DNA repair and human disease. *Mutat Res* **509**(1-2):49-78.
42. de Boer J, Hoeijmakers JH 2000 Nucleotide excision repair and human syndromes. *Carcinogenesis* **21**(3):453-60.
43. Bootsma D, Kraemer KH, Cleaver JE, Hoeijmakers JHJ 2001 Nucleotide excision repair syndromes: xeroderma pigmentosum, Cockayne syndrome and trichothiodystrophy, 8th ed. McGraw-Hill, New York.

44. Hwang BJ, Ford JM, Hanawalt PC, Chu G 1999 Expression of the p48 xeroderma pigmentosum gene is p53-dependent and is involved in global genomic repair. *Proc Natl Acad Sci U S A* **96**(2):424-8.
45. Tang JY, Hwang BJ, Ford JM, Hanawalt PC, Chu G 2000 Xeroderma pigmentosum p48 gene enhances global genomic repair and suppresses UV-induced mutagenesis. *Mol Cell* **5**(4):737-44.
46. Venema J, van Hoffen A, Karcagi V, Natarajan AT, van Zeeland AA, Mullenders LH 1991 Xeroderma pigmentosum complementation group C cells remove pyrimidine dimers selectively from the transcribed strand of active genes. *Mol Cell Biol* **11**(8):4128-34.
47. Venema J, van Hoffen A, Natarajan AT, van Zeeland AA, Mullenders LH 1990 The residual repair capacity of xeroderma pigmentosum complementation group C fibroblasts is highly specific for transcriptionally active DNA. *Nucleic Acids Res* **18**(3):443-8.
48. Kraemer KH, Lee MM, Scotto J 1984 DNA repair protects against cutaneous and internal neoplasia: evidence from xeroderma pigmentosum. *Carcinogenesis* **5**(4):511-4.
49. Kraemer KH, Patronas NJ, Schiffmann R, Brooks BP, Tamura D, DiGiovanna JJ 2007 Xeroderma pigmentosum, trichothiodystrophy and Cockayne syndrome: a complex genotype-phenotype relationship. *Neuroscience* **145**(4):1388-96.
50. Kraemer KH, Lee MM, Scotto J 1987 Xeroderma pigmentosum. Cutaneous, ocular, and neurologic abnormalities in 830 published cases. *Arch Dermatol* **123**(2):241-50.
51. Itoh M, Hayashi M, Shioda K, Minagawa M, Isa F, Tamagawa K, Morimatsu Y, Oda M 1999 Neurodegeneration in hereditary nucleotide repair disorders. *Brain Dev* **21**(5):326-33.
52. Brooks PJ 2002 DNA repair in neural cells: basic science and clinical implications. *Mutat Res* **509**(1-2):93-108.
53. Lehmann AR 2001 The xeroderma pigmentosum group D (XPD) gene: one gene, two functions, three diseases. *Genes Dev* **15**(1):15-23.
54. Brooks PJ, Cheng TF, Cooper L 2008 Do all of the neurologic diseases in patients with DNA repair gene mutations result from the accumulation of DNA damage? *DNA Repair (Amst)* **7**(6):834-48.
55. Nance MA, Berry SA 1992 Cockayne syndrome: review of 140 cases. *Am J Med Genet* **42**(1):68-84.
56. Graham JM, Jr., Anyane-Yeboah K, Raams A, Appeldoorn E, Kleijer WJ, Garritsen VH, Busch D, Ederseim TG, Jaspers NG 2001 Cerebro-oculo-facio-skeletal syndrome with a nucleotide excision-repair defect and a mutated XPD gene, with prenatal diagnosis in a triplet pregnancy. *Am J Hum Genet* **69**(2):291-300.
57. Laugel V, Dalloz C, Tobias ES, Tolmie JL, Martin-Coignard D, Drouin-Garraud V, Valayannopoulos V, Sarasin A, Dollfus H 2008 Cerebro-oculo-facio-skeletal syndrome: three additional cases with CSB mutations, new diagnostic criteria and an approach to investigation. *J Med Genet* **45**(9):564-71.
58. Lindenbaum Y, Dickson D, Rosenbaum P, Kraemer K, Robbins I, Rapin I 2001 Xeroderma pigmentosum/cockayne syndrome complex: first neuropathological study and review of eight other cases. *Eur J Paediatr Neurol* **5**(6):225-42.
59. McCuaig C, Marcoux D, Rasmussen JE, Werner MM, Gentner NE 1993 Trichothiodystrophy associated with photosensitivity, gonadal failure, and striking osteosclerosis. *J Am Acad Dermatol* **28**(5 Pt 2):820-6.
60. Itin PH, Sarasin A, Pittelkow MR 2001 Trichothiodystrophy: update on the sulfur-deficient brittle hair syndromes. *J Am Acad Dermatol* **44**(6):891-920; quiz 921-4.
61. Faghri S, Tamura D, Kraemer KH, DiGiovanna JJ 2008 Trichothiodystrophy: a systematic review of 112 published cases characterises a wide spectrum of clinical manifestations. *J Med Genet* **45**(10):609-21.

62. Bergmann E, Egly JM 2001 Trichothiodystrophy, a transcription syndrome. *Trends Genet* **17**(5):279-86.
63. Price VH, Odom RB, Ward WH, Jones FT 1980 Trichothiodystrophy: sulfur-deficient brittle hair as a marker for a neuroectodermal symptom complex. *Arch Dermatol* **116**(12):1375-84.
64. Weeda G, Eveno E, Donker I, Vermeulen W, Chevallier-Lagente O, Taieb A, Stary A, Hoeijmakers JH, Mezzina M, Sarasin A 1997 A mutation in the XPB/ERCC3 DNA repair transcription gene, associated with trichothiodystrophy. *Am J Hum Genet* **60**(2):320-9.
65. Stefanini M, Lagomarsini P, Arlett CF, Marinoni S, Borrone C, Crovato F, Trevisan G, Cordone G, Nuzzo F 1986 Xeroderma pigmentosum (complementation group D) mutation is present in patients affected by trichothiodystrophy with photosensitivity. *Hum Genet* **74**(2):107-12.
66. Nakabayashi K, Amann D, Ren Y, Saarialho-Kere U, Avidan N, Gentles S, MacDonald JR, Puffenberger EG, Christiano AM, Martinez-Mir A, Salas-Alanis JC, Rizzo R, Vamos E, Raams A, Les C, Seboun E, Jaspers NG, Beckmann JS, Jackson CE, Scherer SW 2005 Identification of C7orf11 (TTDN1) gene mutations and genetic heterogeneity in nonphotosensitive trichothiodystrophy. *Am J Hum Genet* **76**(3):510-6.
67. Giglia-Mari G, Coin F, Ranish JA, Hoogstraten D, Theil A, Wijgers N, Jaspers NG, Raams A, Argentini M, van der Spek PJ, Botta E, Stefanini M, Egly JM, Aebersold R, Hoeijmakers JH, Vermeulen W 2004 A new, tenth subunit of TFIIH is responsible for the DNA repair syndrome trichothiodystrophy group A. *Nat Genet* **36**(7):714-9.
68. Broughton BC, Berneburg M, Fawcett H, Taylor EM, Arlett CF, Nardo T, Stefanini M, Menefee E, Price VH, Queille S, Sarasin A, Bohnert E, Krutmann J, Davidson R, Kraemer KH, Lehmann AR 2001 Two individuals with features of both xeroderma pigmentosum and trichothiodystrophy highlight the complexity of the clinical outcomes of mutations in the XPD gene. *Hum Mol Genet* **10**(22):2539-47.
69. Schaeffer L, Moncollin V, Roy R, Staub A, Mezzina M, Sarasin A, Weeda G, Hoeijmakers JH, Egly JM 1994 The ERCC2/DNA repair protein is associated with the class II BTF2/TFIIH transcription factor. *Embo J* **13**(10):2388-92.
70. Schaeffer L, Roy R, Humbert S, Moncollin V, Vermeulen W, Hoeijmakers JH, Chambon P, Egly JM 1993 DNA repair helicase: a component of BTF2 (TFIIH) basic transcription factor. *Science* **260**(5104):58-63.
71. Bootsma D, Hoeijmakers JH 1993 DNA repair. Engagement with transcription. *Nature* **363**(6425):114-5.
72. Weber CA, Salazar EP, Stewart SA, Thompson LH 1988 Molecular cloning and biological characterization of a human gene, ERCC2, that corrects the nucleotide excision repair defect in CHO UV5 cells. *Mol Cell Biol* **8**(3):1137-46.
73. Holstege FC, van der Vliet PC, Timmers HT 1996 Opening of an RNA polymerase II promoter occurs in two distinct steps and requires the basal transcription factors IIE and IIH. *Embo J* **15**(7):1666-77.
74. Tirode F, Busso D, Coin F, Egly JM 1999 Reconstitution of the transcription factor TFIIH: assignment of functions for the three enzymatic subunits, XPB, XPD, and cdk7. *Mol Cell* **3**(1):87-95.
75. Evans E, Moggs JG, Hwang JR, Egly JM, Wood RD 1997 Mechanism of open complex and dual incision formation by human nucleotide excision repair factors. *Embo J* **16**(21):6559-73.
76. Araujo SJ, Tirode F, Coin F, Pospiech H, Syvaolja JE, Stucki M, Hubscher U, Egly JM, Wood RD 2000 Nucleotide excision repair of DNA with recombinant human proteins: definition of the minimal set of factors, active forms of TFIIH, and modulation by CAK. *Genes Dev* **14**(3):349-59.
77. Sugawara K, Okamoto T, Shimizu Y, Masutani C, Iwai S, Hanaoka F 2001 A multistep damage recognition mechanism for global genomic nucleotide excision repair. *Genes Dev* **15**(5):507-21.

78. Winkler GS, Araujo SJ, Fiedler U, Vermeulen W, Coin F, Egly JM, Hoeijmakers JH, Wood RD, Timmers HT, Weeda G 2000 TFIIH with inactive XPD helicase functions in transcription initiation but is defective in DNA repair. *J Biol Chem* **275**(6):4258-66.
79. Feaver WJ, Svejstrup JQ, Bardwell L, Bardwell AJ, Buratowski S, Gulyas KD, Donahue TF, Friedberg EC, Kornberg RD 1993 Dual roles of a multiprotein complex from *S. cerevisiae* in transcription and DNA repair. *Cell* **75**(7):1379-87.
80. Sung P, Higgins D, Prakash L, Prakash S 1988 Mutation of lysine-48 to arginine in the yeast RAD3 protein abolishes its ATPase and DNA helicase activities but not the ability to bind ATP. *Embo J* **7**(10):3263-9.
81. Coin F, Marinoni JC, Rodolfo C, Fribourg S, Pedrini AM, Egly JM 1998 Mutations in the XPD helicase gene result in XP and TTD phenotypes, preventing interaction between XPD and the p44 subunit of TFIIH. *Nat Genet* **20**(2):184-8.
82. Broughton BC, Steingrimsdottir H, Weber CA, Lehmann AR 1994 Mutations in the xeroderma pigmentosum group D DNA repair/transcription gene in patients with trichothiodystrophy. *Nat Genet* **7**(2):189-94.
83. Takayama K, Salazar EP, Lehmann A, Stefanini M, Thompson LH, Weber CA 1995 Defects in the DNA repair and transcription gene ERCC2 in the cancer-prone disorder xeroderma pigmentosum group D. *Cancer Res* **55**(23):5656-63.
84. Takayama K, Salazar EP, Broughton BC, Lehmann AR, Sarasin A, Thompson LH, Weber CA 1996 Defects in the DNA repair and transcription gene ERCC2(XPD) in trichothiodystrophy. *Am J Hum Genet* **58**(2):263-70.
85. Kobayashi T, Kuraoka I, Saijo M, Nakatsu Y, Tanaka A, Someda Y, Fukuro S, Tanaka K 1997 Mutations in the XPD gene leading to xeroderma pigmentosum symptoms. *Hum Mutat* **9**(4):322-31.
86. Botta E, Nardo T, Broughton BC, Marinoni S, Lehmann AR, Stefanini M 1998 Analysis of mutations in the XPD gene in Italian patients with trichothiodystrophy: site of mutation correlates with repair deficiency, but gene dosage appears to determine clinical severity. *Am J Hum Genet* **63**(4):1036-48.
87. Taylor EM, Broughton BC, Botta E, Stefanini M, Sarasin A, Jaspers NG, Fawcett H, Harcourt SA, Arlett CF, Lehmann AR 1997 Xeroderma pigmentosum and trichothiodystrophy are associated with different mutations in the XPD (ERCC2) repair/transcription gene. *Proc Natl Acad Sci U S A* **94**(16):8658-63.
88. Dubaele S, Proietti De Santis L, Bienstock RJ, Keriell A, Stefanini M, Van Houten B, Egly JM 2003 Basal transcription defect discriminates between xeroderma pigmentosum and trichothiodystrophy in XPD patients. *Mol Cell* **11**(6):1635-46.
89. Boyle J, Ueda T, Oh KS, Imoto K, Tamura D, Jagdeo J, Khan SG, Nadem C, Digiovanna JJ, Kraemer KH 2008 Persistence of repair proteins at unrepaired DNA damage distinguishes diseases with ERCC2 (XPD) mutations: cancer-prone xeroderma pigmentosum vs. non-cancer-prone trichothiodystrophy. *Hum Mutat*.
90. Drapkin R, Le Roy G, Cho H, Akoulitchev S, Reinberg D 1996 Human cyclin-dependent kinase-activating kinase exists in three distinct complexes. *Proc Natl Acad Sci U S A* **93**(13):6488-93.
91. Reardon JT, Ge H, Gibbs E, Sancar A, Hurwitz J, Pan ZQ 1996 Isolation and characterization of two human transcription factor IIH (TFIIH)-related complexes: ERCC2/CAK and TFIIH. *Proc Natl Acad Sci U S A* **93**(13):6482-7.
92. Egly JM 2001 The 14th Datta Lecture. TFIIH: from transcription to clinic. *FEBS Lett* **498**(2-3):124-8.

93. Rochette-Egly C, Adam S, Rossignol M, Egly JM, Chambon P 1997 Stimulation of RAR alpha activation function AF-1 through binding to the general transcription factor TFIID and phosphorylation by CDK7. *Cell* **90**(1):97-107.
94. Harper JW, Elledge SJ 1998 The role of Cdk7 in CAK function, a retro-retrospective. *Genes Dev* **12**(3):285-9.
95. Keriell A, Stary A, Sarasin A, Rochette-Egly C, Egly JM 2002 XPD mutations prevent TFIID-dependent transactivation by nuclear receptors and phosphorylation of RARalpha. *Cell* **109**(1):125-35.
96. Le Page F, Kwok EE, Avrutskaya A, Gentil A, Leadon SA, Sarasin A, Cooper PK 2000 Transcription-coupled repair of 8-oxoguanine: requirement for XPG, TFIID, and CSB and implications for Cockayne syndrome. *Cell* **101**(2):159-71.
97. Chen J, Larochelle S, Li X, Suter B 2003 Xpd/Ercc2 regulates CAK activity and mitotic progression. *Nature* **424**(6945):228-32.
98. Hoeijmakers JH 2001 From xeroderma pigmentosum to the biological clock contributions of Dirk Bootsma to human genetics. *Mutat Res* **485**(1):43-59.
99. Iben S, Tschochner H, Bier M, Hoogstraten D, Hozak P, Egly JM, Grummt I 2002 TFIID plays an essential role in RNA polymerase I transcription. *Cell* **109**(3):297-306.
100. de Boer J, Andressoo JO, de Wit J, Huijijmans J, Beems RB, van Steeg H, Weeda G, van der Horst GT, van Leeuwen W, Themmen AP, Meradji M, Hoeijmakers JH 2002 Premature aging in mice deficient in DNA repair and transcription. *Science* **296**(5571):1276-9.
101. Vermeulen W, Scott RJ, Rodgers S, Muller HJ, Cole J, Arlett CF, Kleijer WJ, Bootsma D, Hoeijmakers JH, Weeda G 1994 Clinical heterogeneity within xeroderma pigmentosum associated with mutations in the DNA repair and transcription gene ERCC3. *Am J Hum Genet* **54**(2):191-200.
102. de Boer J, de Wit J, van Steeg H, Berg RJ, Morreau H, Visser P, Lehmann AR, Duran M, Hoeijmakers JH, Weeda G 1998 A mouse model for the basal transcription/DNA repair syndrome trichothiodystrophy. *Mol Cell* **1**(7):981-90.
103. Botta E, Nardo T, Lehmann AR, Egly JM, Pedrini AM, Stefanini M 2002 Reduced level of the repair/transcription factor TFIID in trichothiodystrophy. *Hum Mol Genet* **11**(23):2919-28.
104. Viprakasit V, Gibbons RJ, Broughton BC, Tolmie JL, Brown D, Lunt P, Winter RM, Marinoni S, Stefanini M, Brueton L, Lehmann AR, Higgs DR 2001 Mutations in the general transcription factor TFIID result in beta-thalassaemia in individuals with trichothiodystrophy. *Hum Mol Genet* **10**(24):2797-802.
105. Compe E, Malerba M, Soler L, Marescaux J, Borrelli E, Egly JM 2007 Neurological defects in trichothiodystrophy reveal a coactivator function of TFIID. *Nat Neurosci* **10**(11):1414-22.
106. Fan L, Fuss JO, Cheng QJ, Arvai AS, Hammel M, Roberts VA, Cooper PK, Tainer JA 2008 XPD helicase structures and activities: insights into the cancer and aging phenotypes from XPD mutations. *Cell* **133**(5):789-800.
107. Liu H, Rudolf J, Johnson KA, McMahon SA, Oke M, Carter L, McRobbie AM, Brown SE, Naismith JH, White MF 2008 Structure of the DNA repair helicase XPD. *Cell* **133**(5):801-12.
108. de Boer J, van Steeg H, Berg RJ, Garssen J, de Wit J, van Oostrum CT, Beems RB, van der Horst GT, van Kreijl CF, de Grujil FR, Bootsma D, Hoeijmakers JH, Weeda G 1999 Mouse model for the DNA repair/basal transcription disorder trichothiodystrophy reveals cancer predisposition. *Cancer Res* **59**(14):3489-94.
109. Wijnhoven SW, Beems RB, Roodbergen M, van den Berg J, Lohman PH, Diderich K, van der Horst GT, Vijg J, Hoeijmakers JH, van Steeg H 2005 Accelerated aging pathology in ad libitum fed Xpd(TTD) mice is accompanied by features suggestive of caloric restriction. *DNA Repair (Amst)*.
110. Kirkwood TB, Austad SN 2000 Why do we age? *Nature* **408**(6809):233-8.

111. Ku HH, Brunk UT, Sohal RS 1993 Relationship between mitochondrial superoxide and hydrogen peroxide production and longevity of mammalian species. *Free Radic Biol Med* **15**(6):621-7.
112. Gorbunova V, Seluanov A, Mao Z, Hine C 2007 Changes in DNA repair during aging. *Nucleic Acids Res* **35**(22):7466-74.
113. Brosh RM, Jr., Bohr VA 2007 Human premature aging, DNA repair and RecQ helicases. *Nucleic Acids Res* **35**(22):7527-44.
114. Martin GM, Oshima J 2000 Lessons from human progeroid syndromes. *Nature* **408**(6809):263-6.
115. Mounkes LC, Stewart CL 2004 Aging and nuclear organization: lamins and progeria. *Curr Opin Cell Biol* **16**(3):322-7.
116. Bootsma D, Kraemer KH, Cleaver JE, Hoeijmakers JHJ 1998 Nucleotide excision repair syndromes: xeroderma pigmentosum, Cockayne syndrome and trichothiodystrophy. In: Vogelstein B, Kinzler KW (eds.) *The genetic basis of human cancer*. McGraw-Hill, New York, pp 245-74.
117. Leupold D 1979 [Ichthyosis congenita, cataract, mental retardation, ataxia, osteosclerosis and immunologic deficiency--a particular syndrome?]. *Monatsschr Kinderheilkd* **127**(5):307-8.
118. Chapman S 1988 The trichothiodystrophy syndrome of Pollitt. *Pediatr Radiol* **18**(2):154-6.
119. Civitelli R, McAlister WH, Teitelbaum SL, Whyte MP 1989 Central osteosclerosis with ectodermal dysplasia: clinical, laboratory, radiologic, and histopathologic characterization with review of the literature. *J Bone Miner Res* **4**(6):863-75.
120. Kousseff BG, Esterly NB 1988 Trichothiodystrophy, IBIDS syndrome or Tay syndrome? *Birth Defects Orig Artic Ser* **24**(2):169-81.
121. Przedborski S, Ferster A, Goldman S, Wolter R, Song M, Tonnesen T, Pollitt RJ, Vamos E 1990 Trichothiodystrophy, mental retardation, short stature, ataxia, and gonadal dysfunction in three Moroccan siblings. *Am J Med Genet* **35**(4):566-73.
122. Toelle SP, Valsangiacomo E, Boltshauser E 2001 Trichothiodystrophy with severe cardiac and neurological involvement in two sisters. *Eur J Pediatr* **160**(12):728-31.
123. Wakeling EL, Cruwys M, Suri M, Brady AF, Aylett SE, Hall C 2004 Central osteosclerosis with trichothiodystrophy. *Pediatr Radiol* **34**(7):541-6.
124. Gerhard GS, Kasales CJ 2003 Aging and kyphosis. *J Gerontol A Biol Sci Med Sci* **58**(11):968.
125. Chan GK, Duque G 2002 Age-related bone loss: old bone, new facts. *Gerontology* **48**(2):62-71.
126. Harada S, Rodan GA 2003 Control of osteoblast function and regulation of bone mass. *Nature* **423**(6937):349-55.
127. Ducy P, Schinke T, Karsenty G 2000 The osteoblast: a sophisticated fibroblast under central surveillance. *Science* **289**(5484):1501-4.
128. Chien KR, Karsenty G 2005 Longevity and lineages: toward the integrative biology of degenerative diseases in heart, muscle, and bone. *Cell* **120**(4):533-44.
129. Knothe Tate ML, Adamson JR, Tami AE, Bauer TW 2004 The osteocyte. *Int J Biochem Cell Biol* **36**(1):1-8.
130. Knothe Tate ML 2003 "Whither flows the fluid in bone?" An osteocyte's perspective. *J Biomech* **36**(10):1409-24.
131. van Bezooijen RL, ten Dijke P, Papapoulos SE, Lowik CW 2005 SOST/sclerostin, an osteocyte-derived negative regulator of bone formation. *Cytokine Growth Factor Rev* **16**(3):319-27.
132. Balemans W, Ebeling M, Patel N, Van Hul E, Olson P, Dioszegi M, Lacza C, Wuyts W, Van Den Ende J, Willems P, Paes-Alves AF, Hill S, Bueno M, Ramos FJ, Tacconi P, Dikkers FG, Stratakis C, Lindpaintner K, Vickery B, Foerzler D, Van Hul W 2001 Increased bone density in sclerosteosis is due to the deficiency of a novel secreted protein (SOST). *Hum Mol Genet* **10**(5):537-43.

133. ten Dijke P, Krause C, de Gorter DJ, Lowik CW, van Bezooijen RL 2008 Osteocyte-derived sclerostin inhibits bone formation: its role in bone morphogenetic protein and Wnt signaling. *J Bone Joint Surg Am* **90 Suppl 1**:31-5.
134. Boyde A 2003 The real response of bone to exercise. *J Anat* **203**(2):173-89.
135. Dunstan CR, Evans RA, Hills E, Wong SY, Higgs RJ 1990 Bone death in hip fracture in the elderly. *Calcif Tissue Int* **47**(5):270-5.
136. Dunstan CR, Somers NM, Evans RA 1993 Osteocyte death and hip fracture. *Calcif Tissue Int* **53 Suppl 1**:S113-6; discussion S116-7.
137. Noble B 2003 Bone microdamage and cell apoptosis. *Eur Cell Mater* **6**:46-55; discussion 55.
138. Verborgt O, Gibson GJ, Schaffler MB 2000 Loss of osteocyte integrity in association with microdamage and bone remodeling after fatigue in vivo. *J Bone Miner Res* **15**(1):60-7.
139. Tomkinson A, Reeve J, Shaw RW, Noble BS 1997 The death of osteocytes via apoptosis accompanies estrogen withdrawal in human bone. *J Clin Endocrinol Metab* **82**(9):3128-35.
140. Mullender MG, van der Meer DD, Huiskes R, Lips P 1996 Osteocyte density changes in aging and osteoporosis. *Bone* **18**(2):109-13.
141. Teitelbaum SL 2000 Bone resorption by osteoclasts. *Science* **289**(5484):1504-8.
142. Boyle WJ, Simonet WS, Lacey DL 2003 Osteoclast differentiation and activation. *Nature* **423**(6937):337-42.
143. Cao J, Venton L, Sakata T, Halloran BP 2003 Expression of RANKL and OPG correlates with age-related bone loss in male C57BL/6 mice. *J Bone Miner Res* **18**(2):270-7.
144. Knott L, Bailey AJ 1998 Collagen cross-links in mineralizing tissues: a review of their chemistry, function, and clinical relevance. *Bone* **22**(3):181-7.
145. Seibel MJ, Woitge HW 1999 Basic principles and clinical applications of biochemical markers of bone metabolism: biochemical and technical aspects. *J Clin Densitom* **2**(3):299-321.
146. Wang X, Bank RA, TeKoppele JM, Hubbard GB, Athanasiou KA, Agrawal CM 2000 Effect of collagen denaturation on the toughness of bone. *Clin Orthop Relat Res* (371):228-39.
147. Williamson AK, Chen AC, Masuda K, Thonar EJ, Sah RL 2003 Tensile mechanical properties of bovine articular cartilage: variations with growth and relationships to collagen network components. *J Orthop Res* **21**(5):872-80.
148. Derx P, Nigg AL, Bosman FT, Birkenhager-Frenkel DH, Houtsmuller AB, Pols HA, van Leeuwen JP 1998 Immunolocalization and quantification of noncollagenous bone matrix proteins in methylmethacrylate-embedded adult human bone in combination with histomorphometry. *Bone* **22**(4):367-73.
149. Price PA, Lothringer JW, Baukol SA, Reddi AH 1981 Developmental appearance of the vitamin K-dependent protein of bone during calcification. Analysis of mineralizing tissues in human, calf, and rat. *J Biol Chem* **256**(8):3781-4.
150. Gundberg CM 2000 Biochemical markers of bone formation. *Clin Lab Med* **20**(3):489-501.
151. Hayden JM, Mohan S, Baylink DJ 1995 The insulin-like growth factor system and the coupling of formation to resorption. *Bone* **17**(2 Suppl):93S-98S.
152. Martin RB 2003 Fatigue microdamage as an essential element of bone mechanics and biology. *Calcif Tissue Int* **73**(2):101-7.
153. Hernandez CJ, Hazelwood SJ, Martin RB 1999 The relationship between basic multicellular unit activation and origination in cancellous bone. *Bone* **25**(5):585-7.
154. Frost HM 1966 Relation between bone tissue and cell population dynamics, histology and tetracycline labeling. *Clin Orthop Relat Res* **49**:65-75.
155. Balasch J 2003 Sex steroids and bone: current perspectives. *Hum Reprod Update* **9**(3):207-22.

156. Riggs BL, Khosla S, Melton LJ, 3rd 2002 Sex steroids and the construction and conservation of the adult skeleton. *Endocr Rev* **23**(3):279-302.
157. Okazaki R, Inoue D, Shibata M, Saika M, Kido S, Ooka H, Tomiyama H, Sakamoto Y, Matsumoto T 2002 Estrogen promotes early osteoblast differentiation and inhibits adipocyte differentiation in mouse bone marrow stromal cell lines that express estrogen receptor (ER) alpha or beta. *Endocrinology* **143**(6):2349-56.
158. Fujita M, Urano T, Horie K, Ikeda K, Tsukui T, Fukuoka H, Tsutsumi O, Ouchi Y, Inoue S 2002 Estrogen activates cyclin-dependent kinases 4 and 6 through induction of cyclin D in rat primary osteoblasts. *Biochem Biophys Res Commun* **299**(2):222-8.
159. Ernst M, Heath JK, Rodan GA 1989 Estradiol effects on proliferation, messenger ribonucleic acid for collagen and insulin-like growth factor-I, and parathyroid hormone-stimulated adenylate cyclase activity in osteoblastic cells from calvariae and long bones. *Endocrinology* **125**(2):825-33.
160. Modder UI, Riggs BL, Spelsberg TC, Fraser DG, Atkinson EJ, Arnold R, Khosla S 2004 Dose-response of estrogen on bone versus the uterus in ovariectomized mice. *Eur J Endocrinol* **151**(4):503-10.
161. Nelson LR, Bulun SE 2001 Estrogen production and action. *J Am Acad Dermatol* **45**(3 Suppl):S116-24.
162. Janssen JM, Bland R, Hewison M, Coughtrie MW, Sharp S, Arts J, Pols HA, van Leeuwen JP 1999 Estradiol formation by human osteoblasts via multiple pathways: relation with osteoblast function. *J Cell Biochem* **75**(3):528-37.
163. Perry RJ, Farquharson C, Ahmed SF 2008 The role of sex steroids in controlling pubertal growth. *Clin Endocrinol (Oxf)* **68**(1):4-15.
164. Manolagas SC 2000 Birth and death of bone cells: basic regulatory mechanisms and implications for the pathogenesis and treatment of osteoporosis. *Endocr Rev* **21**(2):115-37.
165. Orwoll ES 2003 Toward an expanded understanding of the role of the periosteum in skeletal health. *J Bone Miner Res* **18**(6):949-54.
166. Parfitt AM 1994 The two faces of growth: benefits and risks to bone integrity. *Osteoporos Int* **4**(6):382-98.
167. Vanderschueren D, Venken K, Ophoff J, Bouillon R, Boonen S 2006 Clinical Review: Sex steroids and the periosteum--reconsidering the roles of androgens and estrogens in periosteal expansion. *J Clin Endocrinol Metab* **91**(2):378-82.
168. Turner RT, Colvard DS, Spelsberg TC 1990 Estrogen inhibition of periosteal bone formation in rat long bones: down-regulation of gene expression for bone matrix proteins. *Endocrinology* **127**(3):1346-51.
169. Seeman E 2001 Clinical review 137: Sexual dimorphism in skeletal size, density, and strength. *J Clin Endocrinol Metab* **86**(10):4576-84.
170. Bouillon R, Bex M, Vanderschueren D, Boonen S 2004 Estrogens are essential for male pubertal periosteal bone expansion. *J Clin Endocrinol Metab* **89**(12):6025-9.
171. Riggs BL, Melton LJ, 3rd, Robb RA, Camp JJ, Atkinson EJ, Peterson JM, Rouleau PA, McCollough CH, Bouxsein ML, Khosla S 2004 Population-based study of age and sex differences in bone volumetric density, size, geometry, and structure at different skeletal sites. *J Bone Miner Res* **19**(12):1945-54.
172. van der Meulen MC, Ashford MW, Jr., Kiratli BJ, Bachrach LK, Carter DR 1996 Determinants of femoral geometry and structure during adolescent growth. *J Orthop Res* **14**(1):22-9.
173. Beck TJ, Stone KL, Oreskovic TL, Hochberg MC, Nevitt MC, Genant HK, Cummings SR 2001 Effects of current and discontinued estrogen replacement therapy on hip structural geometry: the study of osteoporotic fractures. *J Bone Miner Res* **16**(11):2103-10.

174. Lee KC, Jessop H, Suswillo R, Zaman G, Lanyon LE 2004 The adaptive response of bone to mechanical loading in female transgenic mice is deficient in the absence of oestrogen receptor-alpha and -beta. *J Endocrinol* **182**(2):193-201.
175. Hoff AO, Catala-Lehnen P, Thomas PM, Priemel M, Rueger JM, Nasonkin I, Bradley A, Hughes MR, Ordonez N, Cote GJ, Amling M, Gagel RF 2002 Increased bone mass is an unexpected phenotype associated with deletion of the calcitonin gene. *J Clin Invest* **110**(12):1849-57.
176. Suda T, Ueno Y, Fujii K, Shinki T 2003 Vitamin D and bone. *J Cell Biochem* **88**(2):259-66.
177. Martin TJ, Seeman E 2008 Bone remodelling: its local regulation and the emergence of bone fragility. *Best Pract Res Clin Endocrinol Metab* **22**(5):701-22.
178. Goltzman D, Miao D, Panda DK, Hendy GN 2004 Effects of calcium and of the Vitamin D system on skeletal and calcium homeostasis: lessons from genetic models. *J Steroid Biochem Mol Biol* **89-90**(1-5):485-9.
179. Nemere I, Larsson D 2002 Does PTH have a direct effect on intestine? *J Cell Biochem* **86**(1):29-34.
180. Quarles LD 2008 Endocrine functions of bone in mineral metabolism regulation. *J Clin Invest* **118**(12):3820-8.
181. Ahima RS, Osei SY 2004 Leptin signaling. *Physiol Behav* **81**(2):223-41.
182. Leininger GM 2009 Location, location, location: the CNS sites of leptin action dictate its regulation of homeostatic and hedonic pathways. *Int J Obes (Lond)* **33 Suppl 2**:S14-7.
183. Stepan CM, Crawford DT, Chidsey-Frink KL, Ke H, Swick AG 2000 Leptin is a potent stimulator of bone growth in ob/ob mice. *Regul Pept* **92**(1-3):73-8.
184. Cornish J, Callon KE, Bava U, Lin C, Naot D, Hill BL, Grey AB, Broom N, Myers DE, Nicholson GC, Reid IR 2002 Leptin directly regulates bone cell function in vitro and reduces bone fragility in vivo. *J Endocrinol* **175**(2):405-15.
185. Geusens PP, Boonen S 2002 Osteoporosis and the growth hormone-insulin-like growth factor axis. *Horm Res* **58 Suppl 3**:49-55.
186. Toogood AA 2003 Growth hormone (GH) status and body composition in normal ageing and in elderly adults with GH deficiency. *Horm Res* **60**(Suppl 1):105-11.
187. Zofkova I 2003 Pathophysiological and clinical importance of insulin-like growth factor-I with respect to bone metabolism. *Physiol Res* **52**(6):657-79.
188. Skerry TM, Suva LJ 2003 Investigation of the regulation of bone mass by mechanical loading: from quantitative cytochemistry to gene array. *Cell Biochem Funct* **21**(3):223-9.
189. Schaffler MB, Choi K, Milgrom C 1995 Aging and matrix microdamage accumulation in human compact bone. *Bone* **17**(6):521-25.
190. Warden SJ, Gutschlag FR, Wajswelner H, Crossley KM 2002 Aetiology of rib stress fractures in rowers. *Sports Med* **32**(13):819-36.
191. Norrdin RW, Kawcak CE, Capwell BA, McIlwraith CW 1998 Subchondral bone failure in an equine model of overload arthrosis. *Bone* **22**(2):133-9.
192. Murphy NM, Carroll P 2003 The effect of physical activity and its interaction with nutrition on bone health. *Proc Nutr Soc* **62**(4):829-38.
193. Seeman E 2003 The structural and biomechanical basis of the gain and loss of bone strength in women and men. *Endocrinol Metab Clin North Am* **32**(1):25-38.
194. Martin RB 2002 Is all cortical bone remodeling initiated by microdamage? *Bone* **30**(1):8-13.
195. Taylor D, Lee TC 2003 Microdamage and mechanical behaviour: predicting failure and remodeling in compact bone. *J Anat* **203**(2):203-11.
196. Ahlborg HG, Johnell O, Turner CH, Rannevik G, Karlsson MK 2003 Bone loss and bone size after menopause. *N Engl J Med* **349**(4):327-34.

197. Seeman E 2001 During aging, men lose less bone than women because they gain more periosteal bone, not because they resorb less endosteal bone. *Calcif Tissue Int* **69**(4):205-8.
198. Laib A, Ruegsegger P 1999 Calibration of trabecular bone structure measurements of in vivo three-dimensional peripheral quantitative computed tomography with 28-microm-resolution microcomputed tomography. *Bone* **24**(1):35-9.
199. Laib A, Hauselmann HJ, Ruegsegger P 1998 In vivo high resolution 3D-QCT of the human forearm. *Technol Health Care* **6**(5-6):329-37.
200. Laib A, Hildebrand T, Hauselmann HJ, Ruegsegger P 1997 Ridge number density: a new parameter for in vivo bone structure analysis. *Bone* **21**(6):541-6.
201. Muller R, Hildebrand T, Ruegsegger P 1994 Non-invasive bone biopsy: a new method to analyse and display the three-dimensional structure of trabecular bone. *Phys Med Biol* **39**(1):145-64.
202. Khosla S, Riggs BL, Atkinson EJ, Oberg AL, McDaniel LJ, Holets M, Peterson JM, Melton LJ, 3rd 2006 Effects of sex and age on bone microstructure at the ultradistal radius: a population-based noninvasive in vivo assessment. *J Bone Miner Res* **21**(1):124-31.
203. Aaron JE, Makins NB, Sagreiya K 1987 The microanatomy of trabecular bone loss in normal aging men and women. *Clin Orthop Relat Res* (215):260-71.
204. Silva MJ, Gibson LJ 1997 Modeling the mechanical behavior of vertebral trabecular bone: effects of age-related changes in microstructure. *Bone* **21**(2):191-9.
205. Riggs BL, Melton LJ, Robb RA, Camp JJ, Atkinson EJ, McDaniel L, Amin S, Rouleau PA, Khosla S 2008 A population-based assessment of rates of bone loss at multiple skeletal sites: evidence for substantial trabecular bone loss in young adult women and men. *J Bone Miner Res* **23**(2):205-14.
206. Silbermann M, Weiss A, Reznick AZ, Eilam Y, Szydel N, Gershon D 1987 Age-related trend for osteopenia in femurs of female C57BL/6 mice. *Compr Gerontol [A]* **1**(1):45-51.
207. Weiss A, Arbell I, Steinhagen-Thiessen E, Silbermann M 1991 Structural changes in aging bone: osteopenia in the proximal femurs of female mice. *Bone* **12**(3):165-72.
208. Bar-Shira-Maymon B, Coleman R, Cohen A, Steinhagen-Thiessen E, Silbermann M 1989 Age-related bone loss in lumbar vertebrae of CW-1 female mice: a histomorphometric study. *Calcif Tissue Int* **44**(1):36-45.
209. Mautalen CA, Vega EM, Einhorn TA 1996 Are the etiologies of cervical and trochanteric hip fractures different? *Bone* **18**(3 Suppl):133S-137S.
210. Schaadt O, Bohr H 1988 Different trends of age-related diminution of bone mineral content in the lumbar spine, femoral neck, and femoral shaft in women. *Calcif Tissue Int* **42**(2):71-6.
211. Halloran BP, Ferguson VL, Simske SJ, Burghardt A, Venton LL, Majumdar S 2002 Changes in bone structure and mass with advancing age in the male C57BL/6J mouse. *J Bone Miner Res* **17**(6):1044-50.
212. Ferguson VL, Ayers RA, Bateman TA, Simske SJ 2003 Bone development and age-related bone loss in male C57BL/6J mice. *Bone* **33**(3):387-98.
213. Somerville JM, Aspden RM, Armour KE, Armour KJ, Reid DM 2004 Growth of C57BL/6 mice and the material and mechanical properties of cortical bone from the tibia. *Calcif Tissue Int* **74**(5):469-75.
214. Perkins SL, Gibbons R, Kling S, Kahn AJ 1994 Age-related bone loss in mice is associated with an increased osteoclast progenitor pool. *Bone* **15**(1):65-72.
215. Kodama Y, Dimai HP, Wergedal J, Sheng M, Malpe R, Kutilek S, Beamer W, Donahue LR, Rosen C, Baylink DJ, Farley J 1999 Cortical tibial bone volume in two strains of mice: effects of sciatic neurectomy and genetic regulation of bone response to mechanical loading. *Bone* **25**(2):183-90.

216. Turner CH, Hsieh YF, Muller R, Bouxsein ML, Baylink DJ, Rosen CJ, Grynpas MD, Donahue LR, Beamer WG 2000 Genetic regulation of cortical and trabecular bone strength and microstructure in inbred strains of mice. *J Bone Miner Res* **15**(6):1126-31.
217. Akhter MP, Cullen DM, Pedersen EA, Kimmel DB, Recker RR 1998 Bone response to in vivo mechanical loading in two breeds of mice. *Calcif Tissue Int* **63**(5):442-9.
218. Chen C, Kalu DN 1999 Strain differences in bone density and calcium metabolism between C3H/HeJ and C57BL/6J mice. *Bone* **25**(4):413-20.
219. Kalu DN, Chen C 1999 Ovariectomized murine model of postmenopausal calcium malabsorption. *J Bone Miner Res* **14**(4):593-601.
220. Bouxsein ML, Myers KS, Shultz KL, Donahue LR, Rosen CJ, Beamer WG 2005 Ovariectomy-induced bone loss varies among inbred strains of mice. *J Bone Miner Res* **20**(7):1085-92.
221. Beamer WG, Donahue LR, Rosen CJ, Baylink DJ 1996 Genetic variability in adult bone density among inbred strains of mice. *Bone* **18**(5):397-403.
222. Kaye M, Kusy RP 1995 Genetic lineage, bone mass, and physical activity in mice. *Bone* **17**(2):131-5.
223. Jepsen KJ, Pennington DE, Lee YL, Warman M, Nadeau J 2001 Bone brittleness varies with genetic background in A/J and C57BL/6J inbred mice. *J Bone Miner Res* **16**(10):1854-62.
224. Tommasini SM, Morgan TG, van der Meulen M, Jepsen KJ 2005 Genetic variation in structure-function relationships for the inbred mouse lumbar vertebral body. *J Bone Miner Res* **20**(5):817-27.



CHAPTER 2

Osteoporosis and decline in stem cells in prematurely aging DNA repair deficient trichothiodystrophy mice

Karin E.M. Diderich¹, Claudia Nicolaije², Jan H. Waarsing³, Judd S. Day³, Renata M.C. Brandt¹, Arndt F. Schilling^{4,5}, Matthias Priemel⁴, Sander M. Botter^{1,2}, Harrie Weinans³, Gijsbertus T.J. van der Horst¹, Jan H.J. Hoeijmakers¹, and Johannes P.T.M. van Leeuwen²

¹MGC Dept. of Cell Biology & Genetics, Center for Biomedical Genetics, Erasmus MC, ²Dept. of Internal Medicine, Erasmus MC, ³Dept. of Orthopaedics, Erasmus MC, 3000 DR Rotterdam, The Netherlands, ⁴Center of Biomechanics and Skeletal Biology, Dept. Trauma Surgery, University Medical Center Hamburg Erppendorf, 20246 Hamburg, Germany, ⁵Biomechanics Section, Hamburg University of Technology, 21073 Hamburg, Germany

Abstract

Trichothiodystrophy (TTD) is a rare, autosomal recessive Nucleotide Excision Repair (NER) disorder caused by mutations in components of the dual functional NER/basal transcription factor TFIIH. TTD mice, carrying a patient-based point mutation in the *Xpd* gene, strikingly resemble many features of the human syndrome and exhibit signs of premature aging. Here we show that female TTD mice exhibit accelerated bone aging from 39 weeks onwards as well as lack of periosteal apposition leading to reduced bone strength. Prior to 39 weeks long bones of wild type and TTD mice are identical excluding a developmental defect. Albeit that bone formation is decreased, osteoblasts in TTD mice retain bone-forming capacity as in vivo PTH treatment leads to increased cortical thickness. In vitro bone marrow cell cultures showed that TTD osteoprogenitors retain the capacity to differentiate into osteoblasts. However, after 13 weeks of age TTD females show decreased bone nodule formation. No differences in osteoclasts or bone resorption were detected. In conclusion, TTD mice show premature bone aging, which is preceded by a decrease in mesenchymal stem cells/ osteoprogenitors and a change in systemic factors, identifying DNA damage and repair as key determinants for osteoporosis by influencing osteogenesis and bone metabolism.

Introduction

TTD is a rare, autosomal recessive DNA repair disorder in which patients present an array of symptoms, including photosensitivity, ichthyosis, brittle hair and nails (hallmark feature), impaired intelligence, decreased fertility, short stature and a severely reduced life span (1-3). In addition, skeletal abnormalities have been described (2,4-11). A significant proportion of TTD patients also exhibit marked photosensitivity, due to impaired repair of UV-induced DNA lesions. Complementation analysis of UV-sensitive TTD patients revealed the involvement of three genes (*XPB*, *XPD* and *TTDA*), encoding subunits of the dual functional DNA repair/basal transcription factor TFIIH (12). This 10-subunit protein complex is involved in the Nucleotide Excision Repair (NER) pathway, as well as in the initiation of transcription by RNA polymerases I and II (13-17). NER consists of a complex 'cut and patch' type reaction involving ~30 proteins and is comprised of 2 sub-pathways, differing in the initial steps of DNA damage recognition. Global genome NER removes a wide class of helix-distorting DNA damage (e.g. UV-induced photoproducts) from the overall genome. This pathway is primarily important for preventing DNA damage-induced mutations and thereby for preventing cancer. The second sub-pathway called transcription-coupled NER focuses on the preferential excision of lesions in the transcribed strand of active genes that actually block transcription elongation, to allow rapid resumption of arrested gene expression and thereby promoting cell survival after genotoxic stress (18,19). This sub-pathway is thought to counteract the cytotoxic consequences of DNA damage. TFIIH is as DNA helix opener implicated in both NER sub-pathways as well as in transcription initiation by promoter opening to allow the RNA polymerase to get hold of the transcribed strand for transcription elongation.

We have generated a mouse model in which we precisely mimicked a causative point mutation in the essential *XPD* gene of a TTD patient (TTD1BEL, mutation at the protein level R²²W) (20). TTD mice have a phenotype that strikingly resembles the symptoms of TTD patients and they were found to exhibit several premature aging-like features. Although TTD was not recognized as a segmental premature aging syndrome, some of the features observed in the mouse model were also incidentally reported in patients: deterioration of renal, liver and heart tissues, lymphoid depletion, reduced hypodermal fat, aortic sarcopenia, skeletal abnormalities and an (in patients strongly, in mice moderately) reduced life span (4-11,21-23). For instance, Price and co-workers reported a patient who at the age of 7 years showed decreased bone density in the distal bones on roentgenographic examination (10). Chapman reported a 5-year old child who exhibited decreased bone density in the distal limbs and osteopenia in the most distal parts (9).

In postmenopausal women, accelerated loss of predominantly trabecular bone, due to increased number and activity of osteoclasts, is followed by a slow continuous phase of decrease in bone mass in which the density of trabecular bone reduces and cortical bone thins, leading to an increased fracture risk (24-28). This is partly counteracted by increased

periosteal apposition (29), i.e. bone formation on the outside of the bone (periosteum), a critical process that continues throughout life (26,27,30). Periosteal apposition is thought to be a response to the loss of trabecular bone as well as endosteal resorption and aims to maintain bone strength by increasing the bone perimeter (31). The mechanisms underlying these age-related changes are poorly understood.

To assess the contribution of deficiencies in DNA repair/basal transcription in skeletal aging and to determine to which extent the progeroid features in the mouse and human disorder truly reflect *bona fide* aging we decided to thoroughly examine the skeletal aging as this process has been amply characterized in normal aging. The TTD mouse model may provide a unique tool to study aging and bone metabolism and to assess the impact of DNA repair on skeletal aging.

Materials & Methods

Mice and bones

The cohort of wild type and TTD female mice included 8 animals per age group per genotype. Mice were sacrificed at 13-week intervals up to an age of 104 and 78 weeks for wild type and TTD mice respectively. All mice were on a C57BL/6J background, maintained on a 12:12 h light-dark cycle and fed ad libitum with 'rat and mouse breeder and grower diet' from Special Diet's Services (minimal 0.5% Ca and 0.3% Pi). The animals were injected intra-peritoneal with calcein (10 µg /g body weight) 10 and 3 days before sacrifice in order to study the bone formation occurring in one week. After anaesthetization with isoflurane, blood was collected by an orbital puncture; subsequently the mice were killed by cervical dislocation. Femurs and tibiae were isolated and were either snap frozen in liquid nitrogen and stored at -80°C or fixed in Burkhardt, which was replaced by 70% ethanol after 3 days. As required by Dutch law, formal permission to generate and use genetically modified animals was obtained from the responsible local and national authorities. All animal studies were approved by an independent Animal Ethical Committee (Dutch equivalent of the IACUC).

Micro-computed tomography

Fixed tibiae from wild type and TTD mice of different ages (n = 4-6 per group) were scanned by micro-computed tomography (µCT) from proximal end to mid-diaphysis using the SkyScan 1072 microtomograph (SkyScan, Antwerp, Belgium) with a voxel size of 8.82 µm. The reconstructed data sets were segmented using an automated algorithm based on local thresholds (32). Three-dimensional (3D) morphometric analysis of the bone was performed using freely available software of the 3D-Calculator project (<http://www.erasmusmc.nl/orthopaedie/research/labor/downloads>). For all mice a standardized metaphyseal – diaphyseal area (3.7-6.9 mm from the proximal end; Figure 1) was selected for analysis. This area mainly

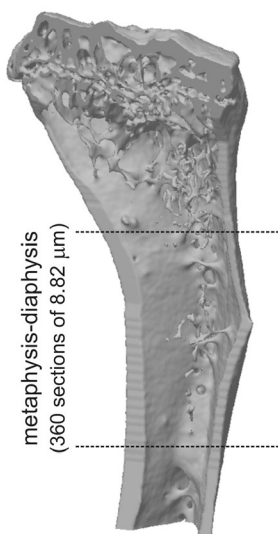


Figure 1: Area of interest for micro-computed tomography analyses.

360 sections of 8,82 μm were analysed in the metaphyseal-diaphyseal area of tibiae from the aging-cohort of wild type and TTD mice.

consists of cortical bone and to a much lesser extent of trabecular bone. This precluded reliable analyses of trabecular bone parameters separately. The parameter bone volume we present reflects mainly cortical bone including the few trabeculae present. In addition, 3D thickness distribution (33), cortical thickness, periosteal perimeter and endocortical volume were determined. Polar moment of inertia (measure of the geometrical distribution and a proxy for mechanical stiffness and strength per transverse cross-section) was determined to analyse the consequence of differences in geometry.

Histomorphometric analysis

To assess dynamic histomorphometric indices, mice received intraperitoneal injections with calcein 10 days and 3 days prior to sacrifice. One tibia of each mouse was dehydrated in ascending alcohol concentrations and embedded in poly-methylmetacrylate (PMMA) as described previously (34). Sections of 5 μm were cut in the sagittal plane on a Microtec rotation microtome (Techno-Med GmbH, Munich, Germany) and stained by toluidine blue, van Gieson/von Kossa and Giemsa procedures as described (34). Parameters of static and dynamic histomorphometry were quantified on these undecalcified proximal tibia sections. Osteocyte numbers were counted and expressed per bone area (per mm^2) according to standardized protocols (35) using the OsteoMeasure histomorphometry system (Osteometrics Inc., Atlanta, Georgia, USA). For each animal, the bone formation rate was determined by fluorochrome (calcein) measurements using two non-consecutive 12 μm -sections per animal.

Mechanical testing

Defrosted femurs from 13, 26, 52 and 78-week old wild type and TTD females as well as from 104-week-old wild type females (5-8 mice/group) were excised from the soft tissues. Femurs were tested in a three-point bending assay using a Lloyd LRX mechanical test frame, constructed with 3mm hemi-cylindrical supports with a 9 mm total span. The femurs were aligned such that the neutral axis was parallel to the sagittal plane (i.e. the femoral head was in the horizontal plane and the posterior aspect of the condyles were facing down). The lesser trochanter was used as a reference point and aligned with one of the two supports. All samples were preconditioned for 5 cycles to 2N at a rate of 0.01 mm/s before testing to failure at a rate of 0.02mm/s.

Backscatter Scanning Electron Microscopy

Processing and analyses were done as described previously (36). In short, from each group (i.e. 26, 52 and 78-week-old wild type and TTD mice) the distal halves of the femurs used for mechanical testing were embedded in blocks of MMA, such that each block contained one distal femur from each genotype and age group. Within a block, all femurs were placed within a plane, such that the longitudinal lateral-medial plane of the femurs coincided with the plane of embedding. Embedding several samples in one block enabled us to image these samples within one scanning electron microscopy (SEM) session, thus decreasing the variance in the measurements.

After embedding, the blocks were cut in two on an electric band saw (Exakt, Norderstedt, Germany), resulting in a slab of plastic with two parallel surfaces, parallel to the plane of embedding of the femurs. Starting from the posterior side of the bones, material was removed using an automatic grinding system (Buehler Phoenix 4000) with p400 grid paper until an interior surface, halfway between the ventral and dorsal external surfaces, was exposed. To reduce the roughness of the surface the blocks were ground with p1200 paper followed by polishing using 3 μm diamond paste with polishing paper (Buehler Texmet 1000). The resulting surface had a roughness (R_a) smaller than 0.05 μm . The blocks were cleaned, sonicated and sputter coated with a thin layer of carbon (Bio-Rad Temcarb Carbon Coater, Bio-Rad Microscience Division) to enable conduction of the electron beam to the sample surface.

Backscatter SEM images were taken of trabecular bone of the metaphyseal and epiphyseal regions of each bone sample, and of the cortex using methods described in detail previously (36). The images were taken at an accelerating voltage of 25 kV, a working distance of 17 mm and 50x magnification. Before and after imaging calibration images were taken of an aluminum standard embedded in each block and of the MMA material. The equivalent Z-value (atomic number) of the MMA was obtained by calibration with aluminum ($Z=13$) and carbon ($Z=6$) standards (Micro Analysis Consultants).

From each image the histogram of equivalent Z-values was calculated of which the mean value represented the mean mineralization of the bone tissue (37).

Tartrate-resistant acid phosphatase assay

Bone resorption was determined by measuring serum tartrate resistant acid phosphatase (TRAP) levels using the TRAP assay purchased from SBA Sciences (Turku, Finland).

Bone marrow isolation, cell culture and cell culture staining

Bone marrow was collected by spinning down the bone marrow into an eppendorf tube at 5000rpm for 2 min. Erythrocytes were lysed using erylisis buffer (1.55M NH_4Cl , 0.1M KHCO_3 , 1mM EDTA (10x)) and cells were washed and seeded at 1.000.000 cells/well (12 wells) for osteoblasts, 100.000 cells/well (96 wells) for osteoclasts and 750.000 cells/well, for adipocytes (24 wells). Cells were cultured at 37°C and 5% CO_2 in a humidified atmosphere in either osteogenic (α -MEM (GIBCO, Paisley, UK) supplemented with P/S, 1.8 mM CaCl_2 (Sigma), Amphotericin B (250 ng/ml, Sigma) and 15% heat-inactivated FCS (GIBCO)), osteoclastogenic (MEM (GIBCO, Paisley, UK) supplemented with P/S, amphotericin B (250 ng/ml, Sigma) and 10% heat-inactivated FCS (GIBCO)) or adipogenic (D-MEM (GIBCO, Paisley, UK) supplemented with P/S, amphotericin B (250 ng/ml, Sigma) and 15% heat-inactivated FCS (GIBCO)) medium. Addition of β -Glycerophosphate (10mM) and Vitamin C (50 μM) from day 3 onwards induced osteoblast differentiation. Osteoclast differentiation was induced by adding RANK-L (20ng/ml, R&D systems) and M-SCF (30ng/ml, R&D systems) to the medium starting at day 0. Osteoclast cultures on plastic or bone slices were cultured for 6 days. Adipogenesis was induced after a 3-week expansion phase by adding insulin (0.1 $\mu\text{g}/\text{ml}$, Sigma), indomethacin (1mM, Sigma) and dexamethasone ($1 \times 10^{-7}\text{M}$, Sigma) to the adipogenic medium for another two weeks.

In osteogenic condition bone nodule formation was measured as parameter of mesenchymal stem cell number and bone forming capacity after 14 days of cultures. At day 14 cultures were stopped by washing with PBS, fixated in 70% EtOH for 10 min., rinsed in 0.2M Tris-HCl (pH 9.5) and stained using NBT (100mg/ml) and BCIP (10mg/ml) diluted in Tris-HCl with MgCl_2 in order to detect alkaline phosphatase as measure for bone nodule formation. Colonies were counted by eye and colony surface area was determined by computer analysis (Bioquant software). The reaction was followed by eye and stopped by washing with PBS. In order to detect mineralisation after 21 days osteoblast cultures were washed with PBS, fixed with cold 70% EtOH O/N at 4°C and stained in a saturated Alizarin Red Solution (Alizarin Red S (Sigma) in H_2O pH 4.2). After staining cells were washed with H_2O . Alizarin Red staining was then extracted from the cultures and measured on a plate reader at 405 nm.

Osteoclast cultures were washed in PBS, fixated for 10 min. in 10% formaline and washed with warm H_2O before they were stained for 30 min. using the Sigma Acid phosphatase leukocyte kit (Sigma), using a 1M Tartrate stocksolution instead of the solution supplied by the kit in order to detect TRAP-positive cells. Washing the cells with PBS stopped the reaction. Cultures were photographed and the number of TRAP-positive cells per photograph was determined. Mature osteoclasts were defined as TRAP-positive cells with more than 2 nuclei. Resorption pits on bone slices were visualised by staining them with Coomassie solution

(Phast Gel Blue R tablet, Coomassie R350). Slices were photographed and the resorption area was determined by computational analysis (Image J).

Adipocyte cultures were fixated O/N with 10% formaline, washed with 60% IPOH and stained with Oil-Red O solution (60-40 dilution of Oil-Red O stock solution (Clin-Tech limited) in H₂O) after which the total amount of adipocytes per well was determined.

PTH treatment

Twenty TTD females were weighed at the age of 45 weeks and randomly divided into the following two groups (n=10 per group): subcutaneous injection with human parathyroid hormone(1-34) (Bachem, Germany) (40 µg/kg body weight) in a weekly alternating regimen (PTH); or subcutaneous injection with phosphate buffered saline in a weekly alternating regimen (VEH). Animals were weighed at the start of every injection week. At 65 weeks of age animals were sacrificed and femurs were prepared for µCT scanning.

Statistics

Micro-CT parameters, histomorphometric data, femur length, ultimate load, bone resorption data and parameters of cell culture analyses were compared between the age groups (significance compared to 13 or 26 weeks of age) of both genotypes separately using one-way ANOVAs with Tukey post-hoc test (Graph Pad InStat version 3.05: Graph Pad Software, San Diego California, USA, www.graphpad.com). In addition, the micro-CT parameters, histomorphometric data, femur length, ultimate load, bone resorption data, and parameters of cell culture analyses were compared between genotypes for all age groups separately using unpaired t-tests. For comparisons of the mineralization data between genotypes unpaired t-tests were performed. The P-values of the unpaired t-test are two-tailed.

Results

To study the bone phenotype in normal and premature aging female TTD mice, we performed a systematic cohort study including 8 mice per age group per genotype. A previous study, performed on a hybrid C57BL/6J 129ola genetic background, showed that TTD mice live shorter than wild type mice (21). In a homogeneous C57Bl/6 genetic background we were able to analyse 13, 26, 39, 52, 65 and 78 weeks-old wild type and TTD mice. For wild type control mice we could in addition analyse 91 and 104 weeks old mice.

Bone geometry

First, 3D thickness distribution was analysed using micro-computed tomography (µCT). In tibiae from wild type mice, a gradual progressive decline in 3D thickness distribution was observed with age (Figure 2A). In TTD mice this process was accelerated with a severe decrease

in 3D thickness distribution after 39 weeks of age (Figure 2B). Already at 52 weeks of age, 3D thickness distribution in TTD tibiae reached a level that in wild type mice was only reached at 91 weeks of age (Figure 2C). Thus age-related decrease in bone mass occurred earlier in TTD mice than in wild type mice.

To study this difference in onset of decrease in bone mass in more detail, we analysed specific μ CT parameters. In wild type mice, bone volume gradually decreased with age, only reaching significance at 104 weeks of age at which time a 12% decrease in bone volume compared to 26-week-old wild type bones was observed (Figure 2D). At 26 and 39 weeks of age, tibiae of TTD mice had a bone volume similar to that of wild type mice (Figure 2D). However, in the period thereafter, bone volume rapidly decreased to 31% (78-week-old TTD mice dropping to 69% of the bone volume of 26-week-old TTD mice), which was significantly lower than the 9% decline in age-matched wild type mice at 78 weeks of age (Figure 2D). Already at 52 weeks of age TTD mice reached a bone volume comparable to that of 104-week-old wild

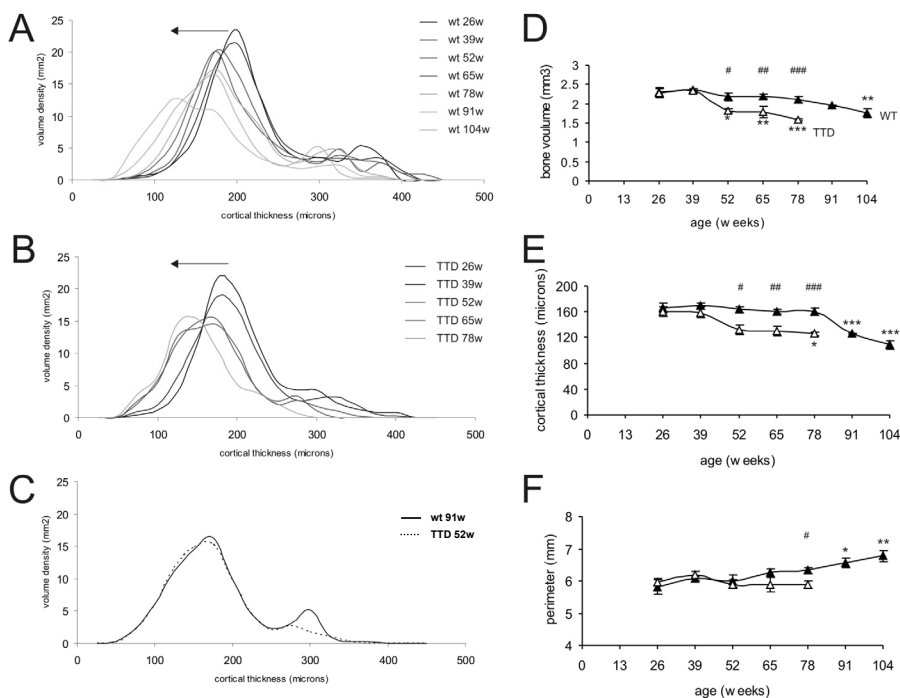


Figure 2: Thickness distribution and bone parameters in wild type and TTD mice.

Cortical thickness distribution in aging wild type (A) and TTD mice (B) with the arrow indicating the direction of change with aging. Comparison of thickness distribution in 52-week-old TTD mice (dotted line) compared to 91-week-old wild type mice (solid line) (C). Bone parameters in aging wild type mice (solid triangles) and TTD mice (open triangles): bone volume (D), cortical thickness (E) and perimeter (F). TTD mice compared to wild type animals: # $p < 0.05$, ## $p < 0.01$, ### $p < 0.001$; TTD mice and wild type animals compared to their 26 week time point: * $p < 0.05$, ** $p < 0.01$, *** $p < 0.001$; error bars represent SEM.

type mice (Figure 2D). In line with bone volume, wild type tibiae maintained their cortical thickness up to 78 weeks of age and showed a decrease thereafter while TTD tibiae already displayed a rapid drop in cortical thickness after 39 weeks of age (Figure 2E).

Next, we analysed the bone perimeter. As depicted in Figure 2F, tibiae from young mice had a similar perimeter (at 26-weeks: 5,80 mm in wild type and 5,96 mm in TTD mice), again indicating normal bone development in TTD mice. From 52 weeks onwards, wild type tibiae showed a progressive increase in perimeter reaching 6,33 mm at 78 weeks (9 % increase) and 6,78 mm at 104 weeks (17% increase). In contrast, TTD mice failed to show an increase in perimeter (5,88 mm at 78 weeks). In 78 week-old wild type mice the perimeter is significantly higher compared to TTD mice (Figure 2F). Thus, TTD mice lack the age-related increase in perimeter as seen in wild type tibiae (Figure 2F).

The endocortical volume was larger in TTD than in wild type mice in the early phase of life but later in life endocortical volume in wild type mice increased and becomes equal to that of TTD mice (data not shown). The temporal dynamics in endocortical volume in wild type mice, showing an increase after 52 weeks, match that observed for perimeter, showing an increase from 52 weeks of age onwards (data not shown). However, periosteal apposition could no longer match the endocortical bone loss in wild type mice after 78 weeks of age leading to a decrease in cortical thickness (Figure 2E).

Histomorphometric analysis of bone

In order to analyse the lack of periosteal expansion in TTD mice in more detail, we examined endosteal and periosteal bone apposition by double labelling studies. In wild type mice both periosteal and endosteal bone formation were present throughout life (Figure 3A). In contrast, in TTD mice endosteal apposition was present whereas periosteal apposition was virtually absent in older TTD mice (Figure 3A). Quantitative analyses revealed no significant difference in endosteal bone formation between 13-week old wild type and TTD mice (Figure 3B). At 39 weeks of age, endosteal bone formation was significantly decreased in TTD mice compared to wild type mice, but after 39 weeks of age endosteal bone formation decreased in wild type mice as well (Figure 3B). At 78 weeks of age, wild type and TTD mice showed a 20-25% decrease in endosteal bone formation when compared to 13-week-old animals. At 13 weeks of age, periosteal apposition showed no significant difference between wild type and TTD mice (Figure 3C). However, after 13 weeks of age, TTD mice showed a dramatic and significant decrease in periosteal apposition compared to wild type mice (Figure 3C). Only at 78 weeks of age, when periosteal apposition in wild type mice decreased as well, there was no significant difference compared to TTD mice anymore (Figure 3C). At that time, however, TTD mice exhibited a 60% decrease in periosteal apposition compared to a 25% decrease in wild type mice when compared to 13-week-old animals. Osteocytes in cortical sections of tibiae of wild type and TTD mice were measured to assess whether a reduced number of osteocytes in TTD mice could play a role in impaired periosteal apposition. However, no significant dif-

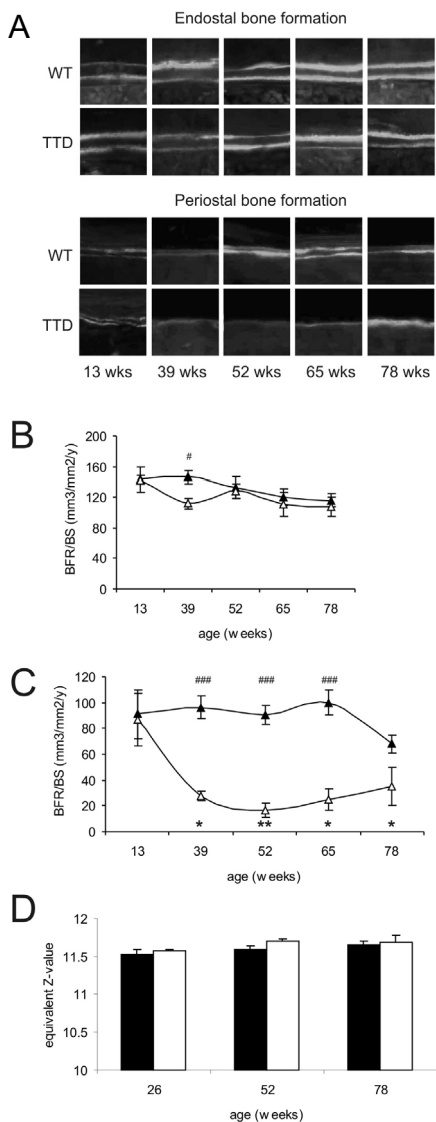


Figure 3: Histomorphometric analysis of cortical bone and Backscatter Scanning Electron Microscopy of wild type and TTD mice.

Calcein double labeling of endosteal and periosteal bone formation in wild type and TTD mice (A). Quantified endosteal apposition (B), quantified periosteal apposition (C) and mineralization status (D) in wild type (solid symbols) and TTD (open symbols) mice. TTD mice compared to wild type mice: # $p < 0.05$, ### $p < 0.001$; TTD mice compared to their 13 week time point: * $p < 0.05$, ** $p < 0.01$; error bars represent SEM.

ference in the number of osteocytes was found between wild type and TTD mice or in aging animals (data not shown). Quantitative Backscatter Scanning Electron Microscopy on femurs

of wild type and TTD mice demonstrated no significant difference in mineralization of the cortex between genotypes or with aging (Figure 3D).

Mechanical testing of bone strength

The overall picture that emerges is that compared to wild type mice, aging TTD mice show an accelerated decrease in bone mass, which initiated between weeks 39 and 52, and that TTD mice lack the age-related increase in perimeter. To analyse the consequence of these geometric changes, we calculated the polar moment of inertia, which is a measure of the geometrical distribution and a proxy for mechanical stiffness and strength per transversal cross-section. This demonstrated that tibiae from wild type mice maintained polar moment of inertia at a constant level throughout life, even at 91 and 104 weeks of age when bone volume and cortical thickness were reduced (Figure 4A). In contrast, TTD tibiae failed to maintain the polar moment of inertia and even showed a progressive decrease throughout life starting at 39 weeks of age (Figure 4A), i.e. 78-week old TTD mice showed a 65% decrease in moment of inertia compared to 39-week old TTD mice whereas the moment of inertia in 78-week old wild type mice showed a 106% increase compared to 39-week old wild type mice. Using a three-point bending assay, we tested whether the differences in polar moment of inertia and lack of periosteal apposition in TTD mice resulted in a difference in bone strength. Femurs from wild type and TTD mice showed a comparable and increasing ultimate fracture load up to 26 weeks of age (Figure 4B). After 26 weeks there was a progressive decrease in ultimate fracture load in both genotypes but this was clearly more prominent and significant in TTD mice showing a 50% decline compared to a 25% decline in wild type mice (Figure 4B). Femurs of TTD mice fractured at a lower ultimate load than femurs of wild type mice, which reached significance in 52 and 78 weeks old animals.

Bone resorption

In wild type and TTD mice the levels of tartrate resistant acid phosphatase (TRAP) were measured to assess whether differences in bone resorption could explain the observed morphometric differences. As expected, bone resorption seemed to increase with aging in both wild type and TTD mice (Figure 4C). In addition, TTD seemed to have higher levels of TRAP. However, no significant differences were observed between genotypes or with age.

Bone marrow cell cultures

To assess whether the differences in bone phenotype in TTD mice are due to an impaired osteoblast and/or osteoclast differentiation we performed bone marrow cultures and assessed the capacity to form osteoblasts and adipocytes from mesenchymal stem cells as well as osteoclasts from hematopoietic stem cells for wild type and TTD mice of various ages. The number of TRAP-positive osteoclasts was similar in 13-weeks-old wild type and TTD cultures (Figure 5A). In the following period wild type but not TTD mice showed a significant decline

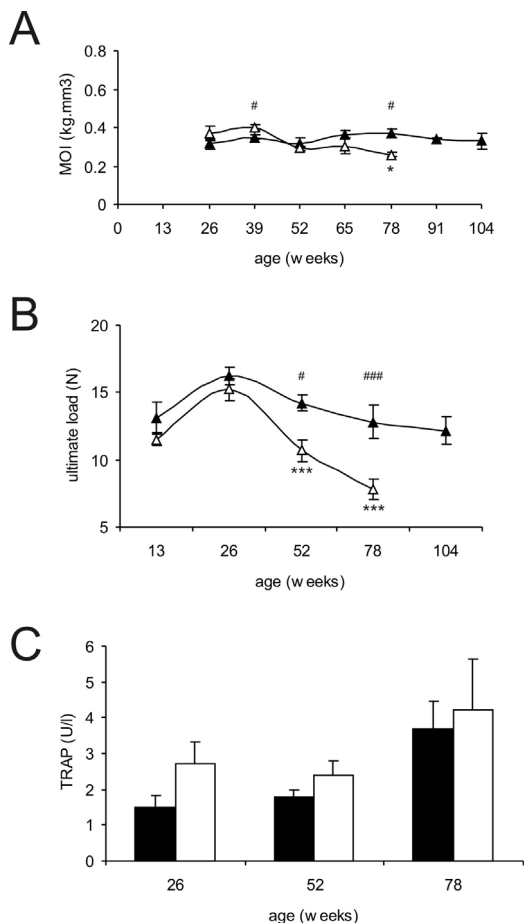


Figure 4: Mechanical testing and TRAP assay in wild type and TTD mice.

Polar moment of inertia in tibiae (A), ultimate load applied on femurs (B) and serum TRAP levels (C) of wild type (solid symbols) and TTD (open symbols) mice. TTD mice compared to wild type animals: # $p < 0.05$, ### $p < 0.001$; TTD and wild type mice compared to their 26 week time point: * $p < 0.05$, *** $p < 0.001$; error bars represent SEM.

in the number of osteoclasts resulting in a significant higher number of osteoclasts at 26 weeks of age in TTD mice. At later ages the number of osteoclasts was similar in wild type and TTD mice (Figure 5A). The amount of resorption by mature osteoclasts was not significantly different between wild type and TTD (Figure 5B). At 13 weeks of age, the number of bone nodules was similar for wild type and TTD mice (Figure 5C). However, the number of bone nodules in TTD mice showed a rapid decline resulting in significantly lower numbers of bone nodules at 26 and 39 weeks of age compared to wild type mice (Figure 5C). Subsequently, the number of bone nodules in wild type mice also declined resulting in similar numbers as in 45-week old TTD mice (Figure 5C). There was no significant difference in bone nodule size

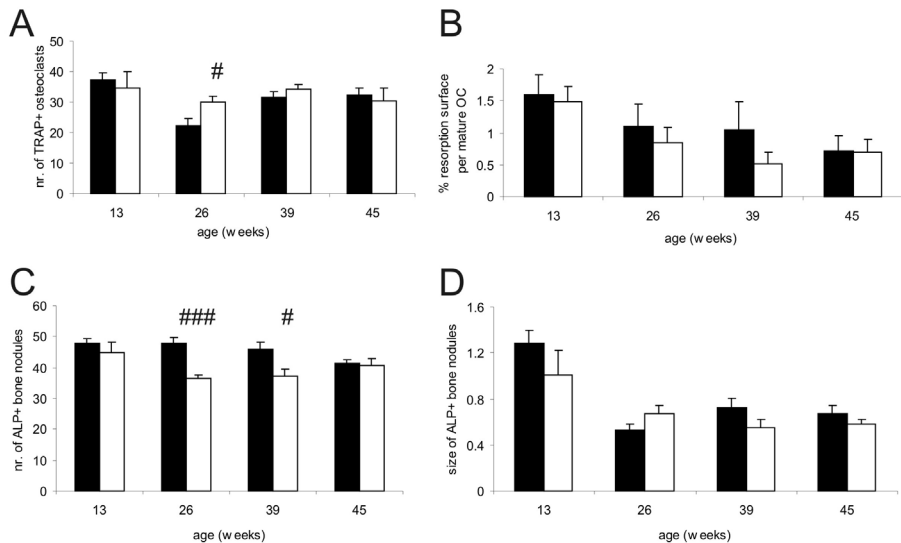


Figure 5: Stem cell cultures of wild type and TTD mice.

Analyses of osteoclast and osteoblast differentiation capacity in bone marrow cell cultures in wild type (solid bars) and TTD mice (open bars). Number of TRAP-positive osteoclasts (A), resorption surface per mature osteoclast (B), number of alkaline phosphatase-positive bone nodules (C) and size of alkaline phosphatase-positive bone nodules (D). TTD mice compared to wild type animals: # $p < 0.05$, ### $p < 0.001$; error bars represent SEM.

between wild type and TTD mice at any age (Figure 5D). Both wild type and TTD nodules mineralized but no significant differences between the genotypes could be detected at any age (data not shown). Similarly, both wild type and TTD mice were able to form adipocytes but no significant differences between the genotypes could be detected at any age (data not shown).

PTH treatment

Albeit with an accelerated decrease in bone nodule formation the bone marrow cultures of TTD mice retained their capacity to generate osteoblasts and form bone. To investigate whether this bone forming capacity is still present and can be stimulated *in vivo* as well, we analyzed the effect of intermittent PTH treatment on bone structure in TTD mice. PTH treatment was started at 45 weeks of age, i.e. after the accelerated bone loss has started. Cortical thickness showed an increase after 20 weeks intermittent PTH treatment as can be seen from the right-shift in the 3D-thickness distribution (Figure 6A). The perimeter was not significantly changed by PTH treatment (data not shown). Although endocortical volume showed a decrease as expected from the increase in cortical thickness and unchanged perimeter, the decrease in endocortical volume after PTH treatment did not reach significance

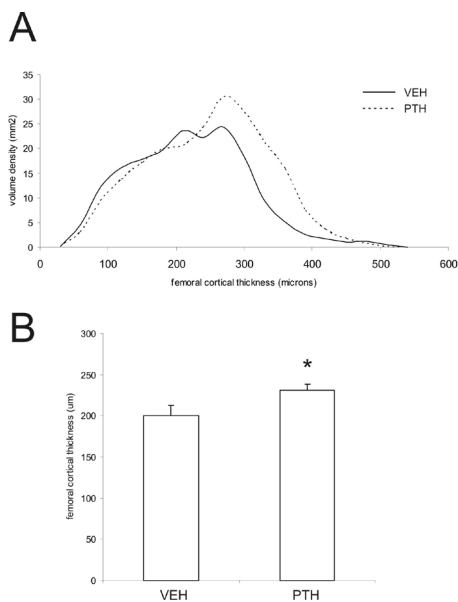


Figure 6: PTH treatment in TTD mice.

Cortical thickness distribution (A) and cortical thickness (B) in femora from PTH treated (PTH) and control (VEH) TTD mice. * $p < 0.05$; error bars represent SEM.

(data not shown). The increase in cortical thickness as well as the increase in trabecular bone volume were significant (Figure 6B and data not shown).

Discussion

TTD mice display features of premature aging in many organs and tissues (21,23), but the progeroid symptoms do not affect all tissues to the same extent. In fact, paradoxically, a detailed, systematic large cohort analysis revealed that some organs and tissues even exhibit features resembling caloric restriction and delayed ageing. For instance, the occurrence of cataract in the eyes in TTD mice was found to be significantly less compared to the isogenic wild type control mice kept under the same conditions (23). This extends the notion that all human progeroid syndromes are segmental (38), i.e. that multiple organs suffer from rapid aging, yet others seem relatively unaffected and as shown by TTD mice may even age slower than wild type controls. Microarray expression analysis of various accelerated aging mice revealed a strong parallel with expression profiles of normal aging (39). To examine at the level of physiology, whether TTD mice are indeed a *bona fide* model for aging and to rule out that it is a developmental disorder, we examined in great detail the effect of aging on bone

parameters of female wild type mice as well as progeroid TTD mice. The systematic analysis uncovered the consequence of a defect in DNA repair and basal transcription on the velocity of age-related skeletal changes and assessed to which extent the skeletal abnormalities reflect normal bone aging.

Normal skeletal development but accelerated skeletal aging in progeroid TTD mice

It should be emphasized that by all parameters measured bone develops normally in TTD female mice, i.e. bone volume, cortical thickness and perimeter are similar in wild type and TTD mice up to 39 weeks of age. In addition, similar numbers of osteoblasts and osteoclasts in bone marrow cultures as well as periosteal apposition are present up to at least 13-weeks of age. This observation excludes a developmental defect as explanation for the TTD phenotype and is in line with other studies on TTD mice (23).

After 39 weeks of age profound accelerated decrease in bone volume is observed in TTD mice. The decrease in bone volume and cortical thickness in TTD mice is almost 40 weeks ahead of that in wild type mice. This accelerated form of natural bone aging strongly underlines the premature aging phenotype of TTD mice.

Notably, the decrease in bone volume is paralleled by an accelerated decrease in bone strength in TTD mice after 26 weeks of age; i.e. an ultimate fracture load as observed in 52-week-old TTD mice was only noticed in 104-week-old wild type mice (Figure 4B). An important mechanism underlying the accelerated decrease in bone strength is that in TTD mice the larger endocortical volume is not compensated by an increase in age-related periosteal apposition and perimeter as seen in wild type mice. The accelerated decrease in bone strength does not appear to be due to a change in mineralization grade of the matrix as assessed by quantitative Backscatter Scanning Electron Microscopy analyses nor due to increased bone resorption as assessed by measurement of serum TRAP.

Lack of periosteal apposition as a cause of decreased bone strength in TTD mice

The lack of effective periosteal apposition in TTD mice is intriguing as it is a localized phenomenon. Despite the important role of periosteal apposition in establishing structural strength during growth and in maintaining strength during aging, little is known about the mechanism and control of periosteal apposition (40). Currently, it is tempting to speculate that, with aging, increased bending stress on the outer surface of bone (due to endosteal bone loss and subsequent cortical thinning) leads to the stimulation of periosteal bone apposition (41-43). The force of mechanical bending and torsion varies linearly with the distance from the neutral axis and therefore bending stress is larger on the periosteal side of the bone (44). Mechanical loading could thus influence periosteal apposition and a change in mechanical loading could consequently affect this process. In wild type mice we see the perfect coupling between thinning of the cortex, increase in endocortical volume, the presence of periosteal apposition and increase in perimeter. In TTD mice this coupling is absent. As TTD mice, in

contrast to wild type mice do not accumulate fat with aging, the difference in weight (23) might contribute to the difference in periosteal apposition. However, we could not detect an obvious correlation between body weight and perimeter (unpublished observations). In addition, it should be noted that controversy exists regarding the influence of fat mass versus muscle mass on bone formation ((45) and references therein). Moreover, in mice a relationship between body weight and femur, vertebral and phalangeal bone parameters has not been found (46). TTD mice may provide an excellent tool to study periosteal apposition and to unravel the underlying mechanisms.

DNA repair defect and bone marrow stem cells in TTD mice

With regard to the accelerated decrease in bone formation and bone mass, the deficiency of DNA damage repair is very likely to have a causative effect. DNA lesions e.g. induced by free radicals, which are a byproduct of normal metabolism, are incompletely repaired by DNA-repair deficient TTD mice (21). The increased damage load will lead to dysfunctional senescent cells or will cause apoptosis (47). Indeed, TTD mice appear to exhibit a decreased spontaneous tumor formation rate likely at least in part by an increased rate of apoptosis (23,48), which protects from cancer but at the same time likely accelerates aging. An increased rate of apoptosis can therefore be expected to cause accelerated depletion of stem cells or early progenitor cells leading to a disturbed osteoblasts and adipocyte differentiation from mesenchymal stem cells and osteoclasts derived from the hematopoietic stem cell lineage. A decrease in mesenchymal stem cell number or disturbed differentiation is suggested by the fact that TTD mice lack abdominal fat mass (49). As the structural differences in bone became apparent after 39 weeks we analysed bone marrow mesenchymal and hematopoietic stem cell differentiation in the period around this age starting at 13 weeks of age. Osteogenic analyses of the bone marrow cultures demonstrated an accelerated decrease in bone nodule formation implicating an accelerated reduction in the number of mesenchymal stem cells that can differentiate into osteoblasts that precedes the decrease in bone mass. The absence of differences in size of the bone nodules shows that the proliferative capacity of the stem cells present is not changed in TTD mice. These data might indicate that DNA damage levels in TTD mice reach a critical threshold in (mesenchymal) stem cells between 13 and 26 weeks, which translates into reduced numbers of differentiated osteoblasts and a bone phenotype between 39 and 52 weeks of age. Although we only studied bone marrow cultures up to 45 weeks, bone nodule formation in wild type mice seems to decrease starting at 45 weeks of age. This is in line with data from the literature; it was shown previously that old mice had significantly fewer stem cells with osteogenic potential than young animals (50,51). In humans, the number of stem cells with osteogenic potential was shown to decrease already at young age (52-54). Only at 26 weeks of age a significant difference in *in vitro* osteoclast formation was observed with TTD mice having an increased osteoclast number without a difference in resorption capacity. This together with the decreased osteoblast differentiation at 26 weeks of

age may explain the decrease in bone volume and structure as first observed after 39 weeks. Obviously, definite proof that the observed accelerated decrease in mesenchymal stem cells in TTD mice is due to accumulation of DNA damage as a consequence of deficient DNA repair is lacking and with current technology very difficult to obtain. However, the most plausible scenario is that loss of DNA repair indeed leads to accumulation of otherwise repaired DNA lesions, which triggers cell death and cellular senescence. In the case of bone metabolism this results in an accelerated decrease in mesenchymal stem cells, suppression of growth and differentiation, deranged bone metabolism and inevitably premature loss of bone strength as shown by the mechanical testing. Although there is an accelerated decrease in bone nodule formation, the current data show that TTD bone marrow mesenchymal stem cells retain bone forming capacity. This is further substantiated by the *in vivo* intermittent PTH treatment studies. Intermittent PTH administration to TTD mice demonstrated an increase in cortical thickness implicating that the stem cells/osteoblasts can still be stimulated to form bone. Considering the above mentioned relationship between DNA repair and apoptosis, it is interesting to note that PTH has been reported to inhibit osteoblast apoptosis (55,56). The PTH effect on cortical thickness in TTD mice appears to be the result of increased endosteal bone formation and not periosteal apposition, as perimeter was not significantly changed. Interestingly, a recent study showed differences in mechanism by which intermittent PTH treatment increases bone formation at the endosteal and at the periosteal surface (57). The increase in endocortical osteoblasts after intermittent PTH treatment is predominantly due to attenuated osteoblast apoptosis (57). In periosteal bone where the rate of osteoblast apoptosis is low, PTH does not increase the number of osteoblasts by attenuating apoptosis, but by exerting pro-differentiating and/or pro-survival effects on post-mitotic pre-osteoblasts (57). These data are suggestive for different age-related mechanisms at the endosteal and periosteal level. The adipocyte cultures support the fact that the intrinsic differentiation capacity of mesenchymal stem cells is not affected. *In vivo* TTD mice lack fat accumulation, but *in vitro* normal adipocyte differentiation is observed. Overall these observations point to an altered systemic environment in TTD mice. Currently, it should be concluded that the observed accelerated skeletal aging observed in TTD mice is the result from a combination of an accelerated decline in the number of osteogenic stem cells together with altered systemic influences.

In conclusion, we demonstrate that the increased and accelerated decrease in bone mass in DNA repair-deficient TTD mice is a premature aging feature, which implies that the other aging-like features in TTD mice and patients may also represent *bona fide* premature aging symptoms and which in a broader context substantiates the importance of DNA repair in healthy aging. Proper DNA repair, notably transcription-coupled repair, is thus required to maintain optimal bone characteristics and strength as long as possible. Prevention and/or limitation of DNA damage may therefore be novel targets for prevention or therapy of osteoporosis and to maintain healthy, strong bones. The TTD mouse mutant constitutes a valid

model for bone aging and the absence of periosteal apposition provides for identification of new targets for maintaining bone strength with aging.

References

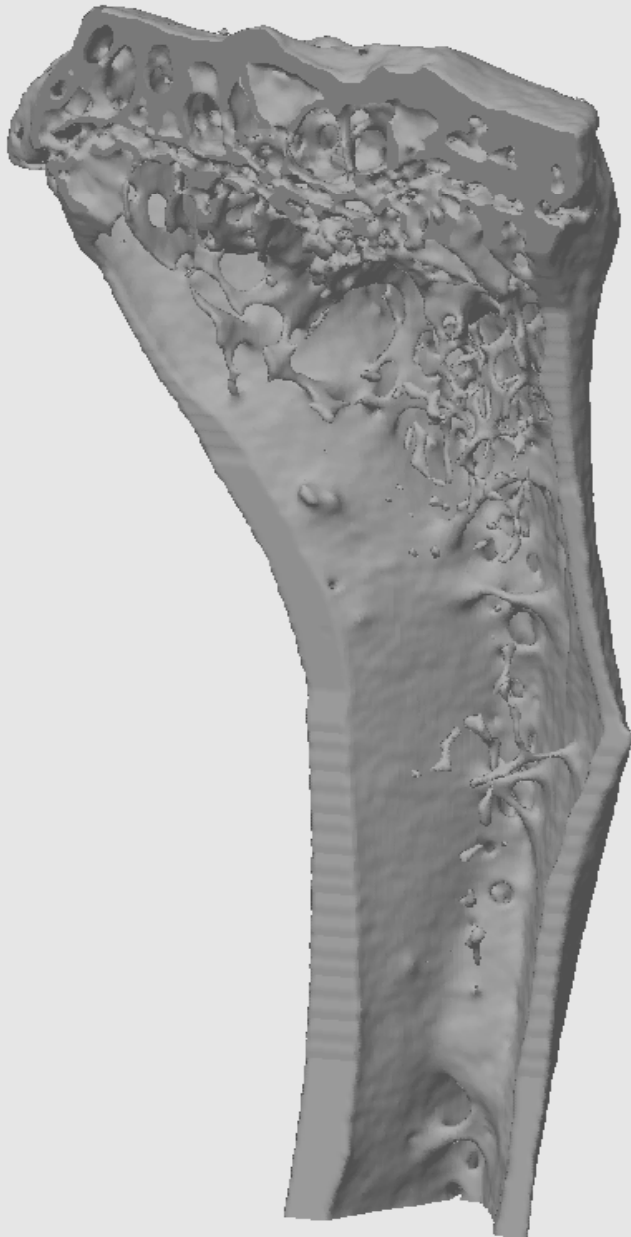
1. Bootsma D, Kraemer KH, Cleaver JE, Hoeijmakers JHJ 1998 Nucleotide excision repair syndromes: xeroderma pigmentosum, Cockayne syndrome and trichothiodystrophy. In: Vogelstein B, Kinzler KW (eds.) *The genetic basis of human cancer*. McGraw-Hill, New York, pp 245-74.
2. Itin PH, Sarasin A, Pittelkow MR 2001 Trichothiodystrophy: update on the sulfur-deficient brittle hair syndromes. *J Am Acad Dermatol* **44**(6):891-920; quiz 921-43. Botta E, Nardo T, Broughton BC, Marinoni S, Lehmann AR, Stefanini M 1998 Analysis of mutations in the XPD gene in Italian patients with trichothiodystrophy: site of mutation correlates with repair deficiency, but gene dosage appears to determine clinical severity. *Am J Hum Genet* **63**(4):1036-48.
4. Wakeling EL, Cruwys M, Suri M, Brady AF, Aylett SE, Hall C 2004 Central osteosclerosis with trichothiodystrophy. *Pediatr Radiol* **34**(7):541-6.
5. Toelle SP, Valsangiacomo E, Boltshauser E 2001 Trichothiodystrophy with severe cardiac and neurological involvement in two sisters. *Eur J Pediatr* **160**(12):728-31.
6. Kousseff BG, Esterly NB 1988 Trichothiodystrophy, IBIDS syndrome or Tay syndrome? *Birth Defects Orig Artic Ser* **24**(2):169-81.
7. Przedborski S, Ferster A, Goldman S, Wolter R, Song M, Tonnesen T, Pollitt RJ, Vamos E 1990 Trichothiodystrophy, mental retardation, short stature, ataxia, and gonadal dysfunction in three Moroccan siblings. *Am J Med Genet* **35**(4):566-73.
8. Civitelli R, McAlister WH, Teitelbaum SL, Whyte MP 1989 Central osteosclerosis with ectodermal dysplasia: clinical, laboratory, radiologic, and histopathologic characterization with review of the literature. *J Bone Miner Res* **4**(6):863-75.
9. Chapman S 1988 The trichothiodystrophy syndrome of Pollitt. *Pediatr Radiol* **18**(2):154-6.
10. Price VH, Odom RB, Ward WH, Jones FT 1980 Trichothiodystrophy: sulfur-deficient brittle hair as a marker for a neuroectodermal symptom complex. *Arch Dermatol* **116**(12):1375-84.
11. McCuaig C, Marcoux D, Rasmussen JE, Werner MM, Gentner NE 1993 Trichothiodystrophy associated with photosensitivity, gonadal failure, and striking osteosclerosis. *J Am Acad Dermatol* **28**(5 Pt 2):820-6.
12. Giglia-Mari G, Coin F, Ranish JA, Hoogstraten D, Theil A, Wijgers N, Jaspers NG, Raams A, Argentini M, van der Spek PJ, Botta E, Stefanini M, Egly JM, Aebersold R, Hoeijmakers JH, Vermeulen W 2004 A new, tenth subunit of TFIIH is responsible for the DNA repair syndrome trichothiodystrophy group A. *Nat Genet* **36**(7):714-9.
13. Chalut C, Moncollin V, Egly JM 1994 Transcription by RNA polymerase II: a process linked to DNA repair. *Bioessays* **16**(9):651-5.
14. Seroz T, Hwang JR, Moncollin V, Egly JM 1995 TFIIH: a link between transcription, DNA repair and cell cycle regulation. *Curr Opin Genet Dev* **5**(2):217-21.
15. Hoeijmakers JH, Egly JM, Vermeulen W 1996 TFIIH: a key component in multiple DNA transactions. *Curr Opin Genet Dev* **6**(1):26-33.
16. Svejstrup JQ, Vichi P, Egly JM 1996 The multiple roles of transcription/repair factor TFIIH. *Trends Biochem Sci* **21**(9):346-50.
17. Hwang JR, Moncollin V, Vermeulen W, Seroz T, van Vuuren H, Hoeijmakers JH, Egly JM 1996 A 3' → 5' XPB helicase defect in repair/transcription factor TFIIH of xeroderma pigmentosum group B affects both DNA repair and transcription. *J Biol Chem* **271**(27):15898-904.
18. Hoeijmakers JH 2001 Genome maintenance mechanisms for preventing cancer. *Nature* **411**(6835):366-74.

19. Hanawalt PC 2002 Subpathways of nucleotide excision repair and their regulation. *Oncogene* **21**(58):8949-56.
20. de Boer J, de Wit J, van Steeg H, Berg RJ, Morreau H, Visser P, Lehmann AR, Duran M, Hoeijmakers JH, Weeda G 1998 A mouse model for the basal transcription/DNA repair syndrome trichothiodystrophy. *Mol Cell* **1**(7):981-90.
21. de Boer J, Andressoo JO, de Wit J, Huijman J, Beems RB, van Steeg H, Weeda G, van der Horst GT, van Leeuwen W, Themmen AP, Meradji M, Hoeijmakers JH 2002 Premature aging in mice deficient in DNA repair and transcription. *Science* **296**(5571):1276-9.
22. Leupold D 1979 [Ichthyosis congenita, cataract, mental retardation, ataxia, osteosclerosis and immunologic deficiency--a particular syndrome?]. *Monatsschr Kinderheilkd* **127**(5):307-8.
23. Wijnhoven SW, Beems RB, Roodbergen M, van den Berg J, Lohman PH, Diderich K, van der Horst GT, Vijg J, Hoeijmakers JH, van Steeg H 2005 Accelerated aging pathology in ad libitum fed Xpd(TTD) mice is accompanied by features suggestive of caloric restriction. *DNA Repair (Amst)*.
24. Chan GK, Duque G 2002 Age-related bone loss: old bone, new facts. *Gerontology* **48**(2):62-71.
25. Harada S, Rodan GA 2003 Control of osteoblast function and regulation of bone mass. *Nature* **423**(6937):349-55.
26. Riggs BL, Khosla S, Melton LJ, 3rd 2002 Sex steroids and the construction and conservation of the adult skeleton. *Endocr Rev* **23**(3):279-302.
27. Seeman E 2002 Pathogenesis of bone fragility in women and men. *Lancet* **359**(9320):1841-50.
28. Kawaguchi H, Manabe N, Miyaura C, Chikuda H, Nakamura K, Kuro-o M 1999 Independent impairment of osteoblast and osteoclast differentiation in klotho mouse exhibiting low-turnover osteopenia. *J Clin Invest* **104**(3):229-37.
29. Seeman E 2001 During aging, men lose less bone than women because they gain more periosteal bone, not because they resorb less endosteal bone. *Calcif Tissue Int* **69**(4):205-8.
30. Seeman E 2003 Invited Review: Pathogenesis of osteoporosis. *J Appl Physiol* **95**(5):2142-51.
31. Russo CR, Lauretani F, Seeman E, Bartali B, Bandinelli S, Di Iorio A, Guralnik J, Ferrucci L 2006 Structural adaptations to bone loss in aging men and women. *Bone* **38**(1):112-8.
32. Waarsing JH, Day JS, Weinans H 2004 An improved segmentation method for in vivo microCT imaging. *J Bone Miner Res* **19**(10):1640-50.
33. Hildebrand T, Laib A, Muller R, Dequeker J, Ruegsegger P 1999 Direct three-dimensional morphometric analysis of human cancellous bone: microstructural data from spine, femur, iliac crest, and calcaneus. *J Bone Miner Res* **14**(7):1167-74.
34. Amling M, Priemel M, Holzmann T, Chapin K, Rueger JM, Baron R, Demay MB 1999 Rescue of the skeletal phenotype of vitamin D receptor-ablated mice in the setting of normal mineral ion homeostasis: formal histomorphometric and biomechanical analyses. *Endocrinology* **140**(11):4982-7.
35. Parfitt AM, Drezner MK, Glorieux FH, Kanis JA, Malluche H, Meunier PJ, Ott SM, Recker RR 1987 Bone histomorphometry: standardization of nomenclature, symbols, and units. Report of the ASBMR Histomorphometry Nomenclature Committee. *J Bone Miner Res* **2**(6):595-610.
36. Broderick E, Infanger S, Turner TM, Sumner DR 2005 Depressed bone mineralization following high dose TGF-beta1 application in an orthopedic implant model. *Calcif Tissue Int* **76**(5):379-84.
37. Roschger P, Fratzl P, Eschberger J, Klaushofer K 1998 Validation of quantitative backscattered electron imaging for the measurement of mineral density distribution in human bone biopsies. *Bone* **23**(4):319-26.
38. Martin GM 2005 Genetic modulation of senescent phenotypes in Homo sapiens. *Cell* **120**(4):523-32.

39. van der Pluijm I, Garinis GA, Brandt RM, Gorgels TG, Wijnhoven SW, Diderich KE, de Wit J, Mitchell JR, van Oostrom C, Beems R, Niedernhofer LJ, Velasco S, Friedberg EC, Tanaka K, van Steeg H, Hoeijmakers JH, van der Horst GT 2007 Impaired genome maintenance suppresses the growth hormone--insulin-like growth factor 1 axis in mice with Cockayne syndrome. *PLoS Biol* **5**(1):e2.
40. Seeman E 2003 Periosteal bone formation--a neglected determinant of bone strength. *N Engl J Med* **349**(4):320-3.
41. Akhter MP, Cullen DM, Recker RR 2002 Bone adaptation response to sham and bending stimuli in mice. *J Clin Densitom* **5**(2):207-16.
42. Beck TJ, Stone KL, Oreskovic TL, Hochberg MC, Nevitt MC, Genant HK, Cummings SR 2001 Effects of current and discontinued estrogen replacement therapy on hip structural geometry: the study of osteoporotic fractures. *J Bone Miner Res* **16**(11):2103-10.
43. Lazenby RA 1990 Continuing periosteal apposition. II: The significance of peak bone mass, strain equilibrium, and age-related activity differentials for mechanical compensation in human tubular bones. *Am J Phys Anthropol* **82**(4):473-84.
44. Currey JD 1999 What determines the bending strength of compact bone? *J Exp Biol* **202**(Pt 18):2495-503.
45. Wires KM 2005 Androgens and bone growth: it's location, location, location. *Curr Opin Pharmacol*.
46. Beamer WG, Donahue LR, Rosen CJ, Baylink DJ 1996 Genetic variability in adult bone density among inbred strains of mice. *Bone* **18**(5):397-403.
47. Campisi J 2005 Senescent cells, tumor suppression, and organismal aging: good citizens, bad neighbors. *Cell* **120**(4):513-22.
48. de Boer J, Hoeijmakers JH 1999 Cancer from the outside, aging from the inside: mouse models to study the consequences of defective nucleotide excision repair. *Biochimie* **81**(1-2):127-37.
49. Compe E, Drane P, Laurent C, Diderich K, Braun C, Hoeijmakers JH, Egly JM 2005 Dysregulation of the peroxisome proliferator-activated receptor target genes by XPD mutations. *Mol Cell Biol* **25**(14):6065-76.
50. Bergman RJ, Gazit D, Kahn AJ, Gruber H, McDougall S, Hahn TJ 1996 Age-related changes in osteogenic stem cells in mice. *J Bone Miner Res* **11**(5):568-77.
51. Moerman EJ, Teng K, Lipschitz DA, Lecka-Czernik B 2004 Aging activates adipogenic and suppresses osteogenic programs in mesenchymal marrow stroma/stem cells: the role of PPAR-gamma2 transcription factor and TGF-beta/BMP signaling pathways. *Aging Cell* **3**(6):379-89.
52. D'ippolito G, Schiller PC, Ricordi C, Roos BA, Howard GA 1999 Age-related osteogenic potential of mesenchymal stromal stem cells from human vertebral bone marrow. *J Bone Miner Res* **14**(7):1115-22.
53. Nishida S, Endo N, Yamagiwa H, Tanizawa T, Takahashi HE 1999 Number of osteoprogenitor cells in human bone marrow markedly decreases after skeletal maturation. *J Bone Miner Metab* **17**(3):171-7.
54. Zhou S, Greenberger JS, Epperly MW, Goff JP, Adler C, Leboff MS, Glowacki J 2008 Age-related intrinsic changes in human bone-marrow-derived mesenchymal stem cells and their differentiation to osteoblasts. *Aging Cell* **7**(3):335-43.
55. Jilka RL, Weinstein RS, Bellido T, Roberson P, Parfitt AM, Manolagas SC 1999 Increased bone formation by prevention of osteoblast apoptosis with parathyroid hormone. *J Clin Invest* **104**(4):439-46.

Chapter 2

56. Sowa H, Kaji H, Lu MF, Tsukamoto T, Sugimoto T, Chihara K 2003 Parathyroid hormone-Smad3 axis exerts anti-apoptotic action and augments anabolic action of transforming growth factor beta in osteoblasts. *J Biol Chem* **278**(52):52240-52.
57. Jilka RL, O'Brien CA, Ali AA, Roberson PK, Weinstein RS, Manolagas SC 2009 Intermittent PTH stimulates periosteal bone formation by actions on post-mitotic preosteoblasts. *Bone* **44**(2):275-86.



CHAPTER 3

Age-related skeletal dynamics in DNA repair deficient male trichothiodystrophy mice

Claudia Nicolaije¹, Karin E.M. Diderich², Jan H. Waarsing³, Judd S. Day³, Renata M.C. Brandt², Arndt F. Schilling⁴, Matthias Priemel⁴, Harrie Weinans³, Gijsbertus T.J. van der Horst², Jan H.J. Hoeijmakers² and Johannes P.T.M. van Leeuwen¹

¹Dept of Internal Medicine, Erasmus MC, ²MGC Dept. of Cell Biology & Genetics, Center for Biomedical Genetics, Erasmus MC, ³Dept. of Orthopaedics, Erasmus MC, 3000 DR Rotterdam, The Netherlands, ⁴Dept. of Trauma, Hand, and Reconstructive Surgery, Hamburg University School of Medicine, 20246 Hamburg, Germany

Abstract

The accumulation of DNA damage is one of the main contributors of human tissue aging. Trichothiodystrophy (TTD) mice have a mutation in a DNA repair gene, resulting in a process of accelerated aging. In order to study the effect of accumulated DNA damage on bone development and mesenchymal stem cell differentiation, we used these mice as a model system for our studies. Analysis of bone parameters, measured by micro computed tomography, displayed an overall accelerated aging of male TTD bone. This was accompanied by a rapid 90% decrease in periosteal apposition at 78 weeks and an overall decline in bone strength of about 25% compared to male wild type mice. After 42 weeks, mesenchymal differentiation potential towards the osteoblast lineage was significantly decreased in male TTD mice. Mineralization of osteoblast colonies was not affected. Adipocyte and osteoclast differentiation was not impaired. Our findings reveal the importance of genome stability and proper DNA repair for skeletal aging. The data show a predominant effect of impaired DNA repair at the osteoblast level. An early disruption in the bone formation-bone resorption balance, caused by a decrease in mesenchymal stem cell differentiation towards the osteoblast lineage, can be the basis of accelerated aging of bone in TTD mice. Periosteal apposition, a hallmark of aging long bones and important to maintain bone strength, is strongly reduced in TTD mice implicating an important role for DNA repair in this process albeit that the precise mechanism remains elusive. However, the absence of periosteal apposition provides a tool to unravel this mechanism and to identify new targets to control bone strength. In comparison with their female counterparts, TTD males are not as strongly affected and the dynamics of their accelerated skeletal aging seem to be slightly delayed.

Introduction

Trichothiodystrophy (TTD) is a rare, autosomal recessive DNA repair disorder presenting a wide range of characteristic features like brittle hair and nails, impaired intelligence, short stature, infertility and a severely reduced lifespan. Additionally, skeletal abnormalities have been described (1). Changes in the *XPB*, *XPD* and *TTDA* genes and their proteins, are described to be the underlying cause of TTD (2). These proteins are all components of the TFIIH complex, which is essential in transcription initiation as well as in the Nucleotide Excision Repair (NER) pathway (3).

The NER pathway is activated during global genome repair in order to remove helix-distorting damage. Similarly, it regulates the excision of lesions in the transcribed strand of active genes during transcription. Consequently NER promotes cell survival and prevents DNA damage induced cancer (4,5). Within this complex, multi-factorial pathway TFIIH opens up the DNA helix to allow other proteins to remove the induced damage. *XPB* and *XPD* are the helicases involved in this process (6).

Previously, an *XPD* mouse model was generated that precisely mimics a causative point mutation in the essential *XPD* gene of a TTD patient (7). TTD mice, in a *C57BL/6J* background, have strikingly similar symptoms and show several premature aging-like features (8). Throughout life, both men and women undergo bone loss due to an unbalanced increase in bone resorption. This usually leads to a reduction of trabecular bone and thinner bone cortices, causing osteoporosis and a severe increase in fracture risk (9-11). Men, unlike women miss the rapid bone loss phase caused by reduced hormone levels, but also develop senile osteoporosis; a fact that can be used to gain insight into the mechanisms behind age-related bone loss (10).

Both osteoblasts and osteoclasts, the main players in bone formation and bone resorption are derived from stem cells that populate the bone marrow cavities of long bones. Osteoblasts rise from mesenchymal stem cells (MSC), which can differentiate into a whole range of cells including adipocytes, chondrocytes and myocytes (12). Osteoclasts on the other hand rise from the hematopoietic stem cells (HSC), which also differentiate into blood cells, immune cells and macrophages (13). A disturbance in either of the differentiation pathways could cause a disbalance in the number of osteoblasts and osteoclasts, leading to either excessive bone gain or bone loss.

We studied the impact of DNA repair deficiency on the dynamics of skeletal aging and the osteoblast/ osteoclast balance in male TTD mice by micro computed tomography (μ CT) analysis of bone architecture and analyses of osteoblast and osteoclast differentiation potential in *in vitro* bone marrow cultures.

Material and Methods

Mice and bones

All mice were on a C57BL/6J background and all mice within one cohort were kept under equal conditions. In the μ CT cohort, 8 wild type and TTD mice were sacrificed at 13, 26, 39, 52, 65 and 78 weeks of age. Wild type mice were also kept until 91 and 104 weeks of age but only few TTD mice survived till this age not allowing age-matched analyses at these ages. The animals were injected intra-peritoneal with calcein (10 μ g /g body weight) 10 and 3 days before sacrifice in order to study the bone formation occurring in one week. The mice were killed by cervical dislocation. Femurs and tibiae were isolated and were either snap frozen in liquid nitrogen and stored at -80°C or fixed in Burkhardt, which was replaced by 70% ethanol after 3 days. For bone marrow isolation 10 wild type and TTD mice were sacrificed at 26, 39, 45 and 78 weeks of age. On the day of sacrifice, bones were isolated and were either used for bone marrow isolation, or fixed in Burkhardt or 10% formalin depending on further testing. As required by Dutch law, formal permission to generate and use genetically modified animals was obtained from the responsible local and national authorities. All animal studies were approved by an independent Animal Ethical Committee (Dutch equivalent of the IACUC).

Micro-computed tomography.

Fixed tibiae from wild type and TTD mice of different ages (n = 4-6 per group) were scanned by micro-computed tomography (μ CT) from proximal end to mid-diaphysis using the SkyScan 1072 microtomograph (SkyScan, Antwerp, Belgium) with a voxel size of 8.82 μ m. The reconstructed data sets were segmented using an automated algorithm based on local thresholds (14). Three-dimensional (3D) morphometric analysis of the bone was performed using freely available software of the 3D-Calculator project (<http://www.erasmusmc.nl/orthopaedie/research/labor/downloads>). For all mice a standardized metaphyseal – diaphyseal area (3.7-6.9 mm from the proximal end) was selected for analysis. This area mainly consists of cortical bone and to a much lesser extent of trabecular bone. This precluded reliable analyses of trabecular bone parameters separately. The parameter bone volume we present reflects mainly cortical bone including the trabeculae present. In addition, 3D thickness distribution (15) cortical volume, cortical thickness, and the periosteal perimeter were determined. Polar moment of inertia (MOI; measure of the geometrical distribution and a proxy for mechanical stiffness and strength per transverse cross-section) was determined to analyse the consequence of differences in geometry.

Histomorphometric analysis

To assess dynamic histomorphometric indices, mice received intraperitoneal injections with calcein 10 days and 3 days prior to sacrifice. One tibia of each mouse was dehydrated in ascending alcohol concentrations and embedded in poly-methylmetacrylate (PMMA)

as described previously (16). Sections of 5 μm were cut in the sagittal plane on a Microtec rotation microtome (Techno-Med GmbH, Munich, Germany) and stained by toluidine blue, van Gieson/von Kossa and Giemsa procedures as described (16). Parameters of static and dynamic histomorphometry were quantified on these undecalcified proximal tibia sections. Osteocyte numbers were counted and expressed per bone area (per mm^2) according to standardized protocols (17) using the OsteoMeasure histomorphometry system (Osteometrics Inc., Atlanta, Georgia, USA). For each animal, the bone formation rate was determined by fluorochrome (calcein) measurements using two non-consecutive 12 μm -sections per animal.

Mechanical testing

Defrosted femurs were excised from the soft tissues. Femurs were tested in a three-point bending assay using a Lloyd LRX mechanical test frame, constructed with 3 mm hemicylindrical supports with a 9 mm total span. The femurs were aligned such that the neutral axis was parallel to the sagittal plane. The lesser trochanter was used as a reference point and aligned with one of the two supports. All samples were preconditioned for 5 cycles to 2 N at a rate of 0.01 mm/s before testing to failure at a rate of 0.02 mm/s.

Backscatter Scanning Electron Microscopy

Processing and analyses were done as described previously (18). In short, from each group (i.e. 26, 52 and 78-week-old wild type and TTD mice) the distal halves of the femurs used for mechanical testing were embedded in blocks of MMA, such that each block contained one distal femur from each genotype and age group. Within a block, all femurs were placed within a plane, such that the longitudinal lateral-medial plane of the femurs coincided with the plane of embedding. Embedding several samples in one block enabled us to image these samples within one scanning electron microscopy (SEM) session, thus decreasing the variance in the measurements.

After embedding, the blocks were cut in two on an electric band saw (Exakt, Norderstedt, Germany), resulting in a slab of plastic with two parallel surfaces, parallel to the plane of embedding of the femurs. Starting from the posterior side of the bones, material was removed using an automatic grinding system (Buehler Phoenix 4000) with p400 grid paper until an interior surface, halfway between the ventral and dorsal external surfaces, was exposed. To reduce the roughness of the surface the blocks were ground with p1200 paper followed by polishing using 3 μm diamond paste with polishing paper (Buehler Texmet 1000). The resulting surface had a roughness (R_a) smaller than 0.05 μm . The blocks were cleaned, sonicated and sputter coated with a thin layer of carbon (Bio-Rad Temcarb Carbon Coater, Bio-Rad Microscience Division) to enable conduction of the electron beam to the sample surface.

Backscatter SEM images were taken of trabecular bone of the metaphyseal and epiphyseal regions of each bone sample, and of the cortex using methods described in detail previously (18). The images were taken at an accelerating voltage of 25 kV, a working distance of

17 mm and 50x magnification. Before and after imaging calibration images were taken of an aluminum standard embedded in each block and of the MMA material. The equivalent Z-value (atomic number) of the MMA was obtained by calibration with aluminum (Z=13) and carbon (Z=6) standards (Micro Analysis Consultants).

From each image the histogram of equivalent Z-values was calculated of which the mean value represented the mean mineralization of the bone tissue (19).

Bone marrow isolation, cell culture and cell culture staining

Bone marrow was collected by spinning down the bone marrow into an eppendorf tube at 5000rpm for 2 min. Erythrocytes were lysed using erylisis buffer (1.55M NH₄Cl, 0.1M KHCO₃, 1mM EDTA (10x)) and cells were washed and seeded at 1.000.000 cells/well (12 wells) for osteoblasts, 100.000 cells/well (96 wells) for osteoclasts and 750.000 cells/well, for adipocytes (24 wells). Cells were cultured at 37°C and 5% CO₂ in a humidified atmosphere in either osteogenic (α -MEM (GIBCO, Paisley, UK) supplemented with P/S, 1.8 mM CaCl₂ (Sigma), Amphotericin B (250 ng/ml, Sigma) and 15% heat-inactivated FCS (GIBCO)), osteoclastogenic (MEM (GIBCO, Paisley, UK) supplemented with P/S, amphotericin B (250 ng/ml, Sigma) and 10% heat-inactivated FCS (GIBCO)) or adipogenic (D-MEM (GIBCO, Paisley, UK) supplemented with P/S, amphotericin B (250 ng/ml, Sigma) and 15% heat-inactivated FCS (GIBCO)) medium. Addition of β -Glycerophosphate (10mM) and Vitamin C (50 μ M) from day 3 onwards induced osteoblast differentiation. Osteoclast differentiation was induced by adding RANK-L (20ng/ml, R&D systems) and M-SCF (30ng/ml, R&D systems) to the medium starting at day 0. Osteoclast cultures on plastic or bone slices were cultured for 6 days. Adipogenesis was induced after a 3-week expansion phase by adding insulin (0.1 μ g/ml, Sigma), indomethacin (1mM, Sigma) and dexamethasone (1*10⁻⁷M, Sigma) to the adipogenic medium for another two weeks.

In osteogenic condition bone nodule formation was measured as parameter of mesenchymal stem cell number and bone forming capacity after 14 days of cultures. At day 14 cultures were stopped by washing with PBS, fixated in 70% EtOH for 10 min., rinsed in 0.2M Tris-HCl (pH 9.5) and stained using NBT (100mg/ml) and BCIP (10mg/ml) diluted in Tris-HCl with MgCl₂ in order to detect alkaline phosphatase as measure for bone nodule formation. Colonies were counted by eye and colony surface area was determined by computer analysis (Bioquant software). The reaction was followed by eye and stopped by washing with PBS. In order to detect mineralisation after 21 days osteoblast cultures were washed with PBS, fixed with cold 70% EtOH O/N at 4°C and stained in a saturated Alizarin Red Solution (Alizarin Red S (Sigma) in H₂O pH 4.2). After staining cells were washed with H₂O. Alizarin Red staining was then extracted from the cultures and measured on a plate reader at 405 nm.

Osteoclast cultures were washed in PBS, fixated for 10 min. in 10% formaline and washed with warm H₂O before they were stained for 30 min. using the Sigma Acid phosphatase leukocyte kit (Sigma), using a 1M Tartrate stocksolution instead of the solution supplied by the kit in order to detect TRAP positive cells. Washing the cells with PBS stopped the reaction. Cultures

were photographed and the number of TRAP positive cells per photograph was determined. Resorption pits on bone slices were visualised by staining them with Coomassie solution (Phast Gel Blue R tablet, Coomassie R350). Slices were photographed and the resorption area was determined by computational analysis (Image J).

Adipocyte cultures were fixated O/N with 10% formaline, washed with 60% IPOH and stained with Oil-Red O solution (60-40 dilution of Oil-Red O stock solution (Clin-Tech limited) in H₂O) after which the total amount of adipocytes per well was determined.

Statistics

Micro-CT parameters, histomorphometric data, femur length, ultimate load, bone resorption data and parameters of cell culture analyses were compared between the age groups (significance compared to 13 or 26 weeks of age) of both genotypes separately using one-way ANOVAs with Tukey post-hoc test (Graph Pad InStat version 3.05: Graph Pad Software, San Diego California, USA, www.graphpad.com). In addition, the micro-CT parameters, histomorphometric data, femur length, ultimate load, bone resorption data, and parameters of cell culture analyses were compared between genotypes for all age groups separately using one-way ANOVAs (SPSS.11.0, SPSS software Chicago, USA). For comparisons of the mineralization data between genotypes unpaired t-tests with two-tailed P-values were performed.

Results

Bone architecture

In order to analyse bone dynamics in wild type and TTD mice throughout life we started out by studying the 3D thickness distribution of bone fragments by μ CT analysis. The bones of wild type mice underwent a gradual decline in 3D thickness throughout life (Fig. 1A left panel). In TTD mice this process was accelerated and showed a large decrease after 39 weeks without clear further changes at later ages (Fig. 1A right panel). The acceleration of skeletal aging in TTD mice is even better illustrated in Figure 1B showing the thickness distribution of 52-week-old TTD left of that of 91-week-old wild type mice.

To study this difference in onset of decrease in bone mass in more detail we analysed specific μ CT parameters. Total cortical bone volume decreased gradually in wild type mice throughout life (Fig. 2A). TTD mice followed the same pattern but the decline observed was steeper and led to a significant decrease in cortical volume at 78 weeks compared to wild type mice (Fig. 2A). In neither wild type nor TTD mice significant changes in cortical thickness were observed throughout life (Fig. 2B). TTD mice however had significantly thinner cortices than wild type mice (Fig. 2B). No significant changes in the endocortical volume of either wild type or TTD mice were observed throughout their lives (Fig. 2C). From 39 weeks onwards, TTD mice showed significantly higher endocortical volumes compared to their age-matched

wild type males (Fig. 2C). This was accompanied by a significantly decreased trabecular bone volume fraction (BV/TV) at 26 and 39 compared to wild type mice (Fig. 2D). At 26 weeks of age, wild type mice had a high BV/TV which decreased up to 52 weeks of age after which it stabilized. TTD mice on the other hand started out with a much lower BV/TV, which only slightly declined (Fig. 2D).

Bone strength

Structural changes in bone architecture, like thinner cortices, or changes in matrix deposition can lead to changes in bone strength. To study changes in bone strength, we performed 3 point bending assays on wild type and TTD femurs. Early on we observed no significant differences between 13-week-old wild type and TTD mice (Fig. 3A). Wild type bones showed a gradual decrease in energy required to break throughout life; from 18 N at 13 weeks to 15,5 N at 78 weeks (Fig. 3A). Albeit not significant, already at 13 weeks of age less energy was required in order to break TTD bones compared to wild type bones. Subsequently, a quick drop to about 12,5 N at 26 weeks of age was observed after which the energy required to break TTD bones remained stable up to 78 weeks (Fig. 3A). Starting at 26 weeks of age, significantly less energy was required in order to break TTD bones compared to their wild type counterparts (Fig. 3A).

Quantitative Backscatter Scanning Electron Microscopic analysis on femurs of wild type and TTD males demonstrated no significant difference in mineralization of the cortex between genotypes or with aging (Fig. 3B). In addition, we studied the decrease in bone strength by analysing two additional μ CT parameters related to bone strength: perimeter and MOI. Perimeter and MOI did not differ significantly between wild type and TTD mice throughout most of their life (Fig. 3C,D). Only at 78 weeks of age both perimeter as well as MOI of wild type mice became significantly larger than that of TTD mice (Fig. 3C,D). Following this observation, we assessed the perimeter and MOI in wild type mice of 91 and 104 weeks of age. This demonstrated that after 78 weeks the perimeter of wild type tibiae increased up to 91 weeks of age followed by an increase in MOI (Fig. 3C,D). The observed increase in bone perimeter in old wild type mice can be explained by the natural process of periosteal apposition, which takes place in order to maintain bone strength by depositing new bone on the outside of the cortex in order to make up for the bone that is removed on the inside. To study this process we measured bone formation rates using calcein labeling (Fig. 3E,F). Endosteal bone formation, on the inside of the bone, was largely unaffected in both genotypes throughout life (Fig. 3G). Periosteal apposition on the other hand, was extremely reduced in old TTD mice (Fig. 3H).

Stem Cell Differentiation Potential

Besides a decrease in bone strength and a lack of periosteal apposition, TTD mice have been reported to lack body fat as well (8,20). This suggests that the mesenchymal stem cell (MSC)

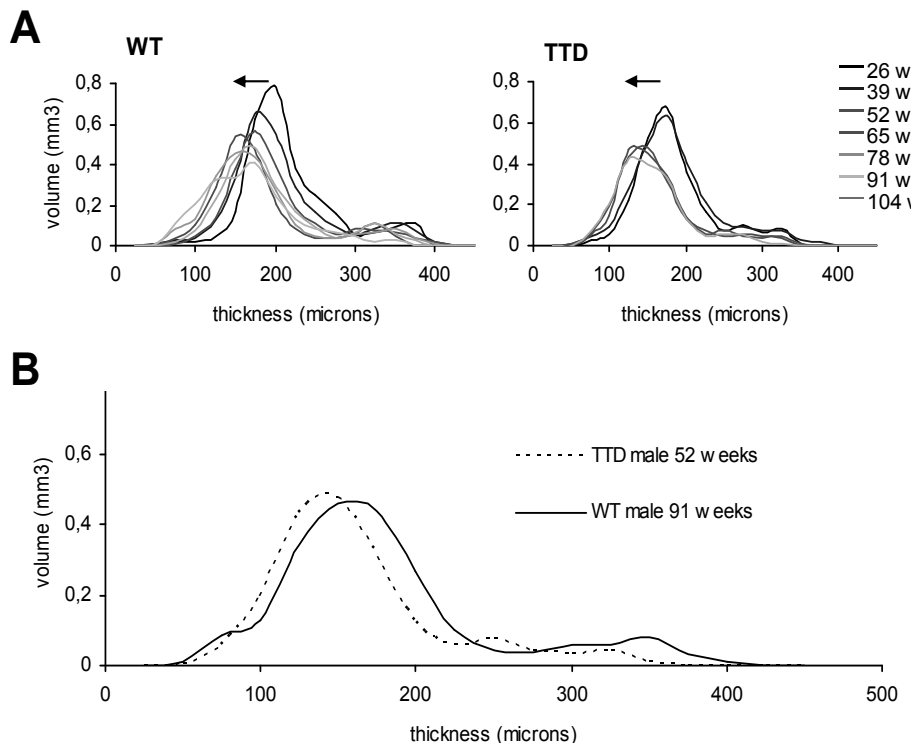


Figure 1: TTD mice show accelerated skeletal aging.

(A) 3D thickness distribution (volume density) in aging male (A left panel) wild type and (A right panel) TTD mice, with the arrow indicating the direction of change with aging. (B) Comparison of thickness distribution in 52-week-old TTD male (dotted line) compared to 91-week-old wild type male (solid line).

differentiation pathway towards osteoblasts and adipocytes might be impaired leading to a decrease in bone and fat formation. In order to study MSC differentiation we set up a new cohort of wild type and TTD mice and isolated bone marrow at 26, 42 and 78 weeks of age and analyzed osteoblast and adipocytes as well as osteoclast differentiation.

Bone nodule formation per se was not affected in *in vitro* TTD cultures, but the number of nodules was significantly reduced in cultures from 42 and 78-week-old TTD mice (Fig. 4A). Both wild type and TTD mice displayed a trend towards reduced bone nodule formation capacity with aging, but this only reached significance in TTD mice (Fig. 4A). Bone nodule size did not differ significantly between wild type and TTD cultures indicating an unaffected proliferation (Fig. 4B). Both wild type and TTD nodules mineralised to the same extent suggesting that mineralisation was not affected in TTD mice (data not shown). In contrast to the number of bone nodules, we did not observe a significant difference between wild type or TTD adipocyte differentiation potential as assessed by the number of lipid-vesicle-forming adipocytes (Fig. 4C).

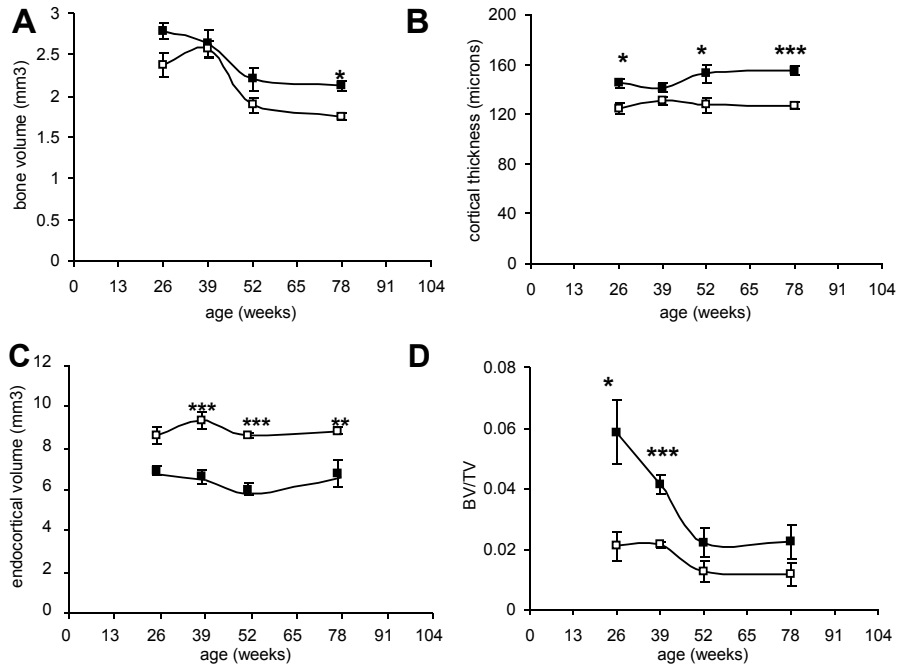


Figure 2: Changes in bone architecture throughout life.

(A-D) Bone parameters in aging wild type (solid squares) and TTD males (open squares). (A) Total bone volume, (B) cortical thickness, (C) endocortical volume, (D) trabecular bone volume fraction (BV/TV). TTD vs. wild type: * $p < 0.05$, ** $p < 0.01$, *** $p < 0.001$; error bars represent SEM.

In parallel to the osteoblast and adipocyte cultures, bone marrow was cultured under osteoclastogenic conditions to assess formation of osteoclasts from hematopoietic stem cells (HSC). The total number of TRAP⁺ osteoclasts found in these *in vitro* cultures was stable throughout life in wild type mice, but significantly decreased in TTD mice (Fig. 4D). When focussing on multinucleated osteoclasts (two nuclei or more), there was no significant difference between wild type and TTD mice although TTD cultures showed a decline in the number of osteoclasts at 78 weeks of age (Fig. 4E). Additionally, osteoclasts were cultured on bone slices to see whether resorption pits could be detected. Since mature osteoclasts are the TRAP⁺ cells responsible for resorption, we calculated the average size of a pit formed by a multinucleated osteoclast (Fig. 4F). For both wild type and TTD mice we observed a decrease in resorbed area with age (Fig. 4F). At none of the ages studied there was a significant difference between wild type and TTD albeit that at both 26 and 42 weeks the resorbed area seemed about twice the size in TTD mice while at 78 weeks it was smaller.

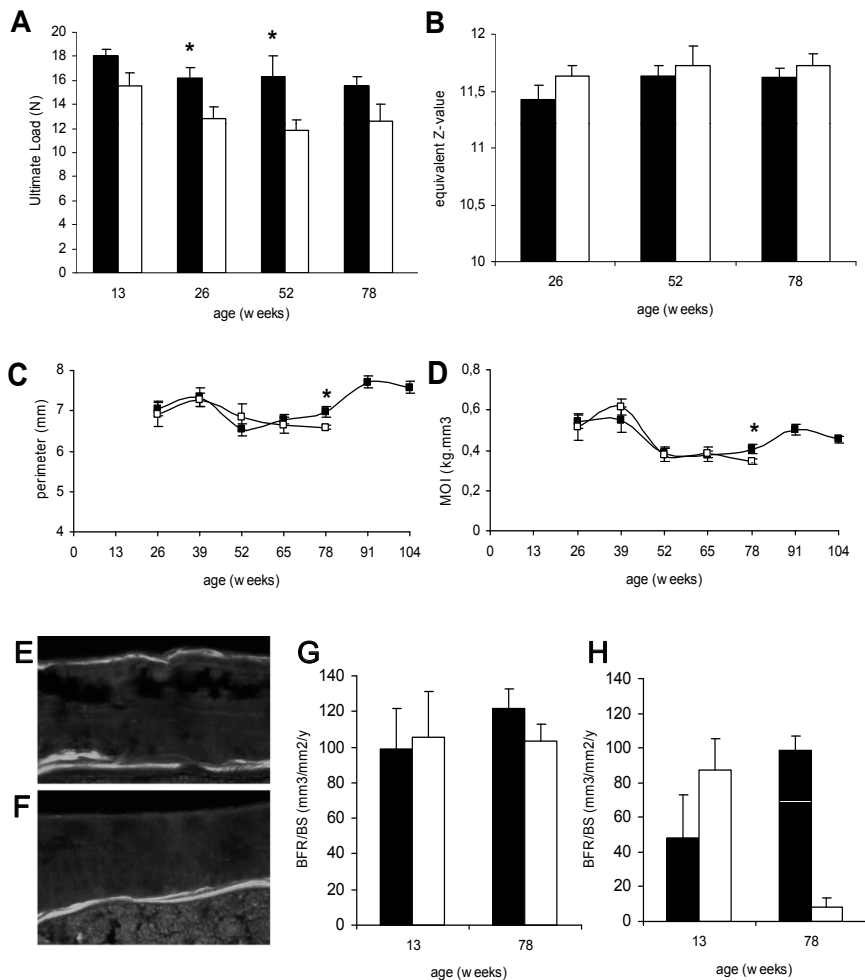


Figure 3: Decreased bone strength in TTD mice.

Bone strength, mineralization and bone formation rates in long bones of aging wild type (solid bars/ symbols) and TTD males (open bars/ symbols). (A) Bone strength depicted as Ultimate Load, (B) bone mineralization, (C) perimeter and (D) MOI. Calcein labelling at sites of periosteal apposition in 78-week-old (E) wild type and (F) TTD mice. (G) Endosteal apposition and (H) periosteal apposition. TTD vs. wild type: ANOVAs * $p < 0.05$, *** $p < 0.001$; error bars represent SEM.

Discussion

In this study, we examined the effect of aging on bone parameters of male wild type mice as well as progeroid TTD males. We showed that a defect in DNA repair and basal transcription leads to accelerated skeletal aging; TTD mice showed an accelerated decrease in 3D thickness distribution, bone volume and bone strength. This is most clearly demonstrated by the

observation that TTD mice reach the same bone volume as wild type males about 40 weeks earlier.

Before discussing our findings it should be emphasized that earlier studies showed that in female TTD mice there is normal early bone development excluding a developmental defect as the cause of our results ((21) and Diderich et al, Chapter 2). However, our current data on male mice show already bone differences, e.g in cortical thickness and BV/TV, starting earlier in life than that observed in female mice. Our observations on cortical thickness and BV/TV in wild type male mice are in line with those reported earlier (22). Whether, in contrast to females, this does reflect developmental differences in male TTD mice is unclear but unlikely as like in females the body weight development is similar for wild type and TTD male mice up to 39 weeks (Diderich et al, Chapter 5). Albeit there are already differences early in life most differences appear later in life or become more pronounced later in life.

At 78 weeks of age, TTD mice show a decreased total bone volume, perimeter and MOI, reduced cortical thickness, and a larger endocortical volume. All these findings point towards a model in which the bone cortex becomes thinner and therefore more fragile at an accelerated speed. This is supported by the lack of periosteal apposition in TTD mice. Together these findings explain (at least part of) the decrease in bone strength.

Periosteal apposition is an important process during skeletal aging. Bone is added to the outside of the cortex in order to compensate loss at the endocortical side in order to maintain bone strength as long as possible (23,24). Disturbances in periosteal apposition and lack to compensate endocortical bone loss will lead to decreased bone strength and increased fracture risk. Involvement of estradiol, with opposite roles for estrogen receptors α and β , testosterone and mechanical loading in the control of periosteal apposition have been reported (10). However the precise mechanisms underlying these age-related changes in bone and periosteal apposition are still poorly understood. The current studies show an important role for age-related DNA repair for proper periosteal apposition and implicate the importance of limiting DNA damage for maintaining bone strength with aging. Albeit the current data do not provide a mechanism explaining the altered periosteal apposition, the TTD mouse model will provide excellent opportunities to further unravel this important skeletal process with aging.

A significant difference in perimeter and MOI is first observed in 78-week-old wild type and TTD mice. Unfortunately, we do not have many data points past the 78 week mark since TTD mice tend to die around this time point. To be able to take this further in at least wild type mice, we obtained perimeter and MOI analyses from older wild type males. This demonstrated an increase in perimeter and MOI between 78 and 91 weeks after which it stabilized. This implies that the loss of bone strength in aging wild type mice will not be as severe as in TTD mice. This is based on the observations of a significant reduction in perimeter, MOI and strength while periosteal apposition is practically absent strongly indicating that TTD mice over 78 week of age would not show restoration of bone strength, but would have

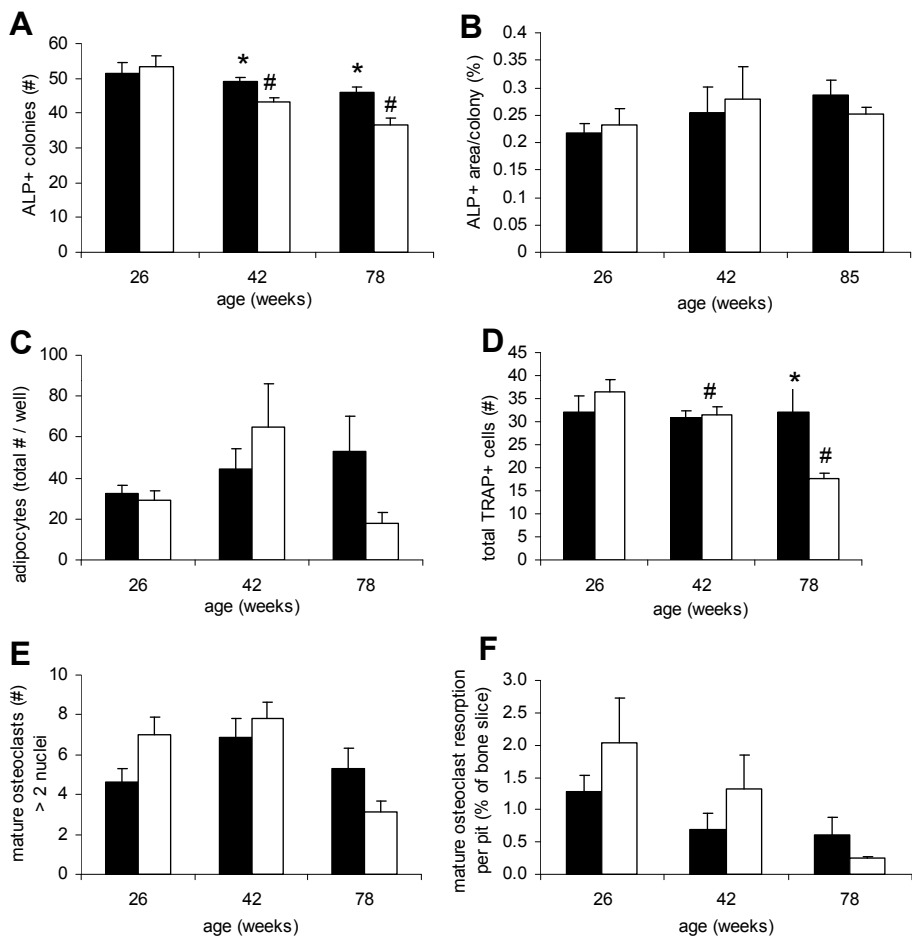


Figure 4: Mesenchymal and hematopoietic stem cell differentiation.

Mesenchymal and hematopoietic stem cell differentiation in aging wild type (solid bars) and TTD males (open bars). (A) Average number of ALP⁺ colonies that rise from bone marrow cultures after 14 days of culture. (B) Average colony size at day 14 of culture. (C) The average number of adipocytes per well. (D) Average number of TRAP positive cells per picture. (E) Average number of mature osteoclasts per picture. (F) Average percentage resorption surface per osteoclast pit per mature osteoclast. TTD vs. wild type: ANOVAs * $p < 0.05$; # value is significantly lower compared to the 26 week time point; error bars represent SEM.

even weaker bones. Our data showing a more or less stable perimeter up to 78 weeks of age are in line with previous reports that showed no change in cross-sectional area after the initial growth phase up to 20 months of age (about 86 weeks) in male wild type mice (22). Apparently, an increase in perimeter is not important to maintain bone strength up to about 86 weeks of age, but becomes important afterwards. The absence of a further increase in perimeter after 91 weeks of age and a decreasing trend in both perimeter and MOI suggest that also in aging wild type mice the process of periosteal apposition to maintain bone strength eventually becomes impaired.

TTD mice have deficient DNA repair which might lead to an increase in cellular DNA damage and an increase in senescent or apoptotic cells. Indeed, it has previously been observed that TTD mice have a decreased tumour formation rate which could protect against cancer, but could also cause accelerated aging (21,25). An increase in damage and apoptosis might lead to a decrease in overall stem cell numbers or precursor cells and changes in their differentiation potential. Both mesenchymal and hematopoietic stem cell differentiation are complex processes that go through a number of precursor stages and are tightly regulated in order to maintain a balance between the number of osteoblasts and osteoclasts present at one time (13,26,27). Additionally the balance between osteoblast and adipocyte formation within the mesenchymal lineage is known to be regulated and can be tipped either way by disrupting one of the differentiation pathways (28). An age-related decrease in osteoblast colony formation potential has been previously described and can also be observed in our aging wild type mice (29).

Our current, *ex vivo* TTD bone marrow cultures showed a reduction in the capacity to form bone nodules and a trend towards reduced osteoclast activity with age. The reduction in osteoblasts and osteoclasts with age may indicate a reduced bone turnover capacity and thereby a reduced capacity to maintain healthy bone in e.g. the case of microcracks. However, this should be proven in further studies focussing on fracture repair. It is tempting to conclude that this is part of the mechanism underlying the observed accelerated skeletal ageing and decrease in bone strength. In addition, earlier in life at 26 and 42 weeks of age the number of multinucleated osteoclasts and resorbed area are higher in TTD mice than in wild type mice which may also contribute to the accelerated bone loss and increased endocortical volume earlier in life. This effect on osteoclasts is supported by FACS analysis of wild type and TTD bone marrow (data not shown) showing a shift in HSC differentiation towards the myeloid lineages in TTD mice. Besides direct effects on MSCs the data on adipocyte development suggest that *in vivo* additional factors are involved to explain the observed phenotype. A very marked characteristic of TTD mice is complete lack of fat deposition ((20) Diderich et al., Chapter 5). This would suggest a severely disturbed adipocyte differentiation from MSCs. However, our current data show no difference in development of adipocytes between wild type and TTD males at any age. This means that the capacity of MSC to differentiate into adipocytes is not impaired and that *in vivo* additional signals or absence of signals explain the

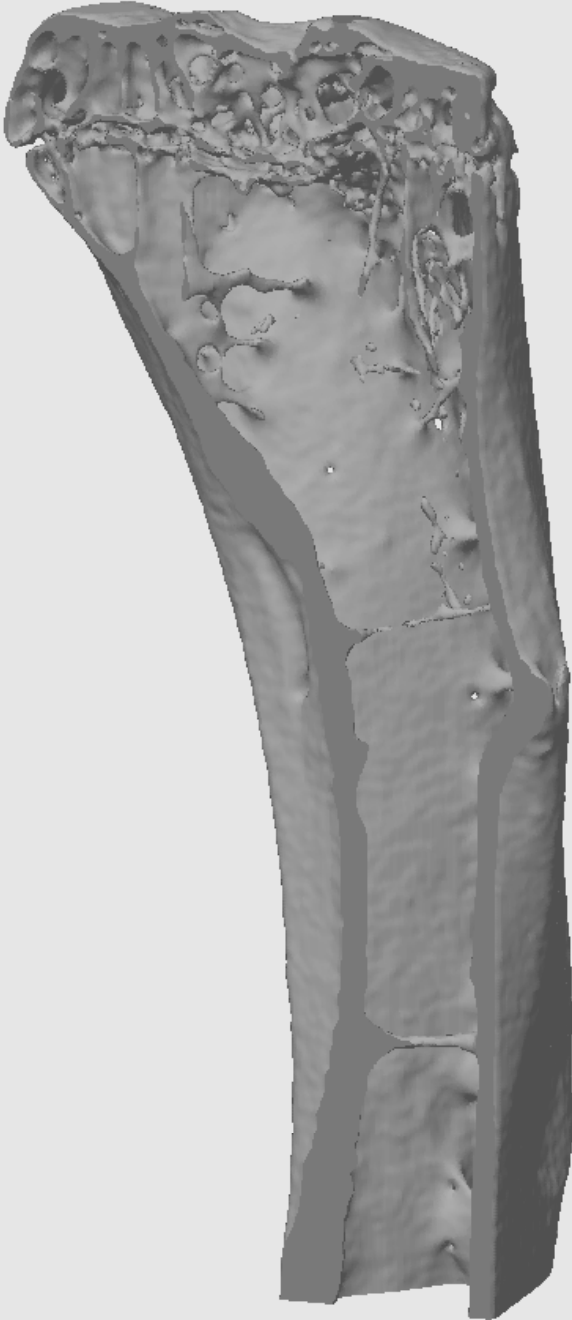
observed fat-less phenotype. At this moment it is elusive which factor(s) form these signals and extensive additional investigation is needed to clarify this. However, it is known that levels of hormones and cytokine and growth factors may change with age and that for example the growth hormone/insulin-like growth factor cascade is impaired in another murine DNA repair deficient mouse model (30). A role for systemic factors in the development of the skeletal phenotype may explain the mild effects on osteoblasts and osteoclasts observed in the *ex vivo* studies.

In conclusion, accumulation of DNA damage due to defective DNA repair causes an acceleration of skeletal aging in male TTD mice. More specifically, aging TTD mice show an accelerated decrease in bone volume and bone strength as well as lack of periosteal apposition. Part of the underlying cause might be the diminished differentiation potential of mesenchymal stem cells towards the osteoblastic lineage, but most likely alterations in additional systemic factors are also implicated. Overall, the data stress the importance of proper DNA repair for healthy skeletal ageing.

References

1. Itin PH, Sarasin A, Pittelkow MR 2001 Trichothiodystrophy: update on the sulfur-deficient brittle hair syndromes. *J Am Acad Dermatol* **44**:891-920.
2. Giglia-Mari G, Coin F, Ranish JA, Hoogstraten D, Theil A, Wijgers N, Jaspers NG, Raams A, Argentini M, van der Spek PJ, Botta E, Stefanini M, Egly JM, Aebersold R, Hoeijmakers JH, Vermeulen W 2004 A new, tenth subunit of TFIIH is responsible for the DNA repair syndrome trichothiodystrophy group A. *Nat Genet* **36**:714-719.
3. Svejstrup JQ, Vichi P, Egly JM 1996 The multiple roles of transcription/repair factor TFIIH. *Trends Biochem Sci* **21**:346-350.
4. Hanawalt PC 2002 Subpathways of nucleotide excision repair and their regulation. *Oncogene* **21**:8949-8956.
5. Hoeijmakers JH 2001 Genome maintenance mechanisms for preventing cancer. *Nature* **411**:366-374.
6. Sung P, Bailly V, Weber C, Thompson LH, Prakash L, Prakash S 1993 Human xeroderma pigmentosum group D gene encodes a DNA helicase. *Nature* **365**:852-855.
7. de Boer J, de Wit J, van Steeg H, Berg RJ, Morreau H, Visser P, Lehmann AR, Duran M, Hoeijmakers JH, Weeda G 1998 A mouse model for the basal transcription/DNA repair syndrome trichothiodystrophy. *Mol Cell* **1**:981-990.
8. de Boer J, Andressou JO, de Wit J, Huijman J, Beems RB, van Steeg H, Weeda G, van der Horst GT, van Leeuwen W, Themmen AP, Meradji M, Hoeijmakers JH 2002 Premature aging in mice deficient in DNA repair and transcription. *Science* **296**:1276-1279.
9. Kawaguchi H, Manabe N, Miyaura C, Chikuda H, Nakamura K, Kuro-o M 1999 Independent impairment of osteoblast and osteoclast differentiation in *klotho* mouse exhibiting low-turnover osteopenia. *J Clin Invest* **104**:229-237.
10. Riggs BL, Khosla S, Melton LJ, III 2002 Sex steroids and the construction and conservation of the adult skeleton. *Endocr Rev* **23**:279-302.
11. Seeman E 2002 Pathogenesis of bone fragility in women and men. *Lancet* **359**:1841-1850.
12. Pittenger MF, Mackay AM, Beck SC, Jaiswal RK, Douglas R, Mosca JD, Moorman MA, Simonetti DW, Craig S, Marshak DR 1999 Multilineage potential of adult human mesenchymal stem cells. *Science* **284**:143-147.
13. Metcalf D 2007 Concise review: hematopoietic stem cells and tissue stem cells: current concepts and unanswered questions. *Stem Cells* **25**:2390-2395.
14. Waarsing JH, Day JS, Weinans H 2004 An improved segmentation method for in vivo microCT imaging. *J Bone Miner Res* **19**:1640-1650.
15. Hildebrand T, Laib A, Muller R, Dequeker J, Ruegsegger P 1999 Direct three-dimensional morphometric analysis of human cancellous bone: microstructural data from spine, femur, iliac crest, and calcaneus. *J Bone Miner Res* **14**:1167-1174.
16. Amling M, Priemel M, Holzmann T, Chapin K, Rueger JM, Baron R, Demay MB 1999 Rescue of the skeletal phenotype of vitamin D receptor-ablated mice in the setting of normal mineral ion homeostasis: formal histomorphometric and biomechanical analyses. *Endocrinology* **140**:4982-4987.
17. Parfitt AM, Drezner MK, Glorieux FH, Kanis JA, Malluche H, Meunier PJ, Ott SM, Recker RR 1987 Bone histomorphometry: standardization of nomenclature, symbols, and units. Report of the ASBMR Histomorphometry Nomenclature Committee. *J Bone Miner Res* **2**:595-610.

18. Broderick E, Infanger S, Turner TM, Sumner DR 2005 Depressed bone mineralization following high dose TGF-beta1 application in an orthopedic implant model. *Calcif Tissue Int* **76**:379-384.
19. Roschger P, Fratzl P, Eschberger J, Klaushofer K 1998 Validation of quantitative backscattered electron imaging for the measurement of mineral density distribution in human bone biopsies. *Bone* **23**:319-326.
20. Compe E, Drane P, Laurent C, Diderich K, Braun C, Hoeijmakers JH, Egly JM 2005 Dysregulation of the peroxisome proliferator-activated receptor target genes by XPD mutations. *Mol Cell Biol* **25**:6065-6076.
21. Wijnhoven SW, Beems RB, Roodbergen M, van den BJ, Lohman PH, Diderich K, van der Horst GT, Vijg J, Hoeijmakers JH, van Steeg H 2005 Accelerated aging pathology in ad libitum fed Xpd(TTD) mice is accompanied by features suggestive of caloric restriction. *DNA Repair (Amst)* **4**:1314-1324.
22. Glatt V, Canalis E, Stadmeier L, Bouxsein ML 2007 Age-related changes in trabecular architecture differ in female and male C57BL/6J mice. *J Bone Miner Res* **22**:1197-1207.
23. Russo CR, Lauretani F, Seeman E, Bartali B, Bandinelli S, Di Iorio A, Guralnik J, Ferrucci L 2006 Structural adaptations to bone loss in aging men and women. *Bone* **38**:112-118.
24. Seeman E 2003 Invited Review: Pathogenesis of osteoporosis. *J Appl Physiol* **95**:2142-2151.
25. de Boer J, Hoeijmakers JH 1999 Cancer from the outside, aging from the inside: mouse models to study the consequences of defective nucleotide excision repair. *Biochimie* **81**:127-137.
26. Horowitz MC, Xi Y, Wilson K, Kacena MA 2001 Control of osteoclastogenesis and bone resorption by members of the TNF family of receptors and ligands. *Cytokine Growth Factor Rev* **12**:9-18.
27. Satija NK, Gurudutta GU, Sharma S, Afrin F, Gupta P, Verma YK, Singh VK, Tripathi RP 2007 Mesenchymal stem cells: molecular targets for tissue engineering. *Stem Cells Dev* **16**:7-23.
28. Atmani H, Chappard D, Basle MF 2003 Proliferation and differentiation of osteoblasts and adipocytes in rat bone marrow stromal cell cultures: effects of dexamethasone and calcitriol. *J Cell Biochem* **89**:364-372.
29. Bergman RJ, Gazit D, Kahn AJ, Gruber H, McDougall S, Hahn TJ 1996 Age-related changes in osteogenic stem cells in mice. *J Bone Miner Res* **11**:568-577.
30. van der Pluijm, I, Garinis GA, Brandt RM, Gorgels TG, Wijnhoven SW, Diderich KE, de Wit J, Mitchell JR, van Oostrom C, Beems R, Niedernhofer LJ, Velasco S, Friedberg EC, Tanaka K, van Steeg H, Hoeijmakers JH, van der Horst GT 2007 Impaired genome maintenance suppresses the growth hormone--insulin-like growth factor 1 axis in mice with Cockayne syndrome. *PLoS Biol* **5**:e2-



CHAPTER 4

Increased bone mass in vertebrae of DNA repair deficient trichothiodystrophy mice strongly resembling patients

K. Diderich¹, J. Waarsing³, Arndt F. Schilling⁴, R. Brandt¹, R. Beems⁵, H. Weinans³, G. van der Horst¹, J. Hoeijmakers¹ and J. van Leeuwen²

¹ErasmusMC, Dept. of Cell Biology & Genetics, ²ErasmusMC, Dept. of Internal Medicine, ³ErasmusMC, Dept. of Orthopedics, ⁴Hamburg University, School of Medicine, ⁵National Institute of Public Health and Environment, Post Office Box 1, 3720BA Bilthoven, The Netherlands

Abstract

Trichothiodystrophy (TTD) is a rare, autosomal recessive Nucleotide Excision Repair (NER) disorder caused by mutations in components of the dual functional NER/basal transcription factor TFIIH. TTD mice, carrying a patient-based point mutation in the *Xpd* gene, strikingly resemble many features of the human syndrome and exhibit signs of premature aging. In TTD patients demineralization of long bones and sclerosis of the vertebrae is observed. Previously, we reported accelerated bone loss in the long bones of TTD mice. Here we show that vertebrae of TTD mice exhibit increased bone mass compared to wild type mice. This osteosclerotic phenotype in vertebrae is strikingly similar to the phenotype observed in TTD patients. In addition, it shows that TTD mice exhibit a different pattern of age-related changes in vertebrae compared to long bones. The bone phenotype in mice thus closely resembles the bone phenotype in TTD patients showing osteopenic long bones and osteosclerotic vertebrae.

Introduction

Trichothiodystrophy (TTD) is a rare, autosomal recessive DNA repair/ basal transcription disorder in which patients present an array of symptoms, including photosensitivity, ichthyosis, brittle hair and nails (hallmark feature), impaired intelligence, decreased fertility, short stature, a severely reduced life span and skeletal abnormalities (1-11).

In TTD patients demineralization of long bones and sclerosis of the vertebrae is observed (4,5,8-10,12-14). In 1980 Price et al. reported a boy who developed axial and cranial sclerosis at the age of 4 years and an osteoporotic phenotype in distal bones at the age of 7 years (10). Several years later, Chapman reported a 5-year old boy who exhibited osteosclerosis in the skull, chest, spine and pelvis with a wooly appearance of the trabeculae in addition to osteopenia of the distal limbs (9). In 1989 Civitelli et al. performed further studies in two boys with axial osteosclerosis and mild osteopenia in the extremities and found no abnormalities of mineral homeostasis (8). Wakeling et al. described a boy who showed normal bone density on a chest radiography at the age of 3 months, but increased bone density at the age of 5 years and who consecutively developed a mild kyphosis between 6 and 7 years of age (4). Toelle et al. reported two sisters who showed marked kyphosis before the age of 4 years (5). In conclusion, TTD patients exhibit a difference in bone phenotype in long bones compared to the axial skeleton.

We have generated a mouse model in which we precisely mimicked a causative point mutation in the essential *XPD* gene of a TTD patient (TTD1BEL) (15). TTD mice have a phenotype that strikingly resembles the symptoms of TTD patients and they exhibit several premature aging-like features some of which incidentally reported in patients: deterioration of renal, liver and heart tissues, lymphoid depletion, thymic involution, reduced hypodermal fat, aortic sarcopenia, early infertility in females, a reduced life span and skeletal abnormalities resembling those observed in TTD patients (4-14,16-18). Previously, we reported an analysis of long bones of an aging cohort of female wild type and TTD mice, which showed accelerated bone aging in TTD females demonstrated by an early decrease in bone volume, cortical thickness and strength in long bones (Diderich et al., Chapter 2).

The aim of the current study was to assess whether the TTD mouse skeletal phenotype truly reflects that observed in patients. To achieve this we investigated the axial skeleton in aging female wild type and TTD mice by microcomputed tomography CT (μ CT) and histological analysis and compared it with our previous data on long bones.

Material & Methods

Mice

We generated a cohort of female wild type and TTD mice including 5 mice per age group per genotype. Mice were sacrificed at 39, 52, 65 and 78 weeks. All mice were in a C57Bl/6

background, maintained on a 12:12 h light-dark cycle and fed ad libitum with a standard rodent diet (0.5% Ca and 0.3% Ph). The mice were killed by cervical dislocation. Bones were isolated and fixed in Burkhardt, which was replaced by 70% ethanol after 3 days. As required by Dutch law, formal permission to generate and use genetically modified animals was obtained from the responsible local and national authorities. All animal studies were approved by an independent Animal Ethical Committee (Dutch equivalent of the IACUC).

Micro-CT

Fixed vertebrae from the lumbar spine (L4-L6) of female, wild type and TTD mice of different ages ($n = 5$) were scanned using a SkyScan 1072 microtomograph (SkyScan, Antwerp, Belgium) with isotropic voxelsize of 8.82 μm . Scans were processed and a three-dimensional morphometric analysis of the bone was performed, using software of the 3D-Calculator project (<http://www.erasmusmc.nl/orthopaedie/research/labor/downloads>). Trabecular thickness distribution, trabecular bone volume (BV), total endocortical volume (TV), trabecular bone volume fraction (BV/TV), trabecular number, trabecular thickness, trabecular spacing, Structure Model Index (SMI) and vertebra width were determined. Figure 1 depicts the area in which BV, TV and vertebra width were determined. Measured parameters were expressed according to bone histomorphometry nomenclature (19).

Histomorphometric analysis

After fixation the skeletons were incubated in 70 % ethanol. The lumbar vertebral bodies (L3 to L5) were thereafter dehydrated in ascending alcohol concentrations and embedded in methylmetacrylate as described previously (20). Sections of 5 μm were cut in the frontal plane on a Microtec rotation microtome (Techno-Med GmbH, Munich, Germany). Static histomorphometry was performed according to standardized protocols (21) using the Osteo-Measure histomorphometry system (Osteometrics Inc., Atlanta, Georgia) on lumbar vertebral sections of 5 μm which were stained by the van Gieson / von Kossa staining procedures as described (20).

Statistics

To analyze the changes in the micro-CT parameters and histomorphometric data over time (significance compared to 39 weeks of age) one-way ANOVAs with Tukey post-hoc test were performed using Graph Pad InStat version 3.05 for Windows 95 (Graph Pad Software, San Diego California, USA, www.graphpad.com). For comparisons of the micro-CT parameters and histomorphometric data between genotypes unpaired t-tests were performed per time point using Graph Pad InStat version 3.05 (Graph Pad Software, San Diego California, USA, www.graphpad.com). The P-values of the unpaired t-test are two-tailed. An univariate General Linear Model (SPSS 15.0) was used to analyze the effect of age in the different genotypes as well as the effect of genotype over all ages.

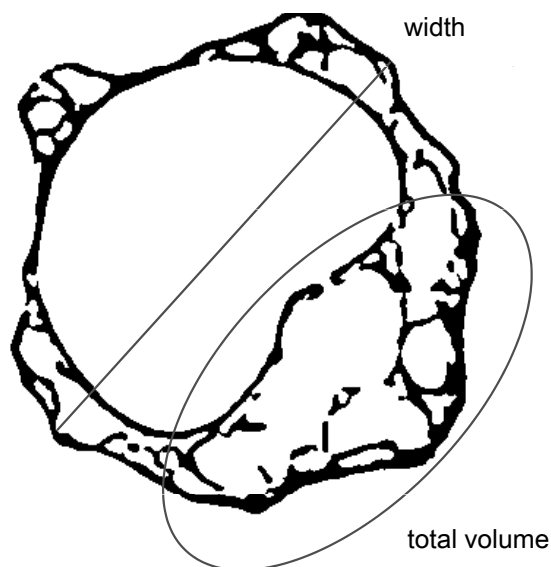


Figure 1: Area of interest for micro-computed tomography analyses.

The bone parameters were measured in the vertebral body. The line represents the width of the vertebra. The ellipse area depicts the total endocortical volume (TV) in which trabecular bone volume (BV) was determined.

Results

Micro-CT analysis of vertebrae

We analyzed various structural parameters including trabecular bone volume fraction, trabecular number and trabecular thickness. Trabecular bone volume fraction (BV/TV) in wild type mice showed a gradual decline with age (Figure 2A). At 78 weeks of age BV/TV had decreased 16% compared to 39-weeks-old wild types. In contrast, TTD mice, which seemed to have higher BV/TV at all ages, showed a 24% decrease up to 65 weeks of age, but a tendency to increase thereafter (Figure 2A). In line with this, the number of trabeculae showed a gradual decrease in wild type mice reaching a 23% decline in 78-week-old wild types while in TTD mice the initial decline was followed by a subsequent increase in the number of trabeculae at 78 weeks of age (Figure 2B). Over all ages the number of trabeculae was significantly higher in TTD mice compared to wild type mice (Figure 2B). Following the changes in BV/TV and trabecular number, wild type mice showed a gradual increase in 2D trabecular spacing with aging whereas TTD mice showed an initial increase up to 65 weeks and a decrease thereafter (Figure 2C). Interestingly, the mean trabecular thickness was higher in TTD mice over all ages; albeit this did not reach statistical significance (Figure 2D). The Structure Model Index (SMI) suggested that TTD mice have a more plate-like structure (lower

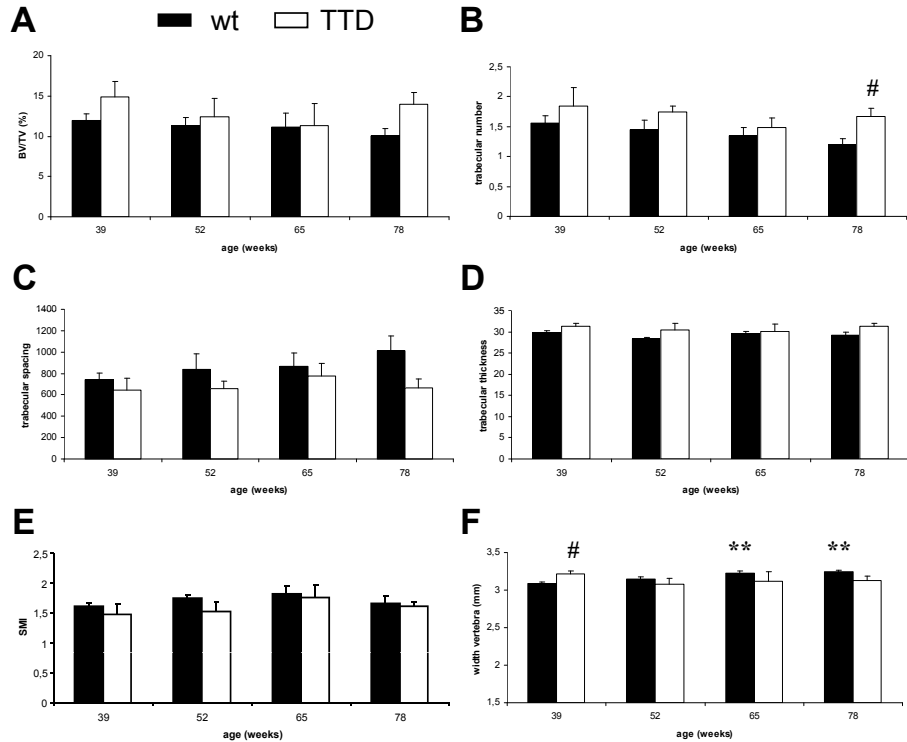


Figure 2: Bone parameters.

Bone parameters in aging wild type mice (solid bars) and TTD mice (open bars): trabecular bone volume fraction (A), trabecular number (B), trabecular thickness; over all ages TTD mice have significantly thicker trabeculae (C), trabecular spacing (D), SMI (E) and width of vertebrae (F). TTD mice compared to wild type animals: # $p < 0.05$; TTD mice and wild type animals compared to their 39 week time point: ** $p < 0.01$; error bars represent SEM.

SMI value) of the bone compared to wild type mice (Figure 2E). Wild type vertebrae showed a significant increase in width with aging (Figure 2F). In contrast, TTD mice had significantly wider vertebrae at 39 weeks and showed no increase in width with ageing (Figure 2F). In line with this observation total cortical volume showed an increase in aging wild type mice whereas this was not observed in TTD mice (data not shown).

To study the difference in trabecular thickness in more detail, we analyzed the thickness distribution of vertebral trabeculae in wild type and TTD mice. Wild type mice showed a highly dynamic pattern in trabecular thickness distribution with aging. This was most prominent for the thinnest trabeculae, i.e. between 20 and 40 μm . However, this dynamic pattern is also observed for the thicker trabeculae, i.e. between 40 and 100 μm , albeit that the differences between the various ages are smaller (Figure 3A). The age-related changes in the TTD mice are clearly less dynamic although there was no stepwise age-related change in trabecular thickness distribution in TTD mice either (compare Figures 3A and B). At 39 weeks of age the

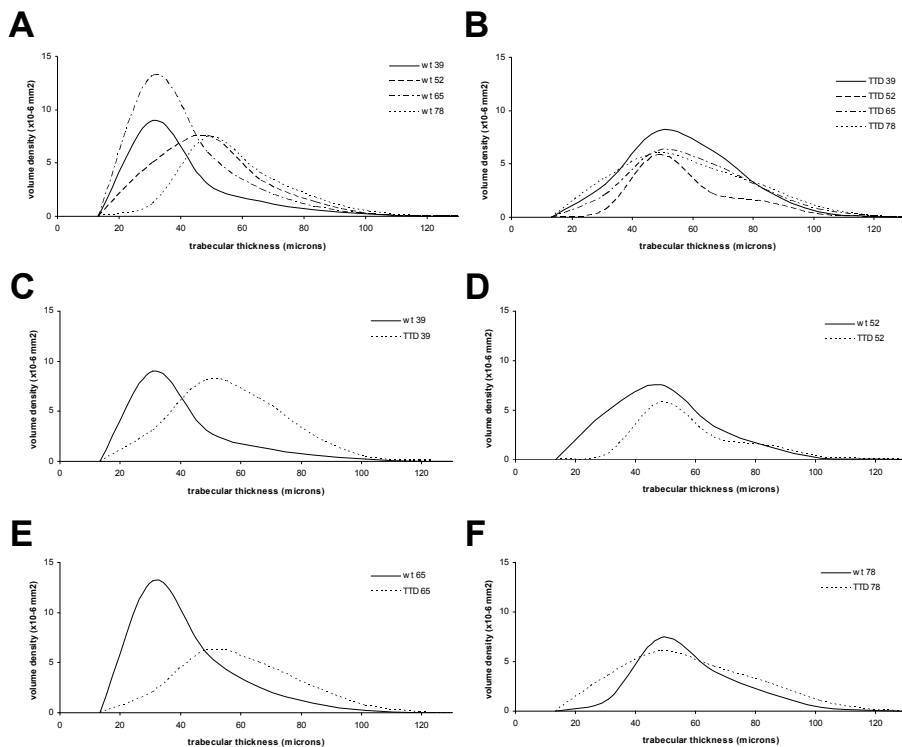


Figure 3: Trabecular thickness distribution.

Trabecular thickness distribution in aging wild type females (A) and TTD females (B). Comparison of trabecular thickness distribution between wild type (solid line) and TTD females (dotted line) at 39 (C), 52 (D), 65 (E) and 78 (F) weeks of age.

number of trabeculae is highest, at 52 weeks of age the number of trabeculae has decreased substantially, whereas the number of trabeculae subsequently increased showing an intermediate number at 65 and 78 weeks of age (Figure 3B). Age-matched comparison of wild type and TTD mice showed that at 39 and 65 weeks of age TTD have clearly thicker trabeculae than wild type mice (Figures 3C and E). While, there were also thicker trabeculae in TTD mice at 78 weeks of age, there were also thinner trabeculae in TTD mice than in wild type mice showing a greater heterogeneity in trabecular bone thickness in TTD mice compared to wild type mice (Figure 3F). At 52 weeks of age, TTD mice showed a completely different pattern with lower volume density than wild type mice except for the trabeculae over 80 μm (Figure 3D). These dynamics and the fact that TTD mice in general have thicker trabeculae could not be observed from the mean BV/TV, trabecular number and trabecular thickness values shown in Figures 2A, B and D, in which the combination of the number of thinner and thicker trabeculae is not taken into account.

Histomorphometric analysis of vertebrae

Histomorphometric analysis of the vertebrae showed higher trabecular bone volume fraction (BV/TV) in TTD mice at all ages reaching statistical significance in 78-week old animals (Figure 4A) thereby supporting the microCT analyses. In addition, the observed dynamics were similar; ie. wild type mice showed a gradual decrease in BV/TV whereas TTD mice exhibited a decrease at week 65 followed by an increase in BV/TV at old age (Figure 4A).

Interestingly, TTD mice exhibited disorganized trabecular structures (illustrated in Figure 4B, panels 1-4), which may explain the greater heterogeneity in trabecular bone thickness, compared to wild type mice (Figure 3F). These typical bone malformations increased with age.

Histopathological analysis of the vertebral column of old TTD mice

TTD and wild type mice kept under different conditions (another location and receiving another diet) appeared to have a longer lifespan, allowing us to analyse animals at even a higher age. In line with our data, an increase in bone mass was observed in these old TTD mice. In transversal samples of the vertebrae of five 104-week-old TTD females a pronounced increase in bone mass (osteosclerosis) accompanied by a distinct reduction of medullary spaces in the thoracic and cervical vertebrae was observed (Figure 4C). Samples from five 104-week-old wild type females did not show osteosclerosis and had normal-sized medullary spaces. These data are supported by results from a life-span study showing slight to moderate osteosclerosis in transversal samples of vertebrae of 33 out of 36 aged TTD females and minimal osteosclerosis in only one out of 40 aged wild type females. In addition, osteonecrosis (defined as empty osteocyte lacunae) was observed in the vertebrae of old TTD mice (Figure 4D).

Discussion

To assess whether the skeletal phenotype in TTD mice truly reflects that observed in patients, ie. osteopenic long bones and osteosclerotic vertebrae, we analyzed the axial skeleton in ageing wild type and TTD females. In agreement with previous studies, wild type mice showed a decline in vertebral trabecular bone volume fraction and trabecular number with ageing (22). While TTD mice showed an initial decrease in trabecular bone volume fraction and trabecular number, they exhibited an increase in bone mass at 78 weeks. In addition, the thickness distribution data demonstrate that TTD mice contain thicker trabeculae than wild type mice and that the dynamics of vertebral trabecular bone turnover is different in wild type and TTD mice. Noteworthy, this telling data could not be observed from the mean microCT data, e.g. BV/TV, trabecular number and trabecular thickness, which are usually presented.

It appears from the data on trabecular bone volume fraction, trabecular number and trabecular thickness distribution that already young TTD mice have more bone mass in their

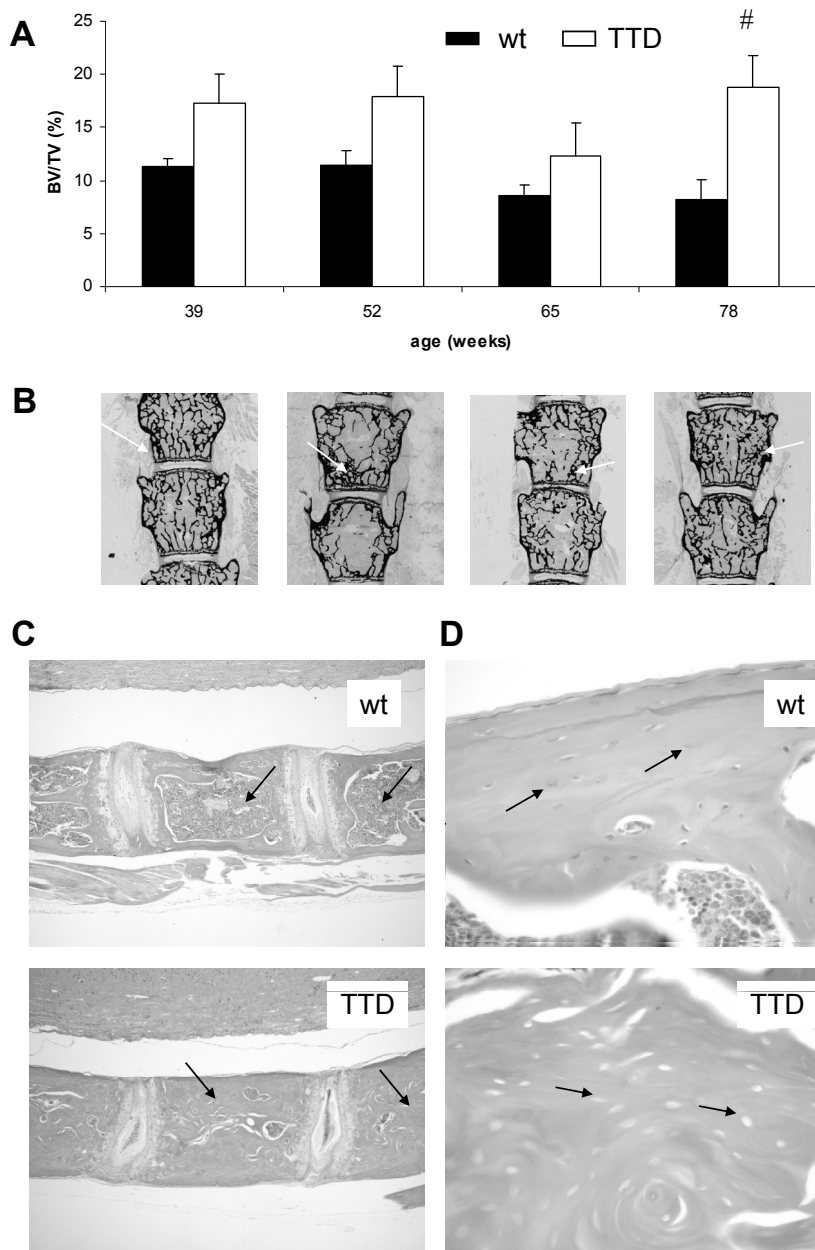


Figure 4: Histomorphometric and histopathological analysis of vertebrae.

Trabecular bone volume fraction in aging wild type mice (solid bars) and TTD mice (open bars) (A), 2D histology (panel 1-4) images of vertebrae of aging TTD mice with the highest trabecular bone volume fraction; disorganized appearance indicated by arrow (B). Transversal section of vertebrae showing an increase in bone mass accompanied by a reduction of medullary spaces (indicated by arrows) in a 104-week old TTD mouse compared to a wild type mouse (C). Increased magnification showing empty osteocyte lacunae (indicated by arrows) in vertebrae of a 104-week old TTD mouse compared to a wild type mouse (D). TTD mice compared to wild type mice: # $p < 0.02$; error bars represent SEM.

vertebrae than wild type mice. As this increased bone mass is also observed in vertebrae of TTD patients, it is intrinsic to the *XPD* mutation and validates the *XPD* point mutant (TTD) mouse as a model for trichothiodystrophy.

The higher bone mass in vertebrae does not represent a premature ageing phenotype. Wild type mice do not show such an extensive increase in bone mass nor is this observed in humans. Quantitative computed tomography studies in aging humans showed large decreases in volumetric bone mineral density (BMD) at several skeletal sites including the spine (23). This decrease in BMD is illustrated by the impression fractures in vertebrae observed in elderly people.

Although, the increased bone mass in old TTD mice which can be observed as disorganized bone might represent a form of cancer, this is not likely to be the case. The analyzed vertebrae contain differentiated bone cells (personal communication, M. Amling) which is not typical of cancer. Furthermore, TTD mice develop less spontaneous cancer than wild type mice (18). However, hyperplasia of tissue, ie. atypical duodenal hyperplasia, has been reported in TTD mice (18). Interestingly, Paget's disease which is a common condition characterised by increased and disorganised bone turnover shows similar bone lesions which can lead to eg. bone deformity. Although Paget's disease was considered to be a disease of the osteoclast, there is evidence that stromal cell function and osteoblast function are also abnormal (24). Genetic factors play an important role in Paget's disease, but environmental factors as e.g. viruses, mechanical loading and environmental toxins have also been implicated as possible disease triggers (24). However, other typical characteristics of Paget's disease, e.g. fibrous replacement of the bone marrow, are not observed in TTD mice (R. Beems, unpublished results).

The increase in trabecular bone volume fraction, which (partly) can be observed as an increase in the disorganized appearance of the vertebrae in old TTD mice might represent a local increase in the number or differentiation of osteogenic mesenchymal stem cells. It would be of interest to study mesenchymal stem cells derived specifically from murine vertebrae. However, this is technically very challenging. We have studied mesenchymal stem cells derived from murine femora (Diderich et al., Chapter 2), but it has been shown that differences between mesenchymal stem cells derived from femora and vertebrae exist (25). Over all ages, TTD mice have significantly lower levels of estradiol compared to wild type mice (our unpublished results). It has been shown that vertebrae of ovariectomized rats exhibit a higher rate of bone formation compared to sham-treated animals (26). Thus, systemic factors may influence the phenotype in TTD vertebrae.

In addition, TTD mice may show reduced mechanical adaptation. TTD vertebrae seem to exhibit less osteocytes (data RIVM,) which are thought to be the mechanosensors in bone (27). Furthermore, TTD vertebral trabeculae have a disorganized appearance which could be due to lack of alignment of trabeculae. Alignment of trabeculae was observed in tibiae of ovariectomized rats and was thought to represent an acceleration of normal bone adapta-

tion (28). The observed increase in the number of trabeculae as well as the disorganized appearance may result from the decrease in osteocytes followed by a decrease in sclerostin expression. Sclerostin is a protein secreted by osteocytes, which inhibits bone formation and mineralization by osteoblasts (29). When osteocytes are absent or their numbers are decreased, it can be expected that (disorganized) bone formation is increased.

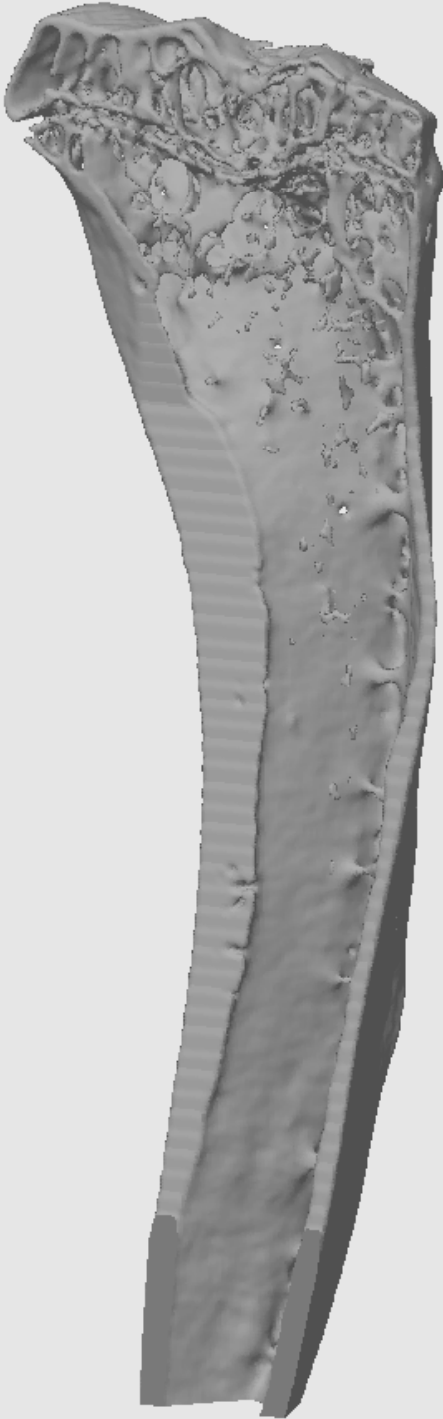
As TTD mice exhibit osteosclerotic vertebrae, kyphosis in TTD mice is not due to osteoporosis of the vertebrae as previously hypothesized and discussed (16,30,31), but may rather be related to deformation of the osteosclerotic vertebrae. Interestingly, TTD vertebrae showed no increase in width. TTD mice also showed a lack of increase in cortical thickness in tibiae which was due to a lack of periosteal apposition (Diderich et al., Chapter 2).

In conclusion, similar to TTD patients TTD mice exhibit increased bone mass in their vertebrae. The bone phenotype in mice thus closely resembles the bone phenotype in TTD patients showing osteosclerotic vertebrae and validates the XPD knockout as a bonafide model for trichothiodystrophy. Furthermore, it shows the importance of proper DNA repair for optimal bone formation in vertebrae and for bone metabolism in general and thus further supports the significance of proper DNA repair in normal aging.

References

1. Bootsma D, Kraemer KH, Cleaver JE, Hoeijmakers JHJ 1998 Nucleotide excision repair syndromes: xeroderma pigmentosum, Cockayne syndrome and trichothiodystrophy. In: Vogelstein B, Kinzler KW (eds.) *The genetic basis of human cancer*. McGraw-Hill, New York, pp 245-74.
2. Itin PH, Sarasin A, Pittelkow MR 2001 Trichothiodystrophy: update on the sulfur-deficient brittle hair syndromes. *J Am Acad Dermatol* **44**(6):891-920; quiz 921-4.
3. Botta E, Nardo T, Broughton BC, Marinoni S, Lehmann AR, Stefanini M 1998 Analysis of mutations in the XPD gene in Italian patients with trichothiodystrophy: site of mutation correlates with repair deficiency, but gene dosage appears to determine clinical severity. *Am J Hum Genet* **63**(4):1036-48.
4. Wakeling EL, Cruwys M, Suri M, Brady AF, Aylett SE, Hall C 2004 Central osteosclerosis with trichothiodystrophy. *Pediatr Radiol* **34**(7):541-6.
5. Toelle SP, Valsangiacomo E, Boltshauser E 2001 Trichothiodystrophy with severe cardiac and neurological involvement in two sisters. *Eur J Pediatr* **160**(12):728-31.
6. Kousseff BG, Esterly NB 1988 Trichothiodystrophy, IBIDS syndrome or Tay syndrome? *Birth Defects Orig Artic Ser* **24**(2):169-81.
7. Przedborski S, Ferster A, Goldman S, Wolter R, Song M, Tonnesen T, Pollitt RJ, Vamos E 1990 Trichothiodystrophy, mental retardation, short stature, ataxia, and gonadal dysfunction in three Moroccan siblings. *Am J Med Genet* **35**(4):566-73.
8. Civitelli R, McAlister WH, Teitelbaum SL, Whyte MP 1989 Central osteosclerosis with ectodermal dysplasia: clinical, laboratory, radiologic, and histopathologic characterization with review of the literature. *J Bone Miner Res* **4**(6):863-75.
9. Chapman S 1988 The trichothiodystrophy syndrome of Pollitt. *Pediatr Radiol* **18**(2):154-6.
10. Price VH, Odom RB, Ward WH, Jones FT 1980 Trichothiodystrophy: sulfur-deficient brittle hair as a marker for a neuroectodermal symptom complex. *Arch Dermatol* **116**(12):1375-84.
11. McCuaig C, Marcoux D, Rasmussen JE, Werner MM, Gentner NE 1993 Trichothiodystrophy associated with photosensitivity, gonadal failure, and striking osteosclerosis. *J Am Acad Dermatol* **28**(5 Pt 2):820-6.
12. Battistella PA, Peserico A 1996 Central nervous system dysmyelination in PIBI(D)S syndrome: a further case. *Childs Nerv Syst* **12**(2):110-3.
13. Happle R, Traupe H, Grobe H, Bonsmann G 1984 The Tay syndrome (congenital ichthyosis with trichothiodystrophy). *Eur J Pediatr* **141**(3):147-52.
14. Hersh JH, Klein LR, Joyce MR, Hordinsky MK, Tsai MY, Paller A, Hyzer R, Zax RH 1993 Trichothiodystrophy and associated anomalies: a variant of SIBIDS or new symptom complex? *Pediatr Dermatol* **10**(2):117-22.
15. de Boer J, de Wit J, van Steeg H, Berg RJ, Morreau H, Visser P, Lehmann AR, Duran M, Hoeijmakers JH, Weeda G 1998 A mouse model for the basal transcription/DNA repair syndrome trichothiodystrophy. *Mol Cell* **1**(7):981-90.
16. de Boer J, Andressoo JO, de Wit J, Huijman J, Beems RB, van Steeg H, Weeda G, van der Horst GT, van Leeuwen W, Themmen AP, Meradji M, Hoeijmakers JH 2002 Premature aging in mice deficient in DNA repair and transcription. *Science* **296**(5571):1276-9.
17. Leupold D 1979 [Ichthyosis congenita, cataract, mental retardation, ataxia, osteosclerosis and immunologic deficiency--a particular syndrome?]. *Monatsschr Kinderheilkd* **127**(5):307-8.

18. Wijnhoven SW, Beems RB, Roodbergen M, van den Berg J, Lohman PH, Diderich K, van der Horst GT, Vijg J, Hoeijmakers JH, van Steeg H 2005 Accelerated aging pathology in ad libitum fed Xpd(TTD) mice is accompanied by features suggestive of caloric restriction. DNA Repair (Amst).
19. Parfitt AM, Drezner MK, Glorieux FH, Kanis JA, Malluche H, Meunier PJ, Ott SM, Recker RR 1987 Bone histomorphometry: standardization of nomenclature, symbols, and units. Report of the ASBMR Histomorphometry Nomenclature Committee. J Bone Miner Res **2**(6):595-610.
20. Amling M, Priemel M, Holzmann T, Chapin K, Rueger JM, Baron R, Demay MB 1999 Rescue of the skeletal phenotype of vitamin D receptor-ablated mice in the setting of normal mineral ion homeostasis: formal histomorphometric and biomechanical analyses. Endocrinology **140**(11):4982-7.
21. Parfitt AM, Mathews CH, Villanueva AR, Kleerekoper M, Frame B, Rao DS 1983 Relationships between surface, volume, and thickness of iliac trabecular bone in aging and in osteoporosis. Implications for the microanatomic and cellular mechanisms of bone loss. J Clin Invest **72**(4):1396-409.
22. Glatt V, Canalis E, Stadmeier L, Bouxsein ML 2007 Age-related changes in trabecular architecture differ in female and male C57BL/6J mice. J Bone Miner Res **22**(8):1197-207.
23. Riggs BL, Melton Iii LJ, 3rd, Robb RA, Camp JJ, Atkinson EJ, Peterson JM, Rouleau PA, McCollough CH, Bouxsein ML, Khosla S 2004 Population-based study of age and sex differences in bone volumetric density, size, geometry, and structure at different skeletal sites. J Bone Miner Res **19**(12):1945-54.
24. Ralston SH 2008 Pathogenesis of Paget's disease of bone. Bone **43**(5):819-25.
25. Pei W, Bellows CG, Elsubeihi ES, Heersche JN 2003 Effect of ovariectomy on dexamethasone- and progesterone-dependent osteoprogenitors in vertebral and femoral rat bone cell populations. Bone **33**(5):822-30.
26. Wronski TJ, Dann LM, Horner SL 1989 Time course of vertebral osteopenia in ovariectomized rats. Bone **10**(4):295-301.
27. Klein-Nulend J, Bacabac RG, Mullender MG 2005 Mechanobiology of bone tissue. Pathol Biol (Paris) **53**(10):576-80.
28. Waarsing JH, Day JS, Verhaar JA, Ederveen AG, Weinans H 2006 Bone loss dynamics result in trabecular alignment in aging and ovariectomized rats. J Orthop Res **24**(5):926-35.
29. ten Dijke P, Krause C, de Gorter DJ, Lowik CW, van Bezooijen RL 2008 Osteocyte-derived sclerostin inhibits bone formation: its role in bone morphogenetic protein and Wnt signaling. J Bone Joint Surg Am **90 Suppl 1**:31-5.
30. Gerhard GS, Kasales CJ 2003 Aging and kyphosis. J Gerontol A Biol Sci Med Sci **58**(11):968.
31. Diderich KE, Hoeijmakers JH, van Leeuwen JP 2003 Accelerated bone aging in the trichothiodysprophy mouse model. J Gerontol A Biol Sci Med Sci **58**(11):969.



CHAPTER 5

Endocrine parameters in relation to accelerated bone loss in prematurely aging DNA repair deficient trichothiodystrophy mice

K.E.M. Diderich¹, C.J. Buurman², I. Westbroek³, R.M.C. Brandt¹, G.T.J. van der Horst¹, F.H. de Jong², J.A. Visser², H. Almeida⁴, J.H.J. Hoeijmakers¹ and J.P.T.M. van Leeuwen²

¹ErasmusMC, Dept. of Cell Biology & Genetics, ²ErasmusMC, Dept. of Internal Medicine, ³DNAge, ⁴Laboratory of Molecular Cell Biology, Faculdade de Medicina da Universidade do Porto

Abstract

Previously, we reported that trichothiodystrophy (TTD) mice show accelerated bone loss and lack of periosteal apposition with aging. In addition, the data suggested that the observed accelerated skeletal aging was the result of a combination of accelerated decline in the number of osteogenic stem cells and altered systemic influences. In this study we analyzed bodyweight, several bone metabolism-related serum parameters, i.e. calcium, parathyroid hormone, vitamin D, alkaline phosphatase, osteocalcin, TRAP, estradiol, testosterone, leptin and corticosterone levels as well as histology of the adrenals and ovaries in aging wild type and TTD mice to assess whether differences in these parameters are related to the previously observed bone phenotype. Aging TTD mice exhibit low estradiol levels which are the result of a lack of fat-mass rather than ovarian dysfunction. In addition, TTD mice showed low levels of parathyroid hormone and 25-hydroxyvitamin D3 while bone turnover markers showed no significant differences and 1,25-dihydroxyvitamin D3 levels were higher in aging TTD females. Analysis of adrenals suggests less effective steroidogenesis in TTD mice. In conclusion, TTD mice show differences in circulating levels of hormones known to control bone metabolism as well as calcium homeostasis. These changes did not result in altered serum calcium but may constitute the systemic influences contributing to the bone phenotype in prematurely aging trichothiodystrophy mice. Following this, the observed bone phenotype may be important to maintain stable serum calcium with aging.

Introduction

Trichothiodystrophy (TTD) is a rare, autosomal recessive DNA repair disorder, in which patients present an array of symptoms, including photosensitivity, ichthyosis, brittle hair and nails, impaired intelligence, decreased fertility, short stature, an aged appearance, a reduced life span and skeletal abnormalities (1-12). Complementation analysis of UV-sensitive TTD patients revealed the involvement of three genes (*XPB*, *XPD* and *TTDA*), encoding subunits of the dual functional DNA repair/basal transcription factor TFIIH. TFIIH is a protein complex involved in the Nucleotide Excision Repair (NER) pathway, a repair mechanism which removes numerous types of helix-distorting and bulky lesions by a 'cut and patch'-like mechanism anywhere in the genome (global genome NER) and also acts when damage blocks ongoing transcription (transcription-coupled repair) (13-17). In addition, TFIIH is implicated in transcription initiation of RNA polymerases I and II (13,18). We have generated a mouse model in which we mimicked a causative point mutation identified in the *XPD* gene of a photosensitive TTD patient (TTD1Bel) (19). The phenotype of TTD mice very much resembles the symptoms of patients, including the presence of premature aging features (20,21).

In previous studies, we examined in great detail the effects of aging on bone parameters of wild type mice as well as progeroid TTD mice (Diderich et al., Chapter 2; Nicolaije et al., Chapter 3). The systematic analysis uncovered the consequence of a defect in DNA repair and basal transcription on the velocity of age-related skeletal changes and assessed to which extent the skeletal abnormalities reflect normal bone aging. We showed that tibiae of TTD mice exhibited normal bone development and metabolism up to 39 weeks of age followed by an accelerated decrease in bone volume compared to wild type mice. In addition, we observed a different temporal pattern of change in bone phenotype in male wild types compared to female wild types. Furthermore, we found that aging TTD mice lack periosteal apposition leading to reduced bone strength compared to wild type mice. These data combined with bone marrow cultures and *in vivo* intermittent PTH treatment suggested that the accelerated decrease in bone mass was caused by a combination of accelerated decline in the number of osteogenic stem cells and altered systemic influences. The focus of the current study was to document changes in body-weight, serum parameters related to bone turnover, and endocrine factors known to affect bone metabolism in relation to the previously reported bone phenotype. For this, the aging cohorts of both female and male wild type mice as well as the prematurely aging TTD mice were investigated.

Material & Methods

Mice

We generated a cohort of wild type and TTD mice including 8 mice per sex per age group per genotype. Wild type mice were held up to 104 weeks while TTD mice die at around 78 weeks of age. Mice were sacrificed at 6, 13, 26, 39, 52, 65 and 78 weeks (wild type and TTD mice) and 91 and 104 weeks of age (wild type mice). All mice were in a C57Bl/6 background, maintained on a 12:12 h light-dark cycle and fed ad libitum with a standard rodent diet (0.5% Calcium and 0.3% Phosphate). The animals were weighed 10 days before sacrifice. Blood was collected by an orbital puncture under isoflurane anesthesia and the mice were subsequently killed by cervical dislocation. Organs were isolated and either snap-frozen and stored at -80°C or fixed. Blood was stored on ice during the procedure after which it was centrifuged at 6000rpm for 10 minutes. Serum was taken off and stored at -20°C . As required by Dutch law, formal permission to generate and use genetically modified animals was obtained from the responsible local and national authorities. All animal studies were approved by an independent Animal Ethical Committee (Dutch equivalent of the IACUC).

Serum parameters

Calcium levels were colorimetrically determined at 595 nm (Packard Spectra Count) after addition of 1M ethanolamine buffer (pH 10.6) containing 0.35 mM o-cresolphthalein complexone, 19.8 mM 8-hydroxy-quinoline, and 0.6 mM hydrochloric acid. Results were adjusted for DNA content of the corresponding cell lysates.

Parathyroid hormone was measured as described by the manufacturer using the mouse intact PTH ELISA kit purchased from Lucron Bioproducts (Gennep, The Netherlands; produced by Immotopics Inc., San Clemente, USA). 25-hydroxyvitamin D3 was measured by a ^{125}I radioimmunoassay purchased from DiaSorin (Minnesota, USA). 1,25-dihydroxyvitamin D3 was measured by a ^{125}I radioimmunoassay using the IDS Gamma-B kit purchased from Immunodiagnostic Systems (Tyne and Wear, UK). Serum levels of osteocalcin were measured using an in house assay with antibodies generously supplied by prof. R. Bouillon (Leuven, Belgium). The levels of alkaline phosphatase were assayed by determining the release of para-nitrophenol from paranitrophenylphosphate (20 mM in 1 M diethanolamin buffer supplemented with 1 mM MgCl_2 at pH 9.8) in the serum for 10 min at 37°C (27). Adding 0.1 M NaOH stopped the reaction and absorption was measured at 405 nm using a Packard Spectra Count. Results were adjusted for DNA content of the serum. Serum tartrate resistant acid phosphatase (TRAP) levels were measured as described by the manufacturer, using the TRAP assay purchased from SBA Sciences (Turku, Finland). Serum levels of estradiol were estimated in duplicate using the ultrasensitive radioimmuno assay (RIA) purchased from Diagnostic Systems Laboratories (Webster, TX, USA). Serum levels of testosterone were measured by coated tube RIA obtained from Siemens DPC (Los Angeles, USA). Serum levels of leptin were measured, as described by

the manufactures, using an ELISA assay purchased from R&D Systems (UK). Serum levels of corticosterone were estimated using enzyme immunoassays provided by Diagnostic Systems Laboratories.

Ovarian histology and follicle counting

Three mice were randomly selected from each age group. Ovaries were isolated, fixed in Bouin (15 picric acid: 5 formaldehyde 37%: 1 acetic acid) overnight, placed in 70% ethanol and stored at 4°C. Follicle count was performed as described previously (22) using one ovary per animal. Follicles were counted in every 10th section.

Analysis of aromatase expression

Fat from the abdomen was snap frozen and stored at -80°C. RNA was isolated using Trizol according to the manufacturer's guidelines. RNA was isolated from fat and ovaries using an adapted RNazo1B procedure. cDNA was made and the PCR product visualized by gelelectrophoresis.

Oil-Red-O staining

Cryosections of male liver were stained with Oil-Red-O to detect triglycerides. All histology images were acquired at 40x objective magnification on an Olympus BX40 microscope (London, United Kingdom), equipped with a CCD camera.

Light microscopy and electron microscopy of adrenals

Adrenals from 13- and 78-week old, male and female, wild type and TTD mice (4 mice per group) were isolated. For light microscopy adrenals were fixed in 3.7% formalin in phosphate buffer for 24-36 hours at roomtemperature. Subsequently, the adrenals were dehydrated in increasing grades of ethanol and embedded in paraffin.

For electron microscopy pieces of adrenals were fixed in glutaraldehyde 2.5% in 0.1 M sodium cacodylate buffer, pH 7.2 at 4°C, for 2 hours and rinsed in 7% sucrose in 0.1 M sodium cacodylate buffer, pH 7.2 (same buffer as above) at 4°C, overnight.

Subsequently, the pieces of adrenals were post-fixed in osmium tetroxide 1% in veronal acetate buffer, pH 7.3, 2 hours at 4°C, dehydrated in ethanol and embedded in Epon.

Statistics

For comparisons in time (significance compared to 6 or 26 weeks of age), between sexes and genotype comparisons of the weight and serum parameters one-way ANOVAs with Tukey post hoc test and unpaired T-tests were performed using Graph Pad InStat version 3.05 for Windows 95, Graph Pad Software, San Diego California, USA, www.graphpad.com. A univariate General Linear Model (SPSS 15.0) was used to analyze the effect of age in the different genotypes as wells as the effect of genotype over all ages for the serum parameters.

Results

Bodyweight

Bodyweight can influence bone volume by the weight bearing effect. We measured the bodyweight of wild type and TTD mice (Figure 1). At 6 weeks of age TTD and wild type mice on average weighed 11 and 14-15 grams, respectively. From 13 weeks of age onwards male mice were heavier compared to female mice (compare Figures 1A and B). From 26 and 39 weeks on the weight of respectively male and female wild type mice started to increase whereas TTD mice showed a stable weight during most of their late adult life span. As a result, significant differences in weight between wild type and TTD mice were observed from 52 weeks of age onwards. In parallel with the increase in bodyweight in wild type mice, we observed accumulation of an increase of fat in the abdominal cavity (Figure 1C). In TTD mice this accumulation of fat was not observed (Figure 1C). At the end of their lifespan a decrease in weight was observed in both sexes of wild type and TTD mice, after 78 and 65 weeks, respectively (Figures 1A and B). Thus, TTD mice have a lower weight after 39 weeks of age compared to wild type mice and lack accumulation of fat in the abdomen. These data are in line with findings reported for other TTD cohort studies (20,21).

Calcium, PTH and vitamin D

Given their importance for bone metabolism, the levels of calcium, parathyroid hormone (PTH), 25-hydroxyvitamin D3 and 1,25-dihydroxyvitamin D3 were measured in serum collected from the aging mice. In both wild type and TTD mice calcium levels were maintained around 2,5-3 mM throughout life with no significant differences between wild type and TTD mice (Figures 2A, B). Over all ages, PTH levels in wild type mice were significantly higher than in TTD mice of similar sex (Figures 2C, D). While 25-hydroxyvitamin D3 levels only showed a significant increase with age in female mice, both male and female wild type mice had significantly higher levels of 25-hydroxyvitamin D3 over all ages compared to TTD mice (Figures 2E, F). Over all ages, 1,25-dihydroxyvitamin D3 levels were significantly higher in TTD females with a clear increase at 39 weeks and onwards (Figure 2G). In contrast, both wild type and TTD males showed a significant increase in 1,25-dihydroxyvitamin D3 levels with age (Figure 2H).

Bone formation markers

In addition, we measured two key markers of bone formation, alkaline phosphatase (ALP) and osteocalcin. As expected the ALP levels were significantly higher in young mice (Figures 3A, B). In adulthood wild type mice seemed to show higher levels of ALP compared to TTD mice. However, this did not reach statistical significance. At 78 weeks of age ALP levels in wild type and TTD mice were similar after which an increase was observed in wild type mice which reached significance in 104-week-old males (Figures 3A, B). Similarly, osteocalcin levels were significantly higher in young animals (Figures 3C, D). Between 6 and 26 weeks

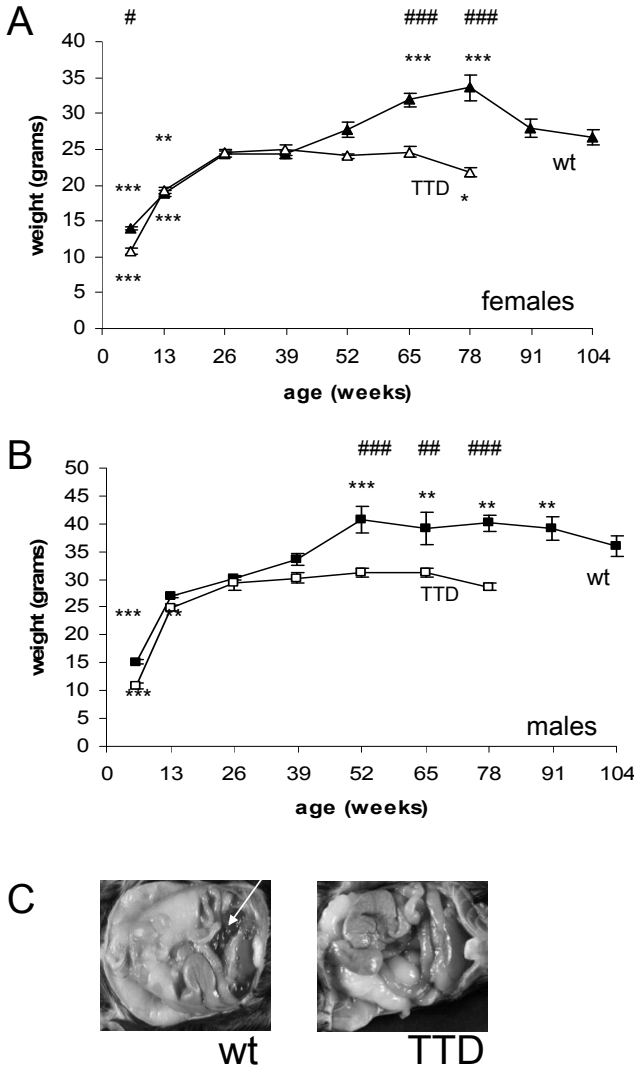


Figure 1: Bodyweight and abdominal cavity in wild type and TTD mice.

Bodyweight in wild type (closed symbols) and TTD mice (open symbols); (A) females and (B) males. Error bars represent SEM; significance compared to 26 w: * = $p < 0.05$, ** = $p < 0.01$, *** = $p < 0.001$ and significance compared between genotypes: ## = $p < 0.01$, ### = $p < 0.001$. (C) abdominal cavity showing (lack of) fat mass in a wild type mouse and a TTD mouse.

of age osteocalcin levels decreased and subsequently remained at a more or less constant level (Figures 3C, D). Overall, male wild type mice showed significantly higher osteocalcin levels compared to TTD mice (Figure 3D). Between 52 and 65 weeks of age and at the age of 65 weeks the curves of the wild type and TTD mice crossed for the female and male mice, respectively (Figures 3C, D).

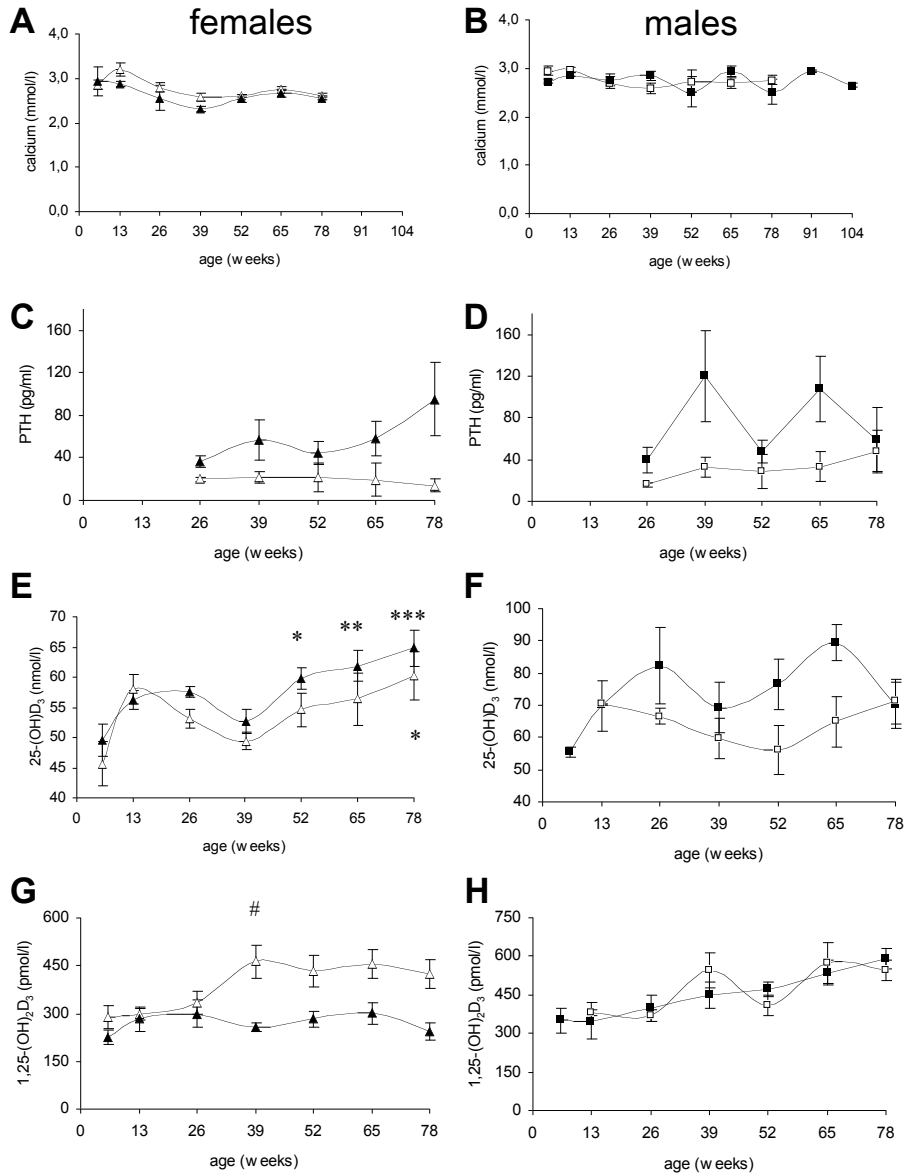


Figure 2: Calcium, PTH and vitamin D in wild type and TTD mice.

Serum parameters in wild type (closed symbols) and TTD mice (open symbols). Levels of calcium in (A) female and (B) male mice, parathyroid hormone in (C) female and (D) male mice, 25-hydroxyvitamin D3 in (E) female and (F) male mice and 1,25-dihydroxyvitamin D3 in (G) female and (H) male mice. Error bars represent SEM; significance compared to 6 w: * = $p < 0.05$, ** = $p < 0.01$, *** = $p < 0.001$ and significance compared between genotypes: # = $p < 0.05$. Over all ages wild type mice had significantly higher levels of parathyroid hormone and 25-hydroxyvitamin D3. Over all ages female TTD mice had significantly higher levels of 1,25-dihydroxyvitamin D3. Female mice showed a significant increase in 25-hydroxyvitamin D3 with age. Male mice showed a significant increase in with age.

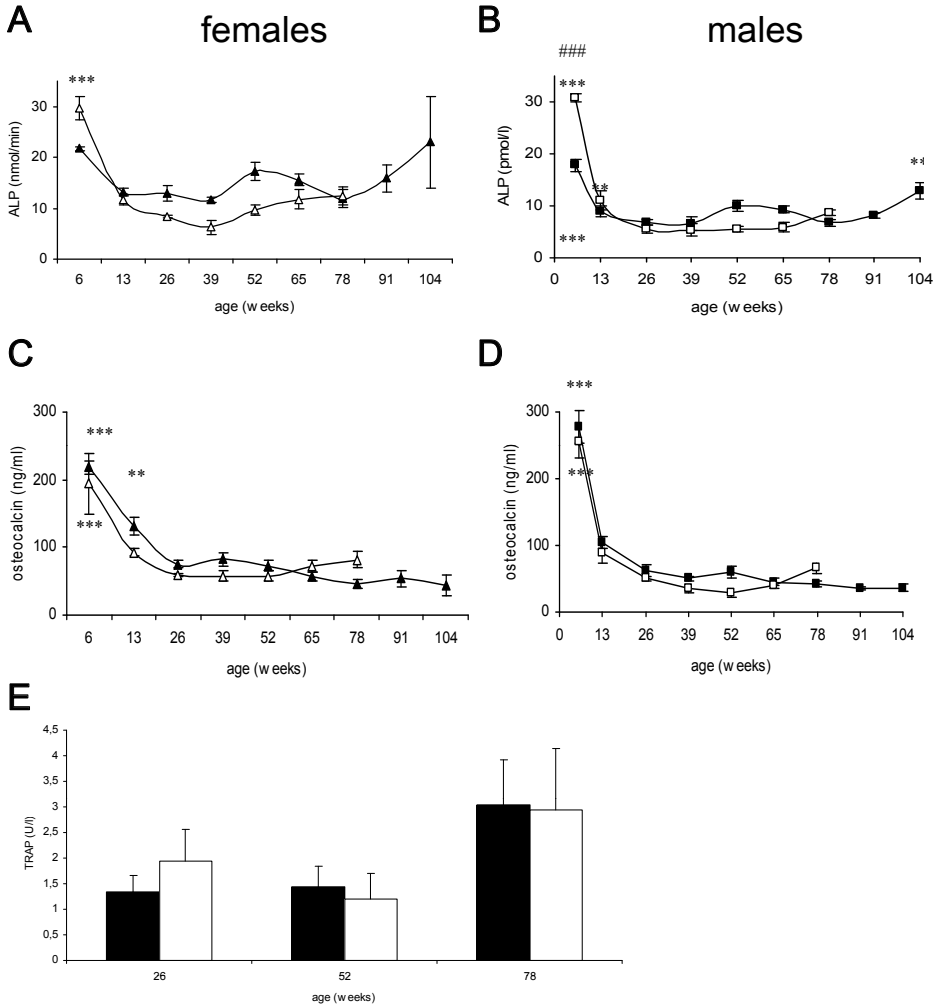


Figure 3: Bone formation markers in wild type and TTD mice.

Serum parameters in wild type (closed symbols) and TTD mice (open symbols). Levels of alkaline phosphatase in (A) female and (B) male mice, osteocalcin in (C) female and (D) male mice and TRAP in female mice (E). Error bars represent SEM; significance compared to 26 w: **= $p < 0.01$, ***= $p < 0.001$, significance compared between genotypes: ###= $p < 0.001$. Young mice had significantly higher levels of alkaline phosphatase and osteocalcin. Over all ages male wild type mice had significantly higher levels of osteocalcin.

Bone resorption

The levels of tartrate resistant acid phosphatase (TRAP) were measured in serum of female mice to assess possible differences in bone resorption. Albeit bone resorption seemed to be higher at 78 weeks of age, it did not significantly change upon aging and no significant difference between wild type and TTD mice was observed (Figure 3E).

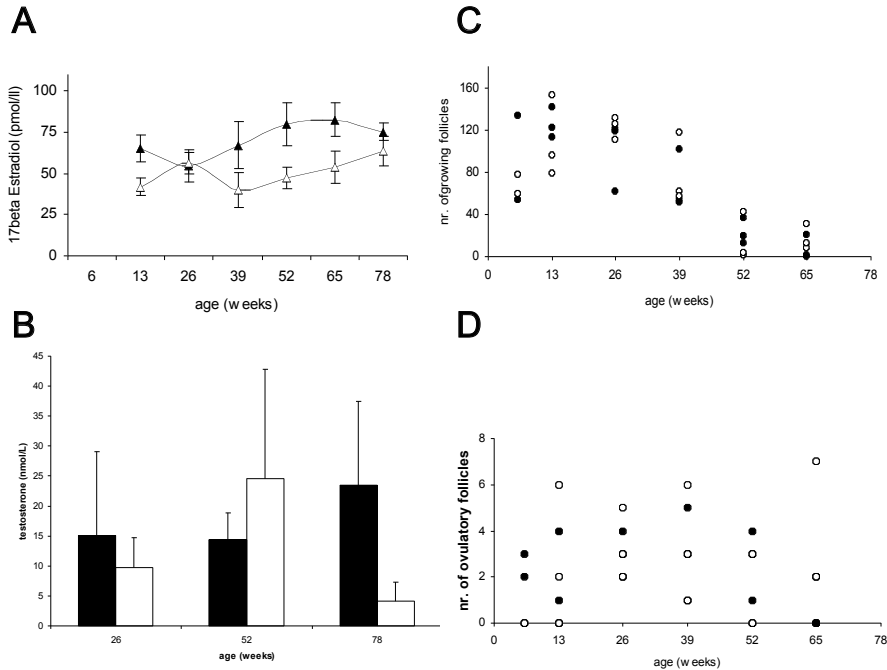


Figure 4: Estradiol, testosterone and ovarian follicles in wild type and TTD mice.

Serum parameters and numbers of growing and ovulatory ovarian follicles in wild type (closed symbols) and TTD mice (open symbols). (A) estradiol levels in female mice; over all ages wild type mice had significantly higher levels of estradiol, (B) testosterone levels in male mice, number of (C) growing and (D) ovulatory follicles. Error bars represent SEM.

Estradiol and testosterone

Over all ages, TTD females had significantly lower estradiol levels compared to wild type mice (Figure 4A). In addition, we measured testosterone levels in aging male mice. However, as expected the testosterone levels showed large variation precluding any significant conclusion about genotype or aging effects (Figure 4B).

Ovarian histology and follicle counting

Next, we went on to see whether the lower estradiol levels in TTD females are caused by a defect in the ovaries. It is known that the primordial follicle pool consists of a set of follicles of which some are selected to grow during initial recruitment. As a result, the size of the primordial follicle pool decreases. During cyclic recruitment a number of these growing follicles is selected to form ovulatory follicles. The granulosa cells in these ovulatory follicles form estradiol.

In both wild type and TTD females, the number of growing follicles gradually decreased from 13 weeks of age onwards (Figure 4C). Up to 39 weeks of age about 50 to 150 growing follicles were detected per ovary. After that the ovaries exhibited a clear drop in follicle number

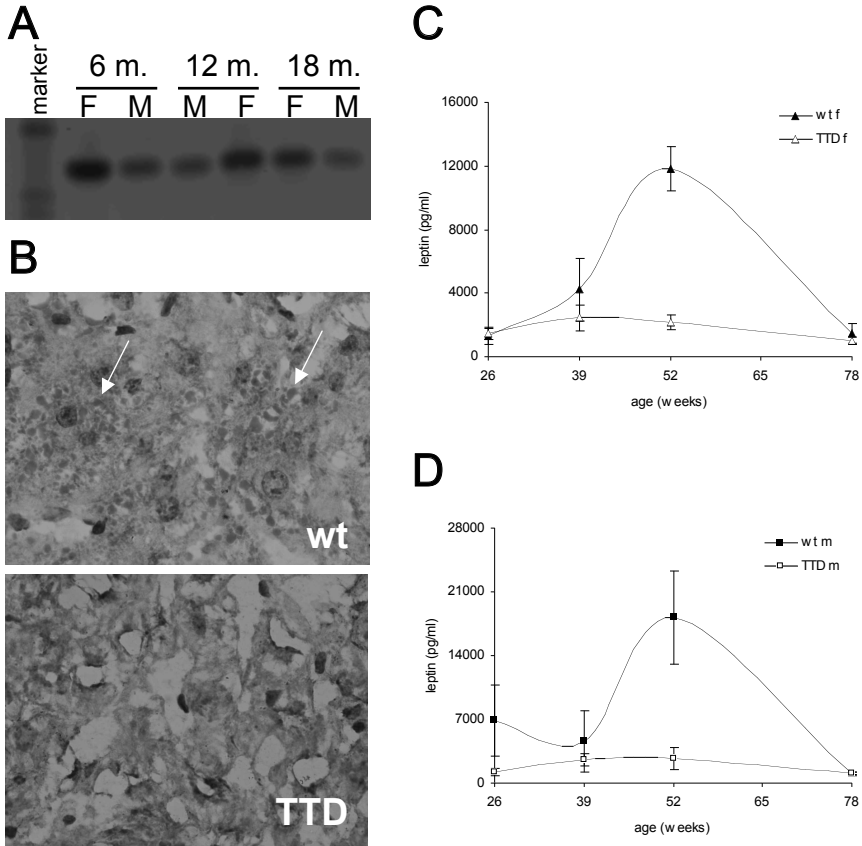


Figure 5: Aromatase expression, Oil-Red-O staining and leptin levels in wild type and TTD mice. (A) aromatase expression in fat of wild type mice. (B) Oil-Red-O staining on livers from a 78-week-old male wild type and TTD mouse. Staining of triglycerides indicated by arrows. Pictures were taken at 100x magnification. Serum leptin levels in wild type (closed symbols) and TTD mice (open symbols); (C) female and (D) male mice. Error bars represent SEM.

reaching follicle numbers between 0 and 42 per ovary (Figure 4C). In contrast, the number of ovulatory follicles showed no evident change with aging (Figure 4D). For none of the ovarian follicle parameters a significant difference between wild type and TTD mice was observed. Thus, wild type and TTD mice have similar numbers of growing and ovulatory follicles.

Aromatase expression

Estrogen levels were lower in TTD mice in spite of a normal number of pre-ovulatory follicles. However, TTD mice lacked accumulation of abdominal fat. We analysed aromatase expression in abdominal fat of wild type mice using RT-PCR to investigate whether this fat could be the source of the additional estrogen that was measured in wild type mice. In abdominal

fat from 6, 12 and 18 month old male and female wild type mice aromatase expression was detected (Figure 5A).

Fat staining

In order to see if the lack of fat is a more generalized phenomenon, we performed Oil-Red-O stainings on liver sections from wild type and TTD males. In 18-month-old male wild type mice abundant staining was present in liver (Figure 5B). In contrast, livers of 18-month-old male TTD mice showed no evident staining (Figure 5B). Thus, TTD mice have less fat accumulation in liver as well as in the abdominal cavity.

Serum leptin

As leptin is produced in fat and plays a role in bone metabolism, we measured leptin levels in wild type and TTD males and females. In line with the increase in abdominal fat, wild type mice showed higher leptin levels at 52 weeks of age (Figures 5C, D). However, at the age of 78 weeks both female and male wild types showed a decrease in leptin levels (Figures 5C, D) while no significant decrease in weight was observed. In contrast, TTD mice showed low leptin levels throughout life (Figures 5C, D). Thus, in agreement with the lower bodyweight and lack of abundant fat, TTD mice have lower leptin levels compared to wild type mice; particularly in the period in which wild type mice show an increase in visceral fat.

Corticosterone levels and microscopy of adrenals

Glucocorticoids (i.e. in mice corticosterone) may affect bone metabolism; in particular in mice high levels of glucocorticoids have a negative effect on bone mass. High levels of glucocorticoids reduce numbers of both osteoblast and osteoclast precursors in mice, but the number of osteoclasts does not decrease as does osteoblast number due to the ability of glucocorticoids to promote osteoclast life span (23).

Serum corticosterone levels were significantly higher in wild type females compared to TTD females (Figure 6A). In male mice a large variation was observed, especially in 78-week-old TTD males, and no significant differences were observed with aging or between genotypes (Figure 6B).

The adrenal cortex consists of the zona reticularis, the zona fasciculata and the zona glomerulosa. Glucocorticoids are secreted from the zona fasciculata and to a lesser extent from the zona reticularis. The zona glomerulosa secretes mineralocorticoids. The X-zone is a zone that can be distinguished from the zona fasciculata in young mice. The X-zone is characterised by whorls of smooth endoplasmic reticulum and peculiar complexes of mitochondria and smooth endoplasmic reticulum (24). More whorls are observed when the X-zone regresses in old mice.

We visualised the zona fasciculata and the zona reticularis by light microscopy. Old TTD mice exhibited a larger cell volume in the zona fasciculata compared to wild type mice as well

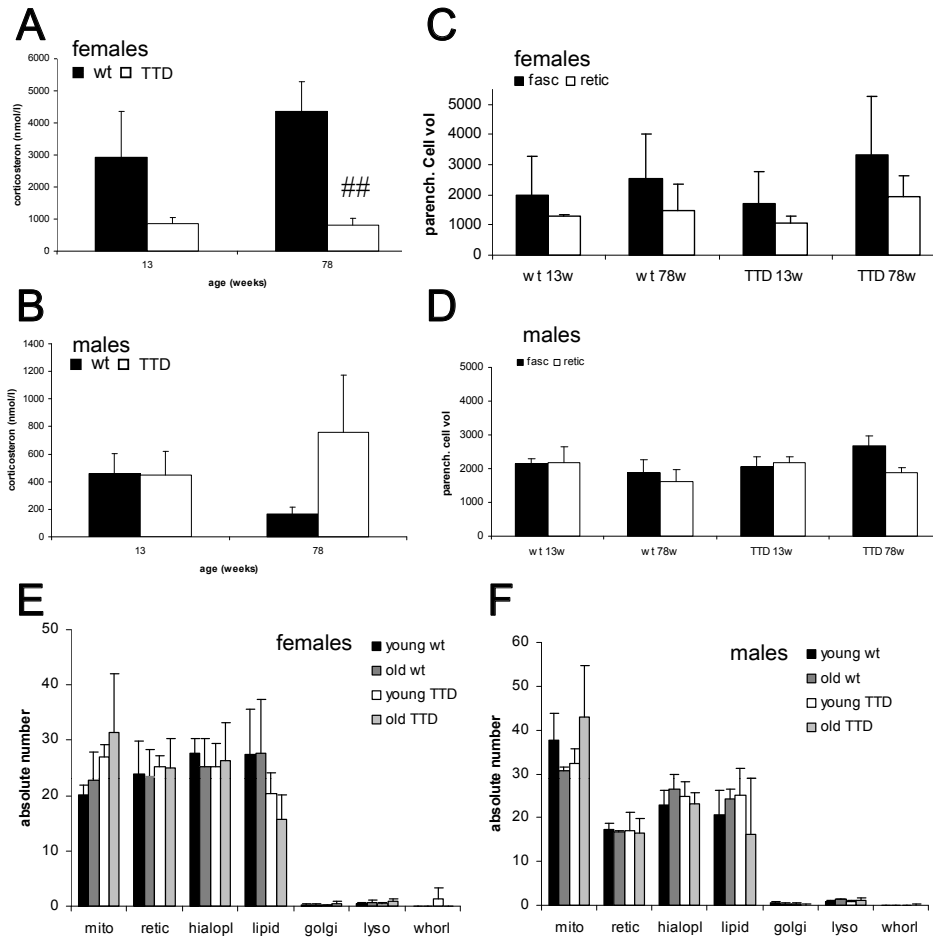


Figure 6 : Serum corticosterone levels and microscopical analysis of adrenals in wild type and TTD mice.

Corticosterone in (A) female and (B) male wild type (closed symbols) and TTD mice (open symbols). Over all ages wild type mice had significantly higher levels of corticosterone. Parenchymal cell volume of (C) female and (D) male adrenals, number of organelles in the zona fasciculata of (E) female and (F) male adrenals. Abbreviations: wt= wild type, fasc= zona fasciculata, retic= zona reticularis, mito= mitochondria, retic= reticulocytes, hialopl= hialoplasma, lyso= lysosomes. Error bars represent SEM; significance compared between genotypes: ##= $p < 0.01$.

as younger TTD mice (Figures 6C, D). Electron microscopy revealed more mitochondria and fewer lipid droplets in the zona fasciculata in old TTD mice compared to wild type mice as well as younger TTD mice (Figures 6E, F). In addition, young TTD females showed more whorls than wild type mice (Figure 6E). Thus, on basis of cell volume and the amount of mitochondria and lipids one would predict highest glucocorticoid synthesis in old TTD mice in contrast to the observed corticosterone data in female TTD mice.

Discussion

Previously, we have shown -by micro-computed tomography analysis- that TTD mice have an accelerated decrease in bone volume in tibiae compared to wild type mice and that they lack an increase in bone perimeter (Diderich et al., Chapter 2). Using double labeling studies, we confirmed that TTD mice lack periosteal apposition and thus have no compensatory mechanism to maintain bone strength (Diderich et al., Chapter 2). Indeed, mechanical testing showed a decrease in bone strength in TTD mice compared to wild type mice (Diderich et al., Chapter 2). In vitro bone marrow cell cultures showed that TTD osteoprogenitors retain the capacity to differentiate into osteoblasts, but show decreased bone nodules after 13-26 weeks of age (Diderich et al., Chapter 2). In addition, after intermittent PTH treatment TTD females demonstrated an increase in cortical thickness implicating that there are still enough stem cells/osteoblasts to maintain the bone phenotype at wild type level (Diderich et al., Chapter 2). The accelerated skeletal aging in TTD mice is likely the result of a combination of an accelerated decline in the number of osteogenic stem cells together with altered systemic influences. Indeed various DNA repair deficient mouse models exhibiting premature aging show a systemic downregulation of various key hormonal axes, including estrogen (25), which may also contribute to the observed loss of osteoprogenitors. To analyze these systemic influences in more detail, we measured several endocrine parameters as well as bodyweight of wild type and TTD mice. In both aging wild type and TTD mice serum levels of calcium, parathyroid hormone, 25-hydroxyvitamin D3, 1,25-dihydroxyvitamin D3, alkaline phosphatase, osteocalcin, TRAP, estradiol, testosterone, leptin, and corticosterone were measured; several of these parameters have not been documented in aging mice before.

Calcium, PTH and vitamin D3 levels

PTH and 25-hydroxyvitamin D3 levels were significantly lower in TTD mice whereas 1,25-dihydroxyvitamin D3 levels were significantly higher in female TTD mice. It is known that a decrease in serum calcium leads to an increase of PTH levels resulting in an increase in 1,25-dihydroxyvitamin D3 levels. 1,25-dihydroxyvitamin D3 is synthesized mainly in the kidney by 25-hydroxy-vitaminD-1 α -hydroxylase which is stimulated by PTH (26). 1,25-dihydroxyvitamin D3 then increases intestinal calcium absorption and renal reabsorption of calcium to restore serum calcium levels (27). In a negative feedback loop the increased level of 1,25-dihydroxyvitamin D3 leads to an inhibition of its own production by 1 α -hydroxylase and also leads to an inhibition of PTH production and secretion leading to reduction of serum PTH levels (26).

We hypothesize that TTD mice have decreased intestinal calcium absorption and/or increased renal calcium loss while maintaining serum calcium (see Figures 2A and B). To maintain this crucial stable level of serum calcium, PTH levels had to increase followed by an increase in 1,25-dihydroxyvitamin D3. The increased levels of 1,25-dihydroxyvitamin D3 will

then repress PTH secretion. Remarkable, the 25-hydroxyvitamin D3 levels were significantly lower in TTD mice. This could be the effect of decreased synthesis in the skin or the liver of TTD mice. TTD mice are known to have specific skin lesions as well as more hepatocellular atrophy compared to wild type mice (21).

Previous studies, including biochemical analysis of aminoacids in serum of TTD mice, showed no indications of malabsorption in TTD mice (20), while just a small number of TTD mice exhibited atypical hyperplasia of the duodenum (21). If, however, there is an imbalance in the absorption and loss of calcium, one would expect to see high levels of 1,25-dihydroxyvitamin D3 and low levels of PTH in addition to normal levels of serum calcium. This is exactly what we observed in TTD mice. Interestingly, long-term administration of 1,25-dihydroxyvitamin D3 has been shown to result in a decrease in bone volume in mice (28). Furthermore, in TRPV5^{-/-} mice which exhibit increased levels of 1,25-dihydroxyvitamin D3 a decrease in bone volume was observed (29). In female TTD mice the 1,25-dihydroxyvitamin D3 levels increase just before the change in bone phenotype is observed.

Interesting, but yet unexplainable are the difference in 1,25-dihydroxyvitamin D3 levels in female and male TTD mice. It is tempting to attribute this to differential effects of estrogens and testosterone.

Estradiol

In addition to the decrease in bone volume that might be caused by increased levels of 1,25-dihydroxyvitamin D3 in TTD mice, the low estradiol levels may result in impaired inhibition of bone resorption as well as in impaired bone formation. Estradiol plays an important role in bone metabolism by controlling bone resorption, by inhibiting osteoclast formation and by decreasing their life-span. In addition estradiol has been shown to have an anabolic effect on bone in mice (30).

The lower levels of estradiol in TTD females do not seem to be caused by ovarian dysfunction as wild type and TTD females have similar numbers of growing and ovulatory follicles. This is in contrast to the previously observed heterogeneous ovarian dysfunction in 6-months-old female TTD mice in a mixed genetic background (20). The pure C57Bl/6 background in our TTD mice, which allows the TTD mice to become older as well, thus alleviates several of the symptoms that were reported for TTD mice in a mixed background. Since the lower estradiol levels are not caused by ovarian dysfunction, we next analysed the abundant fat in wild type mice for aromatase expression. Indeed, aromatase expression is present in fat from wild type females. In men and postmenopausal women, extragonadal aromatase expression plays a key role in estrogen production (31). Recent work has suggested that aromatase expression in adipose tissue of male mice may play an important role in their estrogen biosynthesis (31). Is it possible that aromatase expression in adipose tissue present in wild type mice may contribute to the higher levels of estradiol in old wild type females. On the other hand, it is possible that the breakdown of estrogen is increased in TTD mice.

Much is known about the role of estrogen on bone metabolism. Together with biomechanical strain, estrogen is an important player in bone mass conservation (32). Most importantly, estrogen inhibits bone resorption by inhibiting osteoclastogenesis and osteoclast function and favouring osteoclast apoptosis (33,34). In addition, estrogen promotes the development of osteoblasts from the osteoblast-adipocyte-precursor, and increases the production of a number of osteoblast proteins as e.g. IGF-1 (30,35,36). Thus, a decrease in estrogen due to menopause or ovariectomy results in increased bone loss and adipocyte formation (37). The lower levels of estradiol in TTD mice can thus play a role in the accelerated bone loss resulting in enhanced differences between wild type and TTD mice.

Recently, it was found that estrogens also decrease osteoblast apoptosis (32). In addition, estrogens, like androgens, may be involved in regulation of periosteal apposition. Although estrogens were believed to have a negative effect on periosteal bone formation (32,38,39), recent studies have shown that estrogens may stimulate periosteal apposition (40-42). It is therefore possible that the lower levels of estradiol could have some contribution to the decline in periosteal apposition as observed in TTD mice.

Bone turnover

Total alkaline phosphatase was high in young animals in line with data in other species (43). The measured alkaline phosphatase is not bone-specific, but in dogs it was shown that at young age bone-specific alkaline phosphatase made up 96% of total alkaline phosphatase (43). High bone-specific alkaline phosphatase correlates with increased bone formation (43). Between 13 and 78 weeks of age, total alkaline phosphatase was higher in wild type mice. Higher levels of total alkaline phosphatase are observed in hyperparathyroidism and when corticosteroid levels are higher (43) suggesting that the lower levels of parathyroid hormone and corticosterone in female and young male TTD mice may have had an effect on the levels of alkaline phosphatase. At old age, the percentage of total alkaline phosphatase that is induced by corticosteroids increases (43). However, the majority of alkaline phosphatase is liver-specific alkaline phosphatase (43). The increase in alkaline phosphatase in old mice could thus be a result of liver-associated problems which have been reported in wild type mice (21). In addition, the strong increase in alkaline phosphatase in wild type females may partly result from the increase in corticosterone. However, osteocalcin levels showed an identical pattern as total alkaline phosphatase with aging indicating that the observed changes in alkaline phosphatase reflect changes in bone metabolism with aging.

In spite of the increased levels of 1,25-dihydroxyvitamin D₃ which could increase osteoclastogenesis, the accelerated decrease in bone strength observed in TTD mice does not appear to be due to increased bone resorption as assessed by measurement of serum TRAP.

Bodyweight

Adult wild type mice gain weight from 26-39 weeks of age onwards. Macroscopically, this increase is mainly due to accumulation of fat in the abdominal cavity. In contrast, TTD mice do not increase in weight and lack accumulation of fat in the abdominal cavity as well as in for example liver. Remarkably, with aging a fatty liver can be observed in other DNA repair deficient mouse models; e.g. CSB/XPA double mutants show a fatty liver (25). As TTD mesenchymal stem cells were shown to be able to form adipocytes in vitro (Diderich et al., Chapter 2), systemic effects are likely to cause the lack of fat tissue in TTD mice. Whereas the total lean body mass has not been investigated in TTD mice or patients, it is known that TTD mice have a lower relative heart mass and aortic sarcopenia (21). We may thus assume that the lower bodyweight is not only due to the lack of fat accumulation.

The lower weight in TTD mice could influence bone volume by decreased mechanical loading leading to e.g. decreased periosteal apposition (44) or a decrease in estradiol or leptin. Whether bone formation is influenced by muscle mass or fat mass is under debate ((45) and references therein). The effect of weight on bone volume is most likely a combination of lean body mass and fat mass. Positive correlations have been reported for the relation between lean body mass and bone mineral density (BMD), as well as for fat mass and BMD in postmenopausal women (46,47). An increase in fat mass after the menopause decreases bone resorption without a corresponding decrease in bone formation (48). Even moderate obesity can play a protective role on postmenopausal bone loss (49). Normal mechanical loading maintains bone mass whereas increased mechanical loading stimulates bone formation and decreased mechanical loading is associated with bone loss (50). Two studies, in respectively men and women, compared the relative contribution of lean body mass versus fat mass on bone mineral density and both concluded that lean body mass has a greater effect on bone mineral density (51,52). The lower bodyweight in TTD mice may thus contribute to the accelerated bone loss irrespective whether this predominantly due to lack of fat accumulation, a decrease in lean body mass or a combination of the two. However, we could not detect an obvious correlation between bodyweight and perimeter (our unpublished results). Moreover, in contrast to humans, in mice a relationship between bodyweight and femur, vertebral and phalangeal bone parameters has not been found (46-49,53).

Leptin

An alternative link between altered fat mass and bone metabolism can be leptin. Leptin is a protein hormone that is primarily secreted by white adipose tissue. It seems to be able to modulate the reciprocal differentiation of stromal cells between osteoblast and adipocyte pathways and of inhibiting osteoclastogenesis (54). The lower leptin levels correlate with the lower amount of fat in TTD mice to a certain extent. Whether the somewhat lower leptin levels contribute to the bone phenotype in TTD mice is unknown. In addition, possible effects are not straightforward as correlation studies do not give unequivocal results and it consti-

tutes a complex system also involving central regulatory pathways of bone metabolism (55). The complexity is further demonstrated by the fact that leptin deficient mice are the only hypogonadal animal model with a high bone mass while the high bone mass was unrelated to the increased fat mass (55). Several studies concluded that leptin is not a direct determinant of BMD (56-59) whereas others showed a negative correlation (60-65) or a positive correlation between leptin and BMD (66-68). These differences cannot only be explained by sex or menopausal status as some studies proposed (69-72). Interestingly, aging wild type mice show a drop in leptin levels before the decrease in bodyweight. It has been shown that body fat content correlates with plasma leptin in young males and females, whereas this relationship is disrupted in elderly people (73). For example, anorexia nervosa patients or amenorrhoeic athletes have low leptin levels (33).

Adrenals and corticosterone

Old TTD mice exhibit high steroidogenic activity as assessed by cell volume and the amount of mitochondria and lipids in the adrenal gland while corticosterone levels are relatively high in old male TTD, but not in female TTD mice. Firstly, steroidogenesis might be less effective in TTD mice. Secondly, the break-down-rate of corticosterone in TTD mice might be more rapid leading to a higher production, more stimulation and larger cells in the zona fasciculata. It would be of interest to measure (break-down products of) corticosterone levels in urine. Thirdly, it is possible that 11 β -hydroxysteroid dehydrogenase I, which regenerates active glucocorticoids from their inactive 11-keto derivatives, is less active and thus less corticosterone is formed (74,75). Interestingly, it was found that expression of 11 β -hydroxysteroid dehydrogenase I was reduced in another DNA repair deficient mouse model (25).

Noteworthy, overall the corticosterone levels are higher in female mice compared to male mice. It has been reported that corticosterone levels as well as levels of corticosteroid-binding globulin are higher in stressed female rats compared to stressed male rats (76). Aging C57Bl/6 female mice also showed significantly higher levels of corticosterone compared to male mice (77).

Interestingly, young TTD females showed more whorls, ie. regression of the X-zone, than wild type females. This might be due to the lower levels of estradiol in TTD mice as regression of the X-zone is also delayed in castrated wild type females.

In conclusion, the calciotropic hormone analyses indicate an altered calcium intake and/or increased calcium loss in TTD mice. However, TTD mice are able to adjust their calcium regulatory mechanism of vitamin D and PTH to maintain stable levels of serum calcium up to at least 78 weeks of age. A consequence of these altered levels of PTH and vitamin D3 will be an altered bone metabolism which may lead to a negative effect on bone volume. In addition, the lower bodyweight in TTD mice results in lower levels of serum estradiol which may contribute to the change in bone phenotype in female TTD mice. Furthermore,

microscopy of adrenals suggested that old TTD mice exhibit high, but possibly less effective steroidogenic activity. Further studies are required to fully understand the full contribution of endocrine parameters to the bone phenotype in prematurely aging DNA repair deficient trichothiodystrophy mice.

References

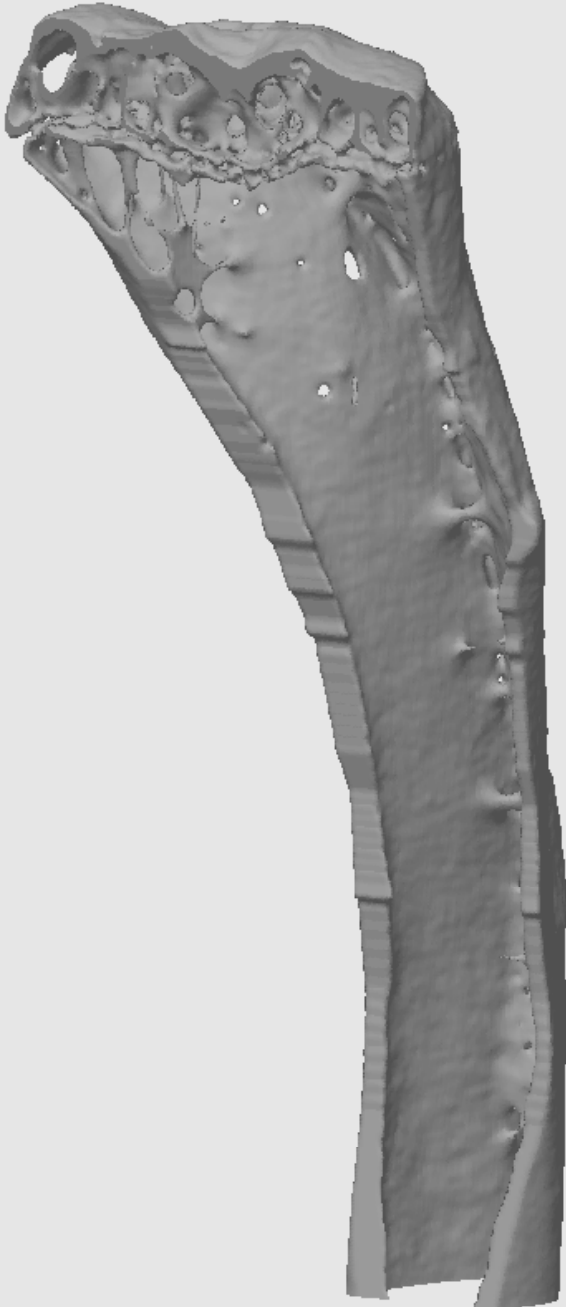
1. Bootsma D, Kraemer KH, Cleaver JE, Hoeijmakers JHJ 2002 Nucleotide excision repair syndromes: xeroderma pigmentosum, Cockayne syndrome and trichothiodystrophy. In: Vogelstein B, Kinzler KW (eds.) *The genetic basis of human cancer*. McGraw-Hill, New York, pp 211-237.
2. Bootsma D, Kraemer KH, Cleaver JE, Hoeijmakers JHJ 1998 Nucleotide excision repair syndromes: xeroderma pigmentosum, Cockayne syndrome and trichothiodystrophy. In: Vogelstein B, Kinzler KW (eds.) *The genetic basis of human cancer*. McGraw-Hill, New York, pp 245-74.
3. Botta E, Nardo T, Broughton BC, Marinoni S, Lehmann AR, Stefanini M 1998 Analysis of mutations in the XPD gene in Italian patients with trichothiodystrophy: site of mutation correlates with repair deficiency, but gene dosage appears to determine clinical severity. *Am J Hum Genet* **63**(4):1036-48.
4. Chapman S 1988 The trichothiodystrophy syndrome of Pollitt. *Pediatr Radiol* **18**(2):154-6.
5. Civitelli R, McAlister WH, Teitelbaum SL, Whyte MP 1989 Central osteosclerosis with ectodermal dysplasia: clinical, laboratory, radiologic, and histopathologic characterization with review of the literature. *J Bone Miner Res* **4**(6):863-75.
6. Itin PH, Sarasin A, Pittelkow MR 2001 Trichothiodystrophy: update on the sulfur-deficient brittle hair syndromes. *J Am Acad Dermatol* **44**(6):891-920; quiz 921-4.
7. Kousseff BG, Esterly NB 1988 Trichothiodystrophy, IBIDS syndrome or Tay syndrome? *Birth Defects Orig Artic Ser* **24**(2):169-81.
8. McCuaig C, Marcoux D, Rasmussen JE, Werner MM, Gentner NE 1993 Trichothiodystrophy associated with photosensitivity, gonadal failure, and striking osteosclerosis. *J Am Acad Dermatol* **28**(5 Pt 2):820-6.
9. Przedborski S, Ferster A, Goldman S, Wolter R, Song M, Tonnesen T, Pollitt RJ, Vamos E 1990 Trichothiodystrophy, mental retardation, short stature, ataxia, and gonadal dysfunction in three Moroccan siblings. *Am J Med Genet* **35**(4):566-73.
10. Price VH, Odom RB, Ward WH, Jones FT 1980 Trichothiodystrophy: sulfur-deficient brittle hair as a marker for a neuroectodermal symptom complex. *Arch Dermatol* **116**(12):1375-84.
11. Toelle SP, Valsangiacomo E, Boltshauser E 2001 Trichothiodystrophy with severe cardiac and neurological involvement in two sisters. *Eur J Pediatr* **160**(12):728-31.
12. Wakeling EL, Cruwys M, Suri M, Brady AF, Aylett SE, Hall C 2004 Central osteosclerosis with trichothiodystrophy. *Pediatr Radiol* **34**(7):541-6.
13. Chalut C, Moncollin V, Egly JM 1994 Transcription by RNA polymerase II: a process linked to DNA repair. *Bioessays* **16**(9):651-5.
14. Seroz T, Hwang JR, Moncollin V, Egly JM 1995 TFIIH: a link between transcription, DNA repair and cell cycle regulation. *Curr Opin Genet Dev* **5**(2):217-21.
15. Hoeijmakers JH, Egly JM, Vermeulen W 1996 TFIIH: a key component in multiple DNA transactions. *Curr Opin Genet Dev* **6**(1):26-33.
16. Svejstrup JQ, Vichi P, Egly JM 1996 The multiple roles of transcription/repair factor TFIIH. *Trends Biochem Sci* **21**(9):346-50.
17. Hwang JR, Moncollin V, Vermeulen W, Seroz T, van Vuuren H, Hoeijmakers JH, Egly JM 1996 A 3' → 5' XPB helicase defect in repair/transcription factor TFIIH of xeroderma pigmentosum group B affects both DNA repair and transcription. *J Biol Chem* **271**(27):15898-904.
18. Iben S, Tschochner H, Bier M, Hoogstraten D, Hozak P, Egly JM, Grummt I 2002 TFIIH plays an essential role in RNA polymerase I transcription. *Cell* **109**(3):297-306.

19. de Boer J, de Wit J, van Steeg H, Berg RJ, Morreau H, Visser P, Lehmann AR, Duran M, Hoeijmakers JH, Weeda G 1998 A mouse model for the basal transcription/DNA repair syndrome trichothiodystrophy. *Mol Cell* **1**(7):981-90.
20. de Boer J, Andressoo JO, de Wit J, Huijmans J, Beems RB, van Steeg H, Weeda G, van der Horst GT, van Leeuwen W, Themmen AP, Meradji M, Hoeijmakers JH 2002 Premature aging in mice deficient in DNA repair and transcription. *Science* **296**(5571):1276-9.
21. Wijnhoven SW, Beems RB, Roodbergen M, van den Berg J, Lohman PH, Diderich K, van der Horst GT, Vijg J, Hoeijmakers JH, van Steeg H 2005 Accelerated aging pathology in ad libitum fed Xpd(TTD) mice is accompanied by features suggestive of caloric restriction. *DNA Repair (Amst)*.
22. Durlinger AL, Kramer P, Karels B, de Jong FH, Uilenbroek JT, Grootegoed JA, Themmen AP 1999 Control of primordial follicle recruitment by anti-Mullerian hormone in the mouse ovary. *Endocrinology* **140**(12):5789-96.
23. Jia D, O'Brien CA, Stewart SA, Manolagas SC, Weinstein RS 2006 Glucocorticoids act directly on osteoclasts to increase their life span and reduce bone density. *Endocrinology* **147**(12):5592-9.
24. Tomooka Y, Yasui T 1978 Electron microscopic study of the response of the adrenocortical X-zone in mice treated with sex steroids. *Cell Tissue Res* **194**(2):269-77.
25. van der Pluijm I, Garinis GA, Brandt RM, Gorgels TG, Wijnhoven SW, Diderich KE, de Wit J, Mitchell JR, van Oostrom C, Beems R, Niedernhofer LJ, Velasco S, Friedberg EC, Tanaka K, van Steeg H, Hoeijmakers JH, van der Horst GT 2007 Impaired genome maintenance suppresses the growth hormone--insulin-like growth factor 1 axis in mice with Cockayne syndrome. *PLoS Biol* **5**(1):e2.
26. Goltzman D, Miao D, Panda DK, Hendy GN 2004 Effects of calcium and of the Vitamin D system on skeletal and calcium homeostasis: lessons from genetic models. *J Steroid Biochem Mol Biol* **89-90**(1-5):485-9.
27. Suda T, Ueno Y, Fujii K, Shinki T 2003 Vitamin D and bone. *J Cell Biochem* **88**(2):259-66.
28. Smith EA, Frankenburg EP, Goldstein SA, Koshizuka K, Elstner E, Said J, Kubota T, Uskokovic M, Koeffler HP 2000 Effects of long-term administration of vitamin D3 analogs to mice. *J Endocrinol* **165**(1):163-72.
29. van der Eerden BC, Hoenderop JG, de Vries TJ, Schoenmaker T, Buurman CJ, Uitterlinden AG, Pols HA, Bindels RJ, van Leeuwen JP 2005 The epithelial Ca²⁺ channel TRPV5 is essential for proper osteoclastic bone resorption. *Proc Natl Acad Sci U S A* **102**(48):17507-12.
30. Okazaki R, Inoue D, Shibata M, Saika M, Kido S, Ooka H, Tomiyama H, Sakamoto Y, Matsumoto T 2002 Estrogen promotes early osteoblast differentiation and inhibits adipocyte differentiation in mouse bone marrow stromal cell lines that express estrogen receptor (ER) alpha or beta. *Endocrinology* **143**(6):2349-56.
31. Zhao H, Innes J, Brooks DC, Reierstad S, Yilmaz MB, Lin Z, Bulun SE 2009 A novel promoter controls Cyp19a1 gene expression in mouse adipose tissue. *Reprod Biol Endocrinol* **7**:37.
32. Riggs BL, Khosla S, Melton LJ, 3rd 2002 Sex steroids and the construction and conservation of the adult skeleton. *Endocr Rev* **23**(3):279-302.
33. Harada S, Rodan GA 2003 Control of osteoblast function and regulation of bone mass. *Nature* **423**(6937):349-55.
34. Chan GK, Duque G 2002 Age-related bone loss: old bone, new facts. *Gerontology* **48**(2):62-71.
35. Fujita M, Urano T, Horie K, Ikeda K, Tsukui T, Fukuoka H, Tsutsumi O, Ouchi Y, Inoue S 2002 Estrogen activates cyclin-dependent kinases 4 and 6 through induction of cyclin D in rat primary osteoblasts. *Biochem Biophys Res Commun* **299**(2):222-8.

36. Ernst M, Heath JK, Rodan GA 1989 Estradiol effects on proliferation, messenger ribonucleic acid for collagen and insulin-like growth factor-I, and parathyroid hormone-stimulated adenylate cyclase activity in osteoblastic cells from calvariae and long bones. *Endocrinology* **125**(2):825-33.
37. Modder UI, Riggs BL, Spelsberg TC, Fraser DG, Atkinson EJ, Arnold R, Khosla S 2004 Dose-response of estrogen on bone versus the uterus in ovariectomized mice. *Eur J Endocrinol* **151**(4):503-10.
38. Duan Y, Beck TJ, Wang XF, Seeman E 2003 Structural and biomechanical basis of sexual dimorphism in femoral neck fragility has its origins in growth and aging. *J Bone Miner Res* **18**(10):1766-74.
39. Turner RT, Colvard DS, Spelsberg TC 1990 Estrogen inhibition of periosteal bone formation in rat long bones: down-regulation of gene expression for bone matrix proteins. *Endocrinology* **127**(3):1346-51.
40. Bouillon R, Bex M, Vanderschueren D, Boonen S 2004 Estrogens are essential for male pubertal periosteal bone expansion. *J Clin Endocrinol Metab* **89**(12):6025-9.
41. Ahlborg HG, Johnell O, Turner CH, Rannevik G, Karlsson MK 2003 Bone loss and bone size after menopause. *N Engl J Med* **349**(4):327-34.
42. Lee K, Jessop H, Suswillo R, Zaman G, Lanyon L 2003 *Endocrinology: bone adaptation requires oestrogen receptor-alpha*. *Nature* **424**(6947):389.
43. Fernandez NJ, Kidney BA 2007 Alkaline phosphatase: beyond the liver. *Vet Clin Pathol* **36**(3):223-33.
44. Mosekilde L 2000 Age-related changes in bone mass, structure, and strength--effects of loading. *Z Rheumatol* **59 Suppl 1**:1-9.
45. Wiren KM 2005 Androgens and bone growth: it's location, location, location. *Curr Opin Pharmacol*.
46. Douchi T, Iemura A, Matsuo T, Kuwahata T, Oki T, Yoshimitsu N, Nagata Y 2003 Relationship of head lean mass to regional bone mineral density in elderly postmenopausal women. *Maturitas* **46**(3):225-30.
47. Dawson-Hughes B, Shipp C, Sadowski L, Dallal G 1987 Bone density of the radius, spine, and hip in relation to percent of ideal body weight in postmenopausal women. *Calcif Tissue Int* **40**(6):310-4.
48. Hassager C, Christiansen C 1989 Influence of soft tissue body composition on bone mass and metabolism. *Bone* **10**(6):415-9.
49. Ribot C, Tremollieres F, Pouilles JM, Bonneau M, Germain F, Louvet JP 1987 Obesity and postmenopausal bone loss: the influence of obesity on vertebral density and bone turnover in postmenopausal women. *Bone* **8**(6):327-31.
50. Skerry TM, Suva LJ 2003 Investigation of the regulation of bone mass by mechanical loading: from quantitative cytochemistry to gene array. *Cell Biochem Funct* **21**(3):223-9.
51. Douchi T, Kuwahata R, Matsuo T, Uto H, Oki T, Nagata Y 2003 Relative contribution of lean and fat mass component to bone mineral density in males. *J Bone Miner Metab* **21**(1):17-21.
52. Wang MC, Bachrach LK, Van Loan M, Hudes M, Flegal KM, Crawford PB 2005 The relative contributions of lean tissue mass and fat mass to bone density in young women. *Bone* **37**(4):474-81.
53. Beamer WG, Donahue LR, Rosen CJ, Baylink DJ 1996 Genetic variability in adult bone density among inbred strains of mice. *Bone* **18**(5):397-403.
54. Thomas T 2003 Leptin: a potential mediator for protective effects of fat mass on bone tissue. *Joint Bone Spine* **70**(1):18-21.
55. Ducy P, Amling M, Takeda S, Priemel M, Schilling AF, Beil FT, Shen J, Vinson C, Rueger JM, Karsenty G 2000 Leptin inhibits bone formation through a hypothalamic relay: a central control of bone mass. *Cell* **100**(2):197-207.

56. Zhong N, Wu XP, Xu ZR, Wang AH, Luo XH, Cao XZ, Xie H, Shan PF, Liao EY 2005 Relationship of serum leptin with age, body weight, body mass index, and bone mineral density in healthy mainland Chinese women. *Clin Chim Acta* **351**(1-2):161-8.
57. Shaarawy M, Abassi AF, Hassan H, Salem ME 2003 Relationship between serum leptin concentrations and bone mineral density as well as biochemical markers of bone turnover in women with postmenopausal osteoporosis. *Fertil Steril* **79**(4):919-24.
58. Ruhl CE, Everhart JE 2002 Relationship of serum leptin concentration with bone mineral density in the United States population. *J Bone Miner Res* **17**(10):1896-903.
59. Martini G, Valenti R, Giovani S, Franci B, Campagna S, Nuti R 2001 Influence of insulin-like growth factor-1 and leptin on bone mass in healthy postmenopausal women. *Bone* **28**(1):113-7.
60. Di Monaco M, Vallero F, Di Monaco R, Mautino F, Cavanna A 2003 Fat body mass, leptin and femur bone mineral density in hip-fractured women. *J Endocrinol Invest* **26**(12):1180-5.
61. Kontogianni MD, Dafni UG, Routsias JG, Skopouli FN 2004 Blood leptin and adiponectin as possible mediators of the relation between fat mass and BMD in perimenopausal women. *J Bone Miner Res* **19**(4):546-51.
62. Morberg CM, Tetens I, Black E, Toubro S, Soerensen TI, Pedersen O, Astrup A 2003 Leptin and bone mineral density: a cross-sectional study in obese and nonobese men. *J Clin Endocrinol Metab* **88**(12):5795-800.
63. Sun AJ, Jing T, Heymsfield SB, Phillips GB 2003 Relationship of leptin and sex hormones to bone mineral density in men. *Acta Diabetol* **40 Suppl 1**:S101-5.
64. Blum M, Harris SS, Must A, Naumova EN, Phillips SM, Rand WM, Dawson-Hughes B 2003 Leptin, body composition and bone mineral density in premenopausal women. *Calcif Tissue Int* **73**(1):27-32.
65. Sato M, Takeda N, Sarui H, Takami R, Takami K, Hayashi M, Sasaki A, Kawachi S, Yoshino K, Yasuda K 2001 Association between serum leptin concentrations and bone mineral density, and biochemical markers of bone turnover in adult men. *J Clin Endocrinol Metab* **86**(11):5273-6.
66. Pasco JA, Henry MJ, Kotowicz MA, Collier GR, Ball MJ, Ugoni AM, Nicholson GC 2001 Serum leptin levels are associated with bone mass in nonobese women. *J Clin Endocrinol Metab* **86**(5):1884-7.
67. Eleftheriou F, Takeda S, Ebihara K, Magre J, Patano N, Kim CA, Ogawa Y, Liu X, Ware SM, Craigen WJ, Robert JJ, Vinson C, Nakao K, Capeau J, Karsenty G 2004 Serum leptin level is a regulator of bone mass. *Proc Natl Acad Sci U S A* **101**(9):3258-63.
68. Blain H, Vuillemin A, Guillemin F, Durant R, Hanesse B, de Talance N, Doucet B, Jeandel C 2002 Serum leptin level is a predictor of bone mineral density in postmenopausal women. *J Clin Endocrinol Metab* **87**(3):1030-5.
69. Chanprasertyothin S, Piaseu N, Chailurkit L, Rajatanavin R, Ongphiphadhanakul B 2005 Association of circulating leptin with bone mineral density in males and females. *J Med Assoc Thai* **88**(5):655-9.
70. Thomas T, Burguera B, Melton LJ, 3rd, Atkinson EJ, O'Fallon WM, Riggs BL, Khosla S 2001 Role of serum leptin, insulin, and estrogen levels as potential mediators of the relationship between fat mass and bone mineral density in men versus women. *Bone* **29**(2):114-20.
71. Iwamoto I, Douchi T, Kosha S, Murakami M, Fujino T, Nagata Y 2000 Relationships between serum leptin level and regional bone mineral density, bone metabolic markers in healthy women. *Acta Obstet Gynecol Scand* **79**(12):1060-4.
72. Nindl BC, Scoville CR, Sheehan KM, Leone CD, Mello RP 2002 Gender differences in regional body composition and somatotrophic influences of IGF-I and leptin. *J Appl Physiol* **92**(4):1611-8.

73. Moller N, O'Brien P, Nair KS 1998 Disruption of the relationship between fat content and leptin levels with aging in humans. *J Clin Endocrinol Metab* **83**(3):931-4.
74. Tomlinson JW, Walker EA, Bujalska IJ, Draper N, Lavery GG, Cooper MS, Hewison M, Stewart PM 2004 11beta-hydroxysteroid dehydrogenase type 1: a tissue-specific regulator of glucocorticoid response. *Endocr Rev* **25**(5):831-66.
75. Holmes MC, Seckl JR 2006 The role of 11beta-hydroxysteroid dehydrogenases in the brain. *Mol Cell Endocrinol* **248**(1-2):9-14.
76. Tinnikov AA 1999 Responses of serum corticosterone and corticosteroid-binding globulin to acute and prolonged stress in the rat. *Endocrine* **11**(2):145-50.
77. Grad B, Khalid R 1968 Circulating corticosterone levels of young and old, male and female C57B1/6J mice. *J Gerontol* **23**(4):522-8.



CHAPTER 6

Concluding remarks and future perspectives

TTD mice display features of premature aging in many organs and tissues (1,2) although the progeroid symptoms do not affect all tissues to the same extent. In fact, paradoxically, a detailed, systematic large cohort analysis revealed that some organs and tissues even exhibit features resembling caloric restriction and delayed aging. For instance, the occurrence of cataract in the eyes in TTD mice was found to be significantly less compared to the isogenic wild type control mice kept under the same conditions (2). This extends the notion that all human progeroid syndromes are segmental (3), i.e. that multiple organs suffer from rapid aging, yet others seem relatively unaffected and as shown by TTD mice may even age slower than wild type controls. Microarray expression analysis of various accelerated aging mice revealed a strong parallel with expression profiles of normal aging (4). To examine at the level of physiology, whether TTD mice are indeed a *bona fide* model for aging and to rule out that it is a developmental disorder, we carried out a detailed comparison of the effect of aging on bone parameters of progeroid TTD females with wild type controls. This systematic analysis uncovered the consequence of a defect in DNA repair and basal transcription on the velocity of age-related skeletal changes and assessed to which extent the skeletal abnormalities reflect normal bone aging.

Bone develops normally in TTD mice, i.e. bone volume, cortical thickness and perimeter in tibiae are similar in wild type and TTD mice up to 39 weeks of age. In addition, similar numbers of osteoblasts and osteoclasts were observed in early bone marrow cultures and periosteal apposition was present in tibiae up to at least 13-weeks of age. This observation excludes a developmental defect as explanation for the TTD phenotype and is in line with other studies on TTD mice (2).

After 39 weeks of age profound accelerated decrease in bone volume is observed in tibiae of TTD mice. The decrease in bone volume is almost 40 weeks ahead of that in wild type mice. In parallel with the decrease in bone volume, an accelerated decrease in bone strength is observed in TTD mice after 26 weeks of age. This accelerated form of natural bone aging strongly underlines the premature aging phenotype of TTD mice, which implies that the other aging-like features in TTD mice and patients may also represent *bona fide* premature aging symptoms and which in a broader context substantiates the importance of DNA repair in healthy aging.

An important mechanism underlying the accelerated decrease in bone strength is that in TTD mice the larger endocortical volume is not fully compensated by periosteal apposition and a subsequent increase in perimeter as seen in wild type mice. In fact, TTD mice show a significant decrease in periosteal apposition between 13 and 39 weeks of age.

The accelerated decrease in bone volume is preceded by an accelerated decrease in bone nodule formation in *ex vivo* osteogenic bone marrow cultures. These data implicate an accelerated reduction in the number of mesenchymal stem cells but also imply that they still

can differentiate into osteoblasts. The adipocyte cultures support the fact that the intrinsic differentiation capacity of mesenchymal stem cells is not significantly affected. Whereas TTD mice lack fat accumulation *in vivo*, normal adipocyte differentiation is observed *in vitro*. We hypothesize that DNA damage levels in TTD mice reach a critical threshold in (mesenchymal) stem cells between 13 and 26 weeks, which triggers apoptosis and cellular senescence and translates into reduced numbers of differentiated osteoblasts and a bone phenotype between 39 and 52 weeks of age.

Although there is an accelerated decrease in bone nodule formation, TTD bone marrow mesenchymal stem cells retain bone forming capacity. In addition to the data from the bone marrow cultures, this is shown by the effect of intermittent PTH administration on long bones of TTD mice. After intermittent PTH administration TTD mice demonstrated an increase in cortical thickness implicating that the stem cells/osteoblasts can still be stimulated to form bone. Considering the above mentioned relationship between DNA repair and apoptosis, it is interesting to note that PTH has been reported to inhibit osteoblast apoptosis (5,6).

The accelerated skeletal aging in TTD mice is likely the result of a combination of an accelerated decline in the number of osteogenic stem cells together with altered systemic influences. Indeed, various DNA repair deficient mouse models exhibiting premature aging show a systemic downregulation of various key hormonal axes, including for example the growth hormone--insulin-like growth factor 1 axis (4), which may also contribute to the observed loss of osteoprogenitors. Although these systemic factors have not been fully identified in TTD mice, we observed several changes in TTD mice suggesting that systemic factors influence the phenotype. For example, TTD females exhibit significantly lower levels of estradiol which may contribute to the accelerated bone loss observed in TTD mice. The lower levels of estradiol in TTD mice are not likely due to ovarian dysfunction as wild type and TTD females have similar numbers of growing and ovulatory follicles. Rather, estradiol levels are higher in wild type females as additional estrogen is produced by aromatase in the fat mass that is strongly reduced in TTD mutants. As TTD mesenchymal stem cells were shown to form adipocytes, systemic effects are likely to cause the lack of fat tissue in TTD mice.

In contrast to the osteopenic phenotype observed in long bones of TTD mice, 78-week-old TTD mutants exhibit significantly increased bone mass in their vertebrae. It appears from the data on trabecular bone volume fraction, trabecular number and trabecular thickness distribution that already young TTD mice have more bone mass in their vertebrae than wild type mice. As increased bone mass is also observed in vertebrae of TTD patients, it is intrinsic to the *XPD* mutation. The increase in trabecular bone volume fraction, which (partly) can be observed as an increase in the disorganized appearance of the vertebrae in old TTD mice might represent a local increase in the number or differentiation of osteogenic mesenchymal stem cells. On the other hand, the observed increase in the number of trabeculae may result from a decrease in the number of osteocytes followed by a decrease in sclerostin expression, i.e. in contrast to TTD tibiae, TTD vertebrae seem to exhibit less osteocytes which are thought

to be the mechanosensors in bone. Osteocytes secrete sclerostin, which inhibits bone formation and mineralization by osteoblasts. When osteocytes are absent or their numbers are decreased, it can thus be expected that bone formation is increased.

The bone phenotype in mice closely resembles the bone phenotype in TTD patients showing osteosclerotic vertebrae and osteopenic long bones and validates the XPD point mutant (TTD) mouse as a *bona fide* model for trichothiodystrophy. Whereas TTD mice exhibit a premature aging phenotype in long bones, the higher bone mass in vertebrae does not represent a premature aging phenotype as wild type mice do not show such an extensive increase in bone mass nor is this observed in humans. TTD mice thus exhibit segmental aging even within the skeleton.

While answering our first questions, many other questions came up during our study. The lack of effective periosteal apposition in adult TTD mice is intriguing as it is a localized phenomenon. While intermittent PTH administration to TTD mice demonstrated an increase in cortical thickness, no increase in perimeter was observed. Thus, the PTH effect on cortical thickness in TTD mice appears to be the result of increased endosteal bone formation and not periosteal apposition. Interestingly, a recent study showed differences in mechanism by which intermittent PTH treatment increases bone formation at the endosteal and at the periosteal surface (7). The increase in endocortical osteoblasts after intermittent PTH treatment is predominantly due to attenuated osteoblast apoptosis (7). In periosteal bone where the rate of osteoblast apoptosis is low, PTH does not increase the number of osteoblasts by attenuating apoptosis, but by exerting pro-differentiating effects on post-mitotic pre-osteoblasts (7). While we observe no difference in endosteal bone formation between aging wild type and TTD mice, endosteal bone formation does show a declining trend with aging. It would be of interest to treat wild type mice with intermittent PTH and assess whether wild type mice show a lower, similar or more pronounced increase in cortical thickness compared to TTD mice and whether they show an increase in periosteal bone formation as well.

A decrease in the number of osteogenic cells was shown in bone marrow cultures from TTD mice. However, *in vivo* TTD mice do not show a decrease in endosteal bone formation compared to wild type mice whereas they do show a significant decrease in periosteal bone formation. It seems that in addition to the decrease in osteogenic stem cells, other factors, e.g. systemic factors and/or mechanical loading, play a major role in periosteal bone formation. TTD mice provide an excellent tool to study periosteal apposition and to analyze the different age-related mechanisms at the endosteal and periosteal level.

Furthermore, while we hypothesize that DNA damage levels in TTD mice reach a critical threshold in (mesenchymal) stem cells, which triggers cell death and cellular senescence and translates into reduced numbers of differentiated osteoblasts, this remains to be proven definitely. At this moment, it is not possible to measure DNA damage in mesenchymal stem cells and to relate this to (altered) gene-expression in bone marrow of TTD mice of different

ages. Alternatively, one could assess the impact of DNA damage induced by oxygen radicals on the development of mesenchymal stem cells. It is possible to culture mesenchymal stem cells at different percentages of oxygen. One expects less DNA damage when culturing cells at a low oxygen percentage (2-3%) compared to the most commonly used (unphysiological) 20% oxygen. It would be interesting to see whether the difference in osteogenic cell numbers is smaller between wild type and TTD mice when cultured at low oxygen. On the other hand, one could culture the cells at a higher oxygen percentage and assess whether the number of osteogenic cells is even lower in TTD mice. In addition, one could isolate DNA from the cultured cells and analyze differences in the number of oxidatively induced lesions by gas chromatography or mass spectrometry (8). In parallel, one could perform micro-array analysis and assess changes in gene-expression in bone marrow cells. Ideally, mesenchymal stem cells should be isolated for this purpose, but at this moment mesenchymal stem cell-specific antibodies are not available. *In vivo*, transplantations of wild type bone marrow to TTD mice may reduce the decline in bone volume that is observed in TTD mice arguing for the role of diminished osteogenic stem cells in TTD mice.

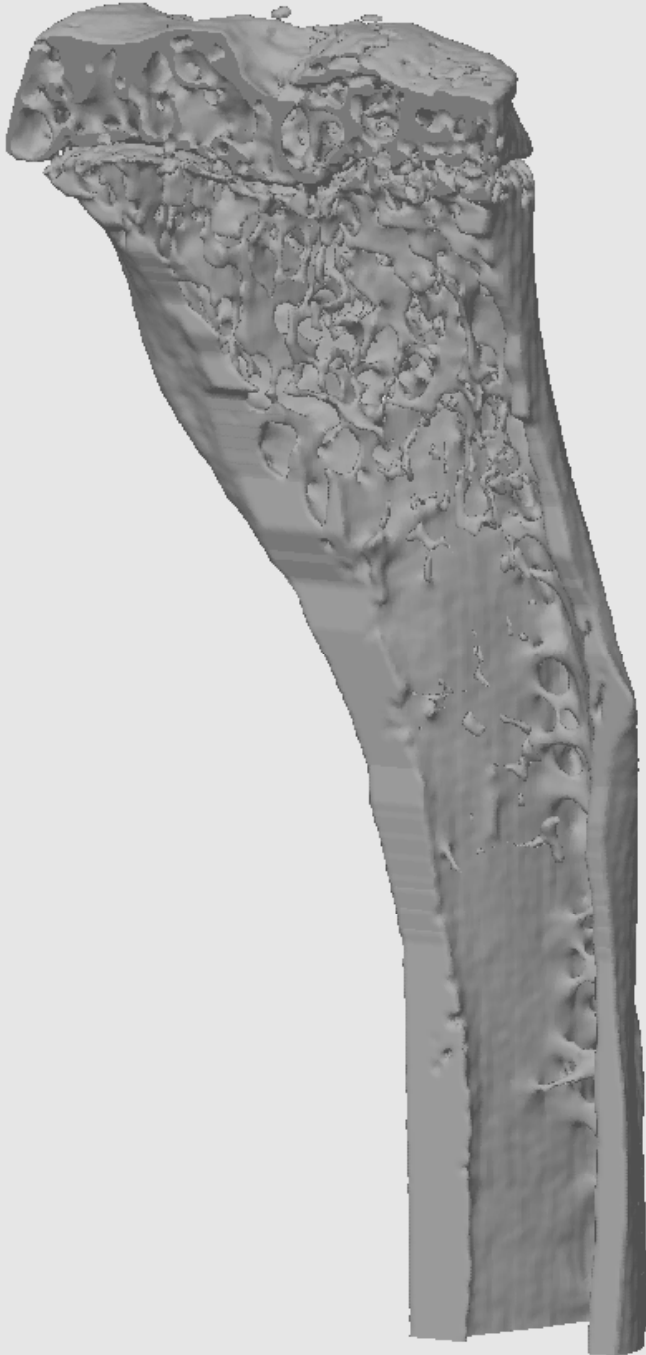
Next to the osteopenic phenotype in long bones, TTD mice displayed a high bone mass phenotype in their vertebrae. It would be of great interest to study mesenchymal stem cells derived specifically from murine vertebrae. However, this is technically very challenging. To analyze the difference between long bones and vertebrae in greater detail, one could assess the effect of intermittent PTH treatment on the phenotype in vertebrae. Furthermore, it would be of interest to exactly measure the number of osteocytes in vertebrae. As we hypothesize that decreased expression of sclerostin by osteocytes might contribute to the high bone mass phenotype in TTD mice, it would also be of interest to measure the expression of sclerostin in long bones and vertebrae (by *in situ* hybridisation, RT-PCR or high throughput sequencing).

In addition to sclerostin measurement, other systemic factors that may contribute to the (bone) phenotype in TTD mice could be analysed; e.g. expression of genes related to calcium homeostasis such as 1 α -hydroxylase in kidney samples. Another possibility to study systemic factors is to perform intervention studies with e.g. estrogen supplementation or to assess the impact of bone resorption inhibition by bone resorption inhibitors like bisphosphonates.

In conclusion, the TTD mouse mutant constitutes a valid model for bone aging in long bones and is an excellent tool to study periosteal apposition as well as age-related differences between long bones and vertebrae. Furthermore, proper DNA repair, notably transcription-coupled repair, is required to maintain optimal bone characteristics and strength as long as possible.

References

1. de Boer J, Andressoo JO, de Wit J, Huijmans J, Beems RB, van Steeg H, Weeda G, van der Horst GT, van Leeuwen W, Themmen AP, Meradji M, Hoeijmakers JH 2002 Premature aging in mice deficient in DNA repair and transcription. *Science* **296**(5571):1276-9.
2. Wijnhoven SW, Beems RB, Roodbergen M, van den Berg J, Lohman PH, Diderich K, van der Horst GT, Vijg J, Hoeijmakers JH, van Steeg H 2005 Accelerated aging pathology in ad libitum fed Xpd(TTD) mice is accompanied by features suggestive of caloric restriction. *DNA Repair (Amst)*.
3. Martin GM 2005 Genetic modulation of senescent phenotypes in Homo sapiens. *Cell* **120**(4):523-32.
4. van der Pluijm I, Garinis GA, Brandt RM, Gorgels TG, Wijnhoven SW, Diderich KE, de Wit J, Mitchell JR, van Oostrom C, Beems R, Niedernhofer LJ, Velasco S, Friedberg EC, Tanaka K, van Steeg H, Hoeijmakers JH, van der Horst GT 2007 Impaired genome maintenance suppresses the growth hormone--insulin-like growth factor 1 axis in mice with Cockayne syndrome. *PLoS Biol* **5**(1):e2.
5. Jilka RL, Weinstein RS, Bellido T, Roberson P, Parfitt AM, Manolagas SC 1999 Increased bone formation by prevention of osteoblast apoptosis with parathyroid hormone. *J Clin Invest* **104**(4):439-46.
6. Sowa H, Kaji H, Lu MF, Tsukamoto T, Sugimoto T, Chihara K 2003 Parathyroid hormone-Smad3 axis exerts anti-apoptotic action and augments anabolic action of transforming growth factor beta in osteoblasts. *J Biol Chem* **278**(52):52240-52.
7. Jilka RL, O'Brien CA, Ali AA, Roberson PK, Weinstein RS, Manolagas SC 2009 Intermittent PTH stimulates periosteal bone formation by actions on post-mitotic preosteoblasts. *Bone* **44**(2):275-86.
8. Anson RM, Senturker S, Dizdaroglu M, Bohr VA 1999 Measurement of oxidatively induced base lesions in liver from Wistar rats of different ages. *Free Radic Biol Med* **27**(3-4):456-62.



SUMMARY

Summary

Trichothiodystrophy (TTD) is a rare, autosomal recessive Nucleotide Excision Repair (NER) disorder caused by mutations in components of the dual functional NER/basal transcription factor TFIIH. TTD mice, carrying a patient-based point mutation in the *Xpd* gene, strikingly resemble many features of the human syndrome and exhibit signs of segmental premature aging. For example, TTD patients exhibit skeletal abnormalities like thoracic kyphosis, axial osteosclerosis, and peripheral osteoporosis while radiographs of 14-month-old TTD mice revealed prominent kyphosis, generalized reduction in radio-density of the skeleton, but higher radio-density in the skull. In this thesis we performed an extensive analysis of the bone phenotype in aging TTD mice to gain insight in the premature aging phenotype of TTD mice.

We showed that female TTD mice exhibit accelerated bone aging from 39 weeks onwards as well as lack of periosteal apposition leading to reduced bone strength. Prior to 39 weeks long bones of wild type and TTD mice are identical excluding a developmental defect. Albeit that bone formation is decreased, osteoblasts in TTD mice retain bone-forming capacity as in vivo PTH treatment leads to increased cortical thickness. In vitro bone marrow cell cultures showed that TTD osteoprogenitors retain the capacity to differentiate into osteoblasts. However, after 13 weeks of age TTD females show decreased bone nodule formation. No differences in osteoclasts or bone resorption were detected. We hypothesize that DNA damage levels in TTD mice reach a critical threshold in (mesenchymal) stem cells between 13 and 26 weeks, which triggers apoptosis and cellular senescence and translates into reduced numbers of differentiated osteoblasts and a bone phenotype between 39 and 52 weeks of age.

Next we showed that male TTD mice also display accelerated bone aging. Long bones of TTD males exhibit a rapid 90% decrease in periosteal apposition at 78 weeks and an overall decline in bone strength of about 25% compared to wild type males. After 42 weeks of development, mesenchymal differentiation potential towards the osteoblast lineage was significantly decreased in TTD males. In contrast, mineralization of osteoblast colonies and adipocyte and osteoclast differentiation were not impaired. In comparison with their female counterparts, TTD males are not as strongly affected and the dynamics of their accelerated skeletal aging seem to be slightly different.

In contrast to the decline in bone volume in long bones of TTD mice, we showed that vertebrae of TTD mice exhibit increased bone mass compared to wild type mice. This osteosclerotic phenotype in vertebrae is strikingly similar to the phenotype observed in TTD patients. The bone phenotype in mice thus closely resembles the bone phenotype in TTD patients showing osteopenic long bones and osteosclerotic vertebrae. Whereas TTD mice exhibit a premature aging phenotype in long bones, the higher bone mass in vertebrae does not represent a premature aging phenotype as wild type mice do not show such an extensive

increase in bone mass nor is this observed in humans. TTD mice thus exhibit segmental aging even within the skeleton.

We hypothesized that altered systemic influences contribute to the observed bone phenotype in TTD mice and analyzed bodyweight, several bone metabolism-related serum parameters as well as histology of the adrenals and ovaries in aging wild type and TTD mice. Aging TTD females exhibit significantly lower levels of estradiol which may contribute to the accelerated bone loss observed in TTD females. In addition, TTD mice showed low levels of parathyroid hormone and 25-hydroxyvitamin D3 while bone turnover markers showed no significant differences and 1,25-dihydroxyvitamin D3 levels were higher in aging TTD females. Analysis of adrenals suggests less effective steroidogenesis in TTD mice. In conclusion, TTD mice show differences in circulating levels of hormones known to control bone metabolism as well as calcium homeostasis. These changes did not result in altered serum calcium but may constitute the systemic influences contributing to the bone phenotype in prematurely aging trichothiodystrophy mice.

TTD mice thus provide an excellent tool to study bone aging in long bones, periosteal apposition, the different age-related mechanisms at the endosteal and periosteal level as well as age-related differences between long bones and vertebrae. Furthermore, proper DNA repair, notably transcription-coupled repair, is required to maintain optimal bone characteristics and strength as long as possible.

Samenvatting

Vrijwel elke cel in ons lichaam bevat het erfelijk materiaal. Dit erfelijk materiaal, het DNA, is van groot belang voor het specifieke functioneren van de verschillende cellen. Het DNA wordt echter continu beschadigd door zowel externe factoren, zoals zonlicht en sigarettenrook, als interne factoren, zoals zuurstofradikalen die ontstaan bij de stofwisseling. Deze schade aan het DNA kan ernstige gevolgen hebben. Bij het kopiëren van beschadigd DNA kunnen permanente veranderingen (mutaties) in de genetische code ontstaan waardoor cellen bijvoorbeeld ongeremd kunnen gaan delen en uiteindelijk kanker kunnen veroorzaken. DNA schade kan ook resulteren in het stoppen van de celdeling of in celdood waardoor (vroegtijdige) veroudering kan optreden. Gelukkig bestaan er verschillende DNA herstelmechanismen die beschadigingen in het DNA verwijderen.

Trichothiodystrofie (TTD) is een zeer zeldzame, autosomaal recessief overervende stoornis in het DNA-schade herstelmechanisme. In het verleden werd een muismodel gemaakt met een mutatie in het *XPD* gen, één van de erfelijke factoren die samen het eiwitcomplex TFIIH vormen. TFIIH is betrokken bij zowel DNA-schade herstel als basale transcriptie. TTD muizen vertonen vele symptomen die overeenkomen met problemen zoals deze bij TTD patiënten worden gezien. Daarnaast vertonen zij kenmerken van vroegtijdige veroudering. Bij TTD patiënten zijn afwijkingen van het skelet, zoals een thoracale kyphose, sclerose van de wervelkolom en osteoporose van de lange pijpbeenderen, beschreven. Bij 14 maanden oude TTD muizen werd op röntgenfoto's een opvallende kyphose, een algeheel verminderde botdichtheid en sclerose van de schedel gezien. In dit proefschrift beschrijven we een uitvoerige analyse van het botfenotype in TTD muizen met als doel het verkrijgen van inzicht in de vroegtijdige veroudering van TTD muizen en in het verlengde daarvan TTD patiënten.

In hoofdstuk 2 laten we zien dat TTD vrouwtjes vanaf de leeftijd van 39 weken een versnelde botveroudering tonen met daarbij een verminderde botvorming aan de buitenzijde van het bot (periosteale appositie) en toenemende zwakte van de botten. Voor de leeftijd van 39 weken vonden wij geen verschil tussen de lange pijpbeenderen van wild type en TTD muizen; er zijn dus geen aanwijzingen voor een stoornis in de ontwikkeling van de lange pijpbeenderen. Hoewel de botvorming is verminderd, hebben TTD muizen nog wel de capaciteit om bot te vormen; dit wordt geïllustreerd door de toename in corticale dikte bij met parathyroid hormoon (PTH) behandelde TTD muizen. PTH wordt door de bijnieren geproduceerd en stimuleert botafbraak. Bij intermitterende toediening van PTH is er echter met name sprake van botaanmaak. Ook de celkweken tonen aan dat stamcellen van TTD muizen zich nog kunnen ontwikkelen tot osteoblasten. Na de leeftijd van 13 weken laten celkweken van TTD vrouwtjes in vergelijking met wild type vrouwtjes een afname in de hoeveelheid botvormende cellen zien terwijl de osteoclasten geen verschil tonen. Onze hypothese is dat de hoeveelheid DNA schade in stamcellen van TTD muizen tussen de 13 en 26

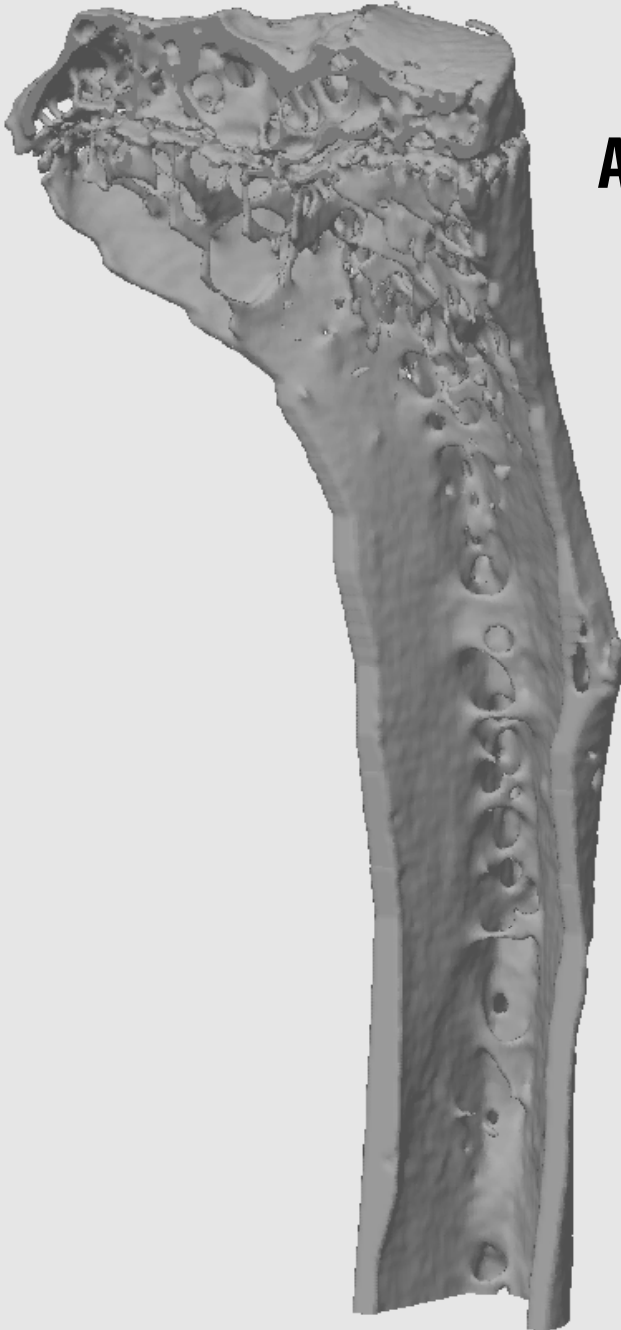
weken een kritische drempel overschrijdt waardoor celdood en celveroudering optreedt en minder osteoblasten worden gevormd met het hiervoor beschreven botfenotype als gevolg.

In hoofdstuk 3 laten we zien dat ook TTD mannetjes versnelde botveroudering, sterk verminderde periosteale appositie en zwakte van de botten tonen. Vergeleken met de vrouwtjes is het effect bij de mannetjes echter minder groot, hetgeen ook bij de mens het geval is.

In hoofdstuk 4 wordt beschreven dat wervels van TTD muizen -in tegenstelling tot het verminderd botvolume in de lange pijpbeenderen- een toename van botmassa tonen. Het beeld in de wervels van TTD muizen vertoont grote gelijkens met het beeld bij TTD patiënten, maar wijkt in dit opzicht af van het beeld bij normale veroudering. Het botfenotype van zowel de lange pijpbeenderen als de wervels vertoont grote gelijkens tussen TTD muizen en TTD patiënten, hetgeen de parallellen tussen het ziektebeeld bij de mens en het muismodel versterkt.

In hoofdstuk 5 beschrijven we de analyse van verschillende endocriene parameters die betrokken zouden kunnen zijn bij het verandere botfenotype in TTD muizen. Oude TTD vrouwtjes hebben significant minder circulerend oestrogeen wat kan bijdrage aan de afname van bot. Daarnaast werd in het bloed van TTD muizen een lagere concentratie van PTH en 25-hydroxyvitamine D3 gemeten. Bij de oude TTD vrouwtjes was de concentratie van 1,25-dihydroxyvitamine D3 hoger. Deze hormonen hebben een effect op botmeta-bolisme zowel als calciumconcentratie welke strikt gereguleerd moet worden. Mogelijk spelen deze systemische factoren een rol in het botfenotype van vroegtijdig verouderende TTD muizen.

Concluderend is het TTD muismodel een goed middel om botveroudering, periosteale appositie, verschillen tussen endosteale en periosteale appositie en de afwijkingen aan het skelet bij TTD te bestuderen. Daarnaast is het goed functioneren van het DNA herstelmechanisme van belang voor een optimale structuur en stevigheid van het bot.



APPENDIX I

Accelerated aging pathology in *ad libitum* fed *Xpd*^{TTD} mice is accompanied by features suggestive of caloric restriction

Susan W.P. Wijnhoven¹, Rudolf B. Beems¹, Marianne Roodbergen¹, Jolanda van den Berg¹, Paul H.M. Lohman¹, Karin Diderich², Gijsbertus T.J. van der Horst², Jan Vijg³, Jan H.J. Hoeijmakers² and Harry van Steeg¹

¹National Institute of Public Health and the Environment, Laboratory of Toxicology, Pathology and Genetics, Bilthoven, the Netherlands

²MGC-Department of Cell Biology and Genetics, Center for Biomedical Genetics, Erasmus University Medical Center, Rotterdam, the Netherlands

³Department of Physiology and Barshop Center for Longevity and Aging Studies, University of Texas Health Science Center, San Antonio, TX, USA

Abstract

Trichothiodystrophy (TTD) patients with a mutation in the *XPB* gene of nucleotide excision repair (NER) have a short life span and show various features of premature aging, thereby linking DNA damage to the aging process. *Xpd*^{TTD} mutant mice share many features with TTD patients, including a shorter life span, accompanied by a segmental progeroid phenotype. Here we report new pathology features supportive to the premature aging phenotype of *Xpd*^{TTD} mice. Strikingly, accelerated aging pathology is accompanied by signs suggestive of caloric restriction (CR), a condition usually linked to retardation of age-related pathology and life extension. Accelerated aging symptoms in *Xpd*^{TTD} mice are most likely due to accumulation of endogenously generated DNA damage and compromised transcription leading to cell death, whereas CR symptoms may reflect the need of *Xpd*^{TTD} mice to reduce metabolism (ROS production) in an attempt to extend their life span. Our current findings in *Xpd*^{TTD} mice further strengthen the link between DNA damage, repair and aging.

Introduction

Aging is a progressive, time-dependent deterioration in the capacity of an organism to properly function and respond adaptively to environmental challenges resulting in an increased vulnerability to death [1]. Within this process, cellular macromolecules like DNA, lipids and proteins accumulate damage leading to the malfunctioning of cellular organelles (like mitochondria) and cellular processes. In addition, damaged macromolecules may cause necrosis and apoptosis of cells resulting in tissue and organismal dysfunction and therefore can be considered as the ultimate driver of aging (reviewed in [2]). Damage to the genome leads to essentially irreversible loss of genetic information and therefore will be more deleterious than damage to RNA, proteins or lipids that can be replaced [3]. A main source of spontaneous somatic DNA damage likely involves reactive oxygen species (ROS), natural by-products of normal oxidative energy metabolism [4, 5]. More than 100 different types of oxidative DNA lesions have been described, ranging from base modifications to single- and double-strand DNA breaks and interstrand cross-links, DNA-protein crosslinks as well as damage to the phosphate-sugar backbone [6, 7]. Oxidative DNA lesions might disrupt vital processes like transcription and replication, resulting in cell death or (transient or permanent) growth arrest or may induce mutations or chromosome aberrations that lead to cancer.

To counteract the effects of (oxidative) DNA damage, an intricate network of DNA repair pathways has evolved, each focusing on a different class of lesions. One major DNA repair pathway is nucleotide excision repair (NER), which removes a broad range of bulky lesions including UV-induced damage, chemical adducts as well as some forms of oxidative damage [7, 8]. NER entails a complex 'cut and patch'-type reaction involving over 30 proteins. Important core components are the XPB and XPD helicases, which are subunits of the TFIIH complex implicated as DNA helix opener in both NER and in basal transcription initiation [9, 10]. The multi-functionality of the XPD (and XPB) protein is further illustrated by the complex genotype-phenotype relationship in human NER patients with a mutation in *XPD*. Site-specific *XPD* mutations can lead to a variety of syndromes; xeroderma pigmentosum (XP), XP combined with Cockayne syndrome (CS), or trichothiodystrophy (TTD). XP patients are highly predisposed to (skin) cancer, CS and TTD patients show various features of premature aging whereas XP-CS patients display both [11, 12].

The connection between NER deficiency and aging can be extended to several other DNA damage repair and response systems. Human segmental progeroid syndromes are frequently caused by genetic alterations that partially or wholly inactivate proteins that sense or repair DNA damage, like in the case of ataxia telangiectasia (AT), Bloom syndrome (BS) and Werner Syndrome (WS) [13]. Hence, accelerated aging symptoms in both humans and mice with genetic defects in genome maintenance, strongly suggest that a wide-spread, strong connection exists between genome care-taking and accelerated aging [14].

In order to further investigate the causes and mechanisms that underlie the aging process and the influence of genome instability on this process, we are currently performing complete lifespan studies of various NER-deficient mouse strains, all defective in one or both sub-pathways of the NER repair system (i.e. *Xpa*, *Csb*, *Xpc* and *Xpd^{TTD}* mice)(reviewed in [15]). For these studies, the mouse mutants were backcrossed over 10 generations into a homogeneous C57BL/6 background and their survival was compared to wild type C57BL/6 controls under strict specific pathogen-free (SPF) conditions.

In this report, we focus on the previously described *Xpd^{TTD}* mouse model and its segmental progeroid phenotype. The results obtained in the present study confirm and significantly extend the previous observations on this mouse model [16]. Here we report many new features not reported before in *Xpd^{TTD}* females. While most of the new features involve additional symptoms of premature aging, we also report phenotypes, consistent with what is normally observed in mice during dietary / caloric restriction, an intervention that significantly increases lifespan and retards aging-related pathology [17]. This observed dichotomy in pathology of aging *Xpd^{TTD}* female mice might be related to the complex roles of the *Xpd* gene in both DNA repair and transcription.

Material and methods

Mice

To perform longevity studies with extensive cohorts of homozygous mutant *Xpd^{TTD}* mice and C57BL/6 controls (Harlan), mice were passed through different rounds of breeding. *Xpd^{TTD}* mice used in this study carry a R722W mutation at the mouse *Xpd* gene. Generation of *Xpd^{TTD}* mice by targeting of the *Xpd^{R722W}* allele has been described previously [18]. To get a genetically homogenous background, *Xpd^{TTD}* mice were back-crossed over 10 times into a C57BL/6 background. To offer the future possibility to monitor genomic instability, heterozygous *Xpd* mutant mice as well as C57BL/6 controls were crossed with pUR288-*lacZ* C57BL/6 transgenic mice line 30, homozygous for *lacZ* integration on chromosome 11 [19], carrying 21 ± 1 copies of the pUR288-*lacZ* plasmid per haploid genome. In the second round of breeding, double heterozygous mice were intercrossed to obtain *Xpd^{TTD}* homozygous mice carrying one locus of the integrated copies of the *lacZ* marker, used in the third breeding round to generate the experimental animals for the aging (and interim) cohorts as described below. Mice were genotyped by a standard PCR reaction using DNA isolated from tail tips. Primers to amplify the wild type and targeted *Xpd* allele, as well as primer sequences for *lacZ* determination have been described previously [18, 19].



Figure 1: Age-matched Xpd^{TMD} and C57BL/6 mice of ~90 wks old.

Picture of two female mice of ~90 weeks old. On the left, a C57BL/6 mouse and right a Xpd^{TMD} mouse which is much smaller and tinier. Also brittle hair and skin lesions are clearly visible.

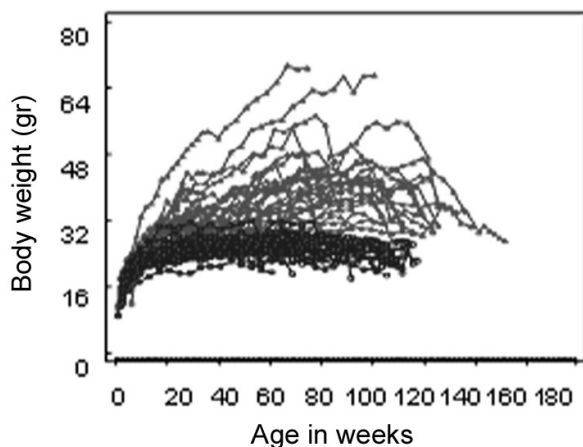


Figure 2: Body weights of Xpd^{TMD} and C57BL/6 female mice.

Body weight curves of female mice during life. Weights of Xpd^{TMD} females are depicted in blue, weights of C57BL/6 control females in red.

Experimental design

Mice were marked and randomized at the day of birth in 9 different groups; i.e. the longevity cohort, or one of the interim cohorts in which the mice were sacrificed at a fixed age of 2, 6, 13, 26, 52, 78, 91, 104, 117 or 130 weeks, respectively (scheduled sacrifice). The interim cohorts consisted of 15 Xpd^{TMD} mice, as well as 15 C57BL/6 control animals per sex per time point. In the longevity cohort, a total of 45 Xpd^{TMD} and 45 C57BL/6 controls per sex were monitored during their entire life span. Additionally, a sub-cohort of 30 wild type Xpd^{TMD} littermate controls was examined in a parallel longevity study to compare survival, pathology and body weight with the true C57BL/6 cohort. In the present study, only the findings of female Xpd^{TMD} and C57BL/6 animals are reported because data obtained with female Xpd^{TMD} wild type littermates were very similar to those from female C57BL/6 mice (data not shown). Furthermore, results from

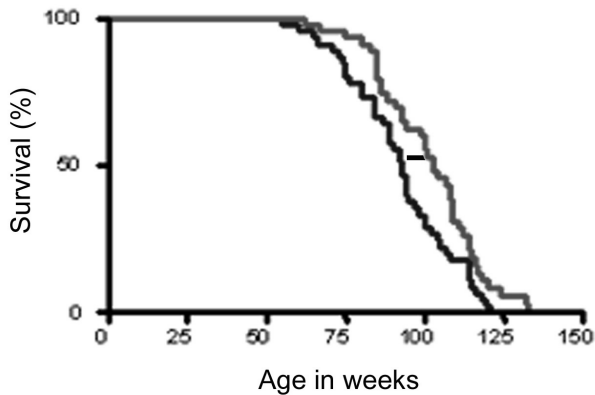


Figure 3: Survival curves of Xpd^{TTD} and C57BL/6 female mice.

Survival curves of Xpd^{TTD} (blue) and C57BL/6 (red) female mice. A statistical significant difference was determined using Kaplan Meier survival statistics with Log Rank test: p-value =0.0163.

male Xpd^{TTD} and C57BL/6 mice were comparable to those from females (data not shown). The health state of the mice was checked daily, beginning at the day of weaning. Individual animals were weighed biweekly to determine live weights. All animals were kept during their entire life span in the same and stringently controlled environment, fed *ad libitum* under a normal day/night rhythm. The microbiological status of the cohorts was monitored every 3 months during the entire study. Food intake was determined in a subgroup of 10 individual animals per genotype. Animals from the longevity cohort were removed from the study only when found dead or moribund. Complete autopsy was performed on animals of all cohorts; a total of 45 different tissues was isolated from each animal and stored for further analysis. Total animal weights as well as various organ weights were determined at time of death.

Pathology

Organ samples (40 organs and tissues) of intact animals and dissected for histopathology, were preserved in a neutral aqueous phosphate-buffered 4% solution of formaldehyde (10% neutral buffered formalin). In addition, samples of 17 different organs were snap-frozen in liquid nitrogen for further molecular biological analyses (to be published elsewhere). Tissues required for microscopic examination were embedded in paraffin wax, sectioned at 5 μm and stained with haematoxylin and eosin. Kidneys were also stained with Periodic Acid Schiff (PAS) and unstained slides were prepared of liver, brain, adrenal, ovaries and heart for lipofuscin UV-fluorescence determination. Other staining methods were used incidentally if necessary. Detailed microscopic examination was performed on all organs and tissues of all female Xpd^{TTD} and C57BL/6 control mice. Histopathological abnormalities were recorded

Table 1: Survival curve summary female mice.

	C57BL/6	<i>Xpd^{TTD}</i>
50% survival ^a	103	93
20% survival ^b	121	115
oldest survivor ^c	133	121

^amedian survival in weeks (first week of 50% mortality)

^bthe average of the longest-lived 20% of a cohort in weeks

^cage in weeks

using the PATHOS pathology data acquisition software and if possible, a cause of death was established for each animal.

Statistical evaluation

Statistical analyses of mortality curves included calculation of Kaplan-Meier distributions of survival of the two different genotypes and comparison by a two-sided log rank test (SPSS, vs 11). Also cause of death (COD) was analyzed using the Kaplan-Meier survival statistics. Incidences of lesions and tumors were analyzed with the Fisher's exact test and with the method of Peto, respectively [20].

Results

Body weights and food intake

Xpd^{TTD} mice have a remarkable phenotype that clearly mimics a segmental progeroid syndrome (Fig. 1) [16]. One striking hallmark of adult *Xpd^{TTD}* mice is a reduced bodyweight. In order to get more knowledge on bodyweight kinetics during life, we determined biweekly the bodyweights of *Xpd^{TTD}* and control C57BL/6 female mice. Results of individual animals (live weights) are plotted in Fig. 2. From this graph it is clear that at early age, growth characteristics for the *Xpd^{TTD}* females were quite similar to those of C57BL/6 control females. However, when female mice reached the age of 13 weeks, striking differences in body weight gain became apparent between *Xpd^{TTD}* and C57BL/6 females, which persisted during the rest of their lives. In general, C57BL/6 females gained weight until the age of 86-90 weeks with a mean weight of 39.0 ± 6.2 gr. After the age of 90 weeks, the majority of the wild type animals started to loose weight to a mean weight of about 32.0 gr. at the time of death. Body weights of female *Xpd^{TTD}* wild type littermates were comparable to those of the C57BL/6 controls (data not shown). *Xpd^{TTD}* females however, remained low in weight during their entire life span. The mean weight was about 25 gr. from the age of 36 wks until 90 wks, showing a remarkable tight distribution for over a 1.5-2 year period. Also *Xpd^{TTD}* female body weights displayed a tendency to decline in the final weeks of their life and as can be expected from mice with a lower body weight and diminished fat reserves; this drop was not as pronounced as observed

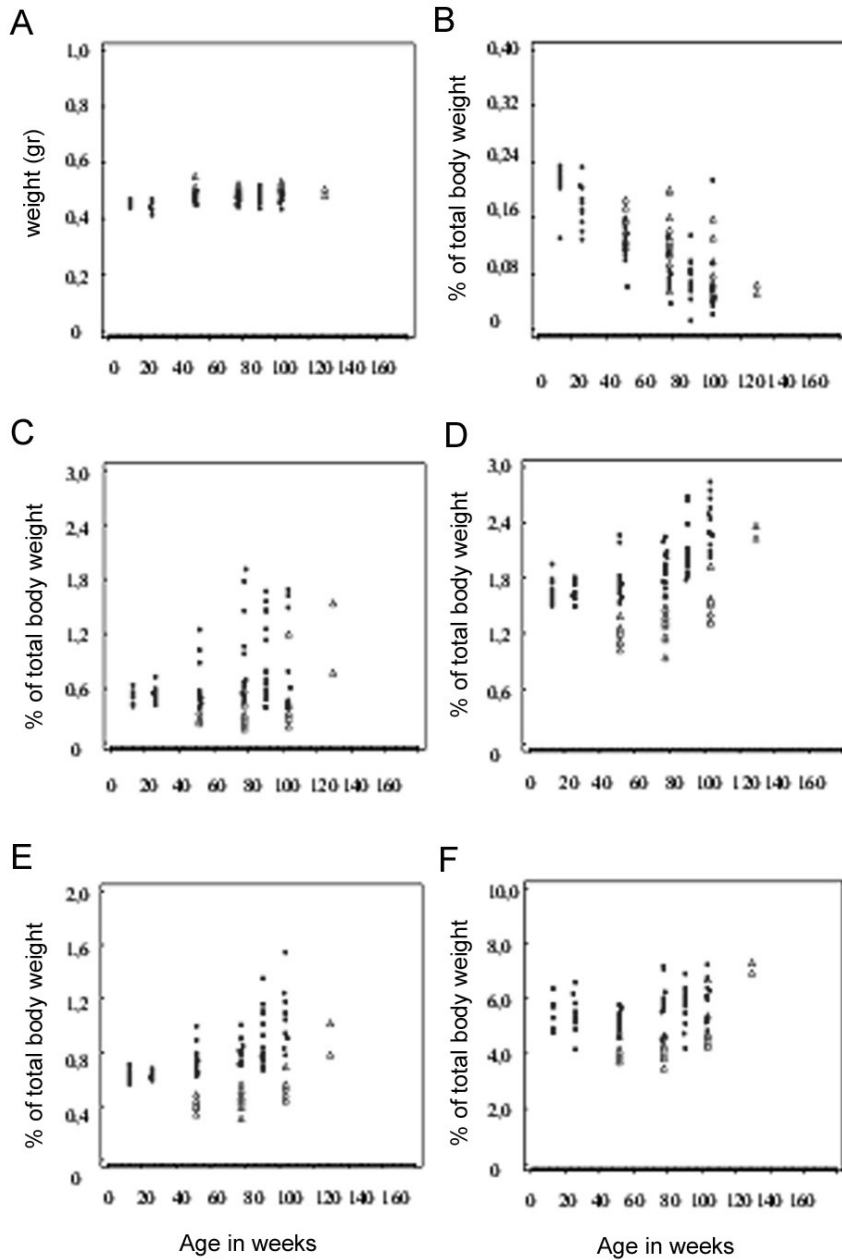


Figure 4: Organ weights at time of schedules sacrifice.

(A) Absolute brain weight in grams. Relative weights (as % of total weight) of thymus (B), spleen (C), kidney (D), heart (E), and liver (F). Organ weights of *Xpd^{TTD}* females are depicted in blue, organ weights of C57BL/6 control females in red.

in C57BL/6 mice. Average weight at the time of death in Xpd^{TTD} females was 23.3 ± 2.5 gr. Importantly, the difference in body weight between Xpd^{TTD} and C57BL/6 mice could not be explained by a difference in food intake as determined in a sub-cohort of female mice during the first 26 weeks of life. Both Xpd^{TTD} females and C57BL/6 control mice consumed 30-35 grams of food per week during this period (data not shown).

Survival of Xpd^{TTD} and C57BL/6 female mice

The survival curves for the aging cohorts of female Xpd^{TTD} as well as C57BL/6 mice as presented in Fig. 3 are based on 45 animals per genotype. All animals were removed from the cohort when found dead or when they appeared moribund. In Table 1, the age of each group at 50% survival (median survival) and maximal survival (mean age of the oldest 20%) are summarized, and the age of the oldest survivor of each genotype is listed. The median survival of Xpd^{TTD} females (93 wks) appeared significantly reduced ($p=0.0163$, Kaplan Meier with Log rank test) compared to the median survival of the C57BL/6 wild type controls (103 wks). Also the average of the longest-lived 20% of the Xpd^{TTD} cohort was lower than in C57BL/6 females, as well as the age of the oldest survivor (Table 1). Again, survival curves of Xpd^{TTD} wild type littermates were comparable to those of C57BL/6 controls (data not shown).

Organ weights

Analysis of organ weights in groups of animals with considerably different growth and terminal body weights is complicated. Absolute and relative organ weights should be evaluated together and in conjunction with body weights. Presented are the organ weights of scheduled interim sacrifices, since these weights give a good impression of the trends in organ weights in time in relatively healthy animals not suffering from terminal diseases. The absolute brain weight (Fig. 4A) was within a narrow range and was only slightly lower in Xpd^{TTD} mice compared to C57BL/6 control females. In contrast to the relatively stable brain weight, the other organs weights determined (heart, kidney, liver, spleen and thymus) are known to be influenced by variations in growth, diet, physiology, or health status. Therefore, relative weights are more informative for these organs (Fig. 4B-F). Evaluation of the lymphoid organs revealed a considerable decrease in relative (and absolute) thymus weights during life in WT mice as expected and consistent with aging, but this decline was distinctly more pronounced in Xpd^{TTD} females (Fig. 4B). The relative spleen weights of both genotypes (Fig. 4C) tended to increase in time and were higher in Xpd^{TTD} than in C57BL/6 mice up to 78 weeks but decreased afterwards in Xpd^{TTD} mice only. The Xpd^{TTD} females showed a higher variation in splenic weight, which is probably due to increased extramedullary hematopoiesis in many animals, whereas others showed lymphoid depletion. The kidney increased in weight over the whole lifespan in both genotypes and relative kidney weights were higher in Xpd^{TTD} than in C57BL/6 mice (Fig. 4D). This implies that the kidney weight stays high while the overall body weight declines, due to loss of subcutaneous and abdominal fat by Xpd^{TTD} females (see

Table 2: Causes of death in *Xpd^{TTD}* and C57BL/6 mice.

	C57BL/6		<i>Xpd^{TTD}</i>	
	n=40	%	n=35	%
Neoplasms	14	35	7	20
Inflammation	20	50	2	6*
Multiple pathology	0	0	2	6
Prolaps	0	0	12	34**
Circulatory disorders	2	5	0	0
Conditional decline	3	8	11	31**
Other	1	3	1	3

N.B. A cause of death was only given when complete autopsy and full histopathology was performed. Autolysed mice were excluded.

Statistically significant difference using Kaplan-Meier survival statistics

* $p < 0.01$ and ** $p < 0.001$

below). The heart weights of all mice increased over the whole experimental period and surprisingly not only the relative but also the absolute heart weights were higher in *Xpd^{TTD}* mice when compared to the C57BL/6 controls, despite the low body weights (Fig. 4E). Liver weights in female mice increased in C57BL/6 mice during aging, whereas the liver weights remained more or less the same in *Xpd^{TTD}* mice over time (Fig. 4F). In summary, the weights of heart, kidney and spleen appeared to be higher and thymus weights were lower in *Xpd^{TTD}* females when compared to C57BL/6 controls.

Hematological findings

In keeping with our previous findings [16], *Xpd^{TTD}* mice showed reduced red blood cell counts (RBC) during their whole life span. For instance, RBC values were 7.4, 6.4 and 7.6 $\times 10^{12}$ cells/l for *Xpd^{TTD}* mice and 8.6, 8.4 and 8.3 $\times 10^{12}$ cells/l for C57BL/6 controls at the age of 52, 78 and 104 weeks, respectively. This RBC decrease in mutant mice was associated with decreased hemoglobin and hematocrit values. However, the mean cellular hemoglobin concentration (MCHC) as well as mean corpuscular volume (MCV) was not altered in *Xpd^{TTD}* mice versus the C57BL/6 controls (data not shown), pointing to a mild normochrome anemia in *Xpd^{TTD}* mice. Platelets increased initially in both genotypes and were relatively high in *Xpd^{TTD}* females but decreased after the age of 78 weeks (from 1392 to 1151 at the age of 104 weeks). The amount of white blood cells showed a considerable variation over the whole experimental period in both genotypes (data not shown).

Causes of death

In Table 2, the causes of death are listed for both *Xpd^{TTD}* and C57BL/6 control mice as determined by combined gross and microscopic pathology. It is clear from this table that striking differences exist between the two genotypes. While in C57BL/6 control females most of the mice died of neoplasms (35%) and (skin) inflammation (50%), these numbers were much

Table 3: Tumor development in *Xpd^{TTD}* and C57BL/6 mice at the time of death.**A. Tumor summary in female mice**

	C57BL/6		<i>Xpd^{TTD}</i>	
	n=40	%	n=35	%
Number of benign tumors	24		12	
Number of malignant tumors	18		10	
Total number of tumors	42		22	
Mean number of tumors per mouse	1.1		0.6	
Number of tumor bearing animals	30	75.0	19*	54.3
Number of multiple tumor bearers	12	30.0	3	8.6
Median latency (50% percentile) ^a	788		699	

Mean age at time of death for the mice analyzed is 99,6 wks for C57BL/6 and 90,8 wks for *Xpd^{TTD}* mice

^aMedian tumor latency in days

* p=0.10 (Fisher exact test 2-sided) and not significant with the Peto method

B. Individual tumor types

		C57BL/6	<i>Xpd^{TTD}</i>
		n=40	n=35
Adrenal	pheochromocytoma (benign)	0	3
Bone	osteosarcoma	2	0
Head	squamous cell carcinoma	0	1
Harderian gland	adenoma	1	0
Lymphatic system	lymphoma	10	3*
Liver	histiocytic sarcoma	3	3
	hepatocellular carcinoma	0	1
Lung	sarcoma	1	0
	bronchiolo-alveolar carcinoma	0	1
Pituitary	pars distalis adenoma	20	3**
Small intestines	leiomyosarcoma	1	0
Skin	melanoma (benign)	0	1
Thyroid	follicular cell adenoma	1	2
Vascular system	hemangioma	2	3
	hemangiosarcoma	1	1

Mean age at time of death for the mice analyzed is 99,6 wks for C57BL/6 and 90,8 wks for *Xpd^{TTD}* mice

Statistically significant difference using Fisher's exact test

* p<0.05 and **p<0.001

Statistically significant difference using method of Peto

**p=0.002

Incidences of all other tumors are too low to reveal statistically significant differences

lower in the *Xpd* mutant mice (20% and 6%, respectively). In contrast, the most common cause of death in *Xpd^{TTD}* mice was anorectal prolapse (34%) or a general conditional decline without major pathological conditions that could be designated as a primary cause of death or a reason for the moribund state (31%). These phenomena were hardly found in the wild type controls (0% and 8% respectively). Using the Kaplan-Meier survival statistics, both decrease in (skin) inflammation (p<0.01) and increase in anorectal prolapse or conditional decline (p<0.001) were statistically significant. However, the decrease of neoplasms as a

Table 4: Histopathology differences in *Xpd^{TTD}* and C57BL/6 mice at the time of death.**A. Differences consistent with accelerated aging**

	C57BL/6 (n=40)		<i>Xpd^{TTD}</i> (n=35)	
	incidence	severity	incidence	severity
Osteoporosis femur	88.2	3.3	97.1	4.1
Hepatic lipofuscin accumulation	85.0	1.6	97.1	3.1
Hepatic intranuclear inclusions	10.0	0.1	28.6	0.5
Hepatocellular atrophy	5.0	0.1	34.3	0.5
Renal karyomegaly	17.9	0.2	38.2	0.7
Renal tubular dilatation	30.8	0.5	85.3	2.2
Renal hyaline glomerulopathy	15.4	0.3	52.9	1.1
Aortic sarcopenia	5.6	0.1	87.9	2.0
Lymphoid depletion spleen	30.8	0.4	85.7	2.0
Lymphoid depletion thymus	82.8	2.6	100	3.7
Skin reduced hypodermal fat	18.9	0.5	85.7	2.9
Heart lipofuscin accumulation	100	1.9	100	2.3

B. Trichothiodystrophy-specific differences

	C57BL/6 (n=40)		<i>Xpd^{TTD}</i> (n=35)	
	incidence	severity	incidence	severity
Anorectal prolapse	0	n.a.	51.4	n.d.
Duodenal atypical hyperplasia	0	n.a.	17.6	0.5
Skin ulcerative dermatitis	45.9	1.5	8.6	0.3
TTD skin lesions ^a	0	n.a.	increased	n.d.

C. Differences consistent with dietary restriction

	C57BL/6 (n=40)		<i>Xpd^{TTD}</i> (n=35)	
	incidence	severity	incidence	severity
Skin ulcerative dermatitis	45.9	1.5	8.6	0.3
Skin reduced hypodermal fat	18.9	0.5	85.7	2.9
Cataract of eye lens	42.1	0.7	9.1	0.1
Nerve demyelination	59.0	1.1	11.8	0.1
Pituitary adenoma	51.3	n.a.	8.6	n.a.
Thyroid follicular cell hyperplasia	21.6	0.4	5.9	0.1
Thyroid follicular distension ("cold follicles")	94.6	2.6	85.7	1.9
Inflammation in various organs			Decreased	
Lacrimal gland lipofuscin accumulation ^b	94.3	1.7	46.9	0.5
Lacrimal gland Harderian type acini ^b	57.1	1.3	21.9	0.4
Adrenal extramedul hematopoiesis ^b	45.0	1.0	34.3	0.6
Brain eosinophilic inclusions thalamus ^b	55.0	1.0	34.0	0.6

Incidences are determined at the time of death and given in %, severity in a score (scale 1-5), mean severity is calculated per group

Mean age at time of death for the mice analyzed is 99,6 wks for C57BL/6 and 90,8 wks for *Xpd^{TTD}* mice

n.a. not applicable, n.d. not determined

^aTTD skin lesions is an assembly of acanthosis, hyperkeratosis, sebaceous hyperplasia, mast cell infiltration, extra-cellular melanin and follicular distention. No quantitative grade of severity is depicted for the separate features

^bpossibly consistent with dietary restriction (not found in literature)

cause of death observed in the Xpd^{TTD} mice did not reach the level of statistical significance (see also next section).

Tumor development during aging

A summary of tumor incidence in old female C57BL/6 wild types and Xpd^{TTD} mice at the time of death is shown in Table 3A. From Table 2 it becomes clear that wild type mice mostly died of neoplasia (fatal tumors) while for Xpd^{TTD} mice other diseases were more life threatening (see above). However, mice of both genotypes showed occult tumors that were not the actual cause of death, but were found incidentally in mice dying of another cause (incidental tumors). In Table 3, when Xpd^{TTD} females were compared with C57BL/6 control mice at the time of death, both the total number of benign and malignant tumors appeared to be lower in Xpd^{TTD} mice. This indicates that there is no difference in tumor progression between the two genotypes. The percentage of tumor-bearing animals (54.3% versus 75%) and the mean number of tumors per mouse (0.6 versus 1.0) appeared to be lower in Xpd^{TTD} mice when compared to wild type controls. Also, as Xpd^{TTD} mice live shorter, the tumors were found earlier than in wild type controls (mean latency time of 699 and 788 days, respectively). However, although there is a clear trend for lower tumor frequencies in Xpd^{TTD} mice, at present no firm conclusion on significant differences in cancer proneness between genotypes can be drawn. For that, further pathology analyses on cross sectional kills are needed.

Incidences of the individual tumor types at the time of death are summarized in Table 3B. All tumors belonged to the spectrum normally observed in aging C57BL/6 mice. The incidences of the majority of these tumors were too low (less than 5%) to reveal any significant differences between the genotypes. As expected, only lymphomas and pituitary pars distalis adenomas had a relatively high incidence in C57BL/6 females and appeared to have a distinctly lower incidence in Xpd^{TTD} mice (Table 3B). These differences were statistically significant for both lymphomas ($p=0.05$) and pituitary adenomas ($p<0.001$, Fisher's exact test). However, when the data were corrected for differences in survival, using the Peto method [20], only the incidence of pituitary adenomas, but not lymphomas, was statistically significantly decreased in Xpd^{TTD} mice ($p=0.002$ and $p=0.26$ two-sided, respectively).

Non-neoplastic pathology

In addition to tumors, both C57BL/6 and Xpd^{TTD} mice showed a large variety of non-neoplastic pathological abnormalities in several organ systems: inflammatory, proliferative, degenerative or regressive. Many of these abnormalities are known to increase with age in C57BL/6 wild type mice. Most of these lesions occurred to about the same degree and incidence in both genotypes and will not be discussed here any further. In addition, pathology features in Xpd^{TTD} wild type littermates were found to be comparable to those in C57BL/6 females (data not shown). Several abnormalities showed biological (and statistical) relevant differences

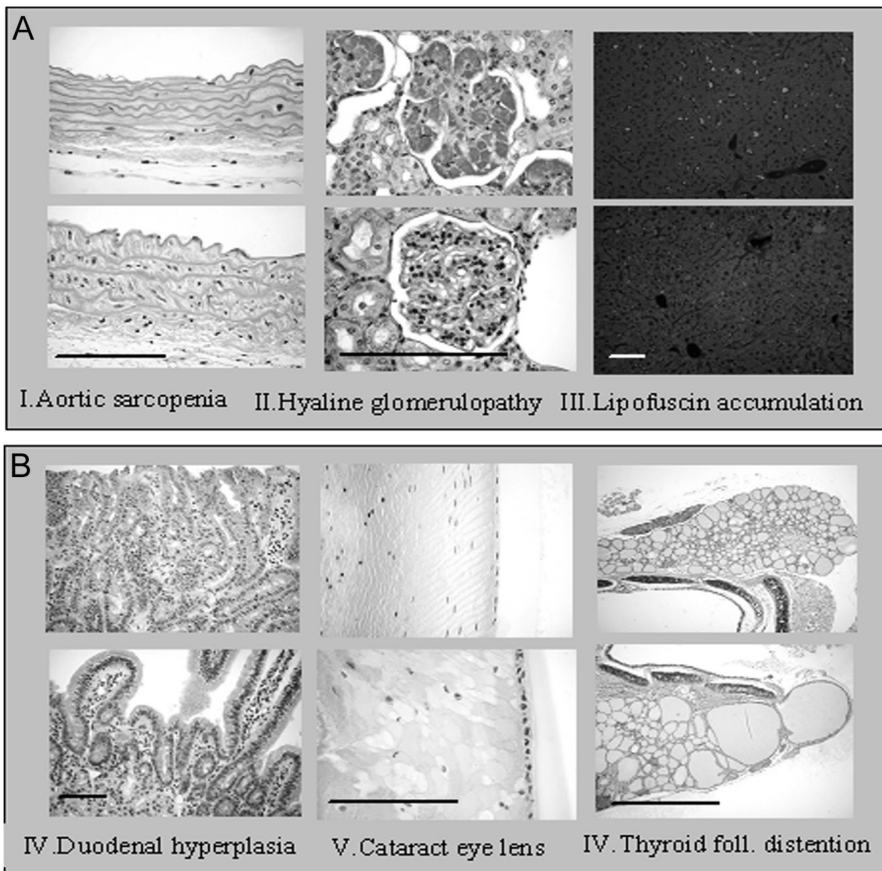


Figure 5: Examples of pathology differences between *Xpd^{TTD}* and C57BL/6 female mice.

Histopathology differences between *Xpd^{TTD}* and C57BL/6 female mice. Examples of age-related (A-I, II, III), TTD-specific (B-IV), and caloric restriction-related differences (B-V, VI) are depicted. The upper picture of every set is of an *Xpd^{TTD}* mouse, the lower picture of a C57BL/6 mouse.

Age-related pathology differences: I. Aortic sarcopenia in an *Xpd^{TTD}* female (644 days) and C57BL/6 mouse (662 days). Note the scarcity of nuclei between the elastic fibers in the *Xpd^{TTD}* aorta. II. Kidney hyaline glomerulopathy in an *Xpd^{TTD}* female (497 days) and C57BL/6 mouse (722 days). PAS-positive purple stained deposits (negative for amyloid) within glomeruli of the *Xpd^{TTD}* kidney, that were absent in the C57BL/6 control kidney. III. Lipofuscin fluorescence (UV) in the liver of an *Xpd^{TTD}* mouse (735 days), which was distinctly less in a C57BL/6 female (855 days). IV: TTD-specific atypical epithelial hyperplasia of the duodenum at the gastroduodenal junction. Note the crowding of nuclei and the disorganized aspect in the *Xpd^{TTD}* duodenum (735 days). Normal duodenum of a C57BL/6 mouse (624 days) is shown for a clear comparison. Dietary restriction-related pathology differences: V. Cataract of the eye lens of a C57BL/6 mouse (722 days), note the swollen and vacuolated lenticular fibers. The lens of the *Xpd^{TTD}* female (659 days) is relatively normal. VI. Thyroid with distended follicles in a C57BL/6 female (764 days) and normal-sized follicles in a *Xpd^{TTD}* female (609 days).

Pictures were obtained using HE staining (I, IV, V, VI) or PAS-staining (II). For III, unstained slides were used. Magnification bars shown represent 0.1 mm in all pictures (except the thyroid (VI): 1 mm). Upper and lower picture in one panel show the same magnification. Objectives used were 5x (VI), 20x (III, IV) or 40x (I, II, V).

in incidence and/or severity between Xpd^{TTD} and C57BL/6 mice. These differences can be subdivided into various categories as pointed out below (see also Table 4).

Accelerated aging features: Histopathological features of this category were consistent with and added on the earlier described premature aging phenotype of the Xpd^{TTD} mice [16]. Age-related pathology at the time of death was found to be most overt in liver, kidney, bone as well as lymphoid tissues (Table 4A, Fig. 5A). Lipofuscin accumulation in the liver was distinctly most severe in Xpd^{TTD} females (Fig.5A-III). The age-related pigment was present mainly in Kupffer cells, but also in hepatocytes. A similar trend was present in the heart of Xpd^{TTD} mice, although to a lesser extent. Eosinophilic or 'empty' hepatic intra-nuclear inclusions occurred to a higher extent in Xpd^{TTD} than in C57BL/6 mice. Hepatic intra-nuclear inclusions increase with age and are generally considered to be invaginations of the nuclear membrane containing cytoplasm [21]. Renal karyomegaly, seen as large, frequently bean-shaped nuclei in epithelial cells of the pars recta of the proximal renal tubules was slightly more pronounced in Xpd^{TTD} mice. Furthermore, the renal tubules were frequently dilated, which might be the cause of the high relative kidney weights of Xpd^{TTD} mice. Renal hyaline glomerulopathy occurred generally to a mild degree in C57BL/6 mice, but was much more pronounced in Xpd^{TTD} females (Fig.5A-II). Evidence for the occurrence of osteoporosis of the femur, characterized by loss of trabecular bone, as well as kyphosis (although not quantified) was found in Xpd^{TTD} mice (Table 4, K. Diderich *et al*, in preparation). The increase of lymphoid depletion of the spleen in Xpd^{TTD} females was characterized by a decreased lymphocytic density and a smaller extent of the splenic white pulp area. This may provide an explanation for the decline in spleen weight observed later in life for the Xpd^{TTD} mutant mice. The normal age-related involution (lymphoid atrophy) of the thymus, with loss of organoid structure and decrease in size, was more pronounced in Xpd^{TTD} than in C57BL/6 mice and correlated with the decreased organ weights. Aortic sarcopenia was defined as loss of muscle cells in the tunica media, a condition that occurred almost exclusively in Xpd^{TTD} mice (Fig.5A-I). Since the number of muscle cells in aortas of 3 and 6 months old Xpd^{TTD} mice did not differ from those of age-matched C57BL/6 controls (data not shown), aortic sarcopenia should be considered as a real aging-related phenomenon. Another conspicuous feature, specifically present in aging Xpd^{TTD} mice, was reduced or absent hypodermal fat as compared to C57BL/6 mice of the same age. This explains the consistent lower body weights of the Xpd^{TTD} animals.

Xpd^{TTD} -specific features: The second category of pathology differences consisted of differences specifically for the TTD phenotype that manifest during the whole lifespan (Table 4B, Fig.5B). One of the most striking hallmarks of TTD patients is the brittleness of hair as was also found in Xpd^{TTD} mice. In more detail, Xpd^{TTD} mice showed acanthosis, hyperkeratosis, sebaceous gland hyperplasia, mast cell infiltration, extra-cellular melanin and follicular distention in the skin (mentioned as TTD skin lesions in Table 4B). Duodenal epithelial hyperplasia just near the gastro-duodenal junction occurred mainly in Xpd^{TTD} mice (Fig.5B-IV). However, no intestinal tumors were observed in this area in any of the mice. A striking feature of Xpd^{TTD}

mice in our study was anorectal prolapse, a condition in which a part of the rectum protrudes through the anus. Since this change was followed by perianal inflammation and ulceration it was a frequent cause of death of *Xpd^{TTD}* mice (see above). The non- protruding part of the rectal mucosa of affected animals appeared not to be altered, however. No evidence of inflammation of the large intestines was found, a condition that has been associated before with rectal prolapse [22]. In conclusion, the observed anorectal prolapse in *Xpd^{TTD}* mice is probably associated with the prolonged cachectic state of the mice or with *Xpd^{TTD}*-specific changes in the perianal musculature and as such there is no relationship with aging *per se*.

Signs of caloric restriction: Apart from the aging-related changes and *Xpd^{TTD}*-specific changes, we found a third unexpected category of altered (reduced) pathology in *Xpd^{TTD}* mice at the time of death, consistent with a phenotype associated with dietary / caloric restriction (CR)(Table 4C, Fig. 5B). These features include a considerably lower incidence and/or severity in *Xpd^{TTD}* mice of the following symptoms: de-myelination of the peripheral nerve, cataract (Fig.5B-V), thyroid follicular distension (Fig.5B-VI), pituitary adenomas, ulcerative dermatitis, etc. (see for further details Table 4C). Most of these abnormalities are known to increase during aging, but under conditions of CR they have been reported to occur with lower incidence and severity [23]. Also age-associated reduction of hypo-dermal fat has been related to CR in rodents [23, 24].

Discussion

Aging is poorly defined at the mechanistic level, because aging is pleiotropic and segmental in its nature. It is a complex process with concurrence of multiple diseases or disabilities on a background of increasing functional decline and failure of homeostasis, associated with reduced stress resistance and an increased risk of dying. The universal driver of the aging process, across species, is likely the accumulation of somatic damage in cellular macromolecules, such as DNA, with ROS as the prime suspect for being the main damage-inducing agent. In view of the importance of DNA as the ultimate template and the discovery that heritable mutations in DNA maintenance genes underlie almost all known human segmental progeroid syndromes, maintenance of genome integrity has now emerged as a major factor in longevity and cell viability. Mice are good model systems to investigate the molecular basis of (accelerated) aging, because of their powerful genetics and the similarity of genomes and genome maintenance systems between mice and man. Many mouse mutants defective in genome maintenance display, like their human counterparts, segmental progeria [14].

In order to further understand the causal relationship between the aging process and genome maintenance, we are currently performing complete life span studies with various mouse models harboring defects in one or both sub-pathways of the NER system (i.e. *Xpa*, *Csb*, *Xpc* and *Xpd^{TTD}* mice). In the present study, we focused on the *Xpd^{TTD}* mouse mutant,

previously shown to display a segmental premature aging phenotype [16] that in retrospect could also be recognized in human trichothiodystrophy (TTD) patients [12]. A cohort of female *Xpd^{TTD}* mice was compared under strict SPF conditions to control mice having the same C57BL/6 genetic background. Such a side-by-side comparison with the normal aging process is the only valid way of identifying genuine symptoms of premature aging [3].

TTD is a segmental progeroid disorder

From present and previous results, it appears that the *Xpd^{TTD}* mice, just like the TTD patients, display wide-spread, premature segmental multi-system aging. *Xpd^{TTD}* mice show accelerated aging for a large number of known aging parameters (Table 4A) and as such they are excellent to study various (not all) premature aging phenotypes. When assumed that the underlying mechanism of aging in *Xpd^{TTD}* mice is similar as that in normal aging, this mouse model could be of potential use in future intervention studies.

Although a statistically significant difference in life span between *Xpd^{TTD}* mice and C57BL/6 control mice was observed, *Xpd^{TTD}* mice in the present study lived significantly longer than reported initially [16]. The major differences between these two studies were differences in genetic background and housing conditions. Either one of these can have impact on the ultimate outcome of longevity studies and underline that genuine comparison of the life span of different strains can only be reliably done under such strict conditions. An important cause of death in *Xpd^{TTD}* mice, and not in C57BL/6 controls, was a general conditional decline (including cachexia), also found in TTD patients [12]. Perhaps this state of conditional decline should be considered as a failure of the organism to maintain homeostasis. Additional causes of death were anorectal prolapse in *Xpd^{TTD}* mice and inflammation (mainly ulcerative dermatitis) in C57BL/6 mice, which was also reported by others [25, 26].

In TTD patients, a specific form of anemia (thalassaemia, trait) has been described [27] that has been related to reduced levels of transcription of the β -globin gene. Although the type of anemia observed in *Xpd^{TTD}* mice (normochrome) appears to be slightly different from that in TTD patients, a similar etiology may be postulated. Pronounced kyphosis and evidence for osteoporosis were found in aging *Xpd^{TTD}* mice, pointing to age-related skeletal abnormalities as were also found in TTD patients [12]. In addition to these known age-related features, the detailed systematic analysis performed in the present study revealed new (histo-) pathological parameters of aging in various organs and tissues of *Xpd^{TTD}* females. Especially lipofuscin accumulation in liver (and heart) cells was a very interesting observation since the accumulation of this pigment can be associated with oxidative damage [28], underlining the theory that defects in genome maintenance may be directly related to accumulating aging features. However, as the XPD protein functions both in DNA repair and transcription (initiation), it needs to be established whether the observed lipofuscin accumulation is due to defects in global genome NER, damage-induced interference of transcription by TCR or inactivated or constitutive transcription initiation of RNA polymerase I and II promoters. Also

renal karyomegaly has been associated with accumulation of DNA damage (M. Luijten *et al*, in preparation). One of the most pronounced age-related pathological differences between old *Xpd^{TTD}* and control females was aortic sarcopenia. This loss of aortic muscle cells was particularly enhanced in old mice. This loss together with the age-related growth retardation and skeletal abnormalities in *Xpd^{TTD}* mice, underlines the hypothesis that TTD is not a developmental disorder, but is truly due to early onset of specific aging-related symptoms.

Besides these genuine progeroid features of *Xpd^{TTD}* mice, we also found (TTD-related) features that do not meet age-related criteria. These are, i) the TTD-specific aberrant brittle hair and skin abnormalities; ii) increase of duodenal atypical hyperplasia and iii) anorectal prolapse probably as a consequence of the cachectic state of the mice. It is our hypothesis that these TTD-specific features are caused by a transcriptional deficit rather than by a defect in the DNA repair function of the XPD protein.

Xpd^{TTD} mice show signs of caloric restriction

A striking finding in the present study, purely based on pathological findings, was the identification of CR features in *Xpd^{TTD}* mice. Pronounced effects of CR on a variety of pathological abnormalities as well as mean and maximum life span in mammalian species are well documented [29, 30]. In C57BL/6 mice on a restricted diet, the frequency of pituitary adenomas as well as dermatitis, other inflammatory changes and cataract appears considerably reduced [23]. The following observations in *Xpd^{TTD}* mice are in line with this CR hypothesis: i) a low body weight accompanied by low hypodermal fat mass and absence of abdominal fat; ii) reduced tumor development; iii) low frequency of inflammation and cataract.

Strikingly however, food intake of *Xpd^{TTD}* mice was comparable to that of the wild type C57BL/6 mice, indicating that the CR phenotypes may be due to metabolic problems in *Xpd^{TTD}* mice owing to mild transcription failures. Supportive to this assumption are our preliminary data on mouse models with true NER defects like *Xpa* and *Xpc*, which lack such an apparent CR phenotype (to be published elsewhere). Definite proof that *Xpd^{TTD}* mice go into a state of metabolic restriction should come from more dedicated studies like biochemical analyses (for instance glucose, insulin, IGF-1), studies that were not possible to combine with our current longevity experiment. Still though, preliminary micro-array analyses further support our CR hypothesis (Suh *et al*, manuscript in preparation).

In conclusion, it is conceivable to assume that inefficient energy uptake is advantageous to *Xpd^{TTD}* mice. Under such conditions, production of harmful metabolic side products (like ROS) will be decreased which is in favor of DNA-repair deficient *Xpd^{TTD}* mice, and clearly more general to all living organisms when survival is considered.

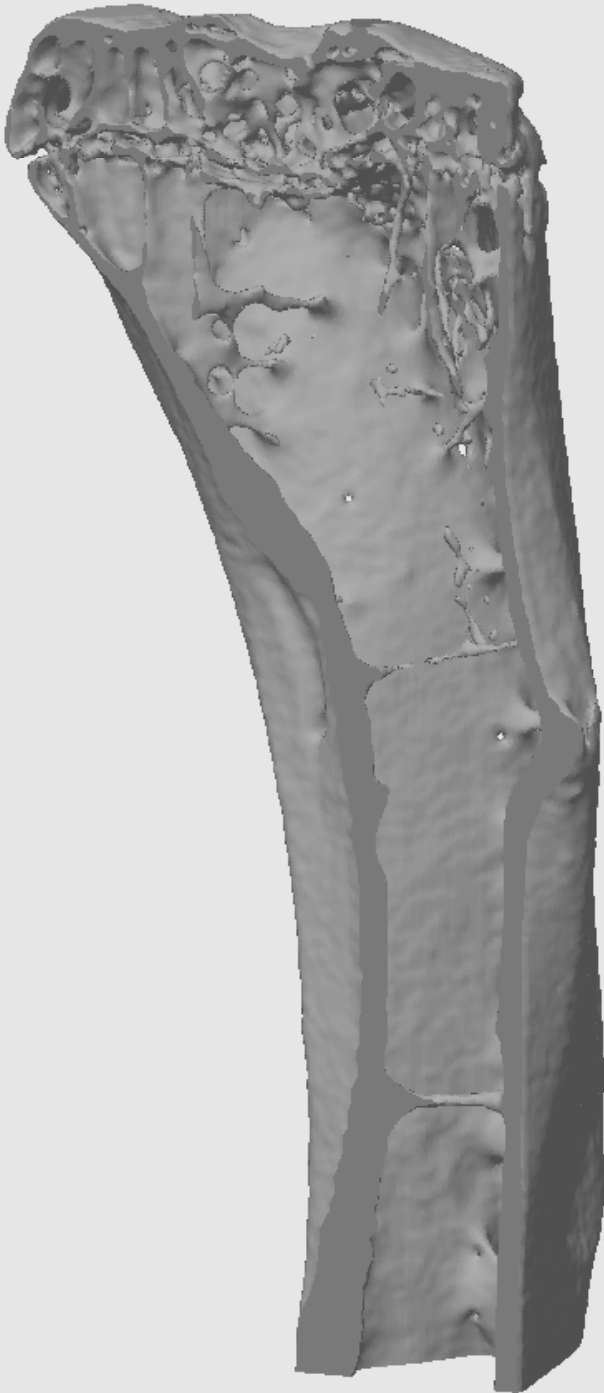
Acknowledgements

We are very grateful to Piet de With, Gwen Intres, Conny van Oostrom, Coen Moolenbeek, Christine Soputan and Henny Loendersloot for their skilful technical assistance. This work was financially supported by National Institute of Health (NIH)/ National Institute of Aging (NIA), grant number 1 PO1 AG-17242, NIEHS (1UO1 ES011044), Netherlands Organization for Scientific Research (NWO) through the foundation of the Research Institute Diseases of the Elderly, as well as grants from the Dutch Cancer Society, (EUR 99-2004) and EC (QRTL-1999-02002).

References

1. R.G. Allen, A.K. Balin. Metabolic rate, free radicals and aging, in: R.G. Cutler, and H. Rodriguez (Eds.) *Oxidative Stress and Aging. Advances in Basic Science, Diagnostics and Intervention. Volume I*, Singapore: World Scientific Publishing, 2003, pp. 3-23.
2. L. Partridge, D. Gems. Mechanisms of ageing: public or private? *Nature Reviews Genetics* 3 (2002) 165-175.
3. P. Hasty, J. Vijg. Accelerating aging by mouse reverse genetics: a rational approach to understanding longevity. *Aging Cell* 3 (2004) 55-65.
4. D. Harman. Aging: A theory based on free radical and radiation chemistry. *Journal of Gerontology* 11 (1956) 298-300.
5. T. Finkel, N.J. Holbrook. Oxidants, oxidative stress and the biology of ageing. *Nature* 408 (2000) 239-247.
6. J. Cadet, M. Berger, T. Douki, J.L. Ravanat. Oxidative damage to DNA: Formation, measurement, and biological significance. *Rev. Physiol. Biochem. Pharmacol.* 131 (1997) 1-87.
7. J.H.J. Hoeijmakers. Genome maintenance mechanisms for preventing cancer. *Nature* 411 (2001) 366-374.
8. E.C. Friedberg, G.C. Walker, W. Siede. *DNA repair and Mutagenesis*. American Society of Microbiology, Washington DC, USA 1995.
9. E. Evans, J.G. Moggs, J.R. Hwang, J.M. Egly, R.D. Wood. Mechanism of open complex and dual incision formation by human nucleotide excision repair factors. *EMBO J.* 16 (1997) 6559-6573.
10. S.J. Araujo, F. Tirode, F. Coin, H. Pospiech, J.E. Syvaoja, M. Stucki, U. Hubscher, J.M. Egly, R.D. Wood. Nucleotide excision repair of DNA with recombinant human proteins: definition of the minimal set of factors, active forms of TFIIH, and modulation by CAK. *Genes Dev.* 14 (2000) 349-359.
11. D. Bootsma, K.H. Kraemer, J.E. Cleaver, J.H.J. Hoeijmakers. Nucleotide excision repair syndromes: xeroderma pigmentosum, Cockayne syndrome and trichothiodystrophy, in: B. Vogelstein, and K.W. Kinzler (Eds.), *The genetic basis of human cancer*. USA: Mc-Graw-Hill Companies, 1998, pp. 245-274.
12. P.H. Itin, A. Sarasin, M.R. Pittelkow. Trichothiodystrophy: Update on the sulfur-deficient brittle hair syndromes. *J. Am. Acad. Dermatology* 44 (2001) 891-920.
13. D.G. Martin. Genetic syndromes in man with potential relevance to the pathobiology of aging, in: *Birth Defects, Original Article Series. Vol 14*, New York: The National Foundation, 1978, pp. 5-39.
14. P. Hasty, J. Campisi, J.H.J. Hoeijmakers, H. van Steeg, J. Vijg. Aging and genome maintenance: lessons from the mouse? *Science* 299 (2003) 1355-1359.
15. J. de Boer, J.H.J. Hoeijmakers. Cancer from the outside, aging from the inside: Mouse models to study the consequences of defective nucleotide excision repair. *Biochimie* 81 (1999) 127-137.
16. J. de Boer, J.O. Andressoo, J. de Wit, J. Huijman, R.B. Beems, H. van Steeg, G. Weeda, G.T.J. van der Horst, W. van Leeuwen, A.P.N. Themmen, M. Meradji, J.H.J. Hoeijmakers. Premature aging in mice deficient in DNA repair and transcription. *Science* 296 (2002) 1276-1279.
17. E. Masoro. Role of sirtuin proteins in life extension by caloric restriction. *Mech. Ageing and Dev.* 125 (2004) 591-594.
18. J. de Boer, J. de Wit, H. van Steeg, R.J.W. Berg, H. Morreau, P. Visser, A.R. Lehmann, M. Duran, J.H.J. Hoeijmakers, G. Weeda. A mouse model for the basal transcription/ DNA repair syndrome trichothiodystrophy. *Molecular Cell* 1 (1998) 981-990.
19. M.E. Dollé, H. Giese, C.L. Hopkins, H.J. Martus, J.M. Hausdorff, J. Vijg. Rapid accumulation of genome rearrangements in liver but not in brain of old mice. *Nat. Genet.* 17 (1997) 431-434.

20. R. Peto, M.C. Pike, N.E. Day, R.G. Gray, P.N. Lee, S. Parish, J. Peto, S. Richards, J. Wahrendorf. Guidelines for simple, sensitive significance tests for carcinogenic effects in long-term animal experiments. *IARC Monogr. Eval. Carcinog. Risk Chem. Hum.* 2 (Suppl) (1980) 311-426.
21. R.R. Maronpot, G.A. Boorman, and B.W. Gaul (Eds.), *Pathology of the Mouse*. Cache River Press, Vienna, IL, USA 1999.
22. H. Takayama, H. Takagi, W.J. Larochelle, R.P. Kapur, G. Merlino. Ulcerative proctitis, rectal prolapse, and intestinal pseudo-obstruction in transgenic mice overexpressing hepatocyte growth factor/scatter factor. *Lab Invest.* 81 (2001) 297-305.
23. A. Turturro, P. Duffy, B. Hass, R. Kodell, R. Hart. Survival characteristics and age-adjusted disease incidences in C57BL/6 mice fed a commonly used cereal-based diet modulated by dietary restriction. *Journal of Gerontology: Biological Sciences* 57A (2002) B379-B389.
24. E. GURSOY, A. CARDOUNEL, Y. HU, M. KALIMI. Biological effects of long-term caloric restriction: adaptation with simultaneous administration of caloric stress plus repeated immobilization stress in rats. *Exp Biol Med.* 226 (2001) 97-102.
25. A.G. Andrews, R.C. Dysco, S.C. Spilman, R.G. Kunkel, D.W. Brammer, K.J. Johnson. Immune complex vasculitis with secondary ulcerative dermatitis in aged C57BL/6Nia mice. *Vet. Pathol.* 31 (1994) 293-300.
26. B.-N. Blackwell, T.J. Bucci, R.W. Hart, A. Turturro. Longevity, body weight, and neoplasia in ad libitum-fed and diet-restricted C57BL/6 mice fed NIH-31 open formula diet. *Toxicol. Pathol.*, **23**, (1995). 570-582.
27. V. Viprakasit, R.J. Gibbons, B.C. Broughton, J.L. Tolmie, D. Brown, P. Lunt, R.M. Winter, S. Marinoni, M. Stefanini, L. Brueton, A.R. Lehmann, D.R. Higgs. Mutations in the general transcription factor TFIIH result in beta-thalassaemia in individuals with trichothiodystrophy. *Hum Mol Genet.* 10 (2001) 2797-2802.
28. D. Harman. Lipofuscin and ceroid formation: the cellular recycling system. *Adv. Exp. Med. Biol.* 266 (1989) 3-15.
29. V.D. Longo, and C.E. Finch. Evolutionary medicine: from dwarf model systems to healthy centenarians? *Science* 299 (2003) 1342-1346.
30. E.J. Masoro. Subfield history: caloric restriction, slowing aging, and extending life. *Sci Aging Knowledge Environ.* 8, (2003) RE2.
31. M. Bluher, B.B. Kahn, and C.R. Kahn. Extended longevity in mice lacking the insulin receptor in adipose tissue. *Science* 299 (2003) 572-574.



APPENDIX II

Dysregulation of the Peroxisome Proliferator-Activated Receptor Target Genes by XPD Mutations

Emmanuel Compe¹, Pascal Drané¹, Camille Laurent¹, Karin Diderich², Cathy Braun¹, Jan H. J. Hoeijmakers², and Jean-Marc Egly¹

¹*Institut de Génétique et de Biologie Moléculaire et Cellulaire, BP 10142, 67404 Illkirch Cedex, C. U. Strasbourg, France, and* ²*MGC-Department of Cell Biology and Genetics, Centre for Biomedical Genetics, Erasmus Medical Center, 3000 DR Rotterdam, The Netherlands*

Abstract

Mutations in the XPD subunit of TFIIH give rise to human genetic disorders initially defined as DNA repair syndromes. Nevertheless, xeroderma pigmentosum (XP) group D (XP-D) patients develop clinical features such as hypoplasia of the adipose tissue, implying a putative transcriptional defect. Knowing that peroxisome proliferator-activated receptors (PPARs) are implicated in lipid metabolism, we investigated the expression of PPAR target genes in the adipose tissues and the livers of XPD-deficient mice and found that (i) some genes are abnormally overexpressed in a ligand-independent manner which parallels an increase in the recruitment of RNA polymerase (pol) II but not PPARs on their promoter and (ii) upon treatment with PPAR ligands, other genes are much less induced compared to the wild type, which is due to a lower recruitment of both PPARs and RNA pol II. The defect in transactivation by PPARs is likely attributable to their weaker phosphorylation by the cdk7 kinase of TFIIH. Having identified the phosphorylated residues in PPAR isotypes, we demonstrate how their transactivation defect in XPD-deficient cells can be circumvented by overexpression of either a wild-type XPD or a constitutively phosphorylated PPAR S/E. This work emphasizes that underphosphorylation of PPARs affects their transactivation and consequently the expression of PPAR target genes, thus contributing in part to the XP-D phenotype.

Introduction

XPD mutations cause the rare autosomal recessive disorder xeroderma pigmentosum (XP), primarily defined as a DNA repair defect, which is sometimes associated with Cockayne syndrome, as well as trichothiodystrophy (TTD) (29, 47). Besides the potential for carcinogenesis caused by photosensitivity, these patients exhibit a large spectrum of clinical abnormalities, such as immature sexual development, mental retardation, skeletal abnormalities, and dwarfism. The principal hallmark of TTD patients is brittle hair and nails, caused by a reduction in cysteine-rich matrix proteins. Some TTD patients have ichthyotic skin and an unusual face that appears aged due to the lack of subcutaneous fatty tissue (15, 21). In women, the breast tissue may be completely absent in spite of normal development of the nipples. Obviously, these various clinical features cannot solely be explained by DNA repair defects (5). While one cannot exclude the biological effects due to the damage itself (that can in some cases prevent one of the ongoing cellular mechanism such as replication or transcription), it however has to be pointed out that the product of the *XPD* gene belongs to the TFIIH complex, which is involved in the DNA repair as well as in the transcription process.

TFIIH can be resolved into two subcomplexes: the core-TFIIH (containing in particular the XPB helicase) and the cdk-activating kinase (CAK) complex containing the cyclindependent kinase cdk7 (40). The core-TFIIH and CAK sub-complexes are bridged by the *XPD* helicase subunit, which interacts with p44 on the one side and MAT1 on the other side (9, 41). In the nucleotide excision reaction, TFIIH, once recruited on the damaged DNA already recognized by the XPCHR23B factor, unwinds the DNA around the lesion upon addition of ATP to allow the recruitment of XPA, RPA, XPG, and XPF/ERCC1 repair factors (37). When *XPD* is mutated in the C-terminal end, its interaction with its regulatory partner p44 is weakened (9). In that case, the *XPD* helicase is no longer upregulated by p44 and cannot optimally operate in the nucleotide excision repair process (49). In the transcription process, TFIIH together with TFIIA, -B, -D, -E, and -F basal transcription factors and RNA polymerase (pol) II, participates in the initiation of RNA synthesis by opening the promoter around the start site via its XPB helicase (18) and by phosphorylating via its cdk7 kinase the carboxy-terminal domain of the largest subunit of RNA pol II and some transcriptional activators including nuclear receptors (7, 12, 25, 32, 38).

The peroxisome proliferator-activated receptors PPAR α , - γ , and - δ are ligand-activated nuclear receptors which form heterodimers with the retinoid X receptor and bind to PPAR-responsive elements of numerous target genes (26). These transcription factors regulate lipid metabolism (3, 28) and are activated by fatty acids, their derivatives, and/or synthetic compounds (11). PPAR α enhances fatty acid combustion in the liver by upregulating genes encoding enzymes in the β -oxidation pathway and hence mediates the hypolipidemic effects of fibrates (35). In contrast, PPAR γ serves as an essential regulator of adipocyte differentiation and promotes lipid storage in mature adipocytes (39). Two PPAR γ isoforms (PPAR γ 1 and -2) are produced

by the differential use of three promoters and alternative splicing (reviewed in reference 11). Lastly, PPAR δ regulates fat burning in peripheral tissues by coordinating fatty acid oxidation and energy expenditure (48). Besides their function in lipid metabolism, many potential roles for PPARs have been named in pathological states observed in XP group D (XP-D) patients, such as infertility and cancers (4).

In order to evaluate whether a transcriptional defect takes part in the XP-D phenotype, we focused on a putative connection between the hypoplasia of adipose tissue observed in XP-D patients and a defect in transactivation by PPARs. Contrary to what was expected, we observed that the expression of PPAR γ target genes is differently affected in the adipose tissues from XPD/TTD-deficient mice. Indeed, whereas some of these genes are abnormally overexpressed in a ligand-independent manner, we also observed a lower induction of PPAR γ target genes after treatment with a specific ligand. We found that the defect in transactivation by PPARs in XPD-deficient cells (isolated from both TTD mice and XP-D patients) is associated with a weaker phosphorylation of these nuclear receptors by cdk7. Having identified the phosphorylated residues in the PPAR isotypes, we demonstrate how their trans-activation defect in XP-D-deficient cells can be circumvented upon the overexpression of either wild-type (WT) XPD or PPAR S/E, in which the glutamic acid mimics a constitutively phosphorylated residue.

Materials and methods

Animals and morphological studies.

The generation of the TTD mouse line R722W has been described previously (10). Mice were fed standard chow with a 5% (wt/wt) fat content (R03 breeding diet; UAR, Villemoisson, France). Fragments of adipose tissues and liver were fixed in 4% formaldehyde for 48 h prior to paraffin embedding. Hematoxylin-and-eosin (H&E)-stained sections were 5 μ m thick, while frozen sections for oil red-O staining were 15 μ m thick. Apoptosis was assessed by the terminal deoxynucleotidyltransferase-mediated dUTPbiotin nick end labeling (TUNEL) method using the ApopTag kit (Chemicon Int.). Briefly, liver sections were deparaffinized, hydrated, and incubated for 15 min at room temperature in 20 mg/ml proteinase K. After being thoroughly washed in distilled water and immersed in terminal deoxynucleotidyltransferase (TDT) buffer for 10 min at room temperature, the sections were incubated in TDT buffer, digoxigenin dUTP, and TDT for 60 min in a humidified chamber at 37°C. The reaction was visualized by an immunohistochemical technique using anti-digoxigenin-peroxidase antibodies. Cell regeneration was evaluated by immunohistochemical studies using antibody against the cell proliferation marker Ki67 according to the manufacturer's instructions (Novocastra). Fragments of various tissues were also frozen for RNA and protein extraction. Three-monthold mice were treated by oral gavage with rosiglitazone (10 mg/kg body weight for 3 days; GlaxoSmithKline), WY14643

(100 mg/kg body weight for 20 h; Calbiochem), or the corresponding vehicle (ethanol at 3 ml/kg or dimethyl sulfoxide at 3 ml/kg, respectively).

Retrotranscription and real-time quantitative PCR.

RNAs were prepared with TRIzol (GIBCO-BRL) and treated with RQ1 DNase (Promega) according to the manufacturer's instructions. For reverse transcriptase PCR, total RNA (2 µg) was reverse transcribed with Moloney murine leukemia virus reverse transcriptase (Invitrogen) using random hexanucleotides. Real-time quantitative PCR was done using the FastStart DNA Master SYBR Green kit and the LightCycler apparatus (Roche Diagnostic). The primer sequences and the PCR conditions for each target gene are available upon request.

Chromatin immunoprecipitation (ChIP).

Hepatic fragments were fixed by adding 37% formaldehyde to a final concentration of 1% and incubated for 15 min at room temperature and 1 h at 4°C. Fragments of white adipose tissue (WAT) and brown adipose tissue (BAT) were pooled from tissues of two animals and fixed as described above. Cross-linking was stopped by addition of glycine to a final concentration of 0.125 M. Fragments were washed twice with cold phosphate-buffered saline and treated with sonicate buffer (50 mM HEPES [pH 7.9], 140 mM NaCl 1 mM EDTA, 1% Triton X-100, 0.1% sodium dodecyl sulfate [SDS], 0.1% Na-deoxycholate) containing protease inhibitors. Fragments were homogenized, and cell lysates were then sheared extensively by sonication on ice to obtain fragments of 200 to 600 bp (as revealed by ethidium bromide staining of aliquots run on agarose gels). Samples were centrifuged to pellet debris, and an aliquot was taken for gel analysis and inputs. Soluble chromatin was pretreated for 2 h at 4°C with protein G (previously saturated with 1 mg/ml of sonicated salmon sperm DNA and 1 mg/ml of bovine serum albumin). Samples were then incubated overnight at 4°C with antibodies of interest; protein G (previously saturated) was then added, and the mixture was incubated for 2 h at 4°C. Sepharose beads were washed twice for 10 min at 4°C with wash 1 (sonicate buffer with 500 mM NaCl) and then with wash 2 (0.25 M LiCl, 0.5% NP-40, 0.5% sodium deoxycholate, 1 mM EDTA, 20 mM Tris-HCl [pH 8.0]), and finally with Tris-EDTA (TE; pH 8.0). Immune complexes were eluted from the beads with 1% SDS in TE (pH 8.0), and protein-DNA cross-links were reversed by adding 200 mM NaCl and heating for 5 h at 65°C. After treatment with proteinase K (2 h at 42°C), the samples were purified by phenol-chloroform-isoamyl alcohol extraction and precipitated with ethanol. One-fifteenth of the immunoprecipitated DNA and 1% of the input DNA were quantified by real-time quantitative PCR (see above). Results are expressed relative to the amount of input DNA per ChIP.

Antibodies.

Monoclonal antibodies against the TFIIF subunits, TATA box binding protein (TBP), and RNA pol II were produced by the Institut de Génétique et de Biologie Moléculaire et Cellulaire

facility. Polyclonal antibodies against VDR (sc-9164; Santa Cruz), PPAR α (H-98; Santa Cruz), PPAR α /S12 (PA1-820; ABR), and PPAR δ (K-20; Santa Cruz) and monoclonal antibodies raised against PPAR γ (E-8 for Western blotting [Santa Cruz], AB12409 for immunoprecipitation [AB Cam LTD]) or phosphorylated S84/S112 PPAR γ 1/2 (1F5; Euromedex) were purchased.

Coimmunoprecipitation assays.

PPAR α and PPAR γ 2 cDNAs were inserted into the pVL1392 vector, and the resulting vectors were recombined with baculovirus DNA (Baculogold; Pharmingen) as previously described (13). Sf9 cells were infected with combinations of baculoviruses encoding the subunits of TFIIH (45) and either VDR (31), PPAR α , or PPAR γ 2. Whole-cell extracts were incubated with an antibody directed against either the p44 subunit of TFIIH, VDR, or the corresponding PPAR isotype. After extensive washing (300 mM KCl), bound proteins were resolved by SDS-polyacrylamide gel electrophoresis (PAGE) and revealed by immunoblotting.

Plasmids and construction of PPAR mutants.

Specific PCR products including the entire coding sequence, the truncated form without the A/B domain, or the A/B domain alone for each PPAR isotype were inserted into the NdeI cloning site of the prokaryotic pET15b expression vector (Novagen). Serine residue changes to alanine or glutamic acid were introduced using the QuikChange site-directed mutagenesis kit (Stratagene).

In vitro kinase assays.

His fusion proteins were produced into *Escherichia coli* strain BL21 and purified on Ni-nitrilotriacetic acid agarose (Qiagen). Equal amounts (1 μ g) of recombinant proteins were incubated with purified recombinant CAK complex (40) or highly purified TFIIH in the presence of [³²P]ATP (0.14 μ M).

Mass spectrometry.

PPAR A/B domains were in vitro phosphorylated by CAK, purified by SDS-PAGE, and in gel digested with *Staphylococcus aureus* V8 protease (for PPAR α and γ) or Asp-N endoproteinase (for PPAR δ). Peptide extracts (0.5 ml) were mixed with an equal volume of saturated 2,5-dihydroxybenzoic acid, dissolved in 20% acetonitrile, and applied to the target. Mass measurements were carried out on a Bruker Reflex IV matrix-assisted laser desorption ionization–time of flight mass spectrometer in the positive-ion reflector mode. Mono-isotopic peptide masses were assigned using the Bruker X-TOF software. Potential phosphorylation sites were searched using the FindMod tool (<http://us.expasy.org/tools/findmod/>) with the following parameters: PPAR A/B domains as user-entered sequences, V8 or Asp-N digestion in phosphate buffer, two missed cleavages allowed, cysteines modified by carbamidomethylation, methionine oxidation, and a mass tolerance of 75 ppm.

Cell culture and transient transfection assays.

HeLa and HD2 cells were grown in Dulbecco's modified Eagle medium (DMEM)-Ham F10 containing 10% (vol/vol) fetal calf serum (FCS) and 40 µg/ml gentamicin and plated to approximately 50% confluency (5×10^5 cells/35-mm plate) before transfection. Normal human fibroblasts (GM03348D; Coriell Cell Repository), XPD-mutated fibroblasts (XPJCL0) (44), TTD8PV, and TTD12PV (isolated from TTD patients bearing the R112H and R722 point mutations, respectively [reviewed in reference 6]) were grown in DMEM (1 g glucose/liter; GIBCO-BRL) supplemented with 10% FCS and 40 µg/ml gentamicin. TTD and WT mouse fibroblasts were grown in DMEM (4.5 g glucose/liter; GIBCO-BRL) and supplemented with 15% FCS and 40 µg/ml gentamicin. Human and mouse fibroblasts were transiently transfected using the transfection reagent Fugene6 (Roche Diagnostics). In all experiments, 1 µg of pPPAR-RE-Luc and 100 ng of each expression vector were used per well in the absence of serum. Control transfections were undertaken with corresponding void plasmids. To normalize transfection efficiencies, pCH110 (1 µg) was cotransfected. Following transfection for 7 h, the cells were treated with red phenol-free medium containing 10% charcoal-treated FCS–40 µg/ml gentamicin. After 12 h of incubation, the appropriate ligand for each PPAR isotype was added and the mixture was incubated for 24 h. Fibroblasts extracts were analyzed for luciferase and β -galactosidase activities as previously described (25). The results are the mean of at least three independent experiments performed in triplicate.

Statistical analysis.

The number of mice for each group used in experiments is indicated in the figure legends. Values are presented as the mean \pm the standard error of the mean. A two-tailed Student test was used to calculate *P* values.

Results***TTD mice exhibit hypoplasia of the adipose tissues.***

TTD mice bearing the *XPD* point mutation R722W were used in our study. These mice develop features similar to those observed in XP-D patients, such as brittle hair, developmental defects, skeletal abnormalities, and cachexia (Fig. 1A; reviewed in reference 10). Indeed, weight differences between WT and TTD mice appear and become more pronounced a few months after birth (TTD mice have about 20% lower body weights at 3 months of age; Fig. 1B). The weight loss is not due to disruption of the daily food intake (3.8 ± 0.2 and 4.2 ± 0.2 g/animal/day for WT and TTD mice, respectively). The appearance and fat composition of the feces of TTD mice are normal (data not shown), arguing against malabsorption as the cause of weight loss.

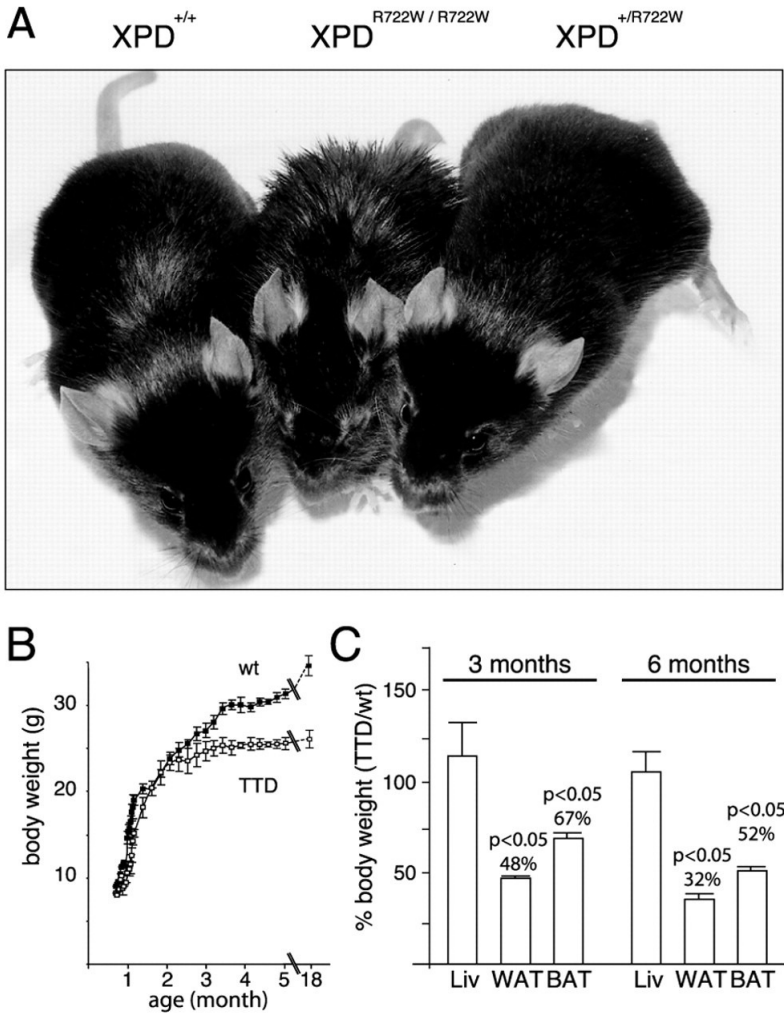


Figure 1: Lean phenotype in TTD mice.

(A) Photographs of representative 3-month-old $XPD^{+/+}$, $XPD^{R722W/R722W}$ and $XPD^{+/R722W}$ mice. (B) Body weights of male WT ($n = 6$) and TTD ($n = 6$) mice were monitored for 18 months. (C) Weights of the liver (Liv), intraperitoneal WAT, and interscapular BAT were normalized to body weight for 3- and 6-month-old male TTD mice ($n = 6$). The values are percentages relative to those observed for WT mice.

The weights of various tissues were then analyzed at different ages (Fig. 1C). Whereas the TTD liver exhibits a weight similar to the WT, we observed a progressive mass reduction for the perivisceral WAT (48% and 32% of that observed in 3- and 6-month-old WT mice, respectively; Fig. 1C and 2A, parts 1 and 2, arrows) and the interscapular BAT (67% and 52% of that observed in 3- and 6-month-old WT mice, respectively; Fig. 1C). Interestingly, the perivisceral WAT and the inter-scapular BAT are almost nonexistent in 18-month-old TTD mice (Fig. 2A). Histological analysis after standard H&E staining revealed that the adipocytes in the intra-

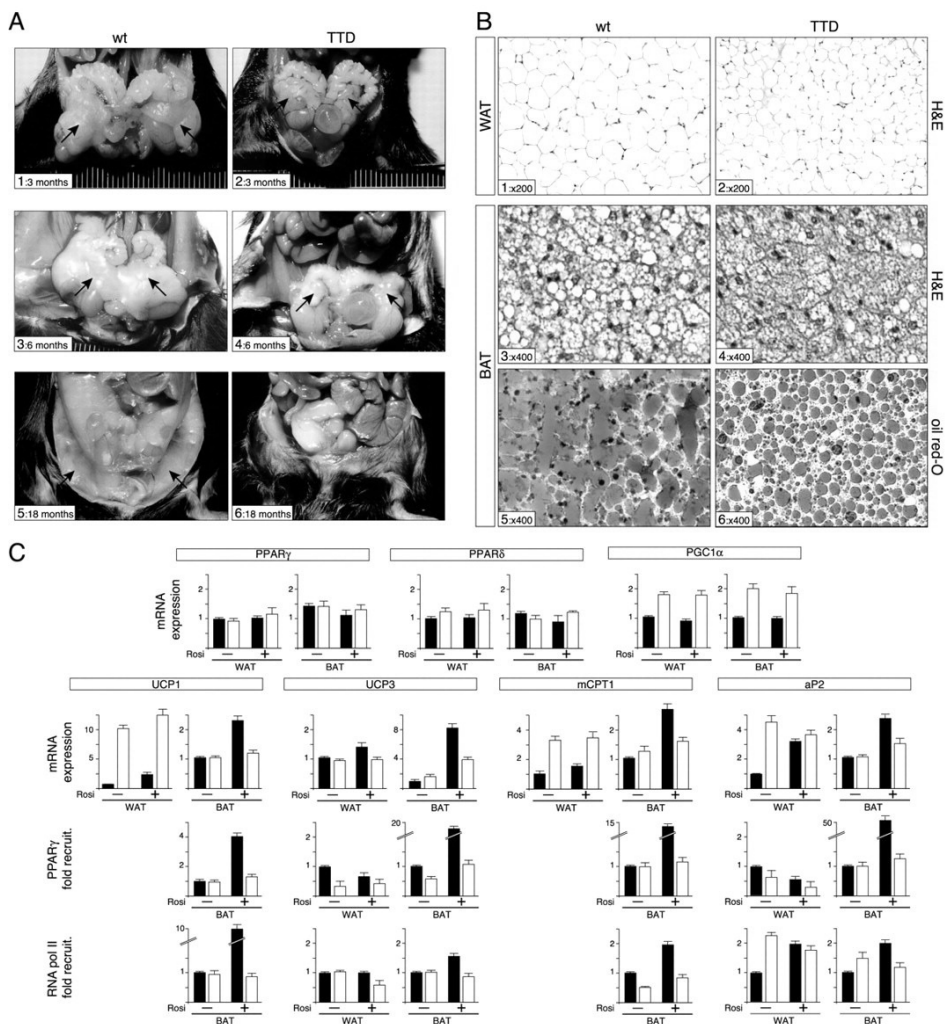


Figure 2: Expression of PPAR γ target genes in TTD adipose tissues.

(A) Ventral view of 3-, 6-, and 18-month-old WT (parts 1, 3, and 5) and TTD (parts 2, 4, and 6) mice. Note the progressive loss of visceral fat pads in TTD mice (arrows). (B) H&E-stained sections of intraperitoneal WAT and interscapular BAT of 3-month-old WT and TTD mice. BAT was also stained with lipid-specific oil red-O dye. Magnification is indicated at the bottom left of each part. (C) Gene expression in WAT and BAT of 3-month-old WT (dark boxes, $n = 4$) and TTD (open boxes, $n = 4$) mice on standard chow (-) or supplemented with rosiglitazone, a specific PPAR γ ligand (+ Rosi; 10 mg/kg body weight for 3 days). The values were normalized relative to 18S RNA expression. The full names of the genes are given in the text. The recruitment of PPAR γ and RNA pol II on the corresponding promoters was also analyzed by ChIP assays in WT (dark boxes) and TTD (open boxes) adipose tissues. Immunoprecipitated DNA was quantified by real-time quantitative PCR. Results are expressed as n -fold recruitment relative to nontreated WT mice.

peritoneal WAT of 3-month-old TTD mice are reduced and heterogeneous in size, whereas they are homogeneous and uniform in the WAT of control littermates (Fig. 2B, parts 1 and 2). In parallel, oil red-O staining of TTD BAT cells reveals a decrease in the accumulation of lipid

droplets (Fig. 2B, parts 5 and 6), which explains the decrease in the intracytoplasmic vacuoles observed in the H&E staining (parts 3 and 4). Similar histological observations were found in TTD mice at different ages (data not shown).

Dysregulation of PPAR γ -responsive genes in the adipose tissues.

We were wondering whether the morphological alterations of the TTD mouse adipose tissues could be associated with dysregulation of some genes. Knowing that PPARs play a preponderant role in these tissues (46, 48), we analyzed the expression of genes known to be controlled by PPARs and/or involved in various pathways of lipid metabolism (Fig. 2C).

WT and TTD mice were thus treated by gavage with rosiglitazone (10 mg/kg body weight for 3 days), a specific ligand of PPAR γ (30). In WT BAT, the rosiglitazone ligand stimulated the expression of UCP-1 and -3 (uncoupling proteins 1 and 3, involved in the uncoupling of oxidative phosphorylation), mCPT1 (the muscle form of carnitine palmitoyltransferase 1, involved in fatty acid β -oxidation), and aP2 (a fatty acid binding protein) (Fig. 2C). More importantly, we observed that the induction of these genes was 50% lower in TTD BAT than in WT BAT. A similar reduction was observed by transfection assays in XPD-deficient cells (see Fig. 5B and C). We also found in TTD WAT an unexpected ligand-independent over-expression of UCP-1 (10-fold), mCPT1 (3.5-fold) (two genes usually expressed in BAT), and aP2 (4.5-fold). Note that PGC1c, a coactivator that regulates the expression of genes involved in biological programs linked to energy homeostasis (such as thermal regulation), is also overexpressed in both TTD BAT and WAT (about twofold). Finally, under both standard and gavage conditions, no significant changes between WT and TTD mice were observed in the expression of some genes, such as PPAR γ , PPAR δ , the very long chain acyl coenzyme A (CoA) synthetase (involved in fatty acid β -oxidation), UCP-2, the lipoprotein lipase (involved in triglyceride hydrolysis), Spot 14 (involved in lipogenesis), and the acyl-CoA binding protein (involved in fatty acid trafficking) (Fig. 2C and data not shown).

To understand whether such dysregulations are due to PPAR γ , we set up ChIP assays. The genomic DNA fragments bound to either PPAR γ or RNA pol II were immunoprecipitated with the corresponding antibodies and further analyzed by quantitative PCR. Upon rosiglitazone treatment, PPAR γ was much less recruited on the promoters of UCP-1, UCP-3, mCPT1, and aP2 in TTD BAT (Fig. 2C). Therefore, it is not surprising that the occupancy on the respective promoters by RNA pol II parallels that of PPAR γ , thus explaining the lower RNA synthesis level. In the case of the abnormal overexpression of aP2 in TTD WAT, we found that mRNA synthesis perfectly parallels RNA pol II recruitment whereas PPAR γ is no longer recruited (Fig. 2C). We next hardly detected PPAR γ recruitment on the promoters of UCP-1 and mCPT1 (masked in the background; data not shown).

Altogether, our data underline a profound dysregulation of PPAR γ -dependent genes in TTD adipose tissues. Whereas the basal dysregulation observed for some of these genes might occur in a PPAR γ (and ligand)-independent manner, the lower response of genes to a

specific PPAR γ treatment is associated with lower PPAR γ recruitment and consequently of the transcription apparatus on their promoters.

Dysregulation of PPAR α -responsive genes in the livers of TTD mice.

We next evaluated whether the transactivity of another PPAR isotype is affected in TTD mice. We focused our attention on PPAR α , the major PPAR isotype in the liver (35). Macroscopic analysis first showed that the livers of 3-, 6-, and 12-month-old TTD mice look normal, with a size, a form, a consistency, and a color similar to the WT (as illustrated for 3-month-old mice in Fig. 3A, parts 1 and 2). Histological analysis further reveals that there is no significant difference in the architecture and structure of the hepatic parenchyma between WT and TTD mice at various ages (parts 3 to 6). A slight reduction of the intrahepatic lipid vacuoles is still observed in TTD mice compared to WT mice (Fig. 3A, parts 7 and 8). It is worth noting that we observed minimal necrotic lesions in the vicinity of the centrilobular and periportal areas of TTD mouse livers, which are associated with granular degeneration of hepatocytes having no or pyknotic nuclei (parts 4 and 6, arrows). Despite their persistence, no age-related accumulation of these necrotic areas was observed in TTD mice. The presence of apoptosis in the 3-month-old TTD liver was assessed by the TUNEL method (Fig. 3, parts 9 and 10). We observed a very slight (5%) increase in apoptosis in the livers of TTD mice compared to their control littermates. More importantly, the apoptotic areas were not colocalized to the necrotic areas. Immunodetection of the cell proliferation marker Ki67 revealed a slight increase in cell regeneration in the livers of WT mice compared to TTD mice (9%, parts 11 and 12). Since neither necrosis accumulation nor other hepatic lesions have been observed, our results led us to suggest the aspecific and isolated status of these necroses.

Although macroscopic and histological analyses did not reveal strong alterations of the TTD liver, we next analyzed the expression of hepatic genes known to be regulated by PPAR α . Three-month-old WT and TTD mice were treated for 20 h with WY14643, a PPAR α agonist, in order to measure the induction of hepatic genes known to be highly and quickly activated by PPAR α (8). Under those conditions, the PPAR α mRNA level remained unchanged in both WT and TTD livers (Fig. 3B). We also noted that the cellular concentrations of PPAR α were similar in WT and TTD mice (see Fig. 5A, right part). Moreover, the expression of CD36 (encoding a glycoprotein involved in the uptake of long-chain fatty acids), the acyl-CoA oxidase (the rate-limiting enzyme in peroxisomal β -oxidation of fatty acids), or the mitochondrial 3-hydroxy-3-methylglutaryl-CoA synthase (involved in ketogenesis) was similarly induced in WT and TTD mice (Fig. 3B and data not shown). On the contrary, pACOTH (peroxisomal acyl-CoA thioesterase, involved in the hydrolysis of acyl-CoAs) and CYP4A1 (cytochrome P450 4A1, involved in the ω -hydroxylation of fatty acids) are much less overexpressed in TTD mice (Fig. 3B). ChIP assays next revealed that PPAR α is much less recruited on the CYP4A1 promoter in TTD liver than in WT liver, while its recruitment on the CD36 promoter is similar in both livers (Fig. 3B). As expected, upon WY14643 treatment, we found that the recruitment of RNA pol

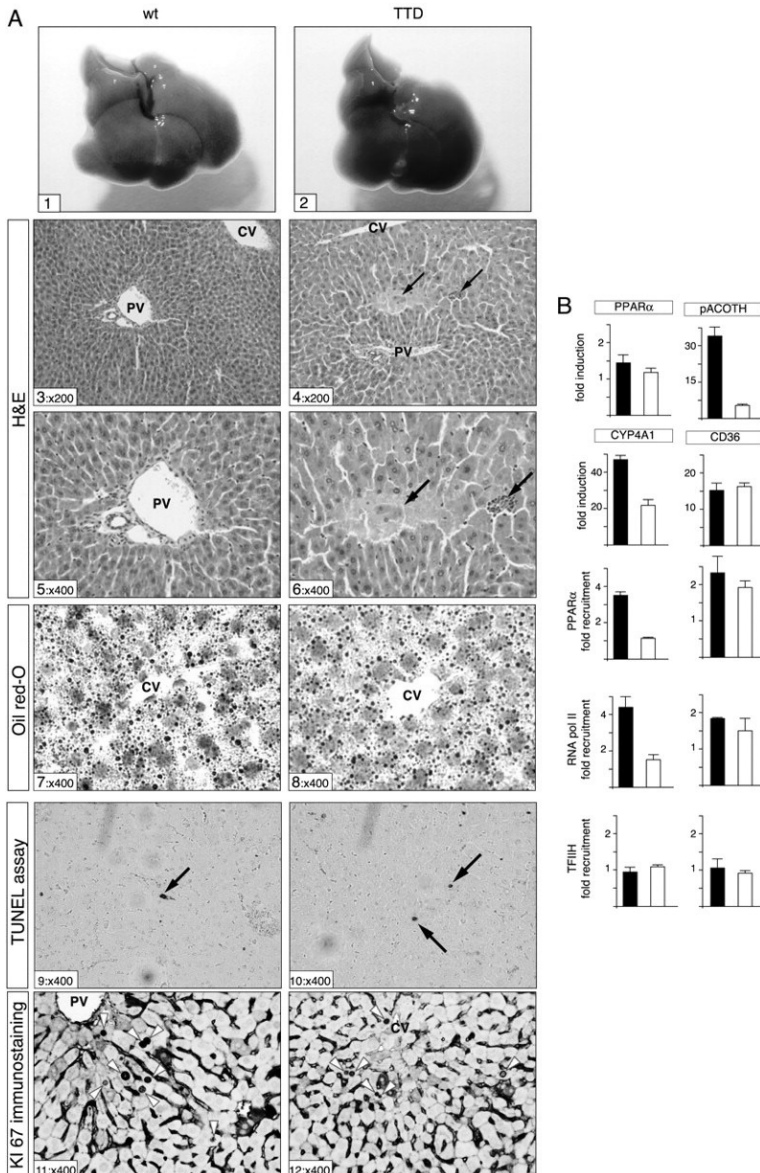


Figure 3: Expression of PPAR α target genes in the TTD liver.

(A) Macroscopic view (parts 1 and 2) of 3-month-old WT and TTD mouse livers. Parts 3 to 6: H&E-stained liver sections. Arrows indicate focal lesions corresponding to hepatic necrosis. Parts 7 and 8: oil red-O-dyed liver sections. Parts 9 and 10: in situ apoptosis detection in liver sections by TUNEL assay (see arrows). Parts 11 and 12: immunoperoxidase staining of liver sections for detection of the Ki67 antigen. Arrows indicate Ki67-positive nuclei. PV and CV, portal and centrolobular veins. Magnifications are indicated. (B) Expression of PPAR α target genes in the livers of 3-month-old WT (black boxes, $n = 4$) and TTD (open boxes, $n = 4$) mice treated for 20 h with WY14643 (100 mg/kg body weight). The results are presented as n -fold induction relative to nontreated mice. ChIP analyses were also performed on the CD36 and CYP4A1 promoters in the liver of WT (dark boxes) and TTD (open boxes) mice. Soluble chromatin was immunoprecipitated with antibodies raised against PPAR α , RNA pol II, or TFIIH (XPB). Immunoprecipitated DNA was quantified by real-time quantitative PCR. Results are expressed as n -fold recruitment relative to nontreated mice.

It was much lower on the CYP4A1 promoter in TTD liver. Lastly, no significant difference was observed between WT and TTD mice in the recruitment of TFIID on the promoters of the CD36 and CYP4A1 genes (Fig. 3B).

Altogether, these results demonstrate that TFIID mutation inhibits the expression of some hepatic PPAR α target genes in response to a specific agonist. This defect is associated with a weaker recruitment of PPAR α and RNA pol II, two components essential for their transcription.

PPARs are phosphorylated by TFIID via cdk7.

Knowing that some nuclear receptors cooperate with TFIID (7, 25, 38), we examined the physical and enzymatic connections between the PPAR nuclear receptors and basal transcription factor TFIID. Extracts from Sf9 insect cells coinfecting with baculoviruses encoding the subunits of TFIID and either PPAR γ 2 or PPAR α were incubated with Ab-p44, a monoclonal antibody directed against the p44 subunit of TFIID (20). Ab-p44 immunoprecipitates either PPAR γ 2 or PPAR α in addition to TFIID (Fig. 4A, left and right parts, lanes 8), while it does not retain PPARs in the absence of TFIID (lanes 6). The presence of a specific ligand does not affect the interaction between TFIID and PPARs (data not shown). As a control, we observed that Ab-C, an unrelated antibody, does not immunoadsorb either of these components (lanes 9). As previously stated (12), no interaction has been observed between TFIID and the vitamin D nuclear receptor (VDR), demonstrating the specificity of the PPAR-TFIID interactions (Fig. 4A, middle part, lane 8). To further determine which TFIID subunit is targeted by PPARs, Sf9 insect cell extracts coinfecting with baculoviruses encoding PPAR α or PPAR γ 2 and either one of the subunits of TFIID were incubated with the corresponding antibodies (Fig. 4B). Both PPAR γ 2 and PPAR α coimmunoprecipitated with XPB, p62, p44, and MAT1.

We also investigated whether PPARs can be used as substrates by cdk7. In vitro kinase assays show that both CAK and TFIID phosphorylate recombinant PPAR γ 2 and PPAR α (Fig. 4D, left and right parts, lanes 1 to 3) and more precisely their A/B domain (both parts, lanes 7 to 9). Indeed, PPAR IA/B, the truncated forms that lack the A/B domain, are not phosphorylated (both parts, lanes 4 to 6). Moreover, the A/B PPARs were not phosphorylated by rIIH-CKmut, a recombinant TFIID in which cdk7 was mutated in its ATP binding site (both parts, lanes 10 to 12). The A/B PPAR motifs were next phosphorylated in vitro by CAK, resolved by SDS-PAGE, and digested for mass spectrometry analysis. Accordingly, and knowing that cdk7s are serine/threonine kinases, each serine or threonine contained in the putative phosphorylated regions of PPAR γ 2 and PPAR α was mutated to alanine. The mutated A/B proteins were produced in *E. coli* and further purified on a nickel chelate column before being tested in in vitro kinase assays. Having observed that some mutations of serine to alanine prevent phosphorylation by either CAK or the entire TFIID, we demonstrate that residue S112 of PPAR γ 2 (corresponding to serine 84 of PPAR γ 1) is a target for cdk7 (Fig. 4E, left part, lanes 4 to 6 and 10 to 12). We also found that the A/B domain of PPAR α contains two phosphorylation sites at positions S12 and S21 (Fig. 4E, right part). Indeed, A/B PPAR α S12A/S21A, in which serines 12 and 21

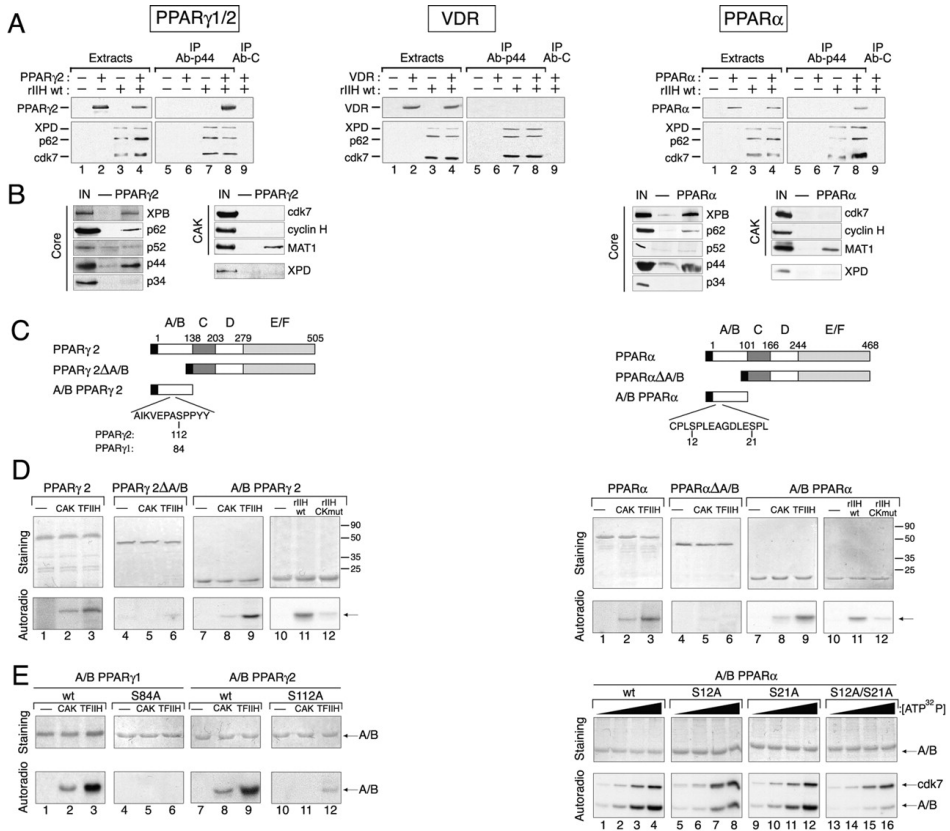


Figure 4: Interaction between TFIIH and PPARs and determination of their cdk7 phosphorylation sites.

(A) Sf9 cells were coinfecting with baculoviruses encoding the subunits of TFIIH (rIIH wt) and PPAR γ 2 (left part), VDR (middle part), or PPAR α (right part). Immunoprecipitation (IP) was done using an antibody directed against the TFIIH/p44 subunit (Ab-p44, lanes 5 to 8) or a control antibody (Ab-C, lanes 9). The bound proteins were analyzed by Western blotting using antibodies against subunits of TFIIH (XPD, p62 and cdk7), PPAR γ 2, VDR, or PPAR α . (B) Sf9 cell extracts overexpressing each TFIIH subunit alone (-) or in combination with PPAR γ 2 or PPAR α (as indicated) were incubated with antibodies directed against the corresponding PPAR isotype. Immunoprecipitated proteins were analyzed by Western blotting using antibodies against each subunit of TFIIH. The input lanes (IN) represent 10% of the total volume of extracts used in each immunoprecipitation.

(C) Schematic representation of the truncated PPAR proteins with a histidine tag (dark box). The different domains (A to F) of PPAR γ 2 and PPAR α and the cdk7 phosphorylation sites are depicted. Serine 112 in PPAR γ 2 corresponds to serine 84 in the PPAR γ 1 isoform. (D) Purified PPAR, PPAR α /B, and A/B PPAR were incubated in the absence (lanes 1, 4, 7, and 10) or presence of either free CAK (lanes 2, 5, and 8), TFIIH isolated from HeLa cells (lanes 3, 6, and 9), recombinant TFIIH (rIIH wt, lanes 11), or recombinant TFIIH mutated in the cdk7 ATP binding site (rIIH CKmut, lanes 12). Coomassie blue-stained gels (top parts) and autoradiography (Autoradio; bottom parts) of the incubated fractions are shown. (E) Left part: A/B PPAR γ 1-wt, A/B PPAR γ 2-wt, A/B PPAR γ 1 S84A, and A/B PPAR γ 2 S112A were incubated with CAK or TFIIH in the presence of 0.14 μ M [32 P]ATP. Right part: purified A/B PPAR α -wt, S12A, S21A, and S12A/S21A were incubated with CAK and increasing concentrations of [32 P]ATP (0.07, 0.14, 0.42, and 0.70 μ M).

were changed to alanine, is no longer phosphorylated by TFIIH (Fig. 4E, right part, lanes 13 to 16), whereas A/B PPAR α -S12A or A/B PPAR α -S21A is less phosphorylated (lanes 5 to 12), suggesting a synergistic effect of the phosphorylation of both serines 12 and 21. Additionally,

preliminary mass spectral data strongly suggest that the PPAR Δ A/B domain is phosphorylated by cdk7 between residues 44 and 55 (DLSQNSSPSSL; data not shown).

Phosphorylation of PPARs is crucial for their transactivation.

We next questioned whether a defect in the phosphorylation of PPARs might explain their lower ability to transactivate their target genes in XPD-mutated cells. Nuclear extracts of WAT, BAT, and liver isolated from 3-month-old WT and TTD mice were resolved by SDS-PAGE, followed by Western blot analysis (Fig. 5A). We found that the cellular concentrations of PPAR γ 1/2 and PPAR α are similar in both WT and TTD mice (left and right parts). Nevertheless, using an antibody specifically designed for either phosphorylated S84/S112 of PPAR γ 1/2 (Ab PPAR γ -P) or phosphorylated S12 of PPAR α (Ab PPAR α /S12), we observed that PPAR γ 1/2 and PPAR α are significantly less phosphorylated in the adipose tissues and liver isolated from TTD mice.

We next designed PPAR expression vectors in which the serine residues phosphorylated by cdk7 were changed to either alanine or glutamic acid, which mimics a constitutively phosphorylated serine residue. Wild-type and TTD mouse fibroblasts were cotransfected with these expression vectors in association with pPPAR-RE-Luc (Fig. 5B). First, we observed that luciferase gene expression was stimulated in WT fibroblasts by PPAR γ 1 (3.3-fold), PPAR γ 2 (4.8-fold), and PPAR α (4.4-fold) following the addition of their corresponding ligands (Fig. 5B, each part, lanes 3 and 4, dark boxes). In contrast, the transactivation directed by PPAR γ 1, PPAR γ 2, or PPAR α was approximately 50% lower in TTD fibroblasts than in WT cells (lanes 3 and 4, open boxes). Control experiments showed that reporter gene activation requires both PPAR overexpression and the presence of the ligand (lanes 1 to 3). Interestingly, the transfection of PPAR γ 1-S84E, PPAR γ 2-S112E, and PPAR α S12E/S21E expression vectors circumvents the transactivation defect observed in TTD fibroblasts (Fig. 5B, compare lane 6 to lane 4, open boxes). Moreover, the overexpression in WT fibroblasts of PPAR γ 1-S84A, PPAR γ 2-S112A, and PPAR α S12A/S21A gives reduced luciferase activity similar to what is usually obtained in TTD cells (compare lane 5 to lane 4, dark boxes).

Finally, we investigated in XPD-mutated cells whether WT XPD would restore the transactivation by PPARs (Fig. 5C) and secondly whether this effect would be correlated with their phosphorylation status (Fig. 5A, middle part). For convenience, we used the established cell line HD2 (22), resulting from the fusion between human fibroblasts harboring the XPD point mutation R683W (an other XPD mutation affecting transactivation by PPARs; see below) and HeLa cells. HD2 and HeLa cells (used as a control) were cotransfected with pPPAR-RE-Luc (a construct containing the luciferase reporter gene placed under the control of three DR1-type PPAR-responsive elements) and expression vectors encoding WT XPD and either PPAR α or PPAR γ 2 (Fig. 5C). Upon addition of the corresponding ligand, the transactivation directed by any PPAR was approximately 50% lower in HD2 than in HeLa cells, as previously observed for PPAR target genes in TTD mice (Fig. 5C, each part, lanes 1, open boxes). Interestingly,

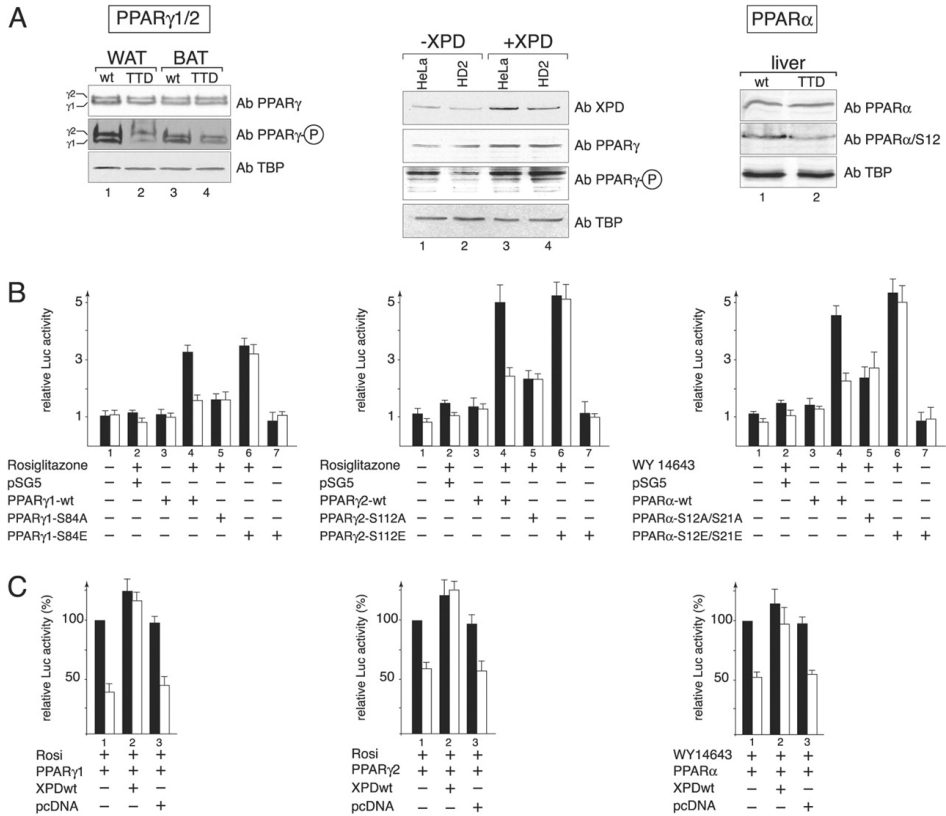


Figure 5: Phosphorylation of PPARs is crucial for their transactivation.

(A) Left part: Western blotting analysis of PPAR γ 1 and -2 (Ab PPAR γ) and their phosphorylated status on serines 84 and 112 (Ab PPAR γ -P) in WAT (10 μ g, lanes 1 and 2) and BAT (25 μ g, lanes 3 and 4) nuclear extracts from 3-month-old WT and TTD mice. TBP (Ab TBP) was used as an internal control. Middle part: detection of PPAR γ 2 (PPAR γ), its phosphorylated status on serine 112 (Ab PPAR-P) and XPD (Ab XPD) in crude extracts (100 μ g) from HeLa and HD2 (bearing XPD point mutation R683W) cells overexpressing PPAR γ 2 (lanes 1 to 4) and WT XPD (+ XPD, lanes 3 and 4). TBP (Ab TBP) was used as an internal control. Right part: detection of PPAR α (Ab PPAR α), phosphorylated S12 PPAR α (Ab PPAR α /S12), and TBP (Ab TBP) in hepatic nuclear extracts (25 μ g) from 3-month-old WT and TTD mice. (B) WT (dark boxes) and TTD (open boxes) mouse fibroblasts were cotransfected with pPPAR-RE-Luc (1 μ g), pCH110 (1 μ g), and either PPAR γ 1-wt, PPAR γ 2-wt, PPAR γ 1S84A, PPAR γ 1S84E, PPAR γ 2S112A, PPAR γ 2S112E, pSG5-PPAR α -wt, PPAR α S12A/S21A, or PPAR α S12E/S21E(100 ng). The cells were next treated with a specific ligand for PPAR γ 1/2 (rosiglitazone, 0.5 μ M) or PPAR α (WY14643, 1 μ M). Luciferase (Luc) activity was measured 24 h later and normalized relative to f-galactosidase activity. Note that the f-galactosidase values were similar in WT and TTD fibroblasts. (C) HeLa (dark boxes) and HD2 (open boxes) cells were transfected with pPPAR-RE-Luc (1 μ g), pCH110 (1 μ g), pSG5-PPAR γ 1 (100 ng), pSG5-PPAR γ 2 (100 ng), pSG5-PPAR α (100 ng), and either pcDNA-XPDwt (XPDwt) or empty pcDNA. Cells were then treated with the corresponding ligand, as mentioned for panel B. The values are presented as percentages, 100% being the level of transactivation obtained in HeLa cells overexpressing each PPAR isotype in the presence of the corresponding ligand. Rosi, rosiglitazone.

overexpression of WT XPD fully restores trans-activation by PPAR γ 1, PPAR γ 2, and PPAR α in HD2 cells (both parts, lanes 2, open boxes). These results clearly demonstrate that the defect in transactivation by PPARs in XPD-deficient cells is due to the XPD mutation itself. In parallel, the phosphorylation status of PPAR γ 2 was evaluated by Western blotting in HD2 cells. WT

Table 1: Transactivation by PPARs in XPD-deficient human fibroblasts^a

Cell line	XPD mutation	Phenotype	PPAR γ 1	PPAR γ 2	PPAR α
TTD8PV	R112H	TTD	100 \pm 8	97 \pm 5	105 \pm 5
XPJCLO	R683W	XP	64 \pm 3	65 \pm 7	61 \pm 3
TTD12PV	R722W	TTD	63 \pm 5	66 \pm 3	63 \pm 1

^aTTD8PV, XPJCLO, and TTD12PV human primary fibroblasts were transfected with pPPAR-RE-Luc (1 μ g), pCH110 (1 μ g), and PPAR expression vectors (100 ng) and subsequently treated with a specific ligand for each PPAR as described Fig. 5B. The transactivation values are indicated as percentages, 100% being the level of transactivation obtained in normal fibroblasts (GM03448D) overexpressing each PPAR isotype in the presence of the appropriate ligand.

and HD2 cells were transfected with expression vectors encoding WT XPD and PPAR γ 2 (Fig. 5A, middle part). Whereas PPAR γ 2 is significantly less phosphorylated in HD2 cells than in HeLa cells (compare lanes 1 and 2), WT XPD overexpression restores the phosphorylation status of PPAR γ 2 in XPD-mutated cells (compare lanes 2 and 4).

Altogether, these results demonstrate unambiguously that an XPD C-terminal mutation affects the phosphorylation of PPARs and consequently their transactivation efficiency.

Other XPD mutations affect transactivation by PPARs.

We then examined whether different XPD mutations alter trans-activation by PPARs. TTD8PV (R112H), XPJCLO (R683W), and TTD12PV (R722W) human primary fibroblasts isolated from XP or TTD patients (44) (<http://www.xpmutations.org/>) and normal human fibroblasts (GM03348D) were transfected with pPPAR-RE-Luc and the expression vector pSG5 PPAR α , pSG5 PPAR γ 1, or pSG5 PPAR γ 2-wt (Table 1). In the presence of ligand, we observed that luciferase gene expression was reduced in cells bearing XPD C-terminal mutations R683W and R722W, while it was normal in TTD8PV cells harboring the N-terminal mutation R112H. These results demonstrate that transactivation by PPARs is altered in fibroblasts from XP or TTD patients and suggest that this deficiency is associated with the position of the XPD mutation rather than with the nature of the disorder.

Discussion

This work is part of a study aiming to better understand the involvement of TFIIH in the transactivation process. We analyzed how a mutation in its XPD subunit affects this process, which in fine might explain the emergence of some clinical features observed in XP-D patients. We thus found that the adipose tissues and livers of TTD mice (bearing the XPD R722W mutation) have a defect in the regulation of their PPAR-responsive genes. We demonstrate that lower PPAR phosphorylation by the cdk7 kinase of TFIIH contributes to the dysregulation of these genes.

PPAR phosphorylation by cdk7.

Our results demonstrate that the activity of PPAR nuclear receptors depends on their ability to be phosphorylated by the DNA repair-transcription factor TFIIH. Mass spectral analysis and mutagenesis show that the phosphorylation sites are located in their A/B domain, also called the AF1 domain, in a serine/proline consensus site, namely, at positions S12 and S21 for PPAR α and S84 and S112 for PPAR γ 1 and -2, respectively. Interestingly, the sites of PPAR phosphorylation by the cdk7 kinase are also targeted by the mitogen-activated protein (MAP) kinases (19, 23). This observation is not restricted to PPARs, since other nuclear receptors are also phosphorylated on the same residue by cdk7 and/or MAP kinases, such as retinoic acid receptor c (38) and estrogen receptor c (7, 24). How do we reconcile that the same residue could be phosphorylated by different kinases? MAP kinases and cdk7 are involved in different signaling pathways, and their actions might occur at different times in cellular life. Whereas PPARs (and in extenso other nuclear receptors) would be phosphorylated in response to some mitogenic signal that activates the MAP kinase pathway, their phosphorylation by cdk7 would occur together with the formation of the trans-activation complex that puts TFIIH (within the preinitiation complex) and PPARs in very close proximity. Consequently, the same phosphorylation performed by various kinases differently affects the activity of the target factor. Along this line, it was demonstrated that serine 5 from the carboxy-terminal domain of RNA pol II could be phosphorylated by both cdk7 and cdk8 kinases with adverse consequences for the transcription process. While phosphorylation by cdk8 (which occurs outside the preinitiation complex) prevents the recruitment of RNA pol II on the promoter, modification of serine 5 by cdk7 (which occurs inside the preinitiation complex) promotes initiation of transcription by facilitating promoter escape (2, 17, 36).

Interestingly, PPAR nuclear receptors are much less phosphorylated by cdk7 in cells bearing an XPD C-terminal mutation, as shown in cells isolated from XP-D R683W patients, as well as in tissues of TTD R722W mice. In these cells, the PPAR underphosphorylation is due to the XPD mutation itself, since overexpression of WT XPD restores PPAR phosphorylation to the normal level. How can one explain that any mutation in the C-terminal end of XPD affects PPAR phosphorylation? XPD C-terminal mutations weaken the interaction between XPD and the p44 subunit, and consequently the anchoring of the CAK to the core-TFIIH (9). This might explain why these mutations not only prevent the regulation of the XPD helicase by p44 to allow elimination of DNA damage (13) but also the ability of cdk7 to phosphorylate the nuclear receptors, such as PPARs.

Incidence of PPAR underphosphorylation.

In the adipose tissues and livers of TTD mice, the XPD mutation R722W affects the phosphorylation of PPAR γ 1/2 and PPAR α and consequently the expression of PPAR target genes.

In some cases, the transactivation by underphosphorylated PPARs is maintained after treatment with a specific ligand, although the PPAR-responsive genes are induced to a much

lower level than in the WT ones, as shown for *aP2* (in WAT), *UCP-1*, *UCP-3* and *mCPT1* (in BAT), and *CYP4A1* and *pACOTH* (in the liver) (Fig. 2C and 3B). Additional ChIP experiments clearly demonstrate that the slight induction of these genes in TTD tissues is consistent with the lower recruitment of PPARs, as well as RNA pol II, on their promoters. Their expression defect is not due to a dysfunction of TFIID in the basal transcription process, since (i) TFIID is normally recruited on their promoters and (ii) a TFIID complex that carries an XPD C-terminal end mutation is able to normally promote RNA synthesis in *in vitro* transcription assays (9, 25). The expression defect (that was also observed in our transienttransfection assays) is rather due to the inability of TFIID to accurately phosphorylate PPAR γ or PPAR α . Indeed, overexpression of WT XPD restores not only transactivation by PPARs but also their phosphorylation in XPD-mutated cells (Fig. 5A, middle part, and C). Moreover, overexpression of the PPAR S-to-E-mutated forms (in which the glutamic acid mimics a constitutively phosphorylated residue) allows normal expression of PPAR-dependent genes even in XPD-mutated cells (Fig. 5B). It remains to be determined whether lower phosphorylation prevents the recruitment of accurate cofactors which are required for the PPAR transactivation process.

In other cases, the expression of PPAR target genes is unexpectedly increased in a tissue-specific manner, as observed for *UCP-1*, *mCPT1*, and *aP2* in TTD WAT. Since such overexpression occurs independently of the presence of a specific ligand, it is not surprising that PPARs are no longer recruited on their corresponding promoters, while the recruitment of RNA pol II is consistent with the expression level (as illustrated for *aP2* in Fig. 2C). Knowing that the expression of any gene requires a subtle combination of several DNA binding factors (14), a defect in the function of one of them might completely reprogram the transcription process. Since PPARs cannot be correctly phosphorylated, one cannot exclude the possibility that their transactivation function is diminished to a such level that they are supplanted by other tissue-specific factors. Further investigations should be undertaken to understand why underphosphorylated PPARs are no longer recruited, giving rise to other regulatory pathways. Altogether, our results show that PPAR target genes are specifically affected by PPAR underphosphorylation in a tissue specific manner. This differential effect can thus explain the apparent discrepancies between our results and data showing that the S112A mutation in PPAR γ 2 increases the expression of responsive genes (1, 19). In the latter case, it is likely that the nonphosphorylated PPAR S112A might be either assisted or supplanted by another transcriptional factor.

Contribution of PPAR defects to the TTD phenotype.

The reduction of adipose mass in TTD mice may occur by a disruption of adipogenesis and/or elevated energy dissipation. Defects in adipogenesis typically result in irregular metabolic features, such as fatty liver, hypertriglyceridemia, and insulin resistance (34, 43). However, in TTD mice, no apparent abnormal fat accumulation was observed in the liver, and the circulating glucose and total triglyceride levels are normal (data not shown). Subtle adipogenic

defects cannot be excluded, since the adipose tissues disappear with age (Fig. 2A) and TTD mouse embryonic fibroblasts have a reduced capability to differentiate into adipocytes in the presence of prostaglandin PGJ₂, a PPAR γ ligand known to induce adipocyte differentiation (data not shown). Besides adipogenic dysfunction, we also observed in TTD mice elevated energy dissipation by indirect calorimetric analysis (1.4 ± 0.06 and 1.6 ± 0.07 kcal/h in WT and TTD mice, respectively; $P < 0.05$; data not shown), as well as the aberrant overexpression in TTD WAT of BAT-specific genes involved in fatty acid catabolism, such as PGC1c and UCP-1 (33, 42). The overexpression of these genes could contribute to the higher energy expenditure in TTD mice, as previously found in transgenic mice overexpressing UCP-1 in WAT (27).

Therefore, the hypoplasia of the adipose tissues observed within the TTD mice might be due at least partially to a dysfunction of the PPAR nuclear receptors, which are essential in the lipid metabolism and both differentiation (46) and *in vivo* survival of the adipocytes (16). However, it seems also clear that the overall pleiotropic nature of the XP-D phenotype might result from the defect of various transcriptional factors, such as other nuclear receptors (12, 25). By using diverse treatments, XPD-deficient mice could provide excellent models to elucidate the contribution of a defect of different nuclear receptors, such as the estrogen receptor or the thyroid receptor, in various physiological pathways.

Our *in vivo* results underline the crucial role of phosphorylation by TFIIF for the transactivation process. Moreover, we demonstrate that a defect in phosphorylating nuclear receptors might simply result in a drop in their transactivation capacity that could (as a function of the tissue and the environmental situation) lead to their being opportunistically replaced by other factors. The major challenge for the future will be to understand how phosphorylation by TFIIF directs the integration of nuclear receptors in the transactivation complex.

Acknowledgements

We thank P. Brousset (CHU Purpan, INSERM U563, Toulouse, France), M. Doffoel (Clinique Med B, Hospices Civils de Strasbourg, Strasbourg, France), and M. P. Chenard (Service d'anatomopathologie, Hôpital Hautepierre, Strasbourg, France) for fruitful discussions and P. Laine for critical reading of the manuscript. We are grateful to I. Kolb-Cheynel and J. L. Weickert for the design and production of recombinant baculoviruses; M. Argentini for mass spectral analysis; M. C. Antal, M. Duval, and M. Selloum for expertise in phenotyping mice; and J. Auwerx, P. Grimaldi, and M. Dauca for the pPPAR-RE-Luc, pSG5-rat PPAR α , pSG5-human PPAR γ 1 and -2, and pcDNAmouse PPAR Δ constructs.

These studies were supported by CNRS, INSERM, and grants from the Association pour la Recherche sur le Cancer, the European Community (QLG1-1999 and QLRT-1999-02002), the Research Ministry ACI Biologie Cellulaire et Structurale (3-2-535), the Institut des Maladies Rares (A03098MS), and the Commissariat à l'Énergie Atomique. E.C. is a recipient of a grant

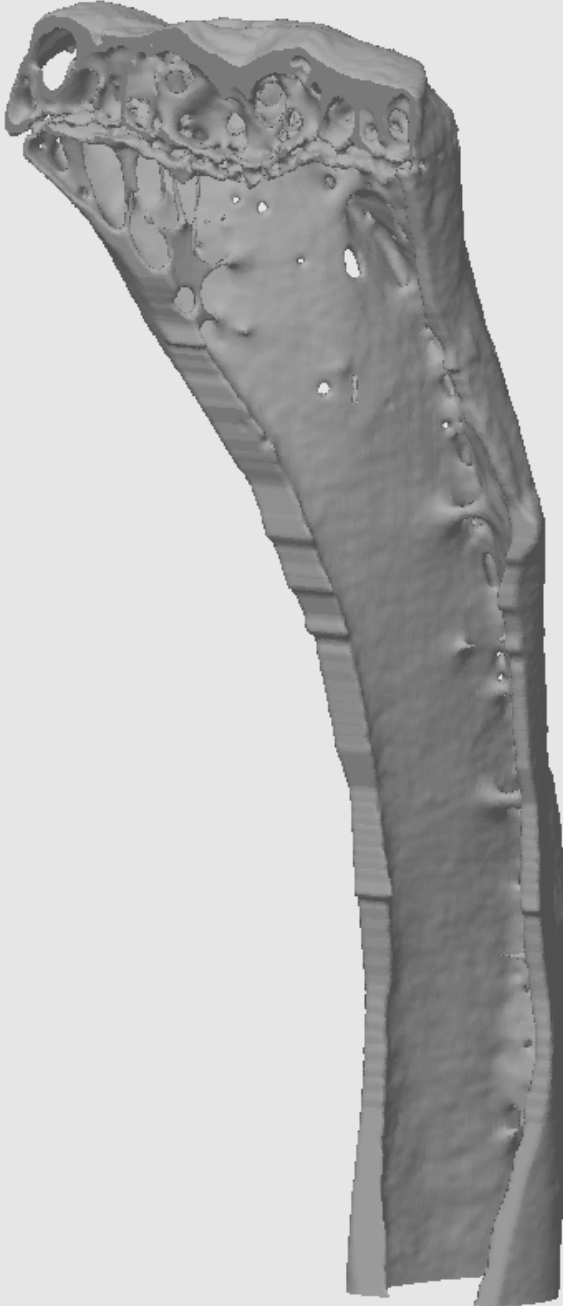
from the Association pour la Recherche contre le Cancer. P.D. is the recipient of a fellowship from the Fondation Lefoulon-Delalande, and the 2000 Descartes Prize was awarded to J.-M.E. by the European Economic Community. C.L. is a recipient of a Fondation pour la Recherche Médicale fellowship.

References

1. **Adams, M., M. J. Reginato, D. Shao, M. A. Lazar, and V. K. Chatterjee.** 1997. Transcriptional activation by peroxisome proliferator-activated receptor gamma is inhibited by phosphorylation at a consensus mitogen-activated protein kinase site. *J. Biol. Chem.* **272**:5128–5132.
2. **Akoulitchev, S., S. Chuikov, and D. Reinberg.** 2000. TFIID is negatively regulated by cdk8-containing mediator complexes. *Nature* **407**:102–106.
3. **Auwerx, J.** 1999. PPAR γ , the ultimate thrifty gene. *Diabetologia* **42**:1033–1049.
4. **Berger, J., and D. E. Moller.** 2002. The mechanisms of action of PPARs. *Annu. Rev. Med.* **53**:409–435.
5. **Bootsma, D., and J. H. J. Hoeijmakers.** 1993. DNA repair. Engagement with transcription. *Nature* **363**:114–115.
6. **Botta, E., T. Nardo, B. C. Broughton, S. Marinoni, A. R. Lehmann, and M. Stefanini.** 1998. Analysis of mutations in the XPD gene in Italian patients with trichothiodystrophy: site of mutation correlates with repair deficiency, but gene dosage appears to determine clinical severity. *Am. J. Hum. Genet.* **63**:1036–1048.
7. **Chen, D., T. Riedl, E. Washbrook, P. E. Pace, R. C. Coombes, J. M. Egly, and S. Ali.** 2000. Activation of estrogen receptor alpha by S118 phosphorylation involves a ligand-dependent interaction with TFIID and participation of CDK7. *Mol. Cell* **6**:127–137.
8. **Cherkaoui-Malki, M., K. Meyer, W. Q. Cao, N. Latruffe, A. V. Yeldandi, M. S. Rao, C. A. Bradfield, and J. K. Reddy.** 2001. Identification of novel peroxisome proliferator-activated receptor alpha (PPAR α) target genes in mouse liver using cDNA microarray analysis. *Gene Expr.* **9**:291–304.
9. **Coin, F., J. C. Marinoni, C. Rodolfo, S. Fribourg, A. M. Pedrini, and J. M. Egly.** 1998. Mutations in the XPD helicase gene result in XP and TTD phenotypes, preventing interaction between XPD and the p44 subunit of TFIID. *Nat. Genet.* **20**:184–188.
10. **de Boer, J., J. de Wit, H. van Steeg, R. J. Berg, H. Morreau, P. Visser, A. R. Lehmann, M. Duran, J. H. Hoeijmakers, and G. Weeda.** 1998. A mouse model for the basal transcription/DNA repair syndrome trichothiodystrophy. *Mol. Cell* **1**:981–990.
11. **Desvergne, B., and W. Wahli.** 1999. Peroxisome proliferator-activated receptors: nuclear control of metabolism. *Endocr. Rev.* **20**:649–688.
12. **Drane, P., E. Compe, P. Catez, P. Chymkowitz, and J. M. Egly.** 2004. Selective regulation of vitamin D receptor-responsive genes by TFIID. *Mol. Cell* **16**:187–197.
13. **Dubaele, S., L. Proietti De Santis, R. Bienstock, A. Keriell, M. Stefanini, B. Van Houten, and J. Egly.** 2003. Basal transcription defect discriminates between xeroderma pigmentosum and trichothiodystrophy in XPD patients. *Mol. Cell* **11**:1635–1646.
14. **Grosschedl, R.** 1995. Higher-order nucleoprotein complexes in transcription: analogies with site-specific recombination. *Curr. Opin. Cell Biol.* **7**:362–370.
15. **Happle, R., H. Traupe, H. Grobe, and G. Bonsmann.** 1984. The Tay syndrome (congenital ichthyosis with trichothiodystrophy). *Eur. J. Pediatr.* **141**: 147–152.
16. **He, W., Y. Barak, A. Hevener, P. Olson, D. Liao, J. Le, M. Nelson, E. Ong, J. M. Olefsky, and R. M. Evans.** 2003. Adipose-specific peroxisome proliferator-activated receptor gamma knockout causes insulin resistance in fat and liver but not in muscle. *Proc. Natl. Acad. Sci. USA* **100**:15712–15717.
17. **Hengartner, C. J., V. E. Myer, S. M. Liao, C. J. Wilson, S. S. Koh, and R. A. Young.** 1998. Temporal regulation of RNA polymerase II by Srb10 and Kin28 cyclin-dependent kinases. *Mol. Cell* **2**:43–53.

18. **Holstege, F. C., P. C. van der Vliet, and H. T. Timmers.** 1996. Opening of an RNA polymerase II promoter occurs in two distinct steps and requires the basal transcription factors IIE and IIH. *EMBO J.* **15**:1666–1677.
19. **Hu, E., J. B. Kim, P. Sarraf, and B. M. Spiegelman.** 1996. Inhibition of adipogenesis through MAP kinase-mediated phosphorylation of PPAR γ . *Science* **274**:2100–2103.
20. **Humbert, S., H. van Vuuren, Y. Lutz, J. H. J. Hoeijmakers, J. M. Egly, and V. Moncollin.** 1994. p44 and p34 subunits of the BTF2/TFIIH transcription factor have homologies with SSL, a yeast protein involved in DNA repair. *EMBO J.* **13**:2393–2398.
21. **Itin, P. H., and M. R. Pittelkow.** 1990. Trichothiodystrophy: review of sulfur-deficient brittle hair syndromes and association with the ectodermal dysplasias. *J. Am. Acad. Dermatol.* **22**:705–717.
22. **Johnson, R. T., S. Squires, G. C. Ellion, G. L. E. Koch, and A. J. Rainbow.** 1985. Xeroderma pigmentosum D-HeLa hybrids with low and high ultraviolet sensitivity associated with normal and diminished DNA repair ability, respectively. *J. Cell Sci.* **76**:115–133.
23. **Juge-Aubry, C. E., E. Hammar, C. Siegrist-Kaiser, A. Pernin, A. Takeshita, W. W. Chin, A. G. Burger, and C. A. Meier.** 1999. Regulation of the transcriptional activity of the peroxisome proliferator-activated receptor alpha by phosphorylation of a ligand-independent trans-activating domain. *J. Biol. Chem.* **274**:10505–10510.
24. **Kato, S., H. Endoh, Y. Masuhiro, T. Kitamoto, S. Uchiyama, H. Sasaki, S. Masushige, Y. Gotoh, E. Nishida, H. Kawashima, et al.** 1995. Activation of the estrogen receptor through phosphorylation by mitogen-activated protein kinase. *Science* **270**:1491–1494.
25. **Keriel, A., A. Stary, A. Sarasin, C. Rochette-Egly, and J. M. Egly.** 2002. XPD mutations prevent TFIIH-dependent transactivation by nuclear receptors and phosphorylation of RAR α . *Cell* **109**:125–135.
26. **Kersten, S., B. Desvergne, and W. Wahli.** 2000. Roles of PPARs in health and disease. *Nature* **405**:421–424.
27. **Kopecky, J., Z. Hodny, M. Rossmeisl, I. Syrový, and L. P. Kozak.** 1996. Reduction of dietary obesity in aP2-Ucp transgenic mice: physiology and adipose tissue distribution. *Am. J. Physiol.* **270**:E768–E775.
28. **Lee, C. H., P. Olson, and R. M. Evans.** 2003. Minireview: lipid metabolism, metabolic diseases, and peroxisome proliferator-activated receptors. *Endocrinology* **144**:2201–2207.
29. **Lehmann, A. R.** 2001. The xeroderma pigmentosum group D (XPD) gene: one gene, two functions, three diseases. *Genes Dev.* **15**:15–23.
30. **Lehmann, J. M., L. B. Moore, T. A. Smith-Oliver, W. O. Wilkison, T. M. Willson, and S. A. Kliewer.** 1995. An antidiabetic thiazolidinedione is a high affinity ligand for peroxisome proliferator-activated receptor gamma (PPAR γ). *J. Biol. Chem.* **270**:12953–12956.
31. **Lemon, B. D., J. D. Fondell, and L. P. Freedman.** 1997. Retinoid X receptor: vitamin D3 receptor heterodimers promote stable preinitiation complex formation and direct 1,25-dihydroxyvitamin D3-dependent cell-free transcription. *Mol. Cell. Biol.* **17**:1923–1937.
32. **Lu, H., L. Zavel, L. Fisher, J. M. Egly, and D. Reinberg.** 1992. Human general transcription factor IIH phosphorylates the C-terminal domain of RNA polymerase II. *Nature* **358**:641–645.
33. **Mascaro, C., E. Acosta, J. A. Ortiz, P. F. Marrero, F. G. Hegardt, and D. Haro.** 1998. Control of human muscle-type carnitine palmitoyltransferase I gene transcription by peroxisome proliferator-activated receptor. *J. Biol. Chem.* **273**:8560–8563.
34. **Moitra, J., M. M. Mason, M. Olive, D. Krylov, O. Gavrilova, B. Marcus-Samuels, L. Feigenbaum, E. Lee, T. Aoyama, M. Eckhaus, M. L. Reitman, and C. Vinson.** 1998. Life without white fat: a transgenic mouse. *Genes Dev.* **12**:3168–3181.

35. **Reddy, J. K., and T. Hashimoto.** 2001. Peroxisomal beta-oxidation and peroxisome proliferator-activated receptor alpha: an adaptive metabolic system. *Annu. Rev. Nutr.* **21**:193–230.
36. **Rickert, P., J. L. Corden, and E. Lees.** 1999. Cyclin C/CDK8 and cyclin H/CDK7/p36 are biochemically distinct CTD kinases. *Oncogene* **18**:1093–1102.
37. **Riedl, T., F. Hanaoka, and J. Egly.** 2003. The comings and goings of nucleotide excision repair factors on damaged DNA. *EMBO J.* **22**:5293–5303.
38. **Rochette-Egly, C., S. Adam, M. Rossignol, J. M. Egly, and P. Chambon.** 1997. Stimulation of RAR α activation function AF-1 through binding to the general transcription factor TFIID and phosphorylation by CDK7. *Cell* **90**: 97–107.
39. **Rosen, E. D., P. Sarraf, A. E. Troy, G. Bradwin, K. Moore, D. S. Milstone, B. M. Spiegelman, and R. M. Mortensen.** 1999. PPAR γ is required for the differentiation of adipose tissue in vivo and in vitro. *Mol. Cell* **4**:611–617.
40. **Roy, R., J. P. Adamczewski, T. Seroz, W. Vermeulen, J. P. Tassan, L. Schaeffer, J. H. J. Hoeijmakers, and J. M. Egly.** 1994. The MO15 cell cycle kinase is associated with the TFIID transcription-DNA repair factor. *Cell* **79**:1093–1101.
41. **Sandrock, B., and J. M. Egly.** 2001. A yeast four-hybrid system identifies Cdk-activating kinase as a regulator of the XPD helicase, a subunit of transcription factor IIF. *J. Biol. Chem.* **276**:35328–35333.
42. **Sears, I. B., M. A. MacGinnitie, L. G. Kovacs, and R. A. Graves.** 1996. Differentiation-dependent expression of the brown adipocyte uncoupling protein gene: regulation by peroxisome proliferator-activated receptor gamma. *Mol. Cell. Biol.* **16**:3410–3419.
43. **Shimomura, I., R. E. Hammer, J. A. Richardson, S. Ikemoto, Y. Bashmakov, J. L. Goldstein, and M. S. Brown.** 1998. Insulin resistance and diabetes mellitus in transgenic mice expressing nuclear SREBP-1c in adipose tissue: model for congenital generalized lipodystrophy. *Genes Dev.* **12**:3182–3194.
44. **Taylor, E. M., B. C. Broughton, E. Botta, M. Stefanini, A. Sarasin, N. G. Jaspers, H. Fawcett, S. A. Harcourt, C. F. Arlett, and A. R. Lehmann.** 1997. Xeroderma pigmentosum and trichothiodystrophy are associated with different mutations in the XPD (ERCC2) repair/transcription gene. *Proc. Natl. Acad. Sci. USA* **94**:8658–8663.
45. **Tirole, F., D. Busso, F. Coin, and J. M. Egly.** 1999. Reconstitution of the transcription factor TFIID: assignment of functions for the three enzymatic subunits, XPB, XPD, and cdk7. *Mol. Cell* **3**:87–95.
46. **Tontonoz, P., E. Hu, and B. M. Spiegelman.** 1994. Stimulation of adipogenesis in fibroblasts by PPAR γ , a lipid-activated transcription factor. *Cell* **79**:1147–1156.
47. **van Steeg, H., and K. H. Kraemer.** 1999. Xeroderma pigmentosum and the role of UV-induced DNA damage in skin cancer. *Mol. Med. Today* **5**:86–94.
48. **Wang, Y. X., C. H. Lee, S. Tjep, R. T. Yu, J. Ham, H. Kang, and R. M. Evans.** 2003. Peroxisome-proliferator-activated receptor delta activates fat metabolism to prevent obesity. *Cell* **113**:159–170.
49. **Zurita, M., and C. Merino.** 2003. The transcriptional complexity of the TFIID complex. *Trends Genet.* **19**:578–584.



APPENDIX III

Impaired Genome Maintenance Suppresses the GH/IGF1 Axis in Cockayne Syndrome Mice

Ingrid van der Pluijm^{1,7}, George A. Garinis^{1,7}, Renata M.C. Brandt¹, Theo G.M.F. Gorgels^{1,2}, Susan W. Wijnhoven³, Karin E.M. Diderich¹, Jan de Wit¹, James R. Mitchell¹, Conny van Oostrom³, Rudolf Beems³, Laura J. Niedernhofer^{1,4}, Susana Velasco⁵, Errol C. Friedberg⁵, Kiyoji Tanaka⁶, Harry van Steeg³, Jan H.J. Hoeijmakers¹, and Gijsbertus T.J. van der Horst¹

¹Department of Genetics, Center for Biomedical Genetics, Erasmus University Medical Center, PO Box 1738, 3000 DR Rotterdam, the Netherlands, ²present address: Department of Molecular Ophthalmology, Netherlands Ophthalmic Research Institute, Royal Netherlands Academy of Arts and Sciences, Meibergdreef 47, 1105 BA Amsterdam, the Netherlands, ³National Institute of Public Health and the Environment (RIVM), Laboratory of Toxicology, Pathology and Genetics (TOX), PO Box 1, 3720 BA Bilthoven, The Netherlands, ⁴present address: University of Pittsburgh Cancer Institute, 5117 Centre Avenue, Pittsburgh PA, USA 15213, ⁵Laboratory of Molecular Pathology, Department of Pathology, University of Texas Southwestern Medical Center, Dallas TX, USA, ⁶Division of Cellular Genetics, Institute for Molecular and Cellular Biology, Osaka University, 1-3 Yamadaoka, Suita, Osaka 565-0871, Japan, ⁷These authors contributed equally.

Abstract

Cockayne syndrome (CS) is a photosensitive, DNA repair disorder associated with progeria caused by a defect in the transcription-coupled repair (TCR) subpathway of nucleotide excision repair (NER). Here, complete inactivation of NER in $Csb^{m/m}/Xpa^{-/-}$ mutants causes a phenotype that reliably mimics the human progeroid CS syndrome. Newborn $Csb^{m/m}/Xpa^{-/-}$ mice display attenuated growth, progressive neurological dysfunction, retinal degeneration, cachexia, kyphosis and die before weaning. Mouse liver transcriptome analysis and several physiological endpoints revealed systemic suppression of the Growth Hormone/

Insulin-like Growth Factor 1 (GH/IGF1) somatotroph axis and oxidative metabolism, increased antioxidant responses, hypoglycemia together with hepatic glycogen and fat accumulation. Broad genome-wide parallels between $Csb^{m/m}/Xpa^{-/-}$ and naturally aged mouse liver transcriptomes suggested that these changes are intrinsic to natural aging and the DNA repair-deficient mice. Importantly, wild type (*wt*) mice exposed to a low dose of chronic genotoxic stress recapitulated this response, thereby pointing to a novel link between genome instability and the age-related decline of the somatotroph axis.

Introduction

A prevailing hypothesis to explain the molecular basis of aging is Harman's "free-radical theory of aging", which states that endogenous reactive oxygen species (ROS), resulting from cellular metabolism, continually damage biomolecules [1]. In line with this hypothesis, it has been shown that increased resistance to oxidative stress (e.g. by improved antioxidant defense) extends the life span of *C. elegans*, *Drosophila*, and rodents [2-4], whereas oppositely, hypersensitivity to oxygen considerably reduces the life span of nematodes [5]. A key macromolecule at risk for ROS-mediated damage is nuclear DNA [1], as evident from the wide range of oxidative DNA lesions that accumulate gradually in rodents and humans with advancing age [6,7].

In humans, the causative role of DNA damage in aging is supported by a variety of progeroid disorders with defects in DNA repair pathways [8,9]. One such condition is *Cockayne syndrome* (CS; affected genes: *CSA* or *CSB*), a photosensitive disorder, originating from a defect in transcription-coupled repair (TCR), that specifically removes DNA lesions, which obstruct RNA polymerases, to allow resumption of transcription and promote cellular survival from DNA damage. TCR of helix-distorting DNA damage is a dedicated subpathway of the multi-step 'cut-and-patch' nucleotide excision repair (NER) system, and is designated Transcription-Coupled Nucleotide Excision Repair (TC-NER) [10] to distinguish it from the so-called global genome NER (GG-NER) subpathway that operates genome wide to eliminate distorting damage. Available evidence suggests that CS cells are also defective in TCR of non-helix distorting, DNA lesions that block transcription such as transcription-blocking oxidative DNA lesions [11,12], which are normally genome-wide removed by base excision repair. We will use TCR, when referring to transcription-coupled repair in general. CS patients present with growth failure (cachectic dwarfism), progressive neurological abnormalities (including delayed psychomotor development, mental retardation, microcephaly, gait ataxia, sensorineural hearing loss, retinal degeneration), along with impaired sexual development, kyphosis, osteoporosis and severely reduced life span (mean age of death: 12.5 years) [13,14]. A related yet distinct disorder is *Trichothiodystrophy* (TTD; affected genes: *XPB*, *XPD* or *TTDA*). TTD patients are partially defective in TCR, as well as in the global genome repair subpathway of NER, and share the symptoms associated with CS. In addition, these patients have a partial defect in transcription itself, causing additional symptoms such as ichthyosis and brittle hair and nails [15]. Many of the CS and TTD features are progressive and resemble premature aging. As patients develop some but not all aspects of normal aging in an accelerated manner, CS and TTD are considered "segmental progeroid syndromes" [8]

Mouse mutants for CS-A and CS-B reliably mimic the UV-sensitivity of CS patients and show accelerated photoreceptor loss, reduced body weight, and mild neurologic abnormalities [16,17]. Similarly, mice homozygous for a causative TTD point mutation in the *Xpd* gene faithfully mirror the symptoms in TTD patients [9] whereas complete inactivation of NER (by

concurrent inactivation of the *Xpa* gene) dramatically aggravates the CS features of partially NER-defective TTD mice [9]. These observations, together with the notion that DNA lesions can provoke a permanent cell cycle arrest or apoptosis, led us to propose that aging can result from (oxidative) DNA lesions that interfere with transcription and/or replication causing cell death or cellular senescence, ultimately leading to loss of tissue homeostasis and onset of age-related diseases [18-20].

Here, we report that mice with engineered mutations in both *Csb* and *Xpa* genes display many CS features in a dramatic form, including postnatal growth attenuation, progressive kyphosis, ataxia, retinal degeneration, motor dysfunction and premature death. Importantly, full genome transcriptome analysis of the *Csb^{m/m}/Xpa^{-/-}* mouse liver at the age of 15 days uncovered a systemic response seen also in wt mice exposed to chronic oxidative stress. These findings disclose a novel link between DNA damage, compromised genome maintenance and the somatotrophic axis that determines life span and shed new light on the etiology of Cockayne syndrome and natural aging.

Methods

Animals

The generation and characterization of NER-deficient *Xpa^{-/-}*, *Xpc^{-/-}*, and *Csb^{m/m}* mice has been previously described [16,22,64,65] *p53^{-/-}* mice [66] were kindly provided by Dr. T. Jacks (MIT, Cambridge, MA). Unless stated otherwise, all mice were kept in a C57BL/6J genetic background. In the DEHP exposure study, 4-week old male wt mice (C57BL/6J; n=6) were put on a di(2-ethylhexyl)phthalate (DEHP; 1500 ppm; Sigma) containing diet or on a regular diet for 9 weeks. Animals were daily screened for discomfort and weighed once a week. Food consumption was registered by weighing the food. In the ionizing irradiation exposure study, 19-day old *Csb^{m/m}/Xpa^{-/-}* and littermate control animals (n=4-6/genotype) were exposed to 10 Gy, sacrificed 20 hours after exposure and eyes were further processed. Additional information on the isolation and processing of the eyes is provided in the supplementary section. As required by Dutch law, all animal studies were approved by an independent Animal Ethical Committee (Dutch equivalent of the IACUC). Further information on mouse crossing, genotyping, housing and macroscopic examination is described in the supplementary section.

Cellular sensitivity studies

UV sensitivity was determined as described [67]. Sparsely seeded Petri dish cultures were exposed to different doses of UV (254 nm, Philips TUV lamp). After 4 days, the number of proliferating cells was estimated from the amount of radioactivity incorporated during a 2 hr pulse with [³H] thymidine. Cell survival was expressed as the percentage of radioactivity in exposed cells in relation to the radioactivity in untreated cells. UV-induced global genome re-

pair was assayed using the UDS method described by [68]. In brief, coverslip-grown cells were exposed to 16 J/m² of 254 nm UV light and labeled with [³H] thymidine. Repair capacity was quantified by grain counting after autoradiography. RNA synthesis recovery was measured according to [69]. In short, coverslip-grown cells were exposed to 10 J/m² of 254 nm UV light, allowed to recover for 16 hr, labeled with [³H] uridine, and processed for autoradiography. The relative rate of RNA synthesis was expressed as G_{UV}/G_C (percentage), where G_{UV} and G_C represent the number of grains over UV-exposed and non-exposed nuclei, respectively.

Ionizing radiation sensitivity of immortalized MEFs was determined using a colony assay. Cells were plated in 6-cm-diameter dishes at various densities. After 16 h, cells were exposed to a single dose of ionizing radiation (¹³⁷Cs source; dose range of 0 to 8 Gy). Cells were grown for another 5 to 14 days, and after fixation and staining, colonies were counted. All experiments were performed in triplicate.

Immunohistological Examination and Blood Parameters

Detailed histopathological examination was performed on all organs and tissues. Paraffin-embedded tissues were sectioned at 5 μm and stained with haematoxylin/eosin solution. Liver sections were stained with Periodic Acid Schiff (PAS) or Oil Red O (cryosections) to detect glycogen and triglycerides respectively. Detailed information on the immunohistochemical procedures is described on the supplementary section. Apoptotic cells were detected using a TdT-mediated dUTP Nick-End Labeling (TUNEL) assay as described by the manufacturer (Apoptag Plus Peroxidase *In Situ* Apoptosis Detection Kit, Chemicon). For retinal evaluation, eyes were marked nasally with Alcian blue (5% Alcian blue in 96% ethanol), enucleated, fixed in 4 % paraformaldehyde in 0.1M phosphate buffer, washed in PBS and embedded in paraffin. Horizontal sections (5 μm thick) of the retina were cut and sections in the middle of the retina were selected by Alcian blue marking and proximity of the optic nerve. Sections were stained for degenerating cells by TdT-mediated dUTP Nick-End Labeling (TUNEL), according to the manufacturer's instructions (Apoptag Plus Peroxidase *In Situ* Apoptosis Detection Kit, Chemicon). For quantification, the number of TUNEL-positive cells in the inner nuclear layer (INL) and outer nuclear layer (ONL) were counted in 6 whole sections per mouse. Differences between the genotypes were tested for statistical significance using multivariate analysis of variance (ANOVA), followed by a posthoc test of Student-Newman-Keuls (S-N-K). Significance was set at $p < 0.05$. Serum IGF1 and GH levels were determined with the Active mouse/rat IGF1 ELISA (Enzyme-Linked Immuno Sorbent Assay) and Active mouse/rat GH ELISA kits respectively, as described by the manufacturer (Diagnostic Systems Laboratories Inc., Texas). Blood glucose was measured using a Freestyle mini blood glucose measurement device (Abbott Diabetes Care).

Radiography and Micro-computed Tomography

Mice were anaesthetized by intraperitoneal injection of ketalin and rompun (120 and 7.5 $\mu\text{g/g}$ body weight). Lateral films were taken at 2x magnification using a CGR Senograph 500T X ray system operated at 30 kV and 32 mAS [9]. Formalin fixed tibiae from wt and mutant mice were scanned from proximal end to mid-diaphysis, using a SkyScan 1072 microtomograph (SkyScan, Antwerp, Belgium) with a voxel size of 8.82 μm . Scans were processed, and 2D images of the bones were obtained.

Footprint Studies

Footprint analysis was performed by painting the hind and fore paws of the mice with different colors of water-soluble non-toxic paints. Animals were allowed to walk along a 30 x 7 cm walled runway, lined with paper, into a darkened, enclosed space. Tests were performed in duplicate at day 15 and 19. Footprint patterns were analyzed for (1) stride length, measured as the average distance between each stride, (2) front base width and (3) hind base width, measured as the average distance between contralateral footprints [70].

Microarray Analysis and Q-PCR Evaluation

Standard procedures were used to obtain total RNA (Qiagen) from the liver of wt, $Xpa^{-/-}$, $Csb^{m/m}$, and $Csb^{m/m}/Xpa^{-/-}$ mice (n=4) at postnatal day 15 and from the liver of 8-, 16-, 96- and 130-week old mice (n=5). Synthesis of double stranded cDNA and biotin labeled cRNA was performed according to the instructions of the manufacturer (Affymetrix, USA). Fragmented cRNA preparations were hybridized to full mouse genome oligonucleotide arrays (430 V2.0; Affymetrix, USA). Q-PCR was performed with a DNA Engine Opticon device (MJ Research). Detailed information on microarray hybridization, microarray data analysis, gene ontology classification, and analysis of overrepresented biological themes, as well as on Q-PCR data analysis and used primer pair sequences is described in the supplementary section. Microarrays complied with the Minimum Information for Microarray Experiments (MIAME, E-MEXP-835 and E-MEXP-839).

Supplementary methods

Animals

Since $Xpa^{-/-}$, $Xpc^{-/-}$ and $Csb^{m/m}$ mice are fertile, $Csb^{m/m}/Xpa^{-/-}$, $Csb^{m/m}/Xpc^{-/-}$ and $Xpa^{-/-}/Xpc^{-/-}$ mice were obtained from crossings between homozygous/heterozygous double mutant animals (e.g. $Csb^{m/m}/Xpa^{+/+}$ x $Csb^{+/m}/Xpa^{-/-}$) to increase the expected proportion of double-mutant mice from 1:16 to 1:4. $Csb^{m/m}/Xpa^{-/-}/p53^{-/-}$ triple-mutant mice were obtained in a similar way after the Xpa and Csb mutant alleles had first been crossed into a $p53$ -deficient background. Mice were genotyped by PCR using a three-primer mix that amplifies both the wt and targeted

allele in a single reaction (see supplementary section). Animals are housed at the Animal Resource Center (Erasmus University Medical Center) and the National Institute of Public Health and the Environment (RIVM), which operate in compliance with the “Animal Welfare Act” of the Dutch government, using the “Guide for the Care and Use of Laboratory Animals” as its standard. As required by Dutch law, formal permission to generate and use genetically modified animals was obtained from the responsible local and national authorities. All animal studies were approved by an independent Animal Ethical Committee (Dutch equivalent of the IACUC).

Exposure to Ionizing Irradiation

For the ionizing irradiation study, 19-day old *Csb^{m/m}/Xpa^{-/-}* and littermate control animals (n=4-6/genotype) were exposed with 10Gy. Animals were sacrificed 20 hours after exposure and eyes were processed for further analysis. For the isolation of the eyes, animals were anaesthetized by CO₂ inhalation, followed by cervical dislocation. Eyes were marked on the nasal side with Alcian blue (5% Alcian blue in 96% ethanol), subsequently enucleated and fixed in 4 % paraformaldehyde in 0.1 M phosphate buffer. Paraffinized sections of 5 µm thickness were subjected to TUNEL staining (see methods), eyes were fixed in 4 % paraformaldehyde in 0.1 M phosphate buffer and embedded in paraffin.

Macroscopic Examination / Blood Parameters

Newborn *Csb^{m/m}/Xpa^{-/-}* mice and their littermates were observed and weighed daily between 11.00 and 13.00 hours. Animals were euthanized at defined time points (as indicated in the text) or when displaying evident worsening of health condition (indicative for imminent death). Internal organs were isolated and either fixed in 10% phosphate-buffered formalin and paraffin-embedded (histopathological analysis) or snap-frozen in liquid N₂ (for transcription profiling by microarray analysis or quantitative PCR). In some cases animals were given an intra-peritoneal injection with bromo-deoxy-uridine (BrdU; 50 µg/gram bodyweight) 45 min. prior to euthanasia in order to measure cell proliferation.

Immunohistochemistry

Immunohistochemical procedures: Paraffin sections (5 µm) were dewaxed and rehydrated, followed by an antigen retrieval step, comprising 1 x 7 minute and 2 x 3 minute incubations of tissue sections with a 0.01M sodium citrate buffer in a 800 Watt microwave. Sections were washed in phosphate buffered saline (PBS) for 2 minutes. Endogenous peroxidase activity was blocked by incubating the sections for 30 minutes in PBS, containing 30% H₂O₂ and 12.5% sodium azide. Sections were washed in PBS (1 x 2 minutes) and PBS, containing 0.5% milk powder, and 0.15% glycine (PBS+ buffer, 2 x 2 minutes).

Immunohistochemical staining was performed by incubating sections with primary antibodies against PCNA (PC10, Abcam, dilution 1:1000) or BrdU (Bu20a, DAKO, dilution 1:100) in

PBS+ (16 hr; 4 °C). In case of BrdU, sections were first covered with 0.1M HCl for 60 minutes at 37 °C and rinsed with PBS, prior to incubation with the primary antibody. Next, sections were washed in PBS+ (3 x 5 minutes) and incubated for 1 hour at room temperature with rat-anti-mouse Immunoglobulins antibody (1:1000) coupled to horseradish peroxidase (DAKO). After sections were washed in PBS+ (3 X 5 minutes) and PBS 1 x 2 minutes), color was developed for 8 minutes in 3, 3'-diaminobenzidine solution (DAKO Liquid DAB substrate-chromogen system), all according to the instructions of the manufacturer. Sections were counterstained in haematoxylin before dehydration and mounting. All histology images were acquired at 40x objective magnification on an Olympus BX40 microscope (London, United Kingdom), equipped with a CCD camera.

Citrate Synthase Enzyme Activity

Frozen livers were transferred into ice-cold buffer (SHE) consisting of 250 mM sucrose, 10 mM HEPES, pH 7.4, and minced. Fresh SHE was added and homogenized by 12 passes in a tight-fitting glass/Teflon power-driven Potter-Elvehjem homogenizer. Citrate synthase activity of the homogenate was measured by monitoring the CoA-coupled conversion of Ellman's reagent into TNB at 412 nm at 37°C in the presence of 0.005% (v/v) Lubrol-WX to solubilize the mitochondrial inner membrane and expressed in mU as nmol 5-thio-2-nitrobenzoate (TNB)/min per mg protein. Protein concentrations were determined by the Bio-Rad DC protein assay (Bio-Rad Laboratories, Inc., Veenendaal, the Netherlands) with BSA as a standard.

Microarray Analysis

Standard procedures were used to obtain total RNA (Qiagen) from the liver of wt, $Xpa^{-/-}$, $Csb^{m/m}$, and $Csb^{m/m}/Xpa^{-/-}$ mice (n=4) at postnatal day 15 and from the liver of 8-, 16-, 96- and 130-week old mice (n=4). Synthesis of double stranded cDNA and biotin labeled cRNA was performed according to the instructions of the manufacturer (Affymetrix, USA). Fragmented cRNA preparations were hybridized to full mouse genome oligonucleotide arrays (Affymetrix, mouse expression 430 V2.0 arrays), using Affymetrix hybridization Oven 640 (Affymetrix, USA), washed, and subsequently scanned on a GeneChip Scanner 3000 (Affymetrix, USA). Initial data extraction and normalization within each array was performed by means of the GCOS software (Affymetrix). By implementing the R statistical package that is based on an open-sourced language, data intensities were log transformed and normalized within and/or between groups of arrays by means of the quantile normalization method. For all 15-day old livers, normalization was performed within and between groups of mice based on the assumption that most genes do not change between the various genotypes ($Csb^{m/m}$, $Xpa^{-/-}$, $Csb^{m/m}/Xpa^{-/-}$ and wt). We also took into account, however, that this assumption may not be true for expression data derived from very distinct groups of mice (e.g. 130-week old compared to 8-week old mice). In those cases, expression data were normalized within age groups. This approach was shown to minimize the variance within each group of mice, thereby increasing

the statistical power between groups of mice. The two normalization approaches used in this study (i.e. within and between groups or only within groups) did not affect the Spearman's rank correlation measures (see below) on the categorical data. Based on the quality report files generated by the manufacturer (Affymetrix, USA), the threshold background noise was set at 40. For each probe set, signals were considered to be valid when they were marked as "Present" and exhibit a signal higher than 40 in at least one microarray experiment. All probe sets with a signal below 40 were set to be equal to 40. Where appropriate, two-tail, pair wise analysis or two-way analysis of variance was employed by means of the Spotfire Decision Site software package 7.2 v10.0 (Spotfire Inc., MA, USA) to extract the statistically significant data from each of the four individual microarrays obtained for each genotype (wt, *Xpa*^{-/-}, *Csb*^{m/m}, and *Csb*^{m/m}/*Xpa*^{-/-} livers) as well as from the four microarrays in each of the three groups of naturally aged mice (16-, 96- and 130-week old mice, n=4) as compared to 8-week old mice. The criteria for significance were set at $p \leq 0.010$ and a $\geq \pm 1.2$ -fold change with the exception of glycogenin 1 where after Q-PCR the difference in expression (1.26-fold up regulation) was considered to be significant despite the slightly deviant p-value of 0.012 (the cut-off was set at 0.010). All correlations were calculated by Spearman's rank correlation coefficient, a non-parametric correlation method and were based on categorical values derived from all significant probe sets (see above). For all correlations, significance was set at $p \leq 0.001$.

Gene Ontology Classification and Overrepresentation of Biological Themes

All significant gene entries were subjected to GO classification (<http://www.geneontology.org>). Significant over-representation of GO-classified biological processes was assessed by comparing the number of pertinent genes in a given biological process to the total number of the relevant genes printed on the array for that particular biological process (Fisher exact test, $p \leq 0.01$, False discovery rate (FDR) ≤ 0.1) using the publicly accessible software Ease (Hosack et al. 2003).

Quantitative PCR Evaluation

Total RNA was isolated from liver, heart, kidney and spleen of wt, *Xpa*^{-/-}, *Csb*^{m/m}, *Csb*^{m/m}/*Xpa*^{-/-} mice at postnatal day 15 using a Total RNA isolation kit (Qiagen) as described by the manufacturer. Quantitative PCR (Q-PCR) was performed with a DNA Engine Opticon device according to the instructions of the manufacturer (MJ Research). Primer pair designed to generate intron-spanning products of 180-210bp were as follows: *Sod1*: 5'-GGG ACA ATA CAC AAG GCT GT-3' and 5'-GCC AAT GAT GGA ATG CTC TC-3'; *Gsr1*: 5'- CCG CCT GAA CAC CAT CTA T -3' and 5'-TTC CCA TTG ACT TCC ACC G-3'; *Ghr*: 5'-ATT CAC CAA GTG TCG TTC CC-3' and 5'-TCC ATT CCT GGG TCC ATT CA-3'; *Igf1*: 5'-TGC TTG CTC ACC TTC ACC A-3' and 5'-CAA CAC TCA TCC ACA ATG CC-3'; *Prlr*: 5'-GCA TCT TTC CAC CAG TTC CG-3' and 5'-GCT CGT CCT CAT TGT CAT CC-3'; *Gstt2*: 5'-GCC CAA GTC CAC GAA TAC CT-3' and 5'-CTC TGT TCC GTT CCA CCT TC-3'; *Ephx1*: 5'-CAG CCA AAG AAG ATG AGA GCA-3' and 5'-AGC CAT AGT GGA AGC GAC T-3'; *Hmox1*: 5'-AAC

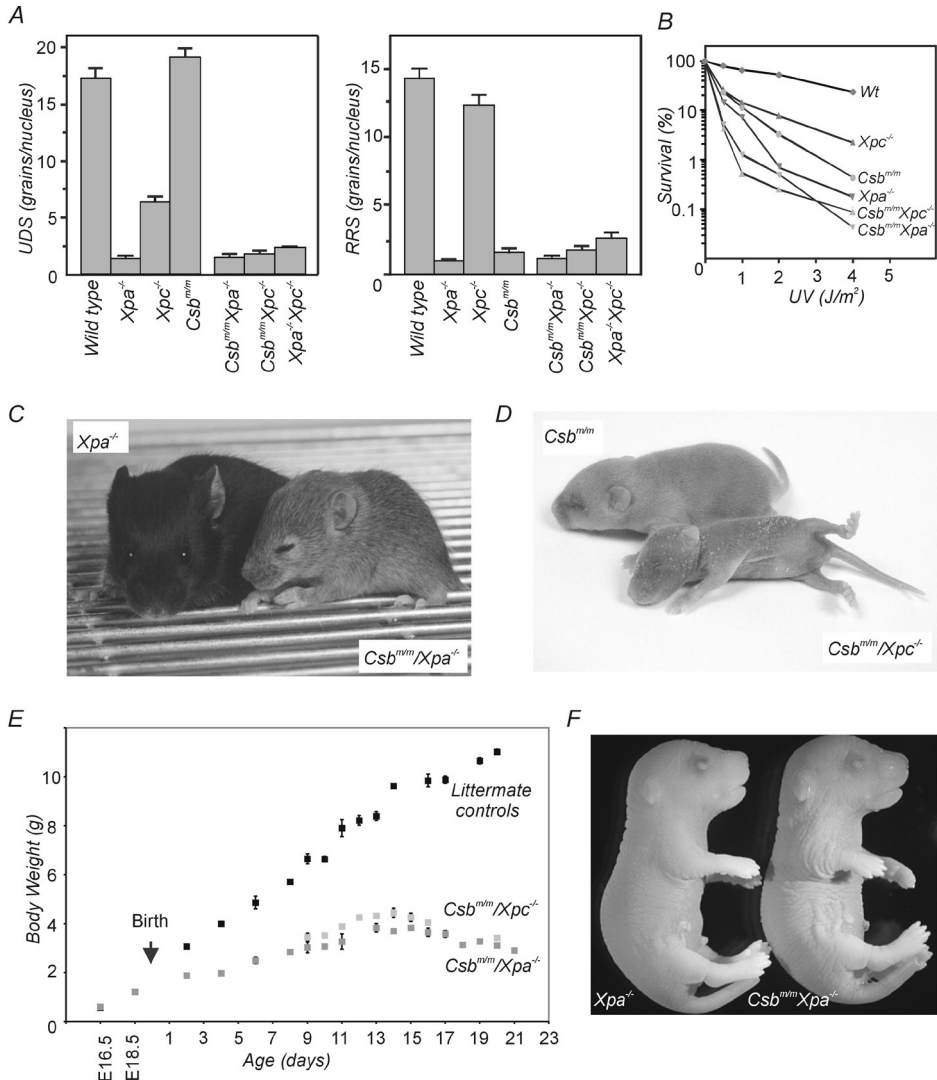


Figure 1: Growth retardation, cachexia, and premature death in $Csb^{m/m}/Xpa^{-/-}$ and $Csb^{m/m}/Xpc^{-/-}$ mice.

(A) UV repair characteristics of wild type, single mutant, and double mutant primary mouse embryonic fibroblasts (MEFs). UV-induced Unscheduled DNA Synthesis (UDS; left panel) and Recovery of RNA Synthesis (RRS, right panel) are indicative for GG-NER and TC-NER capacity, respectively. For a detailed explanation of the procedure, see Method section. Error bars indicate S.E.M. **(B)** Survival of primary MEFs exposed to increasing doses of UV-C light (254 nm), as determined using the with [3H]-thymidine incorporation assay. Error bars (in most cases smaller than symbols used) indicate S.E.M. **(C)** Photograph of a 14-day old $Csb^{m/m}/Xpa^{-/-}$ mouse with an $Xpa^{-/-}$ littermate (hybrid 1290la/C57BL/6J background). **(D)** Photograph of an 8-day old $Csb^{m/m}/Xpc^{-/-}$ mouse with a $Csb^{m/m}$ littermate (hybrid 1290la/C57BL/6J background). **(E)** Body weight curve of $Csb^{m/m}/Xpa^{-/-}$ and $Csb^{m/m}/Xpc^{-/-}$ mice ($n=7$) compared to those defective in a single NER gene ($n=7$) all in a hybrid 1290la/C57BL/6J background. The arrow indicates birth. Error bars (in most cases smaller than symbols used) indicate S.E.M. **(F)** Photographs of day 18.5 $Csb^{m/m}/Xpa^{-/-}$ and $Xpa^{-/-}$ embryos (C57BL/6J).

ACT CTG GAG ATG ACA CCT-3' and 5'-TGT GAG GGA CTC TGG TCT TTG-3'; *ApoA4*: 5'-CAC CGT TTC TTC TGA CTC CG-3' and 5'-AAT CCC ACA CCA CAT TGG C-3'; *Igfbp3*: 5'-GTG ACC GAT TCC AAG TTC CA-3' and 5'-TGT CCT CCA TTT CTC TGC GG-3'; *Dio1*: 5'-CCC TGG TGT TGA ACT TTG GC-3' and 5'-TGA GGA AAT CCG CTG TGG A-3'. The generation of specific PCR products was confirmed by melting curve analysis (which measures product specificity by the decrease in fluorescence signal when the PCR product is denatured) and gel electrophoresis (using Roche Agarose MS for analyzing small PCR products). Each primer pair was tested with a logarithmic dilution of a cDNA mix to generate a linear standard curve (crossing point (CP) plotted versus log of template concentration), which was used to calculate the primer pair efficiency ($E = 10^{(-1/\text{slope})}$). Hypoxanthine guanine phosphoribosyltransferase1 (*Hprt-1*) mRNA was used as an external standard. For data analysis, the second derivative maximum method was applied: $(E_{\text{1gene of interest}}^{\Delta \text{CP (cDNA of wt mice - cDNA of } Xpa^{-/-} \text{ or } Csbm/m \text{ or } Csbm/m/Xpa^{-/-}) \text{ gene of interest}}) / (E_{\text{hprt-1}}^{\Delta \text{CP (cDNA wt mice- cDNA of } Xpa^{-/-} \text{ or } Csbm/m \text{ or } Csbm/m/Xpa^{-/-}) \text{ hprt-1}})$. All Q-PCR experiments were repeated at least three times. In case of the DEHP experiment, we also used the glyceraldehyde-3-phosphate dehydrogenase as an additional housekeeping gene. P values (*) report the one-tail t-test probability that a gene has the same direction in the expression with that shown for the 15-day old *Csb^{m/m}/Xpa^{-/-}* mouse liver as compared to corresponding littermate controls. In addition, we also calculated the probability that all genes examined by Q-PCR demonstrate the same direction in the expression with those previously shown in the liver of *Csb^{m/m}/Xpa^{-/-}* mice by microarrays. Assuming these are independent events, the probability of each gene being up- or down regulated is 0.5 (1/2) whereas the probability of all independent events (13 genes examined) occurring in sequence is 0.00012 (0.5¹³).

Results

Attenuated Growth and Perinatal Death in *Csb^{m/m}/Xpa^{-/-}* and *Csb^{m/m}/Xpc^{-/-}* Mice

TCR-defective *Csb^{m/m}* mutant mice [16] were intercrossed with GG-NER-defective *Xpc^{-/-}* [21] and GG/TC-NER-defective *Xpa^{-/-}* [22] animals to investigate whether an increase in the endogenous burden of unrepaired DNA damage, as provoked by inactivation of GG-NER, enhances the phenotype, including progeroid features. Analysis of UV-induced repair synthesis and RNA synthesis recovery (indicative for GG-NER and TC-NER capacity, respectively) confirmed complete inactivation of NER in *Csb^{m/m}/Xpa^{-/-}* and *Csb^{m/m}/Xpc^{-/-}* animals (Fig. 1A). As expected on the basis of previous work, *Xpa^{-/-}* cells display highest UV-sensitivity, whereas *Xpc^{-/-}* and *Csb^{m/m}* cells show intermediate sensitivities (*Xpa^{-/-}* > *Csb^{m/m}* > *Xpc^{-/-}* > wt; see Fig. 1B). Interestingly, inactivation of GG-NER in *Csb^{m/m}* MEFs (as in *Csb^{m/m}/Xpa^{-/-}* and *Csb^{m/m}/Xpc^{-/-}* cells) renders cells more UV-sensitive than already completely NER-deficient *Xpa^{-/-}* MEFs. We attribute this enhanced sensitivity to the absence of CSB-mediated TCR of UV-induced lesions that do not form a substrate for NER. Thus the repair defect in the double mutant appears to be more

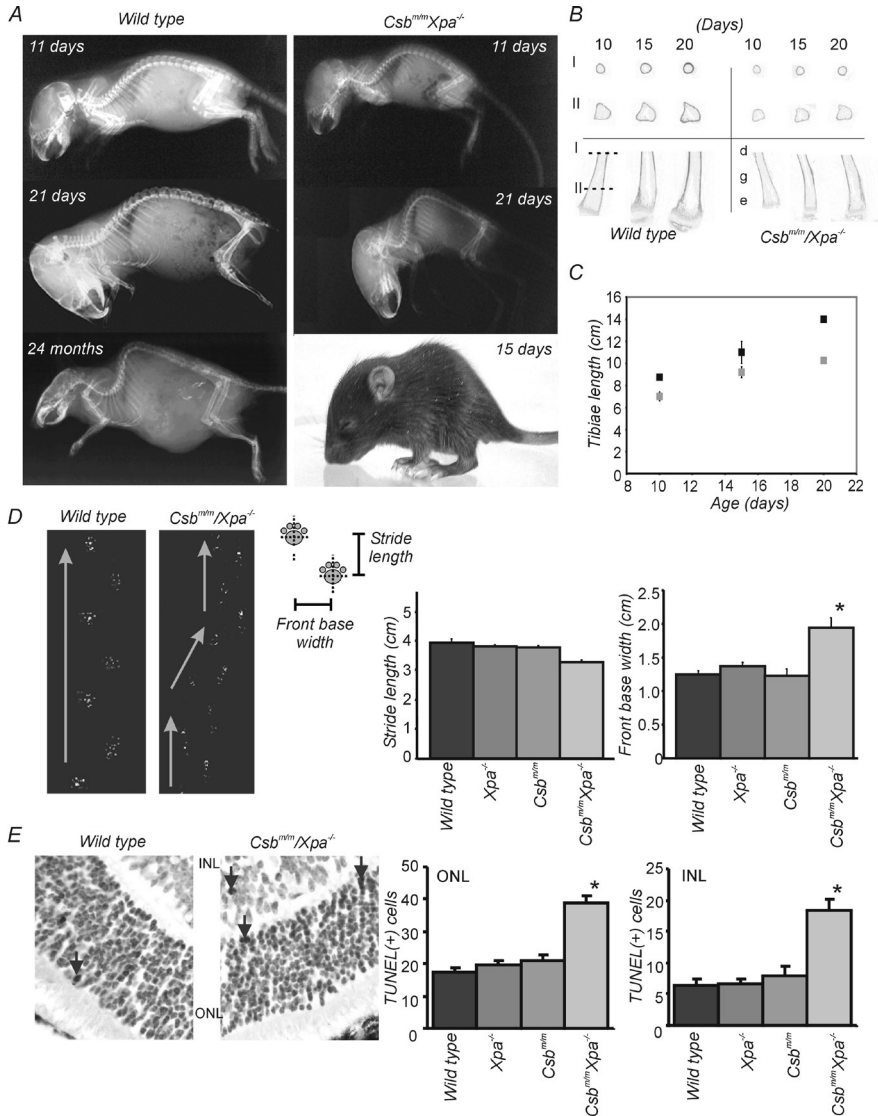


Figure 2: Skeletal and neurological abnormalities in $Csb^{m/m}/Xpa^{-/-}$ mice.

(A) Radiographs of wt and $Csb^{m/m}/Xpa^{-/-}$ mice (age as indicated) and photograph of a 15-day old $Csb^{m/m}/Xpa^{-/-}$ mouse (C57BL/6). **(B)** 2D images of micro-CT scans of tibiae taken from $Csb^{m/m}/Xpa^{-/-}$ animals and wt littermate controls (age indicated in the figure). Horizontal sections are shown of the upper and lower part of the tibiae e = epiphysis, g = growth plate and d = diaphysis. I = the section through the smaller part of the diaphysis, II = section through the broader part of the diaphysis. **(C)** Growth of tibiae, taken from $Csb^{m/m}/Xpa^{-/-}$ animals (light squares) and wt littermate controls (dark squares). **(D)** Representative footprint patterns of 19-day old wt and $Csb^{m/m}/Xpa^{-/-}$ mice. Arrows indicate the trajectory of each mouse. Stride length and front base width measurements on 15-day old wt, $Xpa^{-/-}$, $Csb^{m/m}$ and $Csb^{m/m}/Xpa^{-/-}$ mice. The significantly (asterisk; $p < 0.001$) greater base width in the double mutant mouse indicates ataxia. **(E)** Representative pictures of a TUNEL staining in the retina of wt and $Csb^{m/m}/Xpa^{-/-}$ mice and quantification of the number of TUNEL positive cells. Arrows indicate TUNEL positive cells in the outer nuclear layer (ONL) and inner nuclear layer (INL). Note the significantly higher number of TUNEL-positive cells in both the ONL and the INL in the retina of $Csb^{m/m}/Xpa^{-/-}$ compared to wt mice (asterisk; $p < 0.05$).

severe than that of the single mutants. We could not detect a similar increased sensitivity to ionizing radiation in double mutant cells above that of *Csb^{m/m}* cells ([12], data not shown), supporting the notion that MEFs in culture are already under high oxygen stress [23,24].

As evident from their overall appearance and weight (Fig. 1C to E), *Csb^{m/m}/Xpa^{-/-}* and *Csb^{m/m}/Xpc^{-/-}* pups (hybrid C57BL/6Jx129ola genetic background) displayed a strikingly attenuated growth, resulting in pronounced dwarfism. Whereas the number of double mutant pups was ~3-fold below that expected for Mendelian inheritance (Supplementary Table S1), E18.5 *Csb^{m/m}/Xpa^{-/-}* and *Csb^{m/m}/Xpc^{-/-}* embryos were present at Mendelian frequency, pointing to considerable lethality during or shortly after birth. Importantly, double mutant embryos were morpho- and histologically indistinguishable from wt and single mutant embryos (Fig. 1F, data not shown), indicating that the growth defect was postnatal and did not reflect impaired embryonic development *per se*. In the third week of life, however, *Csb^{m/m}/Xpa^{-/-}* and *Csb^{m/m}/Xpc^{-/-}* pups developed progressive cachexia (evident from the weight loss after day 15; see Fig. 1E), ultimately resulting in death before postnatal day 22. Neither removal of wt or single mutant pups from the litter (to reduce competition for breast milk), nor moistened food pellets (to facilitate intake of solids), improved the physical condition or the lifespan of *Csb^{m/m}/Xpa^{-/-}* and *Csb^{m/m}/Xpc^{-/-}* pups. Necropsy revealed milk or solid food in the stomach, indicating that insufficient access to supplied nutrition was not the underlying cause of growth retardation, weight loss, and early death. Importantly, progressive growth retardation, cachexia and short life expectation (~12.5 years) are also observed in CS patients [13]. Combined inactivation of *Xpa* and *Xpc* rendered mice without any overt phenotype (data not shown), leading us to conclude that the dramatic phenotype of *Csb^{m/m}/Xpa^{-/-}* and *Csb^{m/m}/Xpc^{-/-}* pups results from a combined GG-NER/TC-NER/TCR defect.

Growth and Neurological Abnormalities in *Csb^{m/m}/Xpa^{-/-}* Mice

Further analysis of the *Csb^{m/m}/Xpa^{-/-}* phenotype, performed in an isogenic C57BL/6J background, revealed a near normal size of the skull at day 11 and 21 (autoradiographs shown in Fig. 2A), implying that the (postnatal) growth defect is restricted to the trunk, and to a lesser extent, the extremities. All 21-day old double mutant animals showed kyphosis (abnormal curvature of the spinal column, Fig. 2A, middle left and bottom right), which was also observed in younger *Csb^{m/m}/Xpa^{-/-}* pups, indicating that it is not determined by terminal illness. The normal appearance of the spine in 11-day old double mutant pups excluded a prenatal developmental defect and further pointed to an extremely accelerated onset of kyphosis, a feature observed in naturally aged (2-year old) C57BL/6J mice (see Fig. 2A, bottom left panel). Two-dimensional images of proximal end-to-mid-diaphysis micro-computed tomography (micro-CT) scans of fixed tibiae from 10-, 15- and 20-day old wt and *Csb^{m/m}/Xpa^{-/-}* mice revealed retarded, yet steady longitudinal as well as radial (perimeter) growth, along with a thinner bone cortex and a less developed growth plate (Fig. 2B). In line with this observation, we observed a reduction in tibia length (Fig. 2C). Notably, while *Csb^{m/m}/*

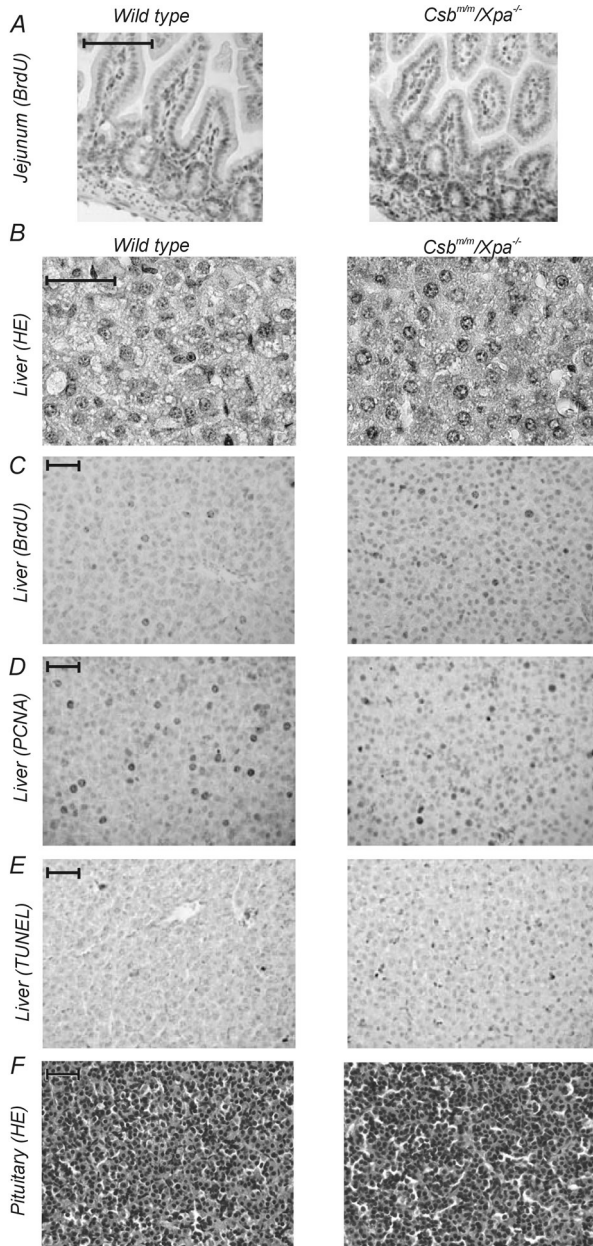


Figure 3: Histological examination of *Csbtm/Xpa^{-/-}* tissues.

(A) BrdU staining of the jejunum of *Csbtm/Xpa^{-/-}* and littermate control mice, showing normal proliferative capacity of the intestine in the double mutant mouse. (B-E) Histological examination of liver sections of 15-day old *Csbtm/Xpa^{-/-}* and littermate control mice, stained with HE (B), immunostained for the proliferation markers (incorporated) BrdU (C) and PCNA protein, or TUNEL-stained for the presence of apoptotic cells (E). Quantification of the number of proliferative or apoptotic cells did not reveal significant differences between *Csbtm/Xpa^{-/-}* and wild type littermate mice. (F) HE staining of the pituitary of *Csbtm/Xpa^{-/-}* and littermate control mice.

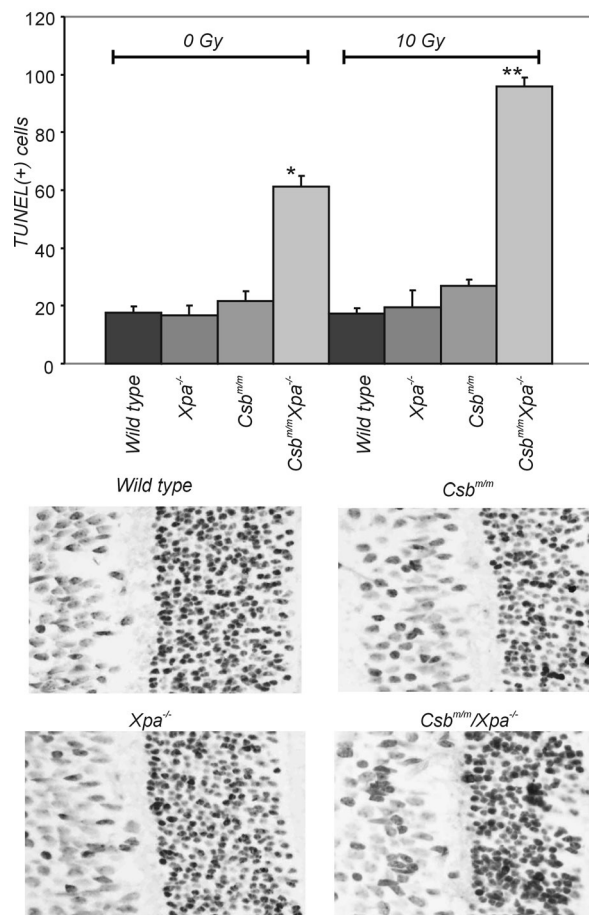


Figure 4: Enhanced sensitivity of *Csb^{m/m}/Xpa^{-/-}* retinal photoreceptor cells to genotoxic insults.

Representative pictures of TUNEL stained retinas of 19-day old wt, *Csb^{m/m}*, *Xpa^{-/-}* and *Csb^{m/m}/Xpa^{-/-}* mice (right panel), 20 hours after exposure of animals to 10 Gy of ionizing radiation, and quantification of the number of TUNEL positive cells in the ONL (left panel). Note the significantly higher number of TUNEL-positive cells in the retina of *Csb^{m/m}/Xpa^{-/-}* mice, as compared to wt and single mutant littermate controls ($p < 0.05$). Asterisks: * indicates statistically significant differences between unirradiated *Csb^{m/m}/Xpa^{-/-}* and littermate control mice ($p < 0.05$), ** indicates statistically significant differences between unirradiated and irradiated *Csb^{m/m}/Xpa^{-/-}* mice ($p < 0.05$).

Xpa^{-/-} pups lose weight in the third week of life, bone growth proceeds, resulting in relatively large extremities, a representative feature of CS and TTD [13].

Motor coordination problems, manifesting as tremors and abnormal posture of the hind limbs (flexion rather than extension in tail suspension test), became evident around day 10 in *Csb^{m/m}/Xpa^{-/-}* mice (data not shown). Foot print analysis revealed a disturbed gait from day 15 onwards. While wt and single mutant animals maintained a straight path with regular alternating strides, *Csb^{m/m}/Xpa^{-/-}* mice demonstrated a non-uniform alternating left-right step

pattern and unevenly spaced shorter strides (Fig. 2D). Despite their runted size, the front base width of *Csb^{m/m}/Xpa^{-/-}* animals was significantly greater than that of wt and single mutant littermates, which likely illustrates an attempt to maintain balance (Fig. 2D). These data are consistent with the profound early postnatal ataxia and abnormal cerebellar development in *Csb^{m/m}/Xpa^{-/-}* mice [25], and the progressive neurodegeneration observed in CS patients [26].

We next examined the retina of 15-day old *Csb^{m/m}/Xpa^{-/-}* pups for the presence of apoptotic cells as retinal degeneration is a prominent neurological feature of CS patients [27] and adult CS mice (Gorgels et al, pending revision). At this age, cell loss occurs as part of the normal development of the retina. Yet, as shown by TUNEL (Fig. 2E) and caspase-3 staining (data not shown), the number of apoptotic cells in the outer (ONL) and inner nuclear (INL) layers of the retina of *Csb^{m/m}/Xpa^{-/-}* pups was significantly increased (ANOVA, S-N-K posthoc test, $p < 0.05$), as compared to wt and single mutant littermates (Fig. 2E). Thus, the *Xpa* defect enhanced the apoptotic sensitivity of photoreceptor cells in *Csb^{m/m}* mice, thereby pointing to DNA damage as a trigger for age-related retinal degeneration. As 15-day old *Csb^{m/m}* mice still have wt levels of apoptotic cells, spontaneous photoreceptor loss in the *Csb^{m/m}* mouse initiates in the second/third month of life.

With the exception of substantial loss of abdominal fat, visual inspection and histological analysis of most internal organs of 15-day old *Csb^{m/m}/Xpa^{-/-}* mice did not reveal any obvious pathological abnormalities (data not shown). As we did not find any sign of infections, necrosis, or abnormal cellular proliferation (as determined by BrdU staining) in the gastrointestinal tract of 15- and 21-day old *Csb^{m/m}/Xpa^{-/-}* animals, intestinal malfunction is an unlikely cause of the growth defect (Fig. 3A). In addition, the liver has a normal histological appearance (Fig. 3B), while neither BrdU (Fig. 3C), PCNA (Fig. 3D), and Ki67 staining (data not shown), nor TUNEL (Fig. 3E) and caspase 3 staining (data not shown) revealed any significant difference between *Csb^{m/m}/Xpa^{-/-}* and wt livers. This finding indicates that aberrant cell proliferation or apoptosis in the liver does not likely contribute to the *Csb^{m/m}/Xpa^{-/-}* phenotype. Moreover, inactivation of the *p53* tumor suppressor gene failed to rescue the mutant phenotype, as *Csb^{m/m}/Xpa^{-/-}/p53^{-/-}* triple mutant pups appeared indistinguishable from *Csb^{m/m}/Xpa^{-/-}* pups (data not shown). Thus, the precise etiology of the overall physical deterioration and the cause of death of *Csb^{m/m}/Xpa^{-/-}* mice remain unknown.

Enhanced Ionizing Radiation Sensitivity of the *Csb^{m/m}/Xpa^{-/-}* Mouse Retina

The spontaneous, age-related and ionizing radiation (IR)-induced loss of post-mitotic photoreceptor cells in *Csb^{m/m}* mice, underscores the relevance of DNA repair in the removal of (oxidative) DNA damage for the long-term survival of terminally differentiated cells in the retina (Gorgels et al, pending revision). To test whether *Csb^{m/m}/Xpa^{-/-}* animals are more sensitive to genotoxic insults than single mutant *Csb^{m/m}* and *Xpa^{-/-}* animals, we next examined if the additional *Xpa* defect further enhances the IR sensitivity of the *Csb^{m/m}* retina. To this end, we exposed 19-day old *Csb^{m/m}/Xpa^{-/-}* pups and wild type and single mutant littermates to γ -rays

Table 1

Code	Title	Symbol	<i>Csb^{mm} Xpa^{-/-}</i>		<i>Xpa^{-/-}</i>		<i>Csb^{mm}</i>	
			FC	P-value	FC	P-value	FC	P-value
The IGF-1/GH growth axis								
1448556_at	prolactin receptor	Prlr	-2.03	0.0000	-1.3	0.1	-1.1	0.66
1419519_at	insulin-like growth factor 1	Igf1	-2.13	0.0000	-1.1	0.16	-1.13	0.19
1421991_a_at	IGF-binding protein 4	Igfbp4	-1.74	0.0000	-1.1	0.82	-1.16	0.39
1458268_s_at	IGF-binding protein 3	Igfbp3	-1.44	0.0010	-1.1	0.25	1.06	0.59
1422826_at	IGF-binding protein, acid labile subunit	Igfbals	-2.36	0.0000	1.06	0.53	1.13	0.26
1417962_s_at	growth hormone receptor	Ghr	-1.53	0.0000	1.03	0.15	1.1	0.05
1425458_a_at	growth factor receptor bound protein 10	Grb10	1.84	0.0000	1.11	0.59	1.24	0.19
1427777_x_at	fibroblast growth factor receptor 4	Fgfr4	-1.32	0.0090	-1.1	0.71	-1.19	0.11
1421841_at	fibroblast growth factor receptor 3	Fgfr3	-1.43	0.0010	-1.3	0.03	-1.12	0.87
1450869_at	fibroblast growth factor 1	Fgfl	-1.38	0.0030	-1.2	0.09	-1.01	0.84
1435663_at	estrogen receptor 1 (alpha)	Esr1	-1.91	0.0010	-1.1	0.32	-1.31	0.12
1417991_at	deiodinase, iodothyronine, type I	Dio1	-2.12	0.0000	1	0.28	-1.04	0.28
Carbohydrate metabolism								
1423644_at	aconitase 1	Aco1	-1.26	0.0020	1.05	0.5	-1	0.96
1422577_at	citrate synthase	Cs	-1.28	0.0060	1.16	0.2	-1.03	0.2
1419146_a_at	glucokinase	Gek	-6.59	0.0040	1.16	0.28	-1.01	0.66
1424815_at	glycogen synthase 2	Gys2	1.78	0.0000	-1	0.22	-1.01	0.3
1459522_s_at	glycogenin 1	Gygl	1.26	0.0140	1.05	0.153	1.03	0.364
1417741_at	liver glycogen phosphorylase	Pygl	-1.42	0.0000	1.02	0.5	1.06	0.03
Steroid metabolism and biosynthesis								
1417871_at	hydroxysteroid (17-beta) dehydrogenase 7	Hsd17b7	-1.5	0.0000	-1.3	0.14	-1.32	0.13
1449038_at	hydroxysteroid 11-beta dehydrogenase 1	Hsd11b1	-1.32	0.0010	1.1	0.34	1.01	0.71
1460192_at	oxysterol binding protein-like 1A	Osbpl1a	-1.38	0.0000	-1.1	0.5	-1.08	0.52
1427345_a_at	sulfotransferase family 1A, member 1	Sult1a1	-1.29	0.0020	-1.1	0.69	-1.05	0.59
1419528_at	sulfotransferase, hydroxysteroid preferring 2	Sth2	-1.61	0.0000	-1.1	0.92	-1.2	0.26
Cytochrome (Cyt) P450, NADH- and NADPH-dependent Oxidative metabolism								
1418821_at	Cyt. P450, family 2, subfam. a, polyp. 12	Cyp2a12	-1.51	0.0000	1.06	0.21	-1.06	0.33
1422257_s_at	Cyt. P450, family 2, subfam. b, polyp. 10	Cyp2b10	-2.81	0.0010	-1.4	0.75	-1.39	0.75
1449479_at	Cyt. P450, family 2, subfam. b, polyp. 13	Cyp2b13	-2.24	0.0020	-1.2	0.77	-1.27	0.98
1425645_s_at	Cyt. P450, family 2, subfam. b, polyp. 20	Cyp2b20	-2.94	0.0010	-1.3	0.95	-1.42	0.36
1419590_at	Cyt. P450, family 2, subfam. b, polyp. 9	Cyp2b9	-1.55	0.0000	-1.1	0.78	-1.04	0.49
1417651_at	Cyt. P450, family 2, subfam. c, polyp. 29	Cyp2c29	-1.59	0.0040	-1.4	0.09	-1.41	0.09
1440327_at	Cyt. P450, family 2, subfam. c, polyp. 70	Cyp2c70	-2.58	0.0010	-1.2	0.15	-1.23	0.58
1448792_a_at	Cyt. P450, family 2, subfam. f, polyp. 2	Cyp2f2	-2.36	0.0010	1.76	0.05	1.3	0.43
1417532_at	Cyt. P450, family 2, subfam. j, polyp. 5	Cyp2j5	-3.08	0.0000	-1.5	0.1	-1.31	0.36
1418767_at	Cyt. P450, family 4, subfam. f, polyp. 13	Cyp4f13	-1.67	0.0080	-1.1	0.46	-1.4	0.36
1419559_at	Cyt. P450, family 4, subfam. f, polyp. 14	Cyp4f14	-3.58	0.0000	1.57	0.06	-1	0.92
1417070_at	Cyt. P450, family 4, subfam. v, polyp. 3	Cyp4v3	-1.41	0.0010	1.04	0.4	-1.09	0.81
1422100_at	Cyt. P450, family 7, subfam. a, polyp. 1	Cyp7a1	-2.36	0.0060	1.14	0.86	-1.39	0.24
1417429_at	flavin containing monooxygenase 1	Fmo1	-1.38	0.0000	1.04	0.23	1	0.57
1422904_at	flavin containing monooxygenase 2	Fmo2	-4.51	0.0080	-2.2	0.4	-2.05	0.49
1449525_at	flavin containing monooxygenase 3	Fmo3	-14.19	0.0040	-2	0.84	-2.34	0.59
1423908_at	NADH dehydrogenase (ubiquinone) Fe-S protein 8	Ndufs8	-1.23	0.0020	1.02	0.87	-1.04	0.13
Antioxidant and detoxification response								
1422438_at	epoxide hydrolase 1, microsomal	Ephx1	2.1	0.0000	1.14	0.3	-1.12	0.02
1421816_at	glutathione reductase 1	Gsr	1.2	0.0090	1.19	0.18	-1.01	0.95
1421041_s_at	glutathione S-transferase, alpha 2 (Yc2)	Gsta2	1.9	0.0030	-1.2	0.09	-1.59	0.51
1416842_at	glutathione S-transferase, mu 5	Gstm5	1.29	0.0000	1.02	0.82	-1.02	0.34
1449575_a_at	glutathione S-transferase, pi 2	Gstp2	1.4	0.0000	1.07	0.64	1.07	0.69
1417883_at	glutathione S-transferase, theta 2	Gstt2	2.76	0.0000	1.18	0.13	-1.3	0.05
1448239_at	heme oxygenase (decycling) 1	Hmox1	2.43	0.0000	-1.5	0.04	-1.17	0.12
1452592_at	microsomal glutathione S-transferase 2	Mgst2	2.89	0.0000	1.02	0.29	1.1	0.29
1448300_at	microsomal glutathione S-transferase 3	Mgst3	1.49	0.0010	1.29	0.04	1.02	0.1
1430979_a_at	peroxiredoxin 2	Prdx2	1.61	0.0010	1.75	0.01	1.34	0.26
1416292_at	peroxiredoxin 3	Prdx3	1.27	0.0100	1.24	0.19	1.09	0.18
1451124_at	superoxide dismutase 1, soluble	Sod1	1.22	0.0030	1.26	0.03	1.16	0.1
1415996_at	thioredoxin interacting protein	Txnip	2.11	0.0080	1.05	0.49	1.05	0.42
1440221_at	thioredoxin-like	Txnl	1.5	0.0020	1.26	0.58	1.17	0.83
Peroxisomal biogenesis								
1416679_at	ATP-binding cassette, sub-family D member 3	Abcd3	-1.29	0.0000	1.03	0.63	1.03	0.6
1449442_at	peroxisomal biogenesis factor 11a	Pex11a	-1.78	0.0100	-1.97	0.04	-1.6	0.37
1451213_at	peroxisomal biogenesis factor 11b	Pex11b	-1.24	0.0100	-1.03	0.82	-1.05	0.69
Fatty acid biosynthesis and elongation								
1455994_x_at	ELOVL1 long chain fatty acid elongation	Elov11	1.28	0.0010	1.24	0.03	1.22	0.68
1417403_at	ELOVL6, long chain fatty acid elongation	Elov16	1.37	0.0010	1.18	0.23	1.09	0.38
1415823_at	stearyl-Coenzyme A desaturase 2	Scd2	1.39	0.0010	1.29	0.15	1.23	0.45
1424119_at	protein kinase beta 1 non-catalytic subunit	Prkab1	1.44	0.0000	1.28	0.15	1.11	0.8
1418438_at	fatty acid binding protein 2, intestinal	Fabp2	1.4	0.0010	1.09	0.21	1.13	0.03
1416021_a_at	fatty acid binding protein 5, epidermal	Fabp5	1.63	0.0000	-1.2	0.17	1.14	0.57
1450779_at	fatty acid binding protein 7, brain	Fabp7	2.16	0.0000	1.52	0.21	1.66	0.05
1425875_a_at	leptin receptor	LepR	2.78	0.0000	-1.6	0.02	-1.3	0.07
1420715_a_at	peroxisome proliferator activated receptor gamma	Pparg	1.99	0.0000	1.53	0.01	1.11	0.73
1417900_a_at	very low density lipoprotein receptor	Vldlr	1.81	0.0010	1.01	0.86	-1.1	0.4

Supplementary Table S2

A. Frequency of viable $Csb^{m/m}Xpa^{-/-}$ mice $Csb^{m/m}Xpa^{+/-}$ x $Csb^{m/m}Xpa^{+/-}$

<i>Xpa</i>	<i>Csb</i>	number	expected (%)	observed (%)
+/+	m/m	20	25	26
+/-	m/m	45	50	60
-/-	m/m	11	25	14*
		76	100	100

*p<0.01

B. Frequency of viable $Csb^{m/m}Xpc^{-/-}$ mice $Csb^{+/-}Xpc^{-/-}$ x $Csb^{+/-}Xpc^{-/-}$

<i>Xpc</i>	<i>Csb</i>	number	expected (%)	observed (%)
-/-	+/+	14	25	23
-/-	+/-	41	50	69
-/-	m/m	5	25	8*
		60	100	100

*p<0.001

C. Parallels of human CS symptoms with the mild $Csb^{m/m}$ and severe $Csb^{m/m}Xpa^{-/-}$ mouse models

CS phenotype	$Csb^{m/m}$	$Csb^{m/m}Xpa^{-/-}$
UV sensitivity	+	++
cachexia	-	+
premature death	-	+
growth retardation	+	++
relatively long limbs	-	+
kyphosis	-	+
ataxia	-	+
dystonia	-	+
Purkinje cell loss	-	+
retinal degeneration	+	++

(10 Gy) and quantified the number of apoptotic cells in the by TUNEL staining 20 hours after exposure. As shown in Fig. 4, the number of apoptotic cells in the ONL of untreated (20-day old) $Csb^{m/m}/Xpa^{-/-}$ pups further increased, as compared to 15-day old double mutant animals (see Fig. 2E). While IR exposure did not increase the frequency of apoptotic photoreceptors in the ONL of wt and $Xpa^{-/-}$ animals, $Csb^{m/m}$ mice already show a tendency to increased photoreceptor loss, as characteristic for mature $Csb^{m/m}$ animals (Gorgels et al., pending decision). In contrast, the retina of IR-exposed $Csb^{m/m}/Xpa^{-/-}$ animals showed an almost two-fold increase

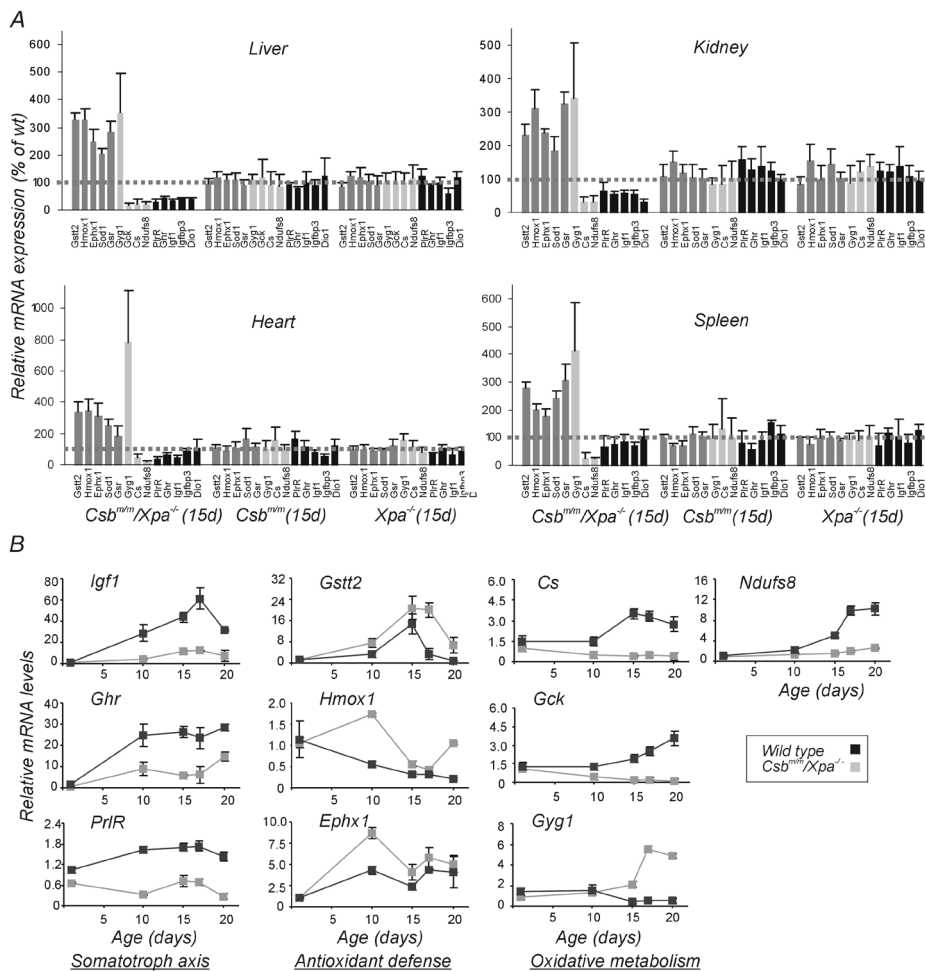
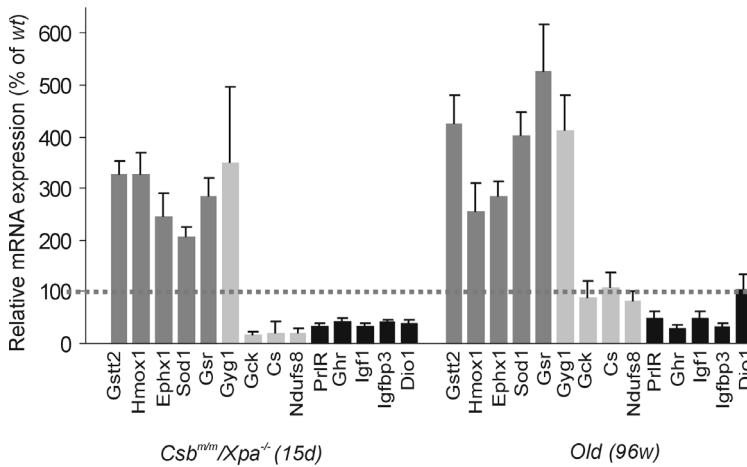


Figure 5: Expression levels of genes associated with the somatotroph axis, antioxidant defense, and metabolism in mutant and wt mouse liver and other organ at various ages.

(A) Q-PCR evaluation of mRNA levels of genes associated with antioxidant defense (dark gray bars), oxidative metabolism (light gray bars) and the GH/IGF1 axis (black bars) in the liver, kidney, heart and spleen of 15-day old *Csb^{tm/m}/Xpa^{-/-}*, *Csb^{tm/m}*, and *Xpa^{-/-}* pups. For each gene, expression levels in the mutant tissue are plotted relative to that of age-matched wt control tissues (dotted line). Error bars indicate S.E.M. between replicates ($n \geq 3$). **(B)** Relative mRNA expression levels (fold changes, relative to embryonic day 18) of genes involved in the GH/IGF1 growth axis, antioxidant defense, and oxidative metabolism in the liver of wt and *Csb^{tm/m}/Xpa^{-/-}* pups, plotted as a function of time. Error bars indicate S.E.M. between replicates ($n \geq 3$).

in the level of TUNEL-positive photoreceptor cells (Student's t-test $p=0.021$). Taken together, these findings not only further point to unrepaired DNA damage (likely originating from oxidative stress) as the underlying trigger for photoreceptor loss, but importantly, also show that inactivation of *Xpa* further enhances the sensitivity of *Csb^{tm/m}* mice to genotoxic stress.



Supplementary Figure 1

Q-PCR evaluation of mRNA levels of genes associated with the GH/IGF1 axis, antioxidant defense, and oxidative metabolism in 2-week old *Csb^{m/m}/Xpa^{-/-}* and 96-week old wt mice.

Analysis of the *Csb^{m/m}/Xpa^{-/-}* Mouse Liver Transcriptome

To investigate whether a disturbance in growth and metabolism could explain the pronounced accelerated organismal deterioration seen in *Csb^{m/m}/Xpa^{-/-}* mice, we evaluated the liver transcriptome of 15-day old wt, single and double mutant mice (n=4). At this age, the *Csb^{m/m}/Xpa^{-/-}* pups have not yet become cachectic. Two-tail, pair wise analysis of variance of Affymetrix full mouse genome arrays revealed 1865 genes with significantly changed expression patterns between wt and *Csb^{m/m}/Xpa^{-/-}* livers ($p \leq 0.01$, 1.2 fold change up- or down regulated, Supplementary Table S2 (not shown)), a number that significantly exceeds the 80 genes that are expected to occur by chance under these selection criteria. Among the set of 1865 genes, we identified those GO-classified biological processes with a significantly disproportionate number of responsive genes relative to those printed on microarrays (False detection rate ≤ 0.10). This unbiased approach revealed processes implicated in the derivation of energy from oxidation of organic compounds, homeostasis of energy reserves, cell growth and maintenance and the redox status of the cell.

Subsequent analysis of these processes led us to identify:

1. a profound attenuation of the somatotroph axis as evidenced by the consistent down-regulation of genes encoding main components of the GH/IGF1 axis (e.g. *IGF1*, *Igfbp3*, *Igfbp4*, *Igfals*, *Ghr*), as well as lactotroph (e.g. *Prlr*) and thyrotroph functions (e.g. *Dio1*) in *Csb^{m/m}/Xpa^{-/-}* livers, in addition to a decrease in the expression of several genes associated with a variety of mitogenic signals (e.g. *Esr1*, *Fgf1*, *Fgfr3*, *Fgfr4*, Table 1 and Supplementary Table S2).
2. an extensive suppression of catabolic metabolism in the *Csb^{m/m}/Xpa^{-/-}* liver, as evident from the significant down-regulation of key genes involved in glycolysis, tricarboxylic acid cycle

and oxidative phosphorylation pathways (Table 1 and Supplementary Table S2), coupled with a significant up-regulation of genes associated with glycogen synthesis (e.g. *Gyg1* and *Gys2* and down-regulation of glycogen phosphorylase, *Pygl*) suggesting that the *Csb^{m/m}/Xpa^{-/-}* liver stores glucose into glycogen, rather than burn it for energy derivation. These changes were further accompanied by the broad down-regulation of genes associated with electron transport and oxidative phosphorylation (e.g. several cytochrome P450 monooxygenases, the NADH dehydrogenase complex and the NADPH-dependent oxidative metabolism; Table 1 and Supplementary Table S2) and the significant down-regulation of several genes associated with peroxisomal biosynthesis (Table 1). Apparently, the complete catabolic metabolism is restrained in the *Csb^{m/m}/Xpa^{-/-}* liver.

3. a broad upregulation of genes associated with fatty acid synthesis and transport (several genes listed in Table 1 and Supplementary Table S2), the up-regulation of the receptor for the adipocyte hormone leptin (*Lepr*) and the central fat regulator peroxisome proliferator-activated receptor-gamma (*Pparγ*). Thus, similar to reserved glucose utilization and enhanced glycogen synthesis, *Csb^{m/m}/Xpa^{-/-}* mice attempt to store rather than burn fat.

4. an up-regulation of genes encoding key enzymatic and non-enzymatic low molecular mass scavengers and antioxidant defense enzymes (e.g. *Sod1*, *Prdx2* and *3*, *Txnip*, *Ephx1*, *Hmox1* and 5 components of the glutathione system; Table 1), suggesting that *Csb^{m/m}/Xpa^{-/-}* mice try to minimize the induction of (DNA) damage by counteracting ROS.

Importantly, none of these genes were identified as significantly differentially expressed in the livers of *Csb^{m/m}* or *Xpa^{-/-}* littermate controls (Table 1). Quantitative real-time PCR (Q-PCR) evaluation of the expression levels of key genes involved in the somatotroph axis, energy metabolism and antioxidant defense in the liver of *Csb^{m/m}/Xpa^{-/-}* mice, and wt, *Csb^{m/m}* and *Xpa^{-/-}* littermates, as well as further biochemical analysis (see below), confirmed the validity of the microarray data (Fig. 5A, upper left panel).

Postnatal Systemic Changes in Somatotroph Axis, Energy Metabolism, and Antioxidant Defense in *Csb^{m/m}/Xpa^{-/-}* Mice

Next, we analyzed whether the onset of aforementioned transcriptional changes paralleled the progressive postnatal growth attenuation, as well as the weight loss observed later. Consistent with the normal embryonic development, the expression levels of genes involved in the somatotroph axis (*Ghr*, *Igf1*, *Prlr*), antioxidant defense (*Gstt2*, *Hmox1*, *Ephx1*) and oxidative metabolism (*Gck*, *Gyg1*, *Cs*, *Ndufs8*) did not differ significantly between wt and *Csb^{m/m}/Xpa^{-/-}* livers at postnatal day 1 (Fig. 5B). In contrast, during the first two weeks of life, wt mice exhibited as expected a robust up-regulation in *Igf1*, *Ghr*, *Prlr* gene expression, a response that was virtually absent in *Csb^{m/m}/Xpa^{-/-}* animals (Fig. 5B, left panels) and well explains the severe growth retardation of double mutant pups after birth. Analysis of *Gstt2*, *Hmox1*, and *Ephx1* mRNA levels revealed that the up-regulation of the antioxidant defense system in the *Csb^{m/m}/Xpa^{-/-}* liver already initiated before postnatal day 10, and thus well ahead of the initia-

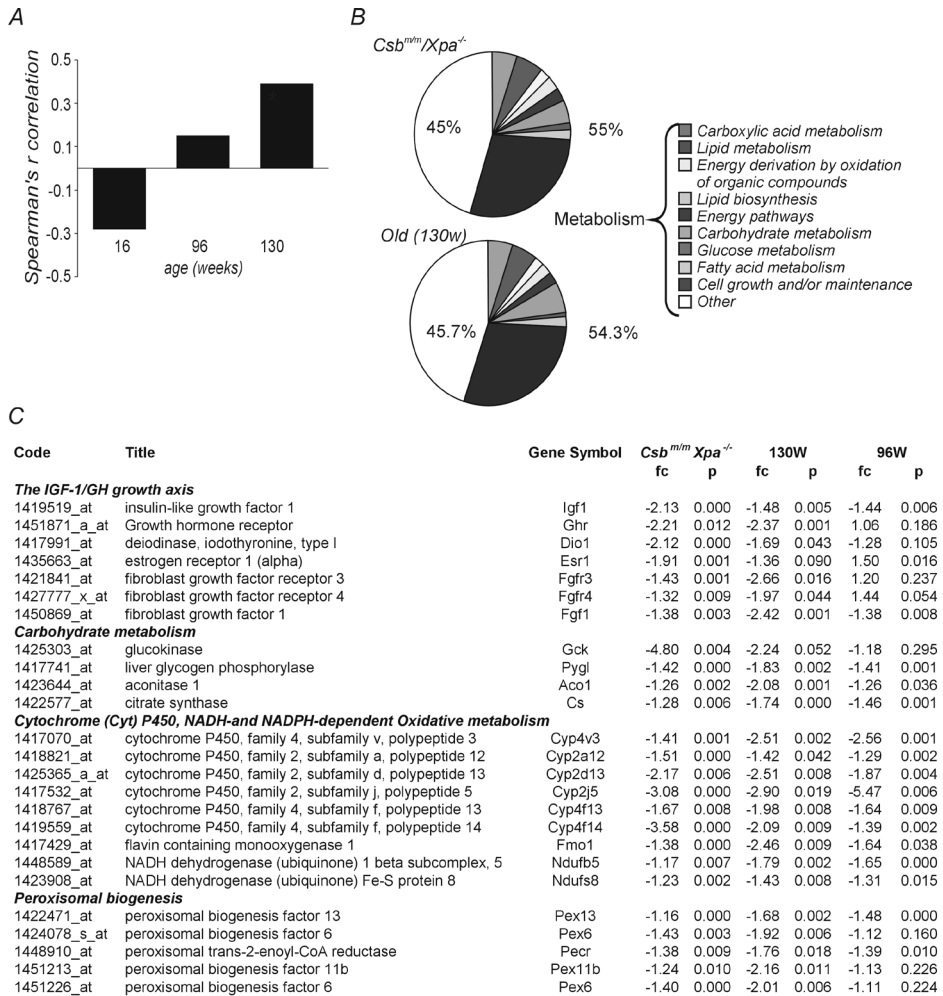


Figure 6: Transcriptome similarities between *Csbtm/Xpa^{-/-}* and naturally aged mice.

(A) Spearman's *r* correlation of 16-, 96- and 130-week old mice with 15-day old *Csbtm/Xpa^{-/-}* mice, where -1.0 is a perfect negative (inverse) correlation, 0.0 is no correlation, and 1.0 is a perfect positive correlation. (B) Similarities between significantly overrepresented biological processes. Note that in both *Csbtm/Xpa^{-/-}* and naturally aged mice, transcriptional changes were mostly associated with metabolic processes. (C) Correlation in significant expression changes of genes associated with the GH/IGF1 axis and oxidative metabolism in the livers of *Csbtm/Xpa^{-/-}* and naturally aged (96- and 130-week old) mice. An extensive overview is listed in Supplementary Tables S3 and S4.

tion of the physiological decline (i.e. weight loss) (Fig. 5B, middle panels). When comparing mRNA levels of key genes in glycolysis (*Gck*), TCA cycle (*Cs*), and mitochondrial oxidative phosphorylation (*Ndufs8*), we noticed that beginning postnatal day 10, *Csbtm/Xpa^{-/-}* livers do not show the prominent up-regulation of these catabolic genes seen in the wt liver (instead expression levels continued to decline), while they up-regulate glycogen synthesis (*Gyg1*, Fig. 2B, right panels). In agreement, the enzymatic activity of citrate synthase was significantly

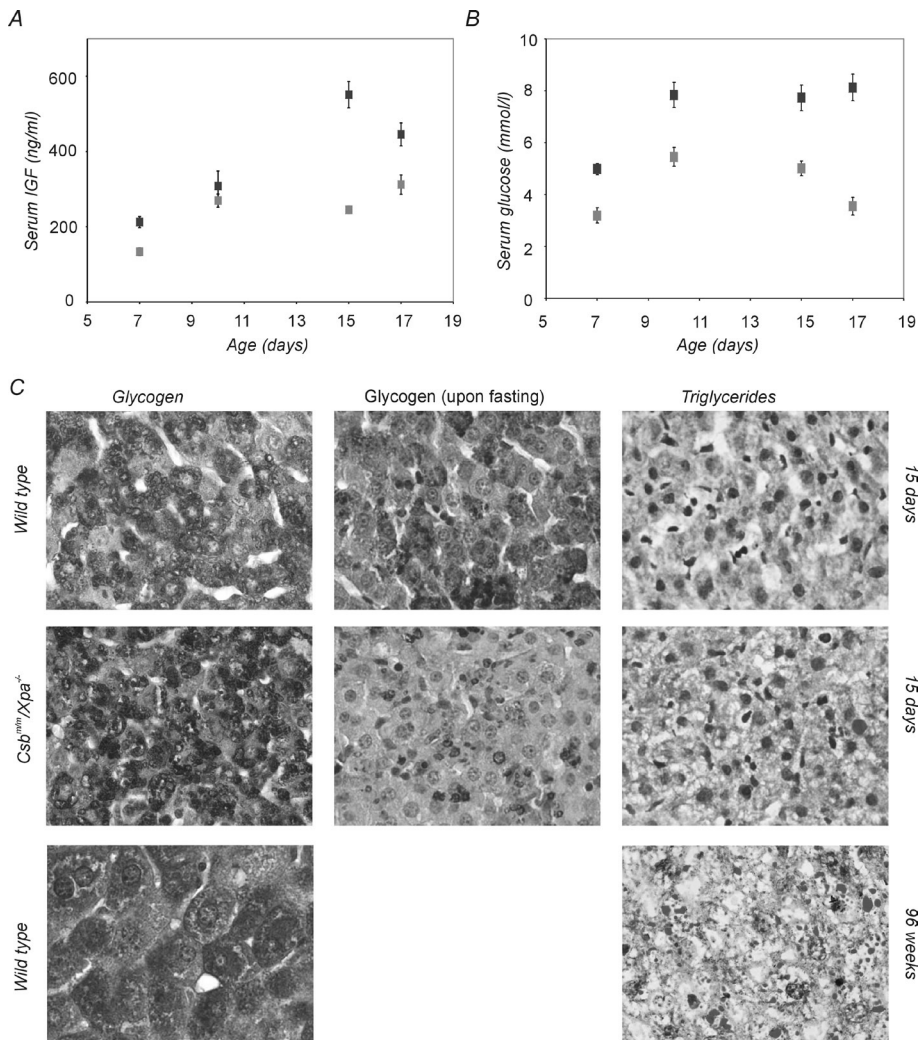


Figure 7: Carbohydrate/fat metabolism and IGF1 serum levels.

IGF1 (**A**) and glucose (**B**) in the serum of 7, 10, 15 and 17-day old wt, *Xpa^{-/-}*, *Csb^{tm/m}* and *Csb^{tm/m}/Xpa^{-/-}* mice (n=6). The levels of IGF1 (ng/ml) and glucose (mmol/l) in the serum of *Csb^{tm/m}/Xpa^{-/-}* mice are significantly lower than that of control littermates ($p < 0.0004$ and $p < 0.04$, respectively). (**C**) PAS staining for glycogen and Oil Red O staining for triglycerides in livers of 15-day old wt and *Csb^{tm/m}/Xpa^{-/-}* mice and 96-week old wt mice. Pictures were taken at 100x magnification. Note the large polyloid nuclei in the 96-week old wt mouse liver and the reduced glycogen levels in the *Csb^{tm/m}/Xpa^{-/-}* liver after overnight fasting.

lower ($p \leq 0.01$) in the liver of 15-day old *Csb^{tm/m}/Xpa^{-/-}* mice (119 ± 15 mU/mg protein), as compared to wt littermate controls (70 ± 13 mU/mg protein).

We next determined the expression levels of aforementioned genes in the kidney, heart and spleen of the same set of animals employed in the microarray experiment. Expression levels markedly mirrored the deviant expression patterns observed in the liver, while mRNA

levels in *Csb^{m/m}* and *Xpa^{-/-}* tissues were not significantly different from wt animals (Fig. 5A). Thus, attenuation of the GH/IGF1 axis and down-regulation of metabolism, along with the enhanced antioxidant/detoxification response, represents a systemic, rather than liver-specific response of the *Csb^{m/m}/Xpa^{-/-}* pups to the DNA repair defect. Interestingly, when 96-week old wild type livers were tested for expression levels of this same set of *Csb^{m/m}/Xpa^{-/-}* responsive genes, we noticed a remarkable resemblance (Supplementary Fig. 1).

Comparison of the *Csb^{m/m}/Xpa^{-/-}* and Naturally Aged Mouse Liver Transcriptomes

The previous result prompted us to investigate whether and to which extent the gene expression changes in the *Csb^{m/m}/Xpa^{-/-}* mouse liver overlap with those observed in a natural aged liver. To this end,, we first compared the full mouse liver transcriptome of adult 16-, 96- and 130-week old wt C57Bl/6J mice (n=4) with that of adult 8-week old wt C57Bl/6J mice (Supplementary Tables S3, S4 and S5 (not shown), n=4). Using the same analytical method as applied to the *Csb^{m/m}/Xpa^{-/-}* mouse livers, we identified homeostasis of energy reserves, oxidative metabolism along with cell growth and maintenance to be significantly overrepresented in 96- and 130-week old wt mice, but not in 16-week old animals (Supplementary Table S6 (not shown)). These findings fit well with previous studies suggesting the repression of oxidative metabolism to represent a conserved response shared by highly diverged species [28]. Next, we implemented a previously described method [29] to evaluate the extent of genome-wide similarity between the liver transcriptomes of 2-week old *Csb^{m/m}/Xpa^{-/-}* mice and, wt animals of various ages. We first classified all significantly differentially expressed genes in the *Csb^{m/m}/Xpa^{-/-}* liver transcriptome as having increased or decreased expression (as compared to wt), and asked how many of these genes respond in a similar direction in the 16/8 wk, 96/8 wk, and 130/8 wk data sets. If the *Csb^{m/m}/Xpa^{-/-}* liver resembles an aged liver, one expects the Spearman's rank correlation coefficient rho (r, +1.0 or -1.0 in case of perfect similarity or dissimilarity, respectively, and 0.0 in case of no correlation) to increase with age. Notably, whereas the liver transcriptome of *Csb^{m/m}/Xpa^{-/-}* mutant mice was dissimilar to that of 16-week old wt mice (Spearman's r = - 0.28), as it was with 15-day old littermates, this turned into a significant positive correlation when the comparison was made between the *Csb^{m/m}/Xpa^{-/-}* and 96-week old mouse liver transcriptomes (r = + 0.15) and even more with the 130-week old wt mouse group (r = + 0.44, p ≤ 0.0001, Fig. 6A). Comparable results were obtained when the same approach was applied over the whole mouse transcriptome (including all Affymetrix probe sets with signals above the detection cut-off value; see Methods), thus avoiding any initial pre-selection or introduction of bias. Using the same approach, we did not find a significant correlation between the liver transcriptomes of 15-day old *Csb^{m/m}* or *Xpa^{-/-}* mice and aged wt mice.

The genome-wide resemblance between the short-lived *Csb^{m/m}/Xpa^{-/-}* mice and the 130-week old mice was substantially higher (>90%) when the comparison was restricted to those functional categories that were significantly overrepresented in the double mutant and

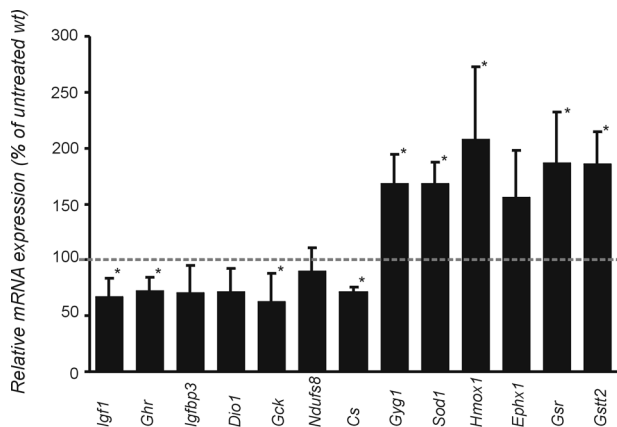


Figure 8: Expression levels of genes associated with the GH/IGF1 axis, oxidative metabolism and antioxidant defense in DEHP-treated wild type mice.

Relative mRNA levels of genes involved in the GH/IGF1 growth axis, oxidative metabolism and antioxidant defense in 13-week old wt mice treated with a low dose of the pro-oxidant DEHP. For each gene, expression levels in the treated wt mouse livers are plotted relative to that of age-matched untreated wt littermate controls (dotted line). Error bars indicate S.E.M. Asterisks indicate statistically significant differences (one-tailed $p \leq 0.05$, see also supplementary methods).

130-week old mice, such as the GH/IGF1 axis, oxidative metabolism (i.e. glycolysis, Krebs and oxidative phosphorylation), cytochrome P450 electron transport and peroxisomal biogenesis (Fig. 6B and C; Supplementary Table S7 (not shown)). Despite the occurrence of dissimilarities between the liver transcriptome of *Csb^{m/m}/Xpa^{-/-}* pups and aged wt mice (the latter animals showing over-representation of genes involved in the immune and inflammatory responses, ATP biosynthesis and protein glycosylation, along with a lack of the anti-oxidant response), these findings strongly underline the genome-wide parallels between the *Csb^{m/m}/Xpa^{-/-}* repair mutants and natural ageing, thereby validating the progeria in the double mutant pups.

Reduced IGF1 Serum Levels, Glucose and Fat Utilization in *Csb^{m/m}/Xpa^{-/-}* Mice

In agreement with the down-regulation of *Igf1* gene expression in the liver (the main source of circulating IGF1 [30]), we observed a significant reduction ($p < 0.004$) in serum IGF1 levels in *Csb^{m/m}/Xpa^{-/-}* mice (Fig. 7A) together with significantly lower blood glucose levels ($p < 0.04$, Fig. 7B). Following an initial reduction of ~30% ($p < 0.04$) in 7- and 10-day old *Csb^{m/m}/Xpa^{-/-}* mice, blood glucose levels started to drop at day 15, gradually reaching low levels in 17-day old *Csb^{m/m}/Xpa^{-/-}* mice (~3 mM), contrasting the steady blood glucose levels (~9 mM) in littermate controls (Fig. 7B). The presence of milk and food in the stomach of the double mutant pups along with the normal appearance of the intestinal epithelium (Fig. 3A) indicates that the hypoglycemia is not due to food intake. Even more, the suppression of the somatotroph axis and subsequent decreased IGF1 production in 15-day old *Csb^{m/m}/Xpa^{-/-}* mice appeared not to originate from a pituitary dysfunction as histological examination (Fig 3F) and TUNEL

staining of sections from the pituitary pars distalis, intermedia and nervosa did not reveal any abnormalities (data not shown). Moreover, serum GH levels in 15-day old *Csb^{m/m}/Xpa^{-/-}* mice (15.2 +/- 4.2 ng/ml, n=8) did not differ significantly from wt littermates (12.8 +/- 2.8 ng/ml, n=6). Interestingly, the normal serum GH levels together with the significant systemic down regulation of GH receptor gene expression, likely points to growth hormone resistance in 15-day old *Csb^{m/m}/Xpa^{-/-}* mice.

PAS staining of liver sections from 10- to 20-day old pups and naturally aged mice revealed enhanced accumulation of glycogen in unusually large vesicles in *Csb^{m/m}/Xpa^{-/-}* pups and 96-week old mice when compared to wt littermates and 8-week old wt mice (Fig. 7C). This observation fits our microarray data, suggesting that both the *Csb^{m/m}/Xpa^{-/-}* and naturally aged mice store, rather than utilize glucose. Overnight fasting of *Csb^{m/m}/Xpa^{-/-}* pups and littermate controls resulted in a near-to-complete depletion of liver glycogen (Fig. 7D) indicating that the glycogen accumulation is not due to inability to split glycogen into its constitutive glucose monomers.

Consistent with the broad up-regulation of genes associated with fatty acid synthesis (Table 1), oil Red O staining of liver sections from 15-day old pups and naturally aged mice revealed enhanced accumulation of triacylglycerides in both compared to control littermates and 8-week old mice (Fig. 7C), indicating hepatic steatosis. This and the absence of adipose tissue suggest that *Csb^{m/m}/Xpa^{-/-}* mice display generalized lipodystrophy (loss and abnormal redistribution of body fat) [31].

Systemic Changes in Somatotroph Axis and Antioxidant Defense in DEHP-Treated wt Mice

To test whether the presence of endogenous (oxidative) DNA damage can provoke the somatotrophic drop and enhanced antioxidant potential, wt C57BL/6J mice (n=6; 4-week old) were fed *ad libitum* for 9 weeks with standard food containing sub-toxic levels of an oxidative DNA damage-inducing agent [di(2-ethylhexyl)phthalate, DEHP, 1500 ppm] [32]. Neither body weight nor appetite and food intake of DEHP-exposed animals deviated from that of untreated control animals. As shown in Figure 8, subsequent analysis revealed suppression of the expression of genes associated with the somatotroph axis (*Igf1*, *Igfbp3*, *Ghr*, and *Dio1*) and oxidative metabolism (*Gck*, *Cs* and *Ndufs8*), along with the up-regulation of glycogenin 1 (*Gyg1*, Fig 5A) in DEHP-exposed animals. Consistent with the ability of DEHP to generate ROS-induced DNA damage in the liver, we also noticed a significant up-regulation of genes associated with the antioxidant and detoxification responses (*Hmox1*, *Ephx1*, *Gsr*, *Sod1*, *Gstt2*). These findings suggest that accumulation of unrepaired (oxidative) DNA damage likely comprises one of the causes underlying the observed suppression of the GH/IGF1 and oxidative metabolism in *Csb^{m/m}/Xpa^{-/-}* mice (see also supplementary methods).

Discussion

Csb^{m/m} mice exhibit several CS features (e.g. attenuated growth, blindness, neurological dysfunction), but their phenotype is overall milder than the human syndrome [16] despite that the truncation in the N-terminal part (mimicking a mutant allele of CS-B patient CS1AN) completely inactivates the protein and TC-NER [16]. Although the severity of clinical features in humans does not seem to correlate with the severity of the molecular defect [33], the absence of the complete spectrum of CS features in the *Csb^{m/m}* mouse model is likely to originate from man-mouse differences (i.e. adaptation to stress, tolerance to DNA damage/genome instability), rather than from the nature of the *Csb^{m/m}* mutation. This idea is supported by our observations that *Xpd^{TTD}* and *Xpd^{XPCS}* mice (all carrying causative point mutations) also fail to show the severe CS features associated with XPCS and TTD [9,34].

Yet, the present study reveals that inactivation of GG-NER or complete abrogation of NER (through inactivation of *Xpc* or *Xpa*, respectively) in TCR-deficient *Csb^{m/m}* mice dramatically aggravates the *Csb^{m/m}* mouse phenotype. As animals were not exposed to exogenous genotoxic agents, we attribute this effect to enhanced levels of unrepaired endogenous (oxidative) DNA damage. In further support of this, we have shown that *Csb^{m/m}/Xpc^{-/-}* and *Csb^{m/m}/Xpa^{-/-}* MEFs, as well as *Csb^{m/m}/Xpa^{-/-}* retinal photoreceptor cells are more sensitive to environmental genotoxic insults (i.e. UV-light, ionizing radiation) than their single mutant counterparts. A comparable phenotypic deterioration has been noticed when *Xpa* was inactivated in *Xpd^{TTD}* [9], *Xpd^{XPCS}* [34], compound heterozygous *Xpd^{TTD/XPCS}* animals (carrying causative mutations for TTD and combined XP/CS; van de Ven et al., pending revision), and *Xpg^{deltaEx15}* mice [35].

Importantly, *Csb^{m/m}/Xpa^{-/-}* mice appeared normal at birth, indicating a normal intra-uterine development and ruling out that this condition is in fact an embryonic developmental disorder. Instead, after birth, the *Csb^{m/m}/Xpa^{-/-}* pups displayed progressive kyphosis, cachexia, photoreceptor loss, and motor dysfunction, all common postnatal manifestations of CS [13], as well as of natural mammalian aging [36-38]. Also similar to CS patients (average age 12.5 years), *Csb^{m/m}/Xpa^{-/-}* pups fail to grow into adulthood and die before weaning. The relation between (residual) repair capacity, time and severity of a particular phenotype is well illustrated by the retinal photoreceptor loss in the *Csb^{m/m}* mouse models. While aging C57Bl/6J mice lose about 5-10% of their rods and cones in 30 months, TCR-deficient *Csb^{m/m}* mice have already lost about 50% of their photoreceptor cells by the age of 16 months (Gorgels et al., pending revision). This spontaneous retinal degeneration in *Csb^{m/m}* mice originates from enhanced apoptotic sensitivity of photoreceptor cells (Gorgels et al., pending revision), evolving in the first one or two months after weaning (this study). Interestingly, further crippling of NER in *Csb^{m/m}* animals by inactivation of *Xpa* accelerates the onset of photoreceptor loss, now becoming visible as early as postnatal day 15, and progressively increasing thereafter. The strong correlation between the severity of the repair deficiency and the onset of photoreceptor loss, as well as the enhanced ionizing radiation hypersensitivity of photoreceptor cells of

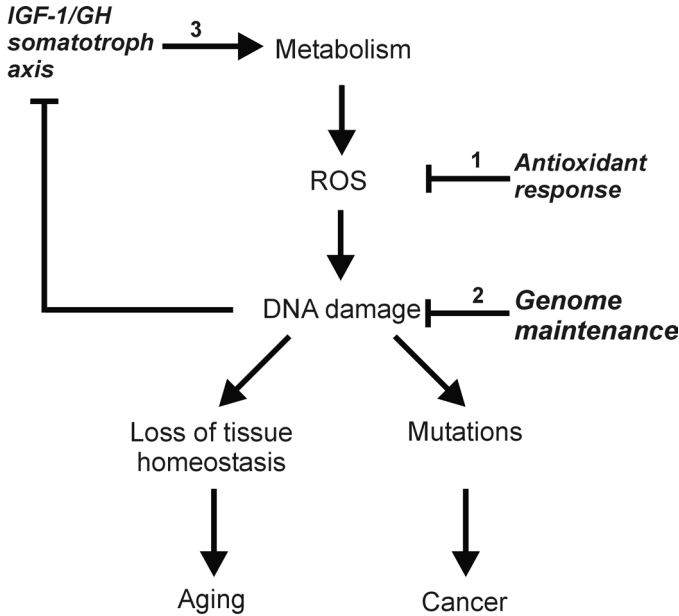


Figure 9: The proposed link between DNA damage and the decline of the GH/IGF1 somatotroph axis.

ROS are natural byproducts of metabolism and can injure several macromolecules including DNA, thus contributing to a slow but steady accumulation of damage, transcriptional stress, impaired replication and eventually the progressive loss of tissue homeostasis and gradual organismal deterioration. Cells and tissues will respond by (1) up regulating their antioxidant defense responses that would moderate the harmful effects of ROS, (2) employing a battery of genome maintenance pathways that would repair or remove damaged macromolecules and help to resist the oxidative stress, and (3) suppressing their GH/IGF1 somatotroph axis along with the oxidative metabolism, thus substantially moderating their metabolic activity that would otherwise lead to high oxygen consumption and increased generation of oxidants. To this end, the physiologic reduction of the somatotroph axis and oxidative metabolism is envisaged to be beneficial in terms of net life span.

$Csb^{m/m}/Xpa^{-/-}$ mice (as compared to age-matched $Csb^{m/m}$ animals), well support the hypothesis that (oxidative) DNA damage likely underlies the retinal degeneration.

Full genome transcriptome analysis of the $Csb^{m/m}/Xpa^{-/-}$ mouse liver, aiming at unraveling the etiology of the severe double mutant phenotype, led us to identify significant genome-wide parallels between the 2-week old $Csb^{m/m}/Xpa^{-/-}$ and 130-week, but not 16-week old wt animals at the fundamental level of gene expression. Importantly, this resemblance was largely attributable to the substantial down regulation of genes associated with processes implicated in oxidative energy and growth metabolism, previously revealed by others to represent a conserved transcriptional response in aging [28].

The down-regulation of genes associated with the GH/IGF1 growth axis in the liver, the systemic reduction in *GH receptor* mRNA levels and the impaired *Igf1* gene expression in liver and other tissues (resulting in low serum IGF1 levels) likely underlies the postnatal growth defect in $Csb^{m/m}/Xpa^{-/-}$ pups. These changes were not due to reduced GH serum levels or

pituitary abnormalities. Importantly, a steady decline in the GH/IGF1 somatotroph axis is also observed in rodents and humans during natural aging [39]. Furthermore, *Csb^{m/m}/Xpa^{-/-}* pups failed to up-regulate metabolism; instead they displayed a sharp, systemic reduction in the expression levels of genes involved in glycolysis, tricarboxylic acid cycle (including decreased citrate synthase activity), and oxidative respiration, which coincided with the onset of weight loss (cachexia). In addition, *Csb^{m/m}/Xpa^{-/-}* pups up-regulated genes associated with glycogen and fatty acid synthesis, leading to increased hepatic glycogen storage and fat accumulation (steatosis) and pronounced hypoglycemia. Simultaneously subcutaneous fat tissue was virtually absent. Given that, in mammals, the GH/IGF1 signaling pathway comprises one of the major regulators of energy homeostasis to integrate metabolism with growth [30,40,41], it is tempting to speculate that reduced IGF1 signaling is responsible for the postnatal metabolic shift and growth defect seen in *Csb^{m/m}/Xpa^{-/-}* mice. Interestingly, several CS patients have been previously reported with hypoglycemia and low IGF1 serum levels [42,43], low metabolic rate [44] and abnormal fat deposition [45].

Paradoxically, however, the systemic suppression of the somatotrophic axis and energy metabolism, along with the up-regulation of antioxidant defenses, low IGF1 serum and blood glucose levels, observed in the *Csb^{m/m}/Xpa^{-/-}* mouse, are all associated with increased longevity, rather than with the short lifespan of this mouse model. In lower paradigms for life span extension (*C. elegans*, *D. melanogaster*), genetic interference in the insulin-signaling pathway can prolong life multi-fold [46,47]. In mammals, IGF1-deficient, Ames and Snell dwarf mice (characterized by defects in the development of the anterior pituitary due to mutations in the *Prop-1* and *Pit1* loci and diminished levels of GH, thyroid stimulating and prolactin hormones) combine hypoglycemia, low body temperature, and increased storage of carbohydrates and lipids [39,41] with up-regulation of antioxidant defense capacity and extended lifespan [48,49]. Conversely, GH-overexpressing transgenic mice display reduced lifespan and antioxidant responses [50]. These findings have also been recently confirmed by our identification of genome-wide parallels between the extremely short-lived DNA repair mutants (i.e. *Csb^{m/m}/Xpa^{-/-}*, *Ercc1^{-/-}*) and the extremely long-lived Ames and Snell dwarfs and growth hormone receptor knockout (*Ghr^{-/-}*) mice (Garinis *et al.* manuscript in preparation). Last but not least, IGF1 plasma levels decline with age in humans and rodents [51-53]. Along with this hormonal shift, aging cells surmount an intricate antioxidant defense response [54,55] that is thought to prevent the detrimental consequences of oxidative stress. Interestingly, the progressive, age-related decrease in the somatotroph axis has been suggested to confer a selective advantage by postponing the onset of age-related disease and prolonging life span through the reduction of toxic free radicals [39].

How would repair-deficient mice benefit from such a response? During development, the mitogenic action of GH and IGF1 fuels cellular metabolism, thereby promoting tissue growth and function [39,56,57]. A high metabolic activity, however, leads to higher oxygen consumption [39] and may also increase the ROS burden through the parallel increase of

mitochondrial electron transport, peroxisomal fatty acid metabolism and/or microsomal cytochrome *P-450* enzymes [58]. Despite antioxidant defense and DNA repair, oxidative DNA damage will still accumulate, leading to transcriptional stress, impaired replication, cellular senescence, malfunction or death and eventually to progressive loss of tissue homeostasis and organismal decline (see model, Fig. 9). We hypothesize that complete abrogation of NER (by inactivation of *Xpa*) renders TCR-deficient *Csb^{m/m}* mice unable to adequately cope with the increased burden of DNA damage in the transcribed strand of active genes. This triggers an adaptive response i.e. reduction of metabolic activity through down-regulation of the GH/IGF1 axis to relieve the pressure on their genome. We interpret this as an attempt to limit the deleterious effects of arrested transcription, such as cellular senescence and death causing accelerated aging. As a consequence, the initially normal growth becomes arrested soon after birth, leading to severe growth retardation. This scenario provides a plausible explanation for the growth defect in CS patients. However, this response is unable to fully compensate for the repair defect, thus damage still accumulates to critical levels and triggers apoptosis and/or senescence, thereby leading to aging-associated pathology such as neurodegeneration (as illustrated by the photoreceptor cells in *Csb^{m/m}/Xpa^{-/-}* mice).

The conceptual link between DNA damage and the systemic adaptive response is supported by our observation that chronic exposure of wt mice to a sub-toxic dose of DEHP (a pro-oxidant that enhances the DNA damage load; see de Waard et al, 2004) triggers a response similar to that observed in (untreated) *Csb^{m/m}/Xpa^{-/-}* mice. Although DEHP at much higher concentrations has been previously documented to affect the endocrine function of the pituitary, proteome analysis revealed that synthesis of prolactin and growth hormone appears unaffected in DEHP-treated rats [59]. This suggests that the observed suppression of genes associated with the somatotroph axis and oxidative metabolism in the liver of DEHP-exposed mice is triggered by DNA damage in the liver, rather than by a pituitary defect or hypothalamic defect.

As one would predict, other short-lived NER mouse models (e.g. *Xpg*, *Xpf* mice, [60,61]) or NER mutant mice with a milder progeroid phenotype could also show accelerated attenuation of the somatotrophic axis in response to their DNA repair defect. Indeed, *Ercc1^{-/-}* animals, carrying a combined NER/crosslink DNA repair defect and a life span of only a few weeks, demonstrate a remarkable genome-wide similarity in liver gene expression profiles with *Csb^{m/m}/Xpa^{-/-}* mice (Niedernhofer et al., pending revision), while *Xpd^{XPCS}/Xpa^{-/-}* and compound heterozygous *Xpd^{TTD/XPCS}/Xpa^{-/-}* mice contain lower serum IGF1 levels (van de Ven et al., submitted). Furthermore, *Xpd^{TTD}* mice, which manifest accelerated aging in many (but not all) organs and tissues, have recently been shown to display features related to a caloric restricted-like phenotype and suppression of the GH/IGF1 axis in a limited set of organs and tissues, stressing the segmental nature that is characteristic of all progeroid syndromes and the systemic nature of the response [62]. Finally, proper glucose homeostasis and normal IGF1 levels were recently shown to require Sirt6 activity, a chromatin deacetylase that may promote DNA

repair [63]. As ROS-mediated DNA damage appears to be the underlying cause of the *Csb^{m/m}/Xpa^{-/-}* progeria, it is tempting to speculate that one can attenuate the premature onset of age-related features by directly counteracting the harmful byproducts of metabolism (*i.e.* ROS), and consequently DNA damage. Interestingly, an antioxidant-based nutraceutical intervention pilot study with *Csb^{m/m}/Xpa^{-/-}* mice, aiming at extending life span and delaying onset of pathology, yielded promising results (van der Pluijm et al., unpublished results).

Acknowledgements

We thank Wiebeke van Leeuwen and Willem Sluiter for assistance with X-ray analysis and citrate synthase activity measurements, respectively. This research was supported by the Netherlands Organization for Scientific Research (NWO) through the foundation of the Research Institute Diseases of the Elderly, as well as grants from SenterNovem IOP-Genomics (IGE03009), NIH (1PO1 AG17242-02), NIEHS (1UO1 ES011044), EC (QRTL-1999-02002; LSHC-CT-2005-512113), and the Dutch Cancer Society (EUR 99-2004). L.J.N. was supported by Post-doctoral Fellowship #PF-99-142 from the American Cancer Society. JHJH is CSO of DNage.

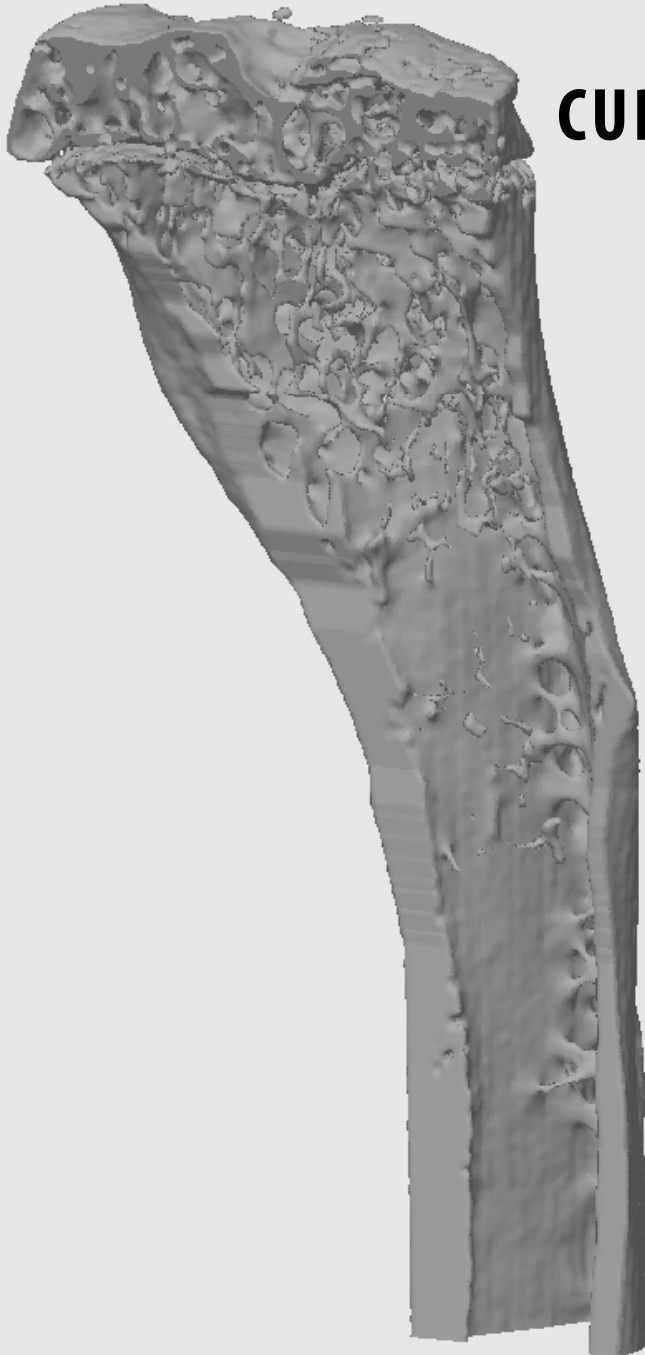
References

1. Harman D (1956) Aging: a theory based on free radical and radiation chemistry. *J Gerontol* 11: 298-300.
2. Schriener SE, Linford NJ, Martin GM, Treuting P, Ogburn CE, et al. (2005) Extension of murine life span by overexpression of catalase targeted to mitochondria. *Science* 308: 1909-1911.
3. Melov S, Ravenscroft J, Malik S, Gill MS, Walker DW, et al. (2000) Extension of life-span with superoxide dismutase/catalase mimetics. *Science* 289: 1567-1569.
4. Orr WC, Sohal RS (1994) Extension of life-span by overexpression of superoxide dismutase and catalase in *Drosophila melanogaster*. *Science* 263: 1128-1130.
5. Ishii N, Fujii M, Hartman PS, Tsuda M, Yasuda K, et al. (1998) A mutation in succinate dehydrogenase cytochrome b causes oxidative stress and ageing in nematodes. *Nature* 394: 694-697.
6. Hamilton ML, Van Remmen H, Drake JA, Yang H, Guo ZM, et al. (2001) Does oxidative damage to DNA increase with age? *Proc Natl Acad Sci U S A* 98: 10469-10474.7. Lu T, Pan Y, Kao SY, Li C, Kohane I, et al. (2004) Gene regulation and DNA damage in the ageing human brain. *Nature* 429: 883-891.
8. Martin GM (2005) Genetic modulation of senescent phenotypes in *Homo sapiens*. *Cell* 120: 523-532.
9. de Boer J, Andressoo JO, de Wit J, Huijijmans J, Beems RB, et al. (2002) Premature aging in mice deficient in DNA repair and transcription. *Science* 296: 1276-1279.
10. Hanawalt PC (2002) Subpathways of nucleotide excision repair and their regulation. *Oncogene* 21: 8949-8956.
11. Spivak G, Hanawalt PC (2005) Host cell reactivation of plasmids containing oxidative DNA lesions is defective in Cockayne syndrome but normal in UV-sensitive syndrome fibroblasts. *DNA Repair (Amst)*.
12. de Waard H, de Wit J, Gorgels TG, van den Aardweg G, Andressoo JO, et al. (2003) Cell type-specific hypersensitivity to oxidative damage in CSB and XPA mice. *DNA Repair (Amst)* 2: 13-25.
13. Nance MA, Berry SA (1992) Cockayne syndrome: review of 140 cases. *Am J Med Genet* 42: 68-84.
14. Bootsma D, Kraemer KH, J.E. C, Hoeijmakers J (2002) Nucleotide excision repair syndromes: Xeroderma Pigmentosum, Cockayne Syndrome and trichthiodystrophy. New York: McGraw-Hill Medical Publishing Division. 211-237 p.
15. Vermeulen W, Rademakers S, Jaspers NG, Appeldoorn E, Raams A, et al. (2001) A temperature-sensitive disorder in basal transcription and DNA repair in humans. *Nat Genet* 27: 299-303.
16. van der Horst GT, van Steeg H, Berg RJ, van Gool AJ, de Wit J, et al. (1997) Defective transcription-coupled repair in Cockayne syndrome B mice is associated with skin cancer predisposition. *Cell* 89: 425-435.
17. van der Horst GT, Meira L, Gorgels TG, de Wit J, Velasco-Miguel S, et al. (2002) UVB radiation-induced cancer predisposition in Cockayne syndrome group A (Csa) mutant mice. *DNA Repair (Amst)* 1: 143-157.
18. Hasty P, Campisi J, Hoeijmakers J, van Steeg H, Vijg J (2003) Aging and genome maintenance: lessons from the mouse? *Science* 299: 1355-1359.
19. de Boer J, Hoeijmakers JH (2000) Nucleotide excision repair and human syndromes. *Carcinogenesis* 21: 453-460.
20. Mitchell JR, Hoeijmakers JH, Niedernhofer LJ (2003) Divide and conquer: nucleotide excision repair battles cancer and ageing. *Curr Opin Cell Biol* 15: 232-240.

21. Cheo DL, Ruven HJ, Meira LB, Hammer RE, Burns DK, et al. (1997) Characterization of defective nucleotide excision repair in XPC mutant mice. *Mutat Res* 374: 1-9.
22. de Vries A, van Oostrom CT, Hofhuis FM, Dortant PM, Berg RJ, et al. (1995) Increased susceptibility to ultraviolet-B and carcinogens of mice lacking the DNA excision repair gene XPA. *Nature* 377: 169-173.
23. Parrinello S, Samper E, Krtolica A, Goldstein J, Melov S, et al. (2003) Oxygen sensitivity severely limits the replicative lifespan of murine fibroblasts. *Nat Cell Biol* 5: 741-747.
24. Busuttill RA, Rubio M, Dolle ME, Campisi J, Vijg J (2003) Oxygen accelerates the accumulation of mutations during the senescence and immortalization of murine cells in culture. *Aging Cell* 2: 287-294.
25. Murai M, Enokido Y, Inamura N, Yoshino M, Nakatsu Y, et al. (2001) Early postnatal ataxia and abnormal cerebellar development in mice lacking Xeroderma pigmentosum Group A and Cockayne syndrome Group B DNA repair genes. *Proc Natl Acad Sci U S A* 98: 13379-13384.
26. Itoh M, Hayashi M, Shioda K, Minagawa M, Isa F, et al. (1999) Neurodegeneration in hereditary nucleotide repair disorders. *Brain Dev* 21: 326-333.
27. Traboulsi EI, De Becker I, Maumenee IH (1992) Ocular findings in Cockayne syndrome. *Am J Ophthalmol* 114: 579-583.
28. McCarroll SA, Murphy CT, Zou S, Pletcher SD, Chin CS, et al. (2004) Comparing genomic expression patterns across species identifies shared transcriptional profile in aging. *Nat Genet* 36: 197-204.
29. Fraser HB, Khaitovich P, Plotkin JB, Paabo S, Eisen MB (2005) Aging and gene expression in the primate brain. *PLoS Biol* 3: e274.
30. Frystyk J (2004) Free insulin-like growth factors -- measurements and relationships to growth hormone secretion and glucose homeostasis. *Growth Horm IGF Res* 14: 337-375.
31. Ahima R, Osei SY (2004) Leptin and appetite control in lipodystrophy. *J Clin Endocrinol Metab* 89: 4254-4257.
32. Seth PK (1982) Hepatic effects of phthalate esters. *Environ Health Perspect* 45: 27-34.
33. Horibata K, Iwamoto Y, Kuraoka I, Jaspers NG, Kurimasa A, et al. (2004) Complete absence of Cockayne syndrome group B gene product gives rise to UV-sensitive syndrome but not Cockayne syndrome. *Proc Natl Acad Sci U S A* 101: 15410-15415.
34. Andressoo JO, Mitchell JR, de Wit J, Hoogstraten D, Volker M, et al. (2006) An Xpd mouse model for the combined xeroderma pigmentosum/Cockayne syndrome exhibiting both cancer predisposition and segmental progeria. *Cancer Cell* 10: 121-132.
35. Shiomi N, Mori M, Kito S, Harada YN, Tanaka K, et al. (2005) Severe growth retardation and short life span of double-mutant mice lacking Xpa and exon 15 of Xpg. *DNA Repair (Amst)* 4: 351-357.
36. Arking R (1998) *Biology of aging; observations and principles*. Sunderland: Sinauer Associates. 528 p.
37. Kalu DN (1995) Bone. In: Masoro, editor. *Handbook of Physiology of Aging*. New York: Oxford University Press. pp. 395-411.
38. Weiss A, Arbell I, Steinhagen-Thiessen E, Silbermann M (1991) Structural changes in aging bone: osteopenia in the proximal femurs of female mice. *Bone* 12: 165-172.
39. Carter CS, Ramsey MM, Sonntag WE (2002) A critical analysis of the role of growth hormone and IGF-1 in aging and lifespan. *Trends Genet* 18: 295-301.
40. Puigserver P, Rhee J, Donovan J, Walkey CJ, Yoon JC, et al. (2003) Insulin-regulated hepatic gluconeogenesis through FOXO1-PGC-1alpha interaction. *Nature* 423: 550-555.
41. Longo VD, Finch CE (2003) Evolutionary medicine: from dwarf model systems to healthy centenarians? *Science* 299: 1342-1346.

42. Park SK, Chang SH, Cho SB, Baek HS, Lee DY (1994) Cockayne syndrome: a case with hyperinsulinemia and growth hormone deficiency. *J Korean Med Sci* 9: 74-77.
43. Fujimoto WY, Green ML, Seegmiller JE (1969) Cockayne's syndrome: report of a case with hyperlipoproteinemia, hyperinsulinemia, renal disease, and normal growth hormone. *J Pediatr* 75: 881-884.
44. Ellaway CJ, Duggins A, Fung VS, Earl JW, Kamath R, et al. (2000) Cockayne syndrome associated with low CSF 5-hydroxyindole acetic acid levels. *J Med Genet* 37: 553-557.
45. Laszlo A, Simon M (1986) Serum lipid and lipoprotein levels in premature ageing syndromes: total lipodystrophy and Cockayne syndrome. *Arch Gerontol Geriatr* 5: 189-196.
46. Kenyon C (2005) The plasticity of aging: insights from long-lived mutants. *Cell* 120: 449-460.
47. Partridge L, Gems D, Withers DJ (2005) Sex and death: what is the connection? *Cell* 120: 461-472.
48. Brown-Borg HM, Bode AM, Bartke A (1999) Antioxidative mechanisms and plasma growth hormone levels: potential relationship in the aging process. *Endocrine* 11: 41-48.
49. Brown-Borg HM, Rakoczy SG (2000) Catalase expression in delayed and premature aging mouse models. *Exp Gerontol* 35: 199-212.
50. Bartke A, Chandrashekar V, Bailey B, Zaczek D, Turyn D (2002) Consequences of growth hormone (GH) overexpression and GH resistance. *Neuropeptides* 36: 201-208.
51. Florini JR, Harned JA, Richman RA, Weiss JP (1981) Effect of rat age on serum levels of growth hormone and somatomedins. *Mech Ageing Dev* 15: 165-176.
52. Johanson AJ, Blizzard RM (1981) Low somatomedin-C levels in older men rise in response to growth hormone administration. *Johns Hopkins Med J* 149: 115-117.
53. Rudman D, Kutner MH, Rogers CM, Lubin MF, Fleming GA, et al. (1981) Impaired growth hormone secretion in the adult population: relation to age and adiposity. *J Clin Invest* 67: 1361-1369.
54. Camougrand N, Rigoulet M (2001) Aging and oxidative stress: studies of some genes involved both in aging and in response to oxidative stress. *Respir Physiol* 128: 393-401.
55. Ji LL, Leeuwenburgh C, Leichtweis S, Gore M, Fiebig R, et al. (1998) Oxidative stress and aging. Role of exercise and its influences on antioxidant systems. *Ann NY Acad Sci* 854: 102-117.
56. Bartke A (2003) Is growth hormone deficiency a beneficial adaptation to aging? Evidence from experimental animals. *Trends Endocrinol Metab* 14: 340-344.
57. Chandrashekar V, Zaczek D, Bartke A (2004) The consequences of altered somatotrophic system on reproduction. *Biol Reprod* 71: 17-27.
58. Beckman KB, Ames BN (1998) The free radical theory of aging matures. *Physiol Rev* 78: 547-581.
59. Hirokawa N, Yano K, Suzuki Y, Sakamoto Y (2006) Endocrine disrupting effect of di-(2-ethylhexyl) phthalate on female rats and proteome analyses of their pituitaries. *Proteomics* 6: 958-971.
60. Harada YN, Shiomi N, Koike M, Ikawa M, Okabe M, et al. (1999) Postnatal growth failure, short life span, and early onset of cellular senescence and subsequent immortalization in mice lacking the xeroderma pigmentosum group G gene. *Mol Cell Biol* 19: 2366-2372.
61. Tian M, Shinkura R, Shinkura N, Alt FW (2004) Growth retardation, early death, and DNA repair defects in mice deficient for the nucleotide excision repair enzyme XPF. *Mol Cell Biol* 24: 1200-1205.
62. Wijnhoven SW, Beems RB, Roodbergen M, van den Berg J, Lohman PH, et al. (2005) Accelerated aging pathology in ad libitum fed Xpd(TTD) mice is accompanied by features suggestive of caloric restriction. *DNA Repair (Amst)*.
63. Mostoslavsky R, Chua KF, Lombard DB, Pang WW, Fischer MR, et al. (2006) Genomic instability and aging-like phenotype in the absence of mammalian SIRT6. *Cell* 124: 315-329.

64. Cheo DL, Meira LB, Hammer RE, Burns DK, Doughty AT, et al. (1996) Synergistic interactions between XPC and p53 mutations in double-mutant mice: neural tube abnormalities and accelerated UV radiation-induced skin cancer. *Curr Biol* 6: 1691-1694.
65. Nakane H, Takeuchi S, Yuba S, Saijo M, Nakatsu Y, et al. (1995) High incidence of ultraviolet-B-or chemical-carcinogen-induced skin tumours in mice lacking the xeroderma pigmentosum group A gene. *Nature* 377: 165-168.
66. Lowe SW, Schmitt EM, Smith SW, Osborne BA, Jacks T (1993) p53 is required for radiation-induced apoptosis in mouse thymocytes. *Nature* 362: 847-849.
67. Sijbers AM, de Laat WL, Ariza RR, Biggerstaff M, Wei YF, et al. (1996) Xeroderma pigmentosum group F caused by a defect in a structure-specific DNA repair endonuclease. *Cell* 86: 811-822.
68. Vermeulen W, Scott RJ, Rodgers S, Muller HJ, Cole J, et al. (1994) Clinical heterogeneity within xeroderma pigmentosum associated with mutations in the DNA repair and transcription gene ERCC3. *Am J Hum Genet* 54: 191-200.
69. Ma GT, Roth ME, Groskopf JC, Tsai FY, Orkin SH, et al. (1997) GATA-2 and GATA-3 regulate trophoblast-specific gene expression in vivo. *Development* 124: 907-914.
70. Carter RJ, Lione LA, Humby T, Mangiarini L, Mahal A, et al. (1999) Characterization of progressive motor deficits in mice transgenic for the human Huntington's disease mutation. *J Neurosci* 19: 3248-3257.



CURRICULUM VITAE

Curriculum vitae

Naam:	Karin Elin Maria Diderich
Geboren:	27 mei 1975, Rotterdam
1987-1993	Erasmiaans gymnasium, Rotterdam
1993-2000	Geneeskunde, Erasmus Universiteit Rotterdam Stages: Klinische Genetica, Karolinska Institutet, Stockholm Celbiologie, Erasmus Universiteit Rotterdam (Dr. P. Fraser) Genetica, University of Maryland, Baltimore (Dr. G. Barcak)
2000-2005	Promotie onderzoek Celbiologie & Genetica, Erasmus Universiteit Rotterdam (Prof.dr. J. Hoeijmakers, Prof.dr. J. van Leeuwen, Prof.dr. G. van der Horst)
2005	Agnio Interne Geneeskunde, Havenziekenhuis, Rotterdam
vanaf 2006	Aios Klinische Genetica, ErasmusMC, Rotterdam

Publications

'Intergenic transcription and developmental remodeling of chromatin sub-domains in the human β globin locus.' by J. Gribnau, **K. Diderich**, S. Pruzina, R. Calzolari and P. Fraser, *Molecular Cell*, Vol. 5(2), 377-386, February 2000

'Accelerated bone aging in the trichothiodystrophy mouse model.' by **K. Diderich**, J. Hoeijmakers and J. van Leeuwen, *Journal of Gerontology*, Vol. 58(11), 969, November 2003

'Dysregulation of the peroxisome proliferator-activated receptor target genes by XPD mutations.' by E. Compe, P. Drane, C. Laurent, **K. Diderich**, C. Braun, J. Hoeijmakers and J. Egly, *Molecular Cell Biology*, Vol. 25(14), 6065-6076, July 2005

'Accelerated aging pathology in ad libitum fed Xpd(TTD) mice is accompanied by features suggestive of caloric restriction.' by S. Wijnhoven, R. Beems, M. Roodbergen, J. van den Berg, P. Lohman, **K. Diderich**, G. van der Horst, J. Vijg, J. Hoeijmakers and H. van Steeg, *DNA Repair*, Vol. 4(11), 1314-1324, November 2005

'Impaired genome maintenance suppresses the growth hormone--insulin-like growth factor 1 axis in mice with Cockayne syndrome.' by I. van der Pluijm, G. Garinis, R. Brandt, T. Gorgels, S. Wijnhoven, **K. Diderich**, J. de Wit, J. Mitchell, C. van Oostrom, R. Beems, L. Niedernhofer, S. Velasco, E. Friedberg, K. Tanaka, H. van Steeg, J. Hoeijmakers and G. van der Horst, *PLoS Biology*, Vol. 5(1):e2, January 2007

'Symptomatic hypoparathyroidism based on a 22q11 deletion first diagnosed in a 43-year-old woman.' by K. van den Berge, **K. Diderich**, P. Poddighe and A. Berghout, *The Netherlands Journal of Medicine*, Vol. 67(3), March 2009

Cursussen

Masters Course in Molecular and Cell Biology, 10 januari -18 mei 2000, Erasmus Universiteit Rotterdam

Classical Methods for Data Analysis, 18 september -6 oktober 2000, Erasmus Universiteit Rotterdam

Cursus Proefdierkunde Art. 9 van de Wet op Dierproeven, 30 oktober -17 november 2000, Erasmus Universiteit Rotterdam

MGC cursus 'Transgenesis, Gene Targeting and Gene Therapy', 8-12 januari 2001, Universiteit Leiden

Microarray course, 2 en 3 april 2001, NKI/AvL-KWF Central Microarray Facility, Amsterdam

MGC cursus 'Oncogenesis and Tumour biology', 2-5 oktober 2001, Erasmus Universiteit Rotterdam

Basiscursus Stralingshygiene en Instellingsgebonden Stralingshygienische Regelgeving EMC, 1 juli 2002, Erasmus Universiteit Rotterdam

Safe Laboratory Techniques/ Risicobeheersing in Laboratoria, oktober 2002, Erasmus Universiteit Rotterdam

MGC cursus 'Towards comprehending scanned array; expression profiling', november 2002, Universiteit Leiden

MGC cursus 'From yeast to man. Comparative Gene Function Analysis', 17-21 februari 2003, Universiteit Leiden

MGC cursus 'From development to disease', 20-22 mei 2003, Erasmus Universiteit Rotterdam

Course Molecular Medicine, 21-25 juni 2004, Erasmus Postgraduate School Molecular Medicine, Erasmus Universiteit Rotterdam

Presentaties en internationale congressen

2nd Joint MGC-ICRF Graduate Student Colloquium, 16-19 mei 2001, Brugge, België

First Conference on Functional genomic of Ageing, 24-27 april 2002, Sevilla, Spanje

4th Joint MGC-Cancer Research UK Graduate Student Conference, 7-10 mei 2003, Lille, Frankrijk

'Genetic Toxicology' Conference, 10-15 augustus 2003, Oxford, Engeland

Posterpresentatie

EU-US Workshop on Molecular signature of DNA damage induced stress responses, 26-30 september 2003, Cortona, Italië

Posterpresentatie

5th Joint MGC-Cancer Research UK Graduate Student Conference, 12-15 mei 2004, Leuven, België

Voordracht

31st European Symposium on Calcified Tissues, 5-9 juni 2004, Nice, Frankrijk

Voordracht en European Calcified Tissue Society Young Investigator Award

Conference of the Research Institute of Diseases in the Elderly, 17 juni 2004, Den Haag

Voordracht

Najaarsvergadering van de Nederlandse Vereniging voor Calcium- en Botstofwisseling, 28 en 29 oktober 2004, Zeist

Voordracht

DANKWOORD



Dankwoord

Nu er eindelijk een boekje ligt, wil ik graag een aantal mensen bedanken die een belangrijke rol hebben gespeeld bij de totstandkoming van dit proefschrift.

Mijn promotoren van de afdeling Genetica, Jan Hoeijmakers en Bert van der Horst wil ik allereerst bedanken voor de mogelijkheden die ik heb gekregen, met name veel dank voor de ruimte om ook te beginnen aan het TTD werk. Beste Jan, ook heel erg bedankt voor je steun en de snelle correcties in de eindfase.

Zonder mijn promotor van de afdeling Inwendige Geneeskunde, Hans van Leeuwen zou dit boekje er zeker niet gekomen zijn. Beste Hans, heel veel dank voor de prettige samenwerking, je inspirerende en opbeurende commentaren!

All the labmembers of 730, 734 and 738, many thanks for the pleasant environment in the lab. Renata, heel erg bedankt voor je hulp met het muizencohort. Inês, heel erg bedankt voor al je hulp met de figuren! Judith, Inês, Hennie, Ingrid, Renata, Phebe en Karin K., bedankt voor de gezelligheid binnen en buiten het lab.

Alle collega's van het 'calcium en botten-lab': Claudia, Cok, Irene, Sander, Bram, Marijke, Marjolein, Ksenija, Halima en Marco, bedankt voor de goede samenwerking, jullie hulp en de gezelligheid.

Alle collega's van de 'endocriene labs': Frank, Axel, Jenny, Piet en Bas, bedankt voor de goede samenwerking, jullie hulp en input.

Many thanks to my colleagues from the Department of Orthopaedics: Harrie, Erwin and Judd for your input and the pleasant collaboration.

Ook heel veel dank aan de collega's van het RIVM; Harry, Dolf, Susan en Evert voor jullie hulp en de plezierige samenwerking.

I would also like to thank our collaborators in Germany and Portugal for their input.

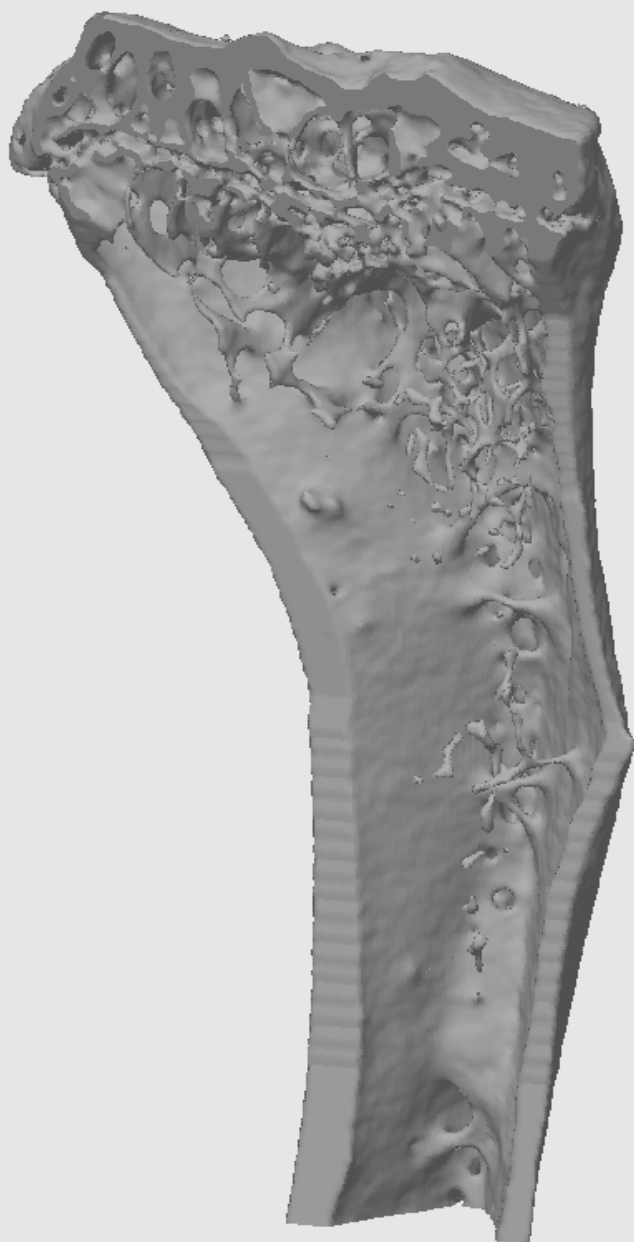
De ondersteuning van de computer-experts, fotografen (Ruud, bedankt voor je hulp met de plaatjes), secretaresses en diervverzorgers (Patrick, bedankt voor je hulp met de orbitapuncties) was onmisbaar, bedankt.

Joost and Peter, thanks for the inspiring introduction in basic science.

Al mijn huidige collega's van de afdeling Klinische Genetica wil ik bedanken voor hun interesse. Beste Anneke en Fred, veel dank voor jullie 'bemoeienissen' en de ruimte om een doorstart te maken. Beste Anja W., veel dank voor je wijze woorden. Beste kamergenoten van de WZD en de 20^e, veel dank voor jullie steun. Lieve Esther, ik vind het meer dan geweldig dat je mijn paranimf wil en kan zijn. Jouw levensinstelling is een groot voorbeeld.

Mijn familie (papa, bedankt voor de typefouten-check) en vrienden wil ik bedanken voor hun interesse en steun gedurende de hele periode. Kära mormor, du var min stora stöd i den största delen av arbetet. Jag är mycket ledsen att du inte fick vara med till slutet. Tack så mycket för ditt ständiga interesse i 'mina celler och möss'. Alex, heel veel dank voor je steun (thuis en als cateraar op de late avonden in het lab) en met name je geduld. Gelukkig heb je

me wel overtuigd niet langer te wachten op het boekje; Thomas is zo geweldig en dat wordt zijn broertje/ zusje vast ook.



**COLOUR
FIGURES**

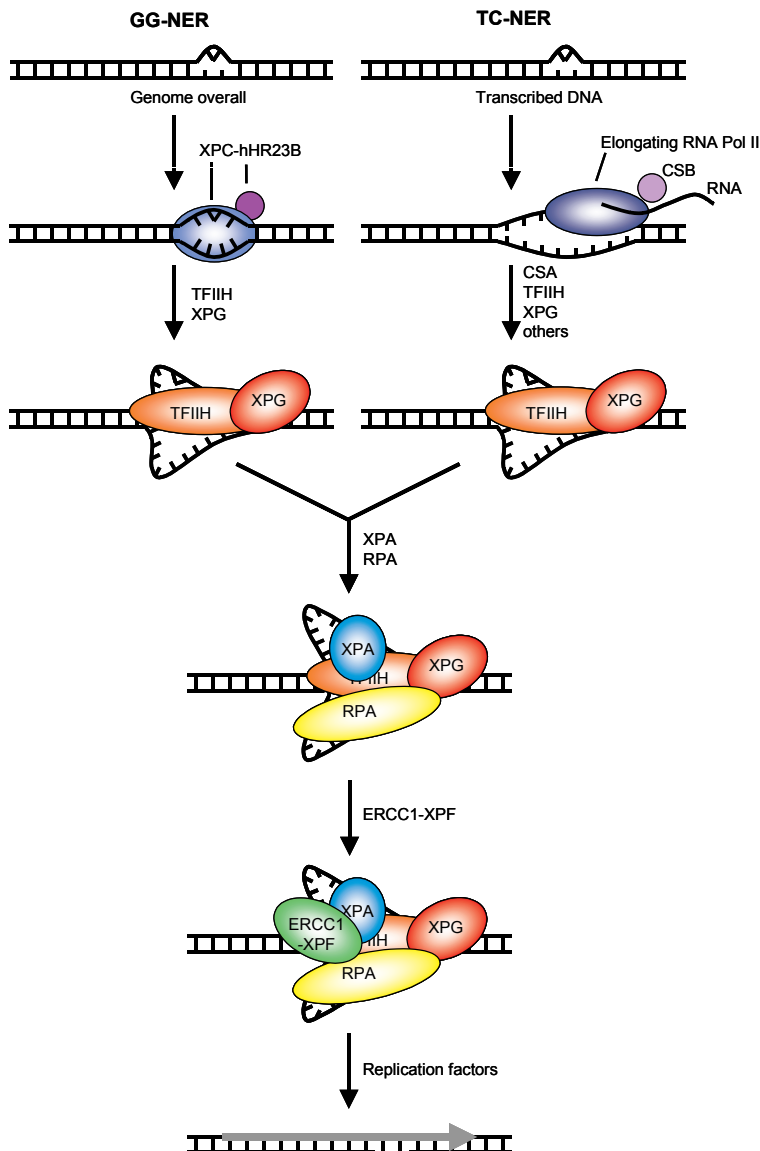


Figure 2: Mechanism of nucleotide excision repair.

This figure shows the principle of nucleotide excision repair (NER) and its two subpathways, global genome NER (GG-NER) and transcription-coupled NER (TC-NER). In GG-NER, the XPC/hHR23B protein complex recognizes the helix distorting lesion. When RNA polymerase II is stalled upon a lesion, TC-NER is initiated by the CSA and CSB protein. In both GG-NER and TC-NER the lesion recognition step is followed by recruitment of TFIIH. The XPB and XPD helicases from the TFIIH complex unwind the DNA around the lesion. The initial open complex is stabilized by XPG. Next, XPA verifies the lesion and RPA stabilizes the open intermediate by binding single stranded DNA. The structure specific endonucleases XPG and ERCC1/XPF cleave 3' and 5' of the lesion, respectively. The resulting 24-32 nucleotide fragment, containing the lesion, is subsequently removed and the remaining single strand gap is filled by the regular replication machinery and the resulting nick is sealed by ligase I or ligase III (adapted from Hoeijmakers, Nature 2001).

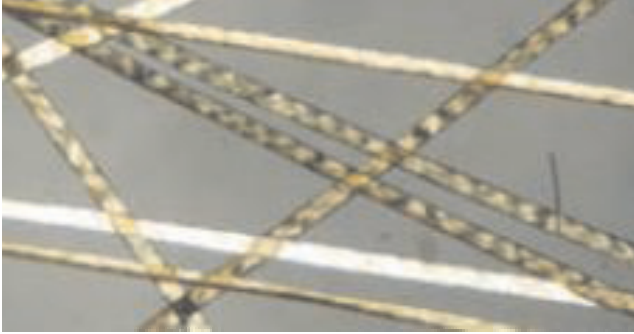


Figure 3: 'Tiger tail banding' in hair from a TTD patient.

Adapted from Liang et al., J Invest Dermatol. 2006.

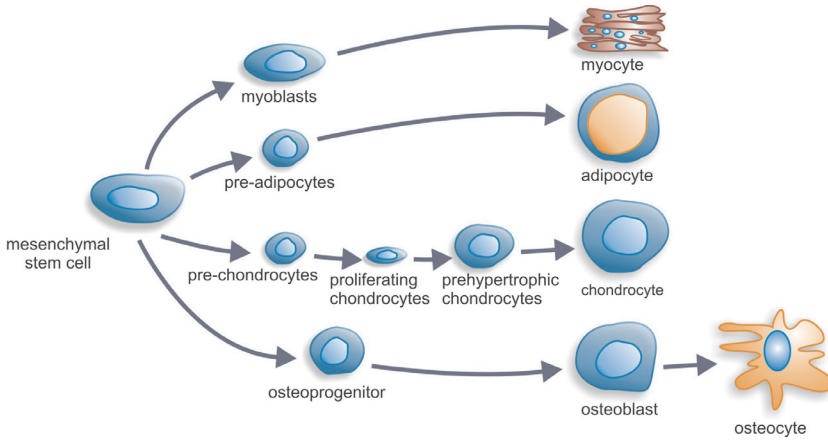


Figure 4: Different lineages derived from the mesenchymal stem cell.

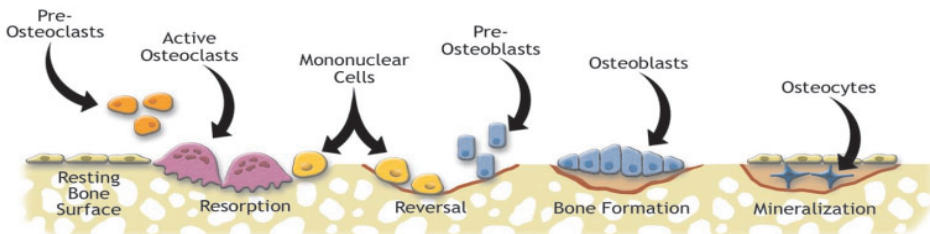


Figure 5: Bone remodelling phases.

During bone remodeling resting bone lining cells secrete RANKL which activates mononuclear cells of the haematopoietic lineage to fuse on the activated bone surface and form differentiated active osteoclasts. Subsequently, osteoclasts resorb bone after which formation is coupled to resorption by the appearance of pre-osteoblasts in the resorption cavity. A cement line is formed which marks the limit of resorption and acts as attachment or glue between the old and new bone. Finally, in the formation phase osteoblasts fill the resorption cavity with new bone. Initially this is osteoid, unmineralized bone matrix, which then becomes mineralized.

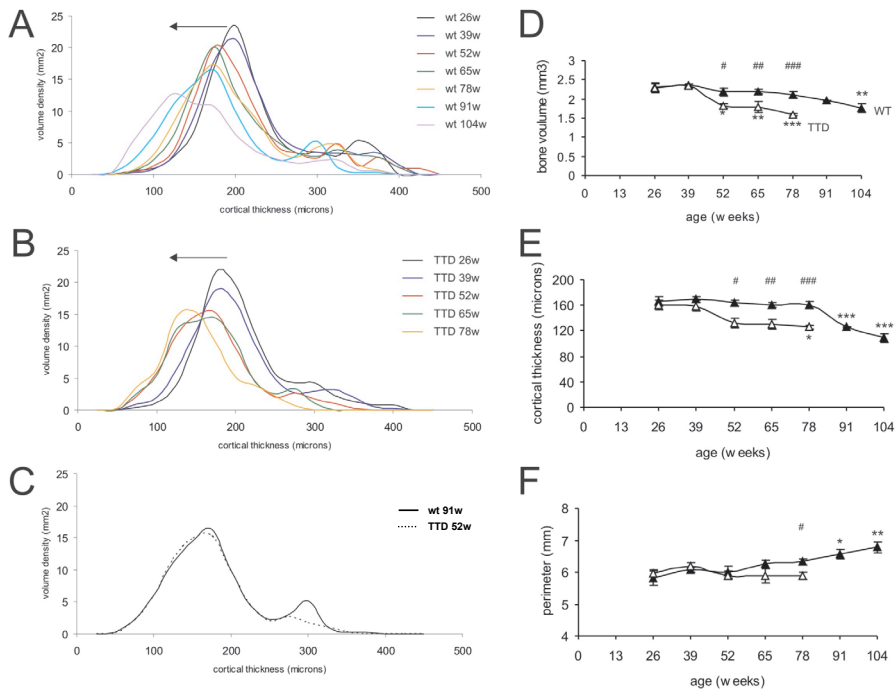


Figure 2: Thickness distribution and bone parameters in wild type and TTD mice.

Cortical thickness distribution in aging wild type (A) and TTD mice (B) with the arrow indicating the direction of change with aging. Comparison of thickness distribution in 52-week-old TTD mice (dotted line) compared to 91-week-old wild type mice (solid line) (C). Bone parameters in aging wild type mice (solid triangles) and TTD mice (open triangles): bone volume (D), cortical thickness (E) and perimeter (F). TTD mice compared to wild type animals: # $p < 0.05$, ## $p < 0.01$, ### $p < 0.001$; TTD mice and wild type animals compared to their 26 week time point: * $p < 0.05$, ** $p < 0.01$, *** $p < 0.001$; error bars represent SEM.

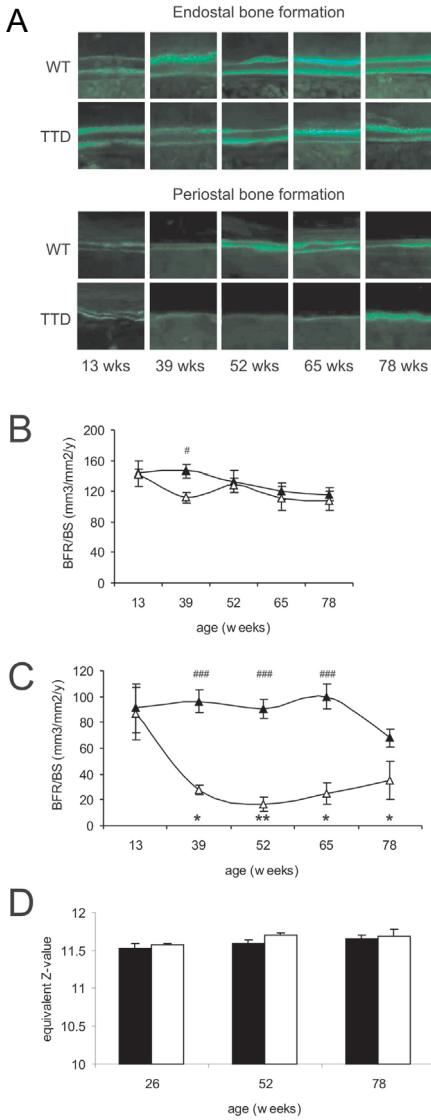


Figure 3: Histomorphometric analysis of cortical bone and Backscatter Scanning Electron Microscopy of wild type and TTD mice.

Calcein double labeling of endosteal and periosteal bone formation in wild type and TTD mice (A). Quantified endosteal apposition (B), quantified periosteal apposition (C) and mineralization status (D) in wild type (solid symbols) and TTD (open symbols) mice. TTD mice compared to wild type mice: # $p < 0.05$, ### $p < 0.001$; TTD mice compared to their 13 week time point: * $p < 0.05$, ** $p < 0.01$; error bars represent SEM.

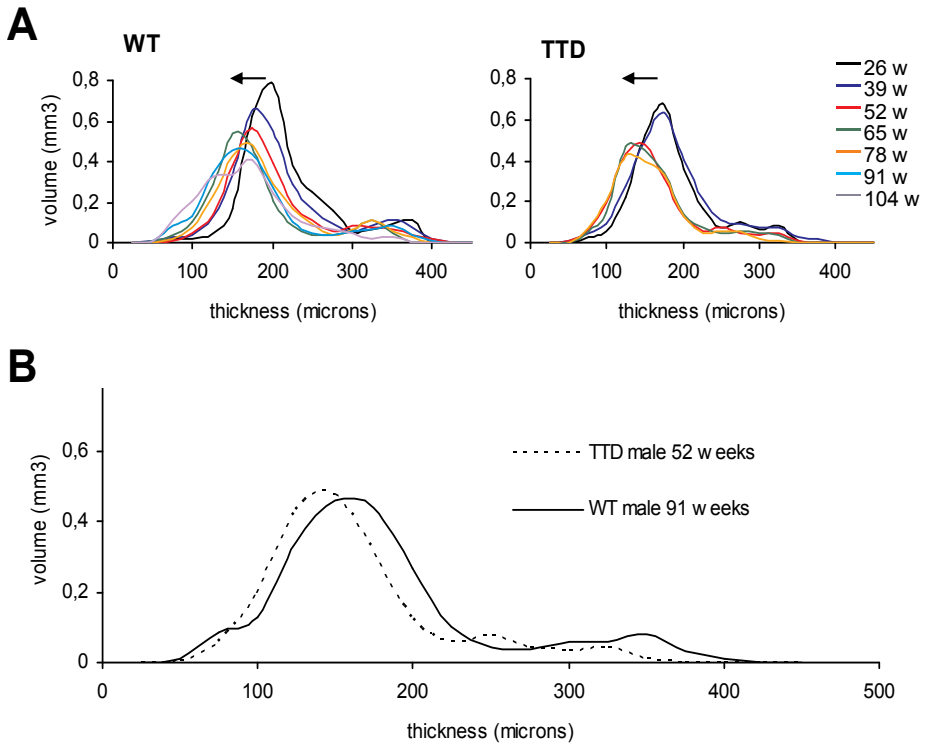


Figure 1: TTD mice show accelerated skeletal aging.

(A) 3D thickness distribution (volume density) in aging male (A left panel) wild type and (A right panel) TTD mice, with the arrow indicating the direction of change with aging. (B) Comparison of thickness distribution in 52-week-old TTD male (dotted line) compared to 91-weeks-old wild type male (solid line).

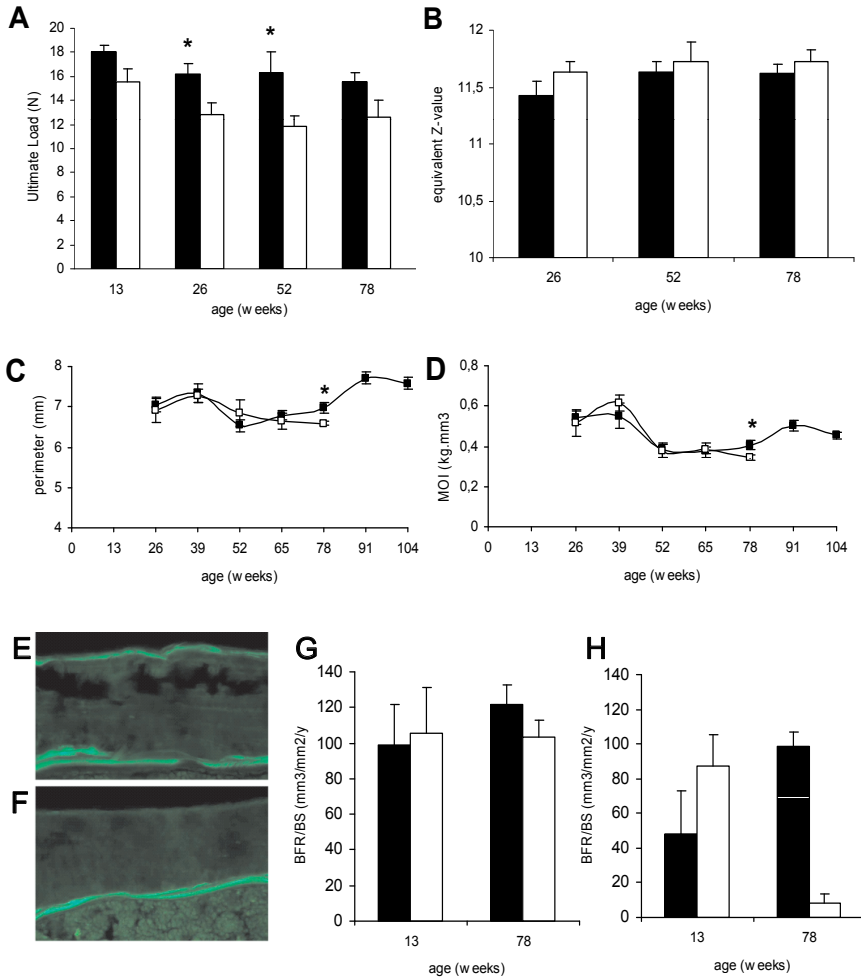


Figure 3: Decreased bone strength in TTD mice.

Bone strength, mineralization and bone formation rates in long bones of aging wild type (solid bars/ symbols) and TTD males (open bars/ symbols). (A) Bone strength depicted as Ultimate Load, (B) bone mineralization, (C) perimeter and (D) MOI. Calcein labelling at sites of periosteal apposition in 78-week-old (E) wild type and (F) TTD mice. (G) Endosteal apposition and (H) periosteal apposition. TTD vs. wild type: ANOVAs * $p < 0.05$, *** $p < 0.001$; error bars represent SEM.

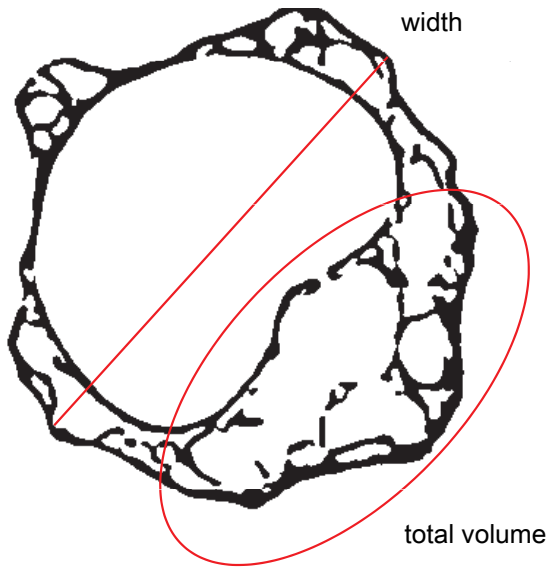


Figure 1: Area of interest for micro-computed tomography analyses.

The bone parameters were measured in the vertebral body. The line represents the width of the vertebra. The ellipse area depicts the total endocortical volume (TV) in which trabecular bone volume (BV) was determined.

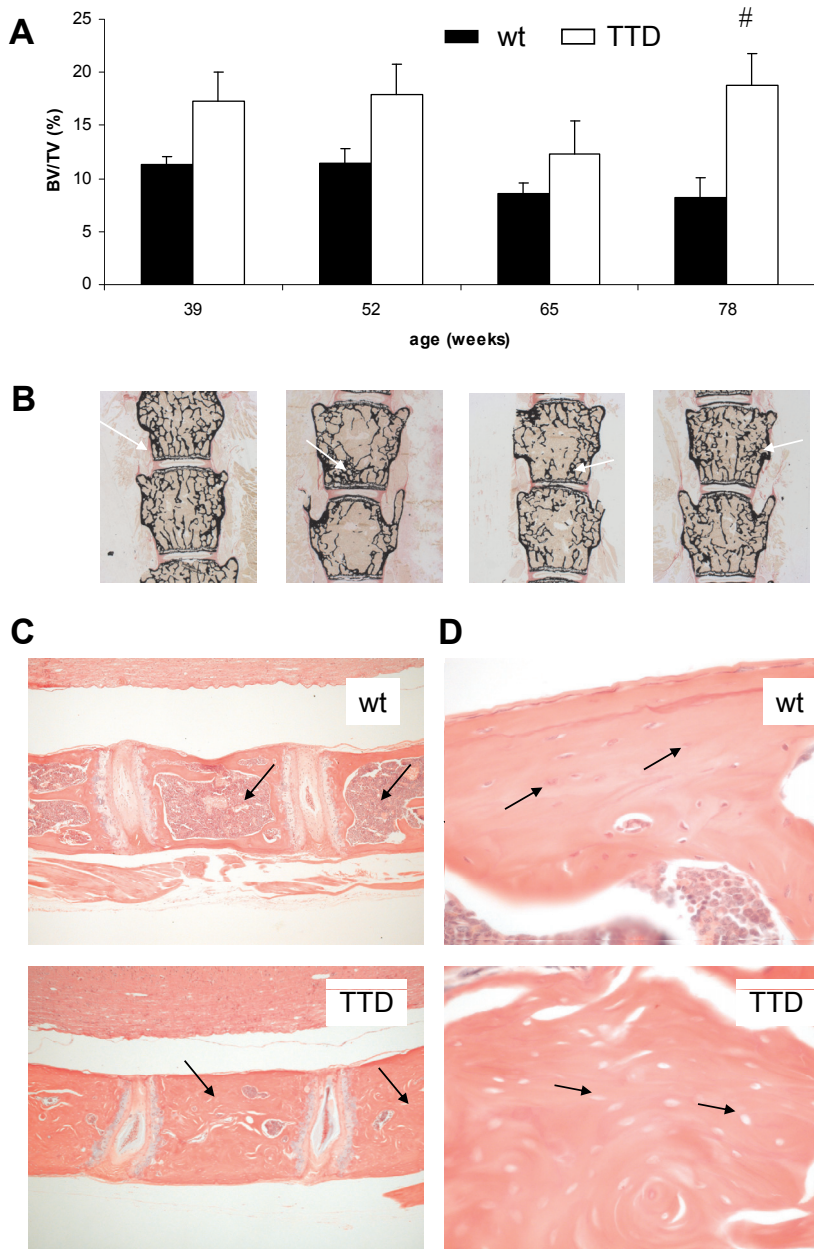


Figure 4: Histomorphometric and histopathological analysis of vertebrae.

Trabecular bone volume fraction in aging wild type mice (solid bars) and TTD mice (open bars) (A), 2D histology (panel 1-4) images of vertebrae of aging TTD mice with the highest trabecular bone volume fraction; disorganized appearance indicated by arrow (B). Transversal section of vertebrae showing an increase in bone mass accompanied by a reduction of medullary spaces (indicated by arrows) in a 104-week old TTD mouse compared to a wild type mouse (C). Increased magnification showing empty osteocyte lacunae (indicated by arrows) in vertebrae of a 104-week old TTD mouse compared to a wild type mouse (D). TTD mice compared to wild type mice: # $p < 0.02$; error bars represent SEM.

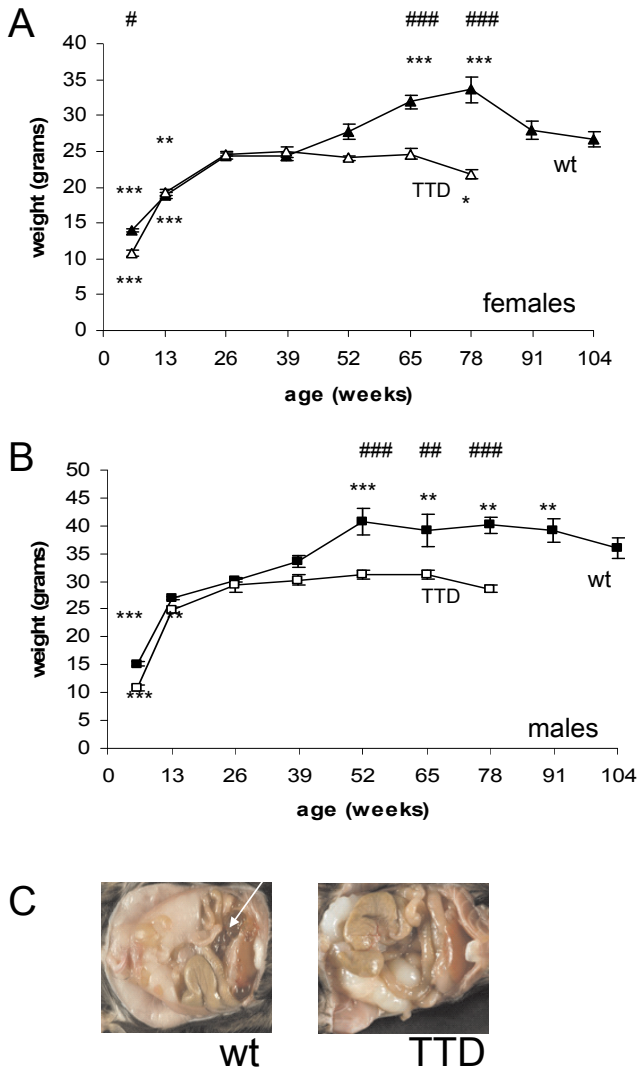


Figure 1: Bodyweight and abdominal cavity in wild type and TTD mice.

Bodyweight in wild type (closed symbols) and TTD mice (open symbols); (A) females and (B) males. Error bars represent SEM; significance compared to 26 w: * = $p < 0.05$, ** = $p < 0.01$, *** = $p < 0.001$ and significance compared between genotypes: ## = $p < 0.01$, ### = $p < 0.001$. (C) abdominal cavity showing (lack of) fat mass in a wild type mouse and a TTD mouse.

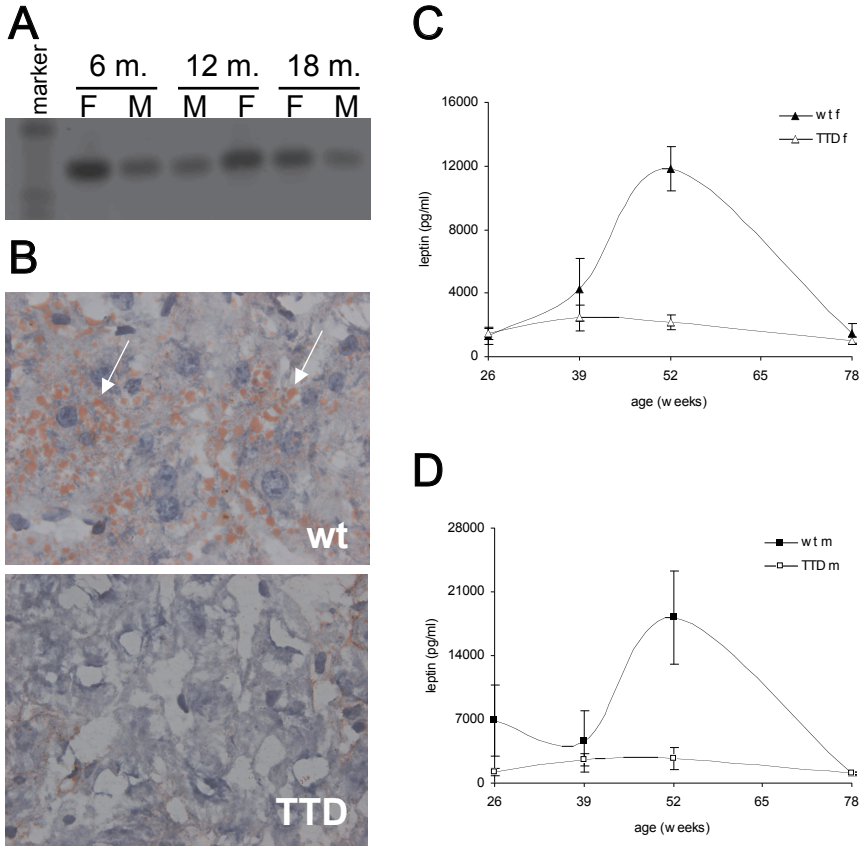


Figure 5: Aromatase expression, Oil-Red-O staining and leptin levels in wild type and TTD mice. (A) aromatase expression in fat of wild type mice. (B) Oil-Red-O staining on livers from a 78-week-old male wild type and TTD mouse. Staining of triglycerides indicated by arrows. Pictures were taken at 100x magnification. Serum leptin levels in wild type (closed symbols) and TTD mice (open symbols); (C) female and (D) male mice. Error bars represent SEM.